Proprioceptor subtype identity specified by limb-derived signals

Amy L. Norovich

Submitted in partial fulfillment of the

requirements for the degree of

Doctor of Philosophy

in the Graduate School of Arts and Sciences

COLUMBIA UNIVERSITY

2017

Abstract

Proprioceptor subtype identity specified by limb-derived signals

Amy L. Norovich

The provision of proprioceptive feedback from limb muscle to spinal motor neuron is essential for the generation of coordinated movement. Proprioceptive sensory neurons form a precise matrix of connections with motor neurons and do so in the absence of patterned activity, implying the existence of proprioceptor subtype identities that mediate selective connectivity. The developing limb has been shown to influence the pattern of connections made by proprioceptors with motor neurons, suggesting that the patterning cues distributed along its cardinal axes are capable of influencing the molecular identities of proprioceptors.

In this thesis, I describe efforts to characterize the molecular diversity of proprioceptors supplying distinct muscles located at different dorsoventral and proximodistal positions within the mouse hindlimb. I demonstrate the selective expression of several genes – *cdh13*, *vstm2b*, *sema5a*, and *crtac1* – by proprioceptors supplying defined positional domains of the limb. I proceed to determine the limb tissue source of proprioceptor patterning information by examining the expression of these genes in mice in which one of three tissues encountered by proprioceptors – the motor axon, limb mesenchyme, and target muscle – has been genetically manipulated, revealing that both mesenchyme and muscle supply cues capable of

directing proprioceptor gene expression. Finally, I show that one marker of proprioceptor muscle-type identity, *cdh13*, mediates the formation of selective connections between proprioceptors and motor neurons, thereby establishing a molecular link between proprioceptor subtype identity and patterned central connectivity.

Contents

List of figures

List of tables

Acknowledgements

During my time in the Jessell Lab I have had the honor and privilege of working with many extraordinary scientists, each of whom has contributed to my own growth as a scientist and has therefore influenced the work presented in this thesis.

First and foremost, I would like to thank Tom Jessell for the opportunity to perform my thesis work in his laboratory. He has been a kind, patient and encouraging mentor during my years in the lab yet has always held me to the highest standards, which I will undoubtedly carry forward into future scientific endeavors. I am greatly indebted to Sebastian Poliak, who initiated the investigation of proprioceptor muscle-type identity and with whom all experiments addressing the mechanism of *cdh13* induction and its role in sensory-motor connectivity were performed. I am also grateful to Joriene de Nooij, for many helpful discussions of proprioceptor diversity; Niccolo Zampieri, for supervising my rotation in the lab; Andy Murray, for being an ever-affable benchmate and for teaching me everything I know about Photoshop and Illustrator; and David Ng and Nikos Balaskas, for cloning and circuit tracing advice.

Several members of the Jessell Lab have provided invaluable assistance with the experimental work presented in this thesis: Monica Mendelsohn and Nataliya Zabello assisted with the generation of *Vstm2b* transgenic mice; Susan Morton continues to work to generate a Vstm2b antibody; and David Wu and Qiaolin Liu

provided genotyping assistance. Sean O'Keefe, formerly of the Maniatis Lab, was instrumental in performing RNA-Seq data analysis. Thank you all for sharing your time and expertise. I would also like to thank Joshua Sanes of Harvard University and Martyn Goulding of the Salk Institute for their respective gifts of *Cdh13*::CreER and *Lbx1*$^{-/-}$ mice, without which the work presented here would have been impossible.

I am grateful to Jessell Lab managers former and current – Barbara Han, Erica Famojure, and Myles Marshall – for ensuring that everything works, and to Kathy MacArthur, for ensuring that everything runs smoothly.

I would like to thank Richard Mann and Franck Polleux for thoughtful advice during their years serving on my thesis committee. I am also grateful to Chris Henderson, who was a member of my committee while at Columbia, and to Darcy Kelley, for participating in my defense. I am especially grateful to Eric Frank for agreeing to be my external examiner and for his many landmark contributions to the field of spinal circuit formation, several of which provided the foundation and inspiration for the work presented in this thesis.

I am grateful for the close friends that I've made among my fellow graduate students at Columbia: Thomas Reardon, Tim Machado, Alana Mendelsohn, Claire Warriner, Shobhit Singla, Kara Marshall, Mariano Gabitto, Armen Enikolopov and Ashley Jurado, who I am fortunate to count as both friends and colleagues. I am especially

grateful to my friends outside of science for their steadying influence and support: Alissa Randall, Catherine Hancock, Heather Boaz, Adriana Socoski, and Arden Hegele; and friends in the Greenwich Village Orchestra, which has become my musical home in New York.

Finally, I am forever thankful to my loving parents, Steve and Cindy Norovich, who have supported and encouraged me in every conceivable way, and to Imri Talgam, for his love, support and encouragement, and for eliminating the clutter in my life.

1 Proprioceptor subtypes are required for motor control

Proprioceptive feedback plays an essential role in the refinement and coordination of motor behavior. The ability of proprioceptors to modulate motor output is predicated on their formation of highly stereotyped patterns of excitatory monosynaptic connections with motor neurons. The requirement that proprioceptors innervating each of the approximately 50 muscles of the limb locate and synapse with a distinct subpopulation of spinal motor neurons represents a significant developmental challenge. The complex pattern of sensory-motor synapses forms largely in the absence of patterned neuronal activity, suggesting that proprioceptors possess distinct molecular identities that underlie their ability to synapse with discrete populations of motor neurons. Nevertheless, the nature of proprioceptor subtype identity with respect to peripheral target innervation remains uncharacterized.

In this thesis, I describe our efforts to characterize proprioceptor "muscle-type" identities. I first discuss the results of a comparative screen designed to probe proprioceptor gene expression along the dorsoventral and proximodistal axes of the limb. I show that proprioceptors exhibit apparently hierarchical subtype identities that respect the biomechanical organization of the limb and, by extension, their patterns of connectivity within the spinal cord. I then assess the impact of manipulating several peripheral tissues – motor axon, limb mesenchyme, and muscle – on the expression of proprioceptor muscle-type genes, thereby

demonstrating that limb mesenchyme and muscle supply independent yet overlapping programs of patterning information that may enable specification of the ~50 proprioceptor subtypes presumed necessary to establish selective connectivity with motor neurons. Finally, I provide evidence of a functional link between proprioceptor muscle-type identity and the ability of these neurons to selectively target spinal motor subsets. This work suggests that positionally restricted limb signals from multiple tissue sources are integrated by proprioceptors to specify molecular recognition programs that underly the accurate formation of spinal circuitry, thereby enabling coordinated limbed movement.

Proprioceptive feedback is essential for movement

Proprioceptive sensory neurons play a critical role in refining the output of the spinal motor system by supplying feedback signals that convey the state of muscle activity to motor neurons (Figure 1.1). Axons extending into the periphery from proprioceptor cell bodies located in dorsal root ganglia (DRG) supply specialized sensory receptors known as muscle spindles and Golgi tendon organs (GTOs) in skeletal muscle, where they detect changes in muscle tension. Proprioceptors innervating the muscle spindle respond to increases in muscle fiber length through the monosynaptic excitation of spinal motor neurons innervating the same muscle (Brown, 1981; Burke and Nelson, 1966), thereby causing the muscle to contract in opposition to the original force.

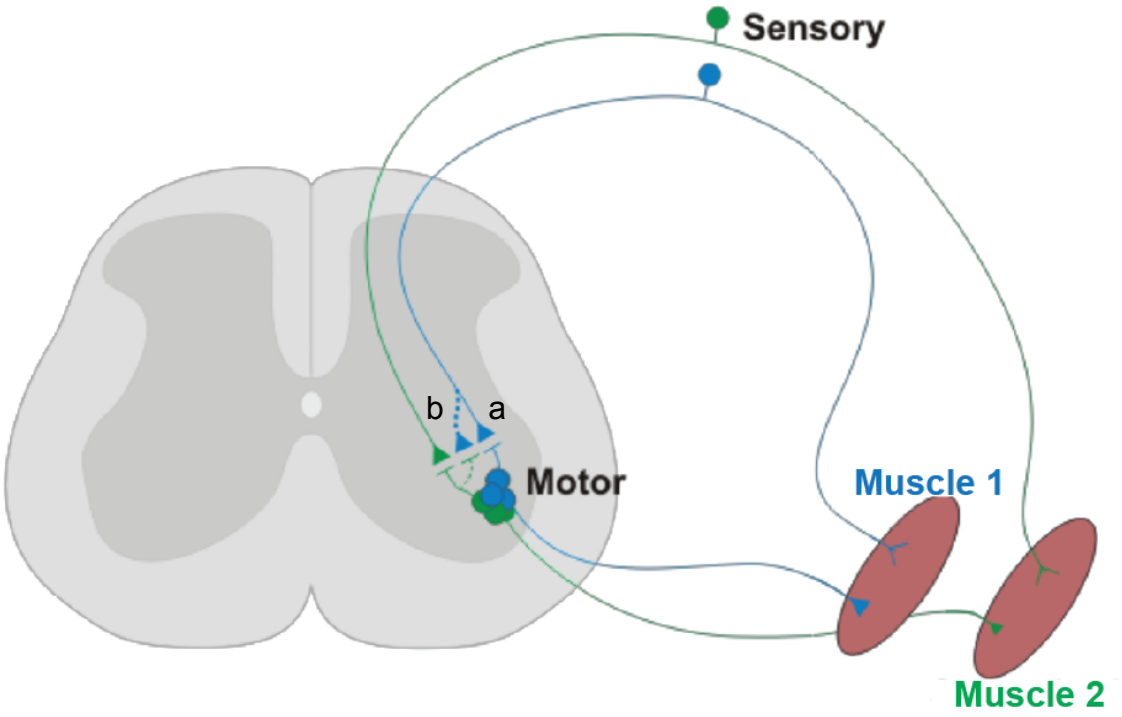

Figure 1.1 Structure of the stretch reflex

Motor neurons located in the ventral spinal cord project to individual muscles in the limb and trigger the contraction of muscle fibers upon excitation. Proprioceptors located in the dorsal root ganglion (DRG) innervate these muscles and detect changes in muscle fiber length, upon which they provide excitatory monosynaptic feedback to the motor neuron (a), resulting in contraction to restore the length of the muscle (Muscle 1: a joint flexor). Joint position is stabilized in part through the provision of proprioceptive feedback to inhibitory interneurons, which negatively regulate the activity of motor neurons controlling opposing muscles (Muscle 2: a joint extensor).

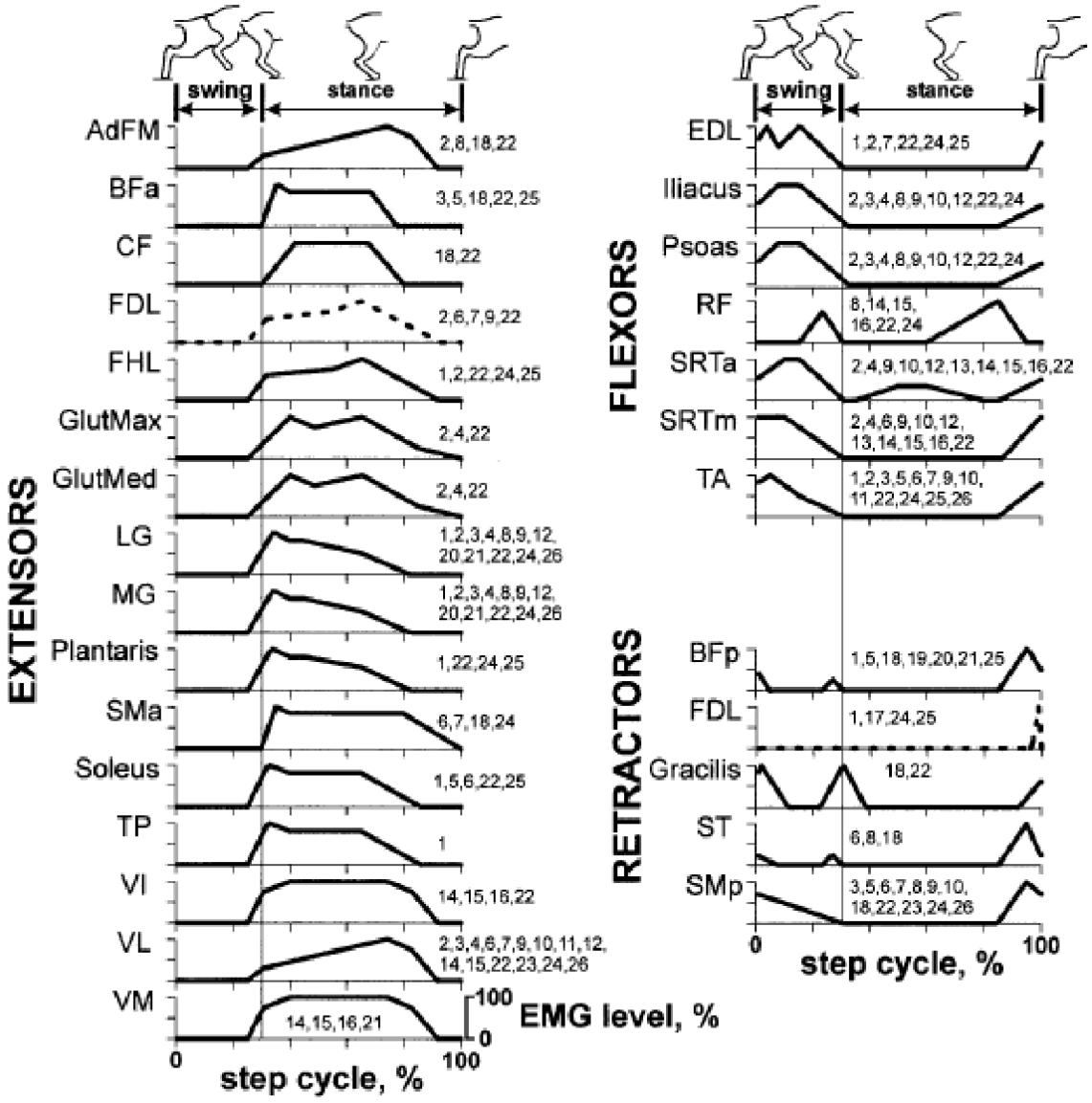

Figure 1.2 Patterns of muscle activation during the step cycle

Electromyographic (EMG) patterns of hindlimb muscle activation during the locomotor step cycle. Adapted from Yakovenko et al., 2002.

The most basic function of this feedback circuit is the provision of a homeostatic mechanism by which the resting position of the muscle is restored. This reflex circuitry has also been suggested to contribute to the stability of individual joints and to postural support (Sherrington, 1906). However, the requirement for proprioception is perhaps most marked during limbed movement. Limb-based locomotion requires the precise temporal activation of spinal motor neurons in order to coordinate the activity of the approximately 50 muscles of the limb across the duration of the step cycle (Figure 1.2; Machado et al., 2015; Rossignol; Yakovenko et al., 2002). The activation of motor neurons is gated by their presynaptic inputs, which are supplied by three distinct cellular sources: descending tract neurons, local spinal interneurons, and proprioceptors (Kiehn, 2016). Of these, monosynaptic proprioceptive feedback represents the most direct mechanism by which motor neuron activity is regulated.

Evidence from multiple model systems has demonstrated the importance of peripheral sensory information in coordinating locomotor output. Transections of hindlimb dorsal roots in cat result in varying degrees of perturbation of the EMG muscle activity pattern observed during locomotion (Grillner and Zangger, 1984; Hiebert and Pearson, 1999). In addition, cats treated with an overdose of pyroxidine (vitamin B6) exhibit loss of proprioceptive and large-diameter cutaneous proprioceptive sensory afferents, resulting in delayed postural reactions and ataxic locomotor behavior (Stapley et al., 2002). Mice in which spindle afferent activation has been impaired by mutation of the gene Egr3, which is required for muscle

spindle development, exhibit attenuated proprioceptive sensory feedback, resulting in a degraded ambulatory pattern characterized by loss of the inter-joint coordination and flexor-extensor alternation typical of limbed movement (Akay et al., 2014).

Thus, the role of information supplied by muscle spindle and GTO afferents extends beyond the unconscious, reflexive regulation of posture and movement. Proprioception plays an active role in coordinating limb trajectory during locomotion.

Anatomical and physiological features of proprioceptors

Proprioceptors terminate in one of two transduction systems within muscles: muscle spindles and Golgi tendon organs (GTOs) (Figures 1.3 and 1.4; Matthews, 1972). Muscle spindles are composed of several intrafusal muscle fibers enveloped by a collagen sheath called the outer capsule. There are three types of intrafusal fibers, each with specialized characteristics: (i) dynamic nuclear bag fibers (bag1), (ii) static nuclear bag fibers (bag2), and (iii) nuclear chain fibers. Muscle spindles typically receive innervation from one group Ia afferent and two group II afferents (Hunt, 1974), as well as gamma motor neurons. Group Ia afferents contact each type of intrafusal fiber and form primary endings with a characteristic annulospiral morphology. Terminations of group II afferents are referred to as secondary endings and are found predominantly on chain intrafusal fibers, where they display either

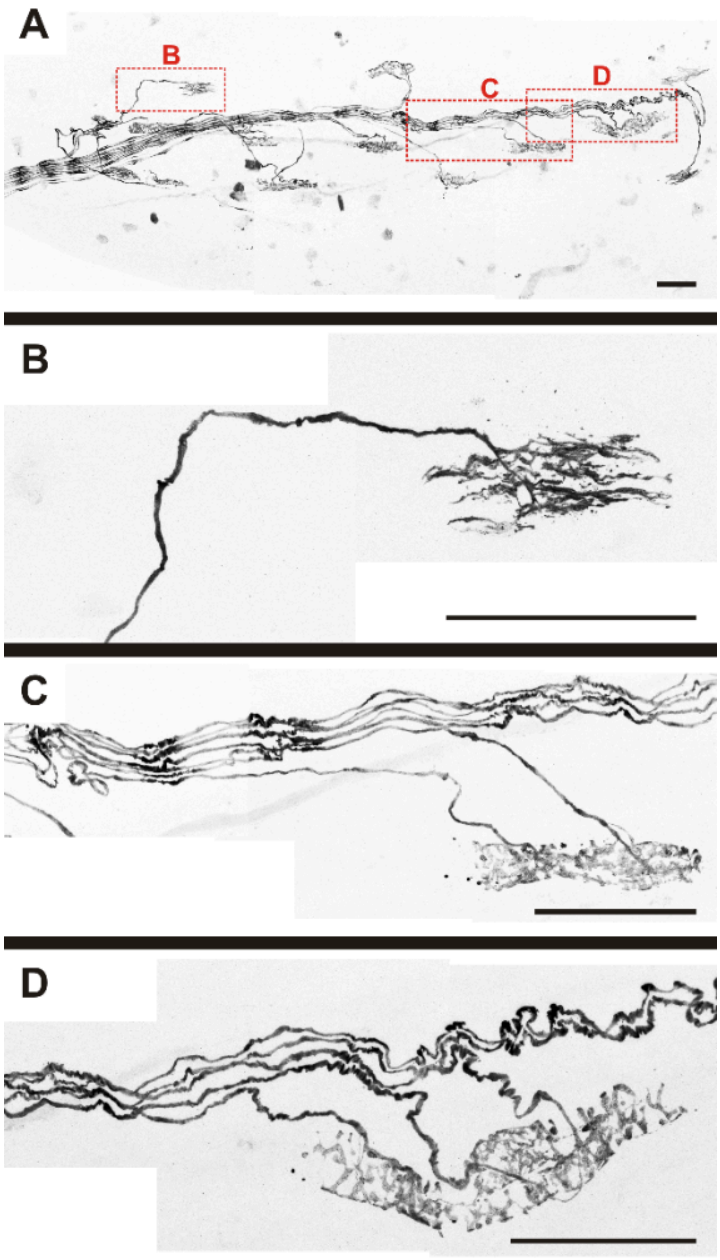

Figure 1.3 Morphology of proprioceptor sensory endings

(A-D) Whole-mount muscle preparation revealing intact proprioceptive innervation of the mouse soleus muscle. (A) Composite 20X confocal image from a P5 mouse genetically manipulated to express the fluorescent reporter tdTomato in proprioceptors. (B-D) Representative composite 60X confocal images of a GTO and two muscle spindles are shown, identified in (A) by red boxes. (B) GTOs are invariably supplied by a single Ib afferent. (C) Example of a muscle spindle supplied by two afferents, likely one group Ia and one group II. (D) Example of a muscle spindle supplied by three afferents, likely one group Ia and two group II. Scale bars represent 100 μm. Adapted from Sonner et al., 2017.

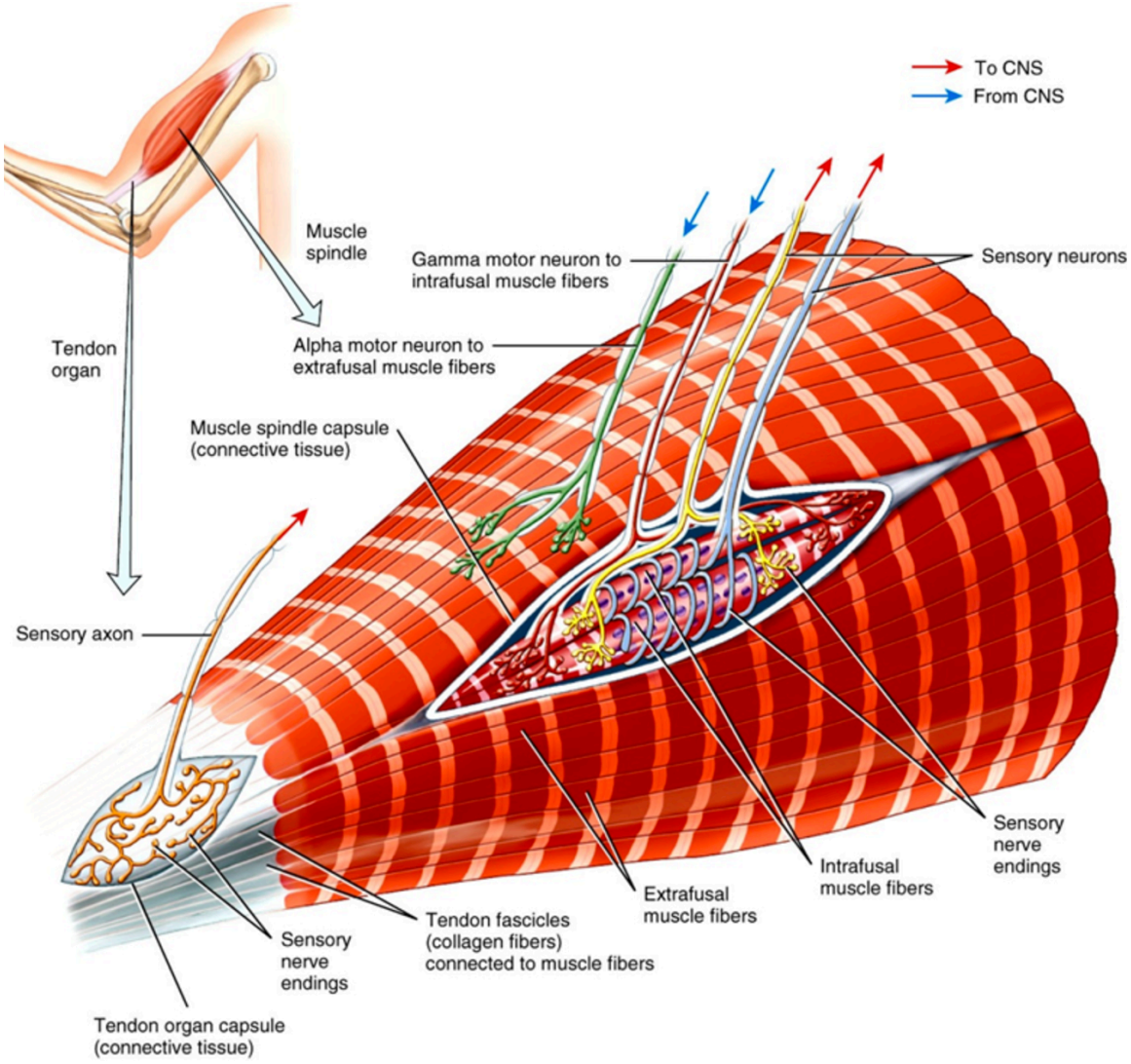

Figure 1.4 Diagrammatic representation of the muscle spindle

Sensory nerve endings supplying the muscle spindle include group Ia and II afferents, whereas those terminating in the GTO are group Ib. Efferent nerves are indicated by blue arrows and afferent nerves by red arrows.

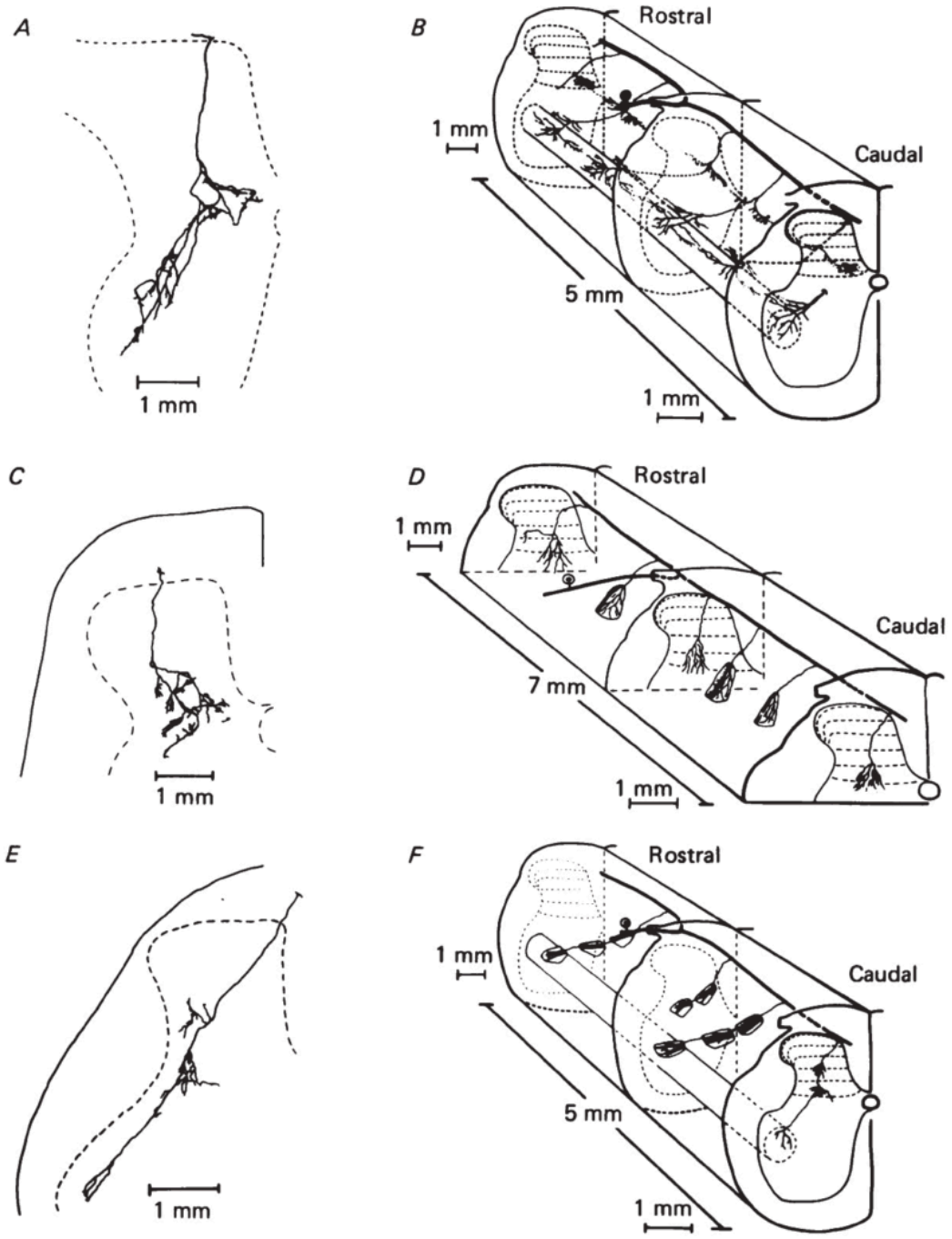

Figure 1.5 Dorsoventral termination zones of proprioceptive afferents

(A, C, E) Transverse sections depict the innervation pattern of single proprioceptive afferent fibers as they enter the lumbosacral spinal cord in cat. (B, D, F) The pattern of axon collateral innervation across segments displays precise and segmental organization. (A and B) Group Ia afferent; (C and D) group Ib afferent; (E and F) group II afferent. Adapted from Brown, 1982.

spiral-like or flower-spray morphology. The number of muscle spindles present in a given muscle is variable; in the mouse soleus muscle, for example, the number of spindles ranges between 8 and 16 per muscle (Sonner et al., 2017). Furthermore, the number of spindles found in a muscle tends to scale with the size of the muscle.

GTOs are located at the junction between tendon and muscle fiber, where their arrangement in series with muscle fibers enables sensitivity to muscle contraction. GTOs are innervated by a single group Ib proprioceptive afferent (Hunt, 1974), which branches extensively and intercalates with collagen fibers that are connected at one end to muscle fibers and at the other merge with the tendon. Increases in tensile forces upon muscle contraction cause these collagen bundles to tighten, thereby distorting Ib terminals (Schoultz and Swett, 1972). As with muscle spindles, there is substantial variability in the number of GTOs in a given muscle; in mouse soleus, the number of GTOs per muscle ranges between 3 and 7 (Sonner et al., 2017). Typical GTOs associate with small groups of muscle fibers, and not all muscle fibers feed into GTOs (Scott, 2005). However, calculations performed on data from cat hindlimb experiments indicate that the relatively small number of GTOs populating a given muscle is sufficient to adequately track motor unit activity.

Proprioceptive afferents innervating muscle spindles and GTOs adopt distinct axonal trajectories within the spinal cord that result in their termination in different dorsoventral zones (Figure 1.5; Brown, 1981b; Chen et al., 2006). All proprioceptive afferents – groups Ia, II, and Ib – project to an intermediate target

zone within the spinal cord (Windhorst, 2007). While group Ib afferents do not extend beyond the intermediate zone (Figures 1C and D), group II afferents project sparsely and group Ia afferents extensively into the ventral spinal cord (Figures 1.4A and B, E and F; Windhorst, 2007). These projection patterns restrict the repertoire of postsynaptic partners available to each class of proprioceptive afferents. In the intermediate zone, muscle spindle and GTO afferents form synapses with spinal interneuron populations, thereby exerting a polysynaptic influence on motor neuron activity. In the ventral horn, muscle spindle afferents – overwhelmingly group Ia - form monosynaptic connections with motor neurons (Eccles et al., 1957). Consequently, the most direct mechanism by which proprioceptive sensory neurons influence the output of spinal motor neurons is the monosynaptic reflex mediated by group Ia proprioceptive afferents.

Monosynaptic connectivity between proprioceptors and motor neurons conforms to limb biomechanics

The range of motion available to the limb is dictated by constraints of the musculoskeletal system. The mouse hindlimb contains approximately 50 muscles, the biomechanical properties of which are determined by muscle fiber content, fiber length, and sites of tendon origin and insertion with respect to bone (Biewener, 2016). Each muscle produces a unique torque at a joint, the direction of which is determined by its sites of origin and insertion and can be represented by the degrees of flexion versus extension with respect to the joint and abduction versus

adduction with respect to the body axis. Across these axes, muscles can be categorized according to biomechanical similarity as producing synergistic (cooperative) or antagonistic (opposing) functions at a joint (Nichols et al., 2002, 2016). The ability of a proprioceptive sensory afferent to refine and coordinate limbed motor output is dependent on its pattern of monosynaptic connectivity with motor neurons supplying synergist and antagonist muscles.

The pattern of monosynaptic input from limb-innervating proprioceptors to motor neurons was first characterized through intracellular recording. After identifying the muscle connectivity of an individual motor neuron by antidromic stimulation, EPSPs were recorded in the same motor neuron following stimulation of distinct muscle nerves containing the proprioceptive sensory afferents innervating the same muscle (Eccles et al., 1957). Direct monosynaptic input to motor neurons can be differentiated from polysynaptic sensory input relayed via interneuronal populations by the latency between stimulus and EPSP. In every vertebrate characterized, motor neurons innervating a given muscle have been found to receive strong proprioceptive input from the same muscle, termed homonymous proprioceptive feedback, and weaker feedback from muscles with synergist function at a joint, termed heteronymous feedback (Figure 1.6; Eccles et al., 1957; Frank and Westerfield, 1983; Hongo, 1984). This selective innervation establishes a negative feedback loop: the stretch of a muscle results in its strong contraction and the weaker contraction of synergist muscles via monosynaptic input from homonymous sensory neurons. In contrast, proprioceptive feedback is not

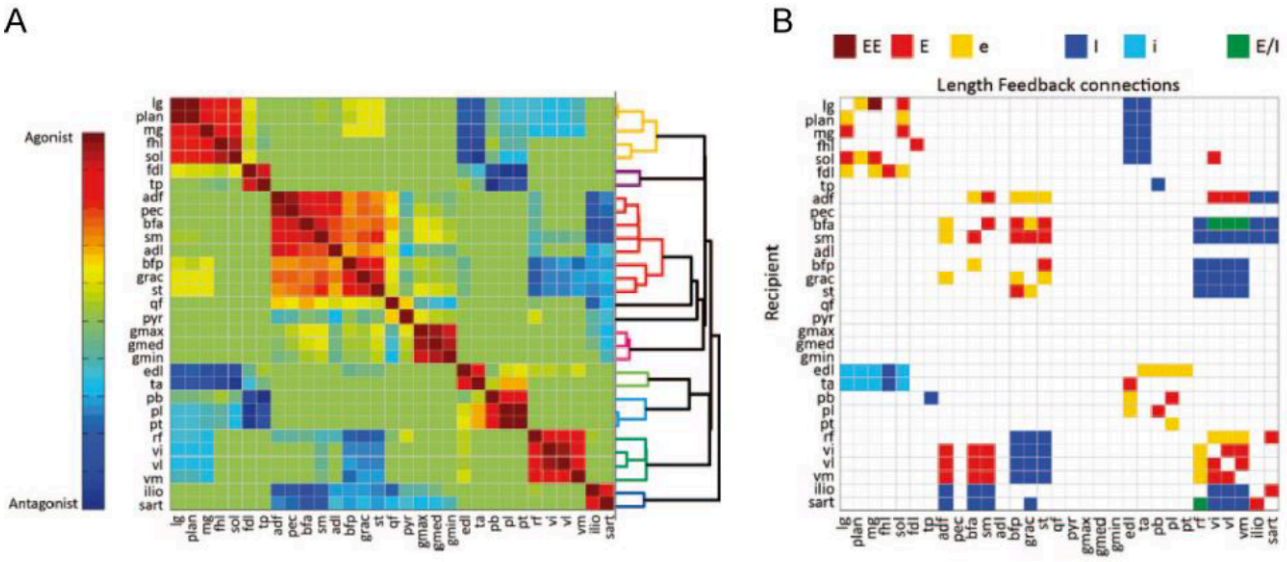

Figure 1.6 Proprioceptive feedback respects limb biomechanics

(A) Mechanical similarity of muscle actions. Cells are coded according to the cosine of the angle between the lines of action of each pair of muscles. The colors depict a continuum ranging from completely agonistic muscles (dark red) to completely antagonistic muscles (dark blue), with a midpoint where muscle pairs have no shared actions at a joint (light green). The order of the muscles in the rows and columns was chosen based on a cluster analysis that groups muscles according to their normalized moment arm vector. (B) Magnitude of proprioceptive length feedback between muscle pairs. Excitatory connections are shown in yellow, red and dark red, with darker color representing increased strength of excitation. Inhibitory connections are shown in cyan and blue. Connections that can be either excitatory or inhibitory are shown in green. Adapted from Nichols et al., 2016.

supplied to motor neurons innervating muscles of unrelated or antagonist function. Rather, these Ia afferents contact Ia inhibitory interneurons to form reciprocal inhibitory circuits that silence motor neurons of opposing function (refer to Figure 1.1).

Several cellular properties account for the relative strength of heteronymous compared to homonymous sensory-motor connections. Individual Ia afferent fibers contact both homonymous and heteronymous motor neurons (Scott and Mendell, 1976). However, while nearly all motor neurons innervating a given muscle receive homonymous input, only ~40-70% of these motor neurons receive heteronymous input (Mendell and Henneman, 1968; Nelson and Mendell, 1978; Scott and Mendell, 1976). On individual motor neurons, heteronymous boutons are observed at a lower density than their homonymous counterparts (Brown and Fyffe, 1981; Burke and Glenn, 1996). The size of EPSP evoked by a heteronymous synapse is comparable to that of a homonymous synapse, suggesting that the difference in strength between these types of feedback is due to the difference in the number of synaptic contacts supplied by proprioceptor subtypes (Kuno and Miyahara, 1969).

The role of activity in patterning monosynaptic sensory-motor connectivity

Activity-dependent refinement acts throughout the developing CNS to shape neural circuits by eliminating inappropriate synapses and strengthening desired connections (Okawa et al., 2014). It is therefore possible that the stereotyped matrix

of monosynaptic connections formed between proprioceptors and motor neurons is the result of patterned neural activity.

Agonist-antagonist specificity is apparent in mouse, chick and frog at late embryonic stages and remains stable through early postnatal development, suggesting that these connections are not subject to postnatal refinement (Frank and Westerfield, 1983; Lee and O'Donovan, 1991; Mears and Frank, 1997). Furthermore, coordinated electrical activity in sensory and motor neurons is not required for these connections to form correctly (Frank and Jackson, 1986; Mendelson and Frank, 1991; Shneider et al., 2009; Wang et al., 2012). In one study performed in chick, coordinated neurogenic muscle contractions were blocked in developing embryos by treatment with d-turbocurarine (dtc), which inhibits the nicotinic acetylcholine receptor at the neuromuscular junction. Electrophysiological examination of sensory-motor innervation in experimental animals revealed that antagonist specificity was unaltered following peripheral activity blockade (Figure 1.7; Mendelson and Frank, 1991).

The fidelity of sensory-motor connections has also been examined in the context of impaired muscle spindle function (Shneider et al., 2009; Wang et al., 2012). Genetic elimination of the ErbB2 receptor or the transcription factor Egr3 from developing intrafusal muscle fibers blocks the maturation of muscle spindles but does not impact the survival of proprioceptive sensory afferents and results in only a modest reduction in the density of anatomically defined sensory-motor

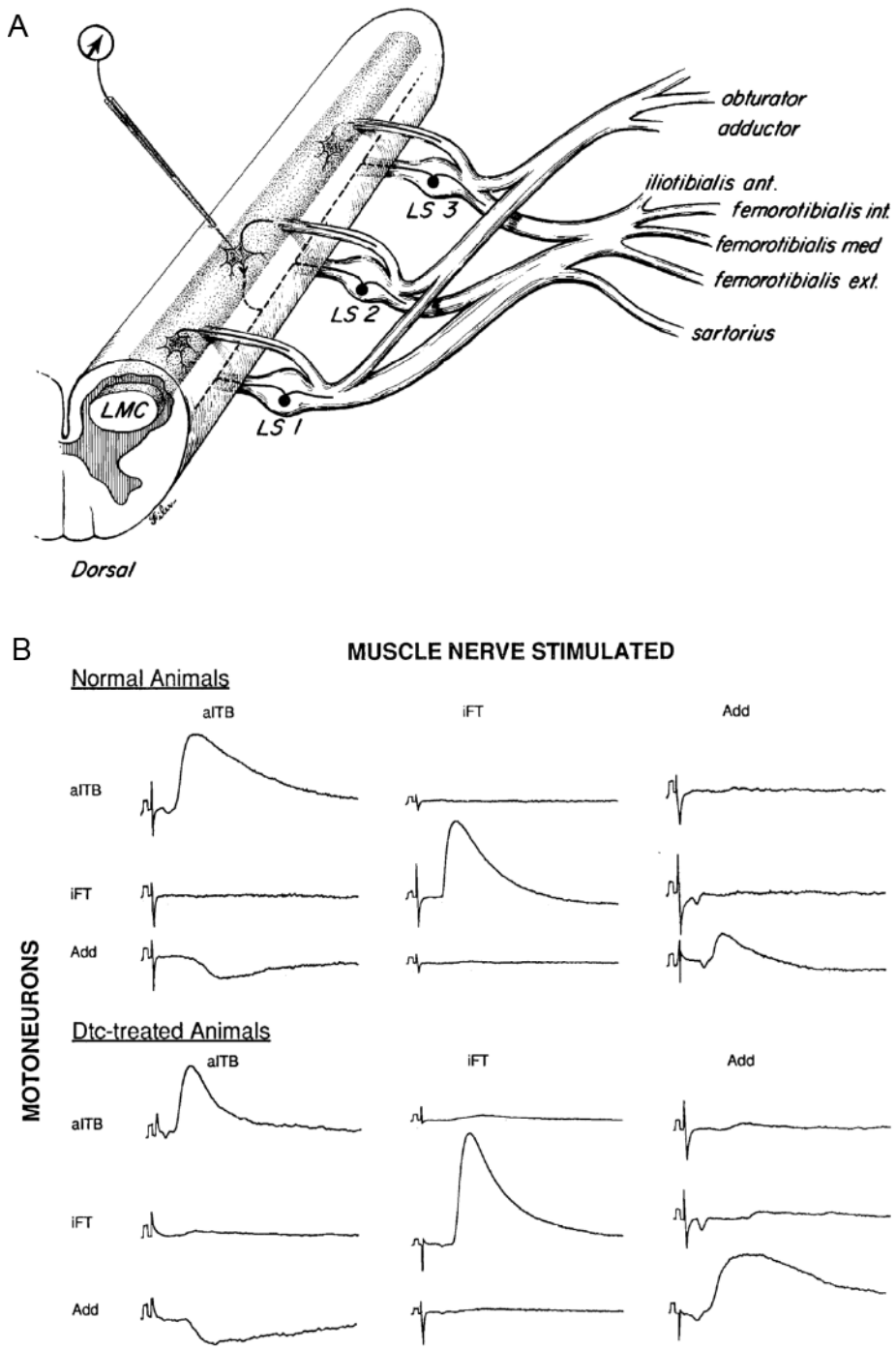

Figure 1.7 Activity-independent formation of monosynaptic contacts in chick

(A) Strength of input from Group Ia proprioceptive afferents to identified motor neurons was assayed by intracellular recording following peripheral nerve stimulation. (B) The gross pattern of homonymous input to motor neurons was unchanged in embryos treated with dtc. Adapted from Mendelson and Frank, 1991.

synapses (Shneider et al., 2009; Wang et al., 2012). Despite the fact that sensory-motor synapses in these mutants are functionally silent, they form with appropriate antagonist specificity, corroborating the notion that sensory activity is dispensable for sensory avoidance of antagonist motor neurons.

These studies, however, reached the conclusion that sensory-motor connections are shaped independent of activity based on the presence homonymous connections and persistence of antagonist avoidance in experimental preparations. More recent genetic studies in mouse have demonstrated a limited but selective role for activity in refining heteronymous connections between proprioceptors and motor neurons (Mendelsohn et al., 2015). Sensory-motor transmission was blocked presynaptically through proprioceptor-specific expression of tetanus toxin, which prevents neurotransmitter release through the cleavage of synaptic vesicle fusion proteins (Humeau et al., 2000). In these animals, the density of heteronymous connections observed by anatomical tracing methods increased 2-fold, while the incidence of homonymous synapses was unaffected (Mendelsohn et al., 2015). If activity were the sole determinant of heteronymous synaptic density, one might expect blockade of sensory transmission to equalize homonymous and heteronymous input strengths. Instead, the overall incidence of heteronymous synapses remained substantially lower than that of homonymous synapses (Mendelsohn et al., 2015), suggesting that molecular recognition may nevertheless contribute to the specificity of heteronymous reflex arcs.

Thus, while the weighting of heteronymous synapses seems to rely in part on activity-dependent refinement, activity does not appear to be involved in establishing the pattern of homonymous inputs by proprioceptors to motor neurons. This conclusion, combined with the selectivity of connections formed between spindle afferents and motor neurons, implies that proprioceptors possess muscle-specific molecular identities capable of directing monosynaptic connectivity within the spinal cord. I will now discuss current knowledge of the molecular events underlying specification of the proprioceptive lineage (Figure 1.8), followed by efforts to characterize proprioceptor subtype diversity.

Genetic specification of the proprioceptive lineage

All DRG sensory neurons are derived from neural crest cells, which arise as a seemingly homogenous population of multipotent cells along the dorsal neural tube and migrate on a ventral path between somite and neural tube to coalesce into segmentally reiterated ganglia (Horstadius, 1950). The earliest steps of sensory neuron specification are controlled by the basic helix-loop-helix transcription factors Ngn1 and Ngn2 (Perez et al., 1999; Sommer et al., 1996). In the mouse, Ngn2 is expressed in early migratory neural crest cells and is responsible for an initial wave of neurogenesis that gives rise exclusively to proprioceptive and cutaneous mechanosensitive neurons, whereas Ngn1 is required by a later-differentiating lineage that generates most or all nociceptive neurons, as well as a subset of proprioceptors and mechanoreceptors (Ma et al., 1999). The requirement for Ngn1

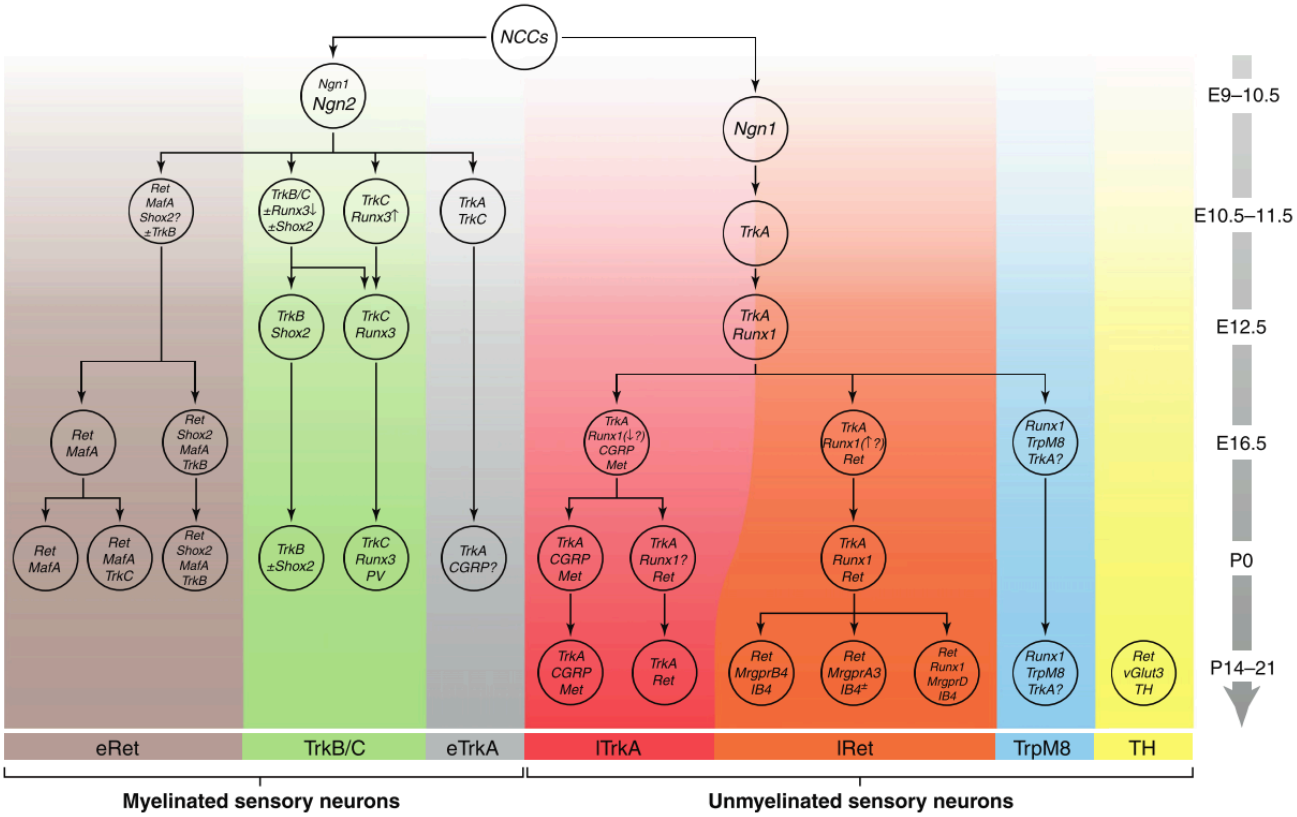

Figure 1.8 Molecular hierarchy governing the specification of proprioceptors

DRG neuron diversification during development. Schematic representation of the main lineages (outlined by color shading) during the course of sensory neuron differentiation in mouse. Proprioceptors are located in the green column and are defined by the expression of TrkC, Runx3 and Pv. Adapted from Lallemend and Ernfors, 2012.

and Ngn2 in distinct classes of sensory neurons does not mean that these factors necessarily encode sensory neuron subtype: Ngn1 compensates for the loss of Ngn2 by supplementing neurons of the proprioceptive and mechanosensitive lineages (Ma et al., 1999). Nevertheless, the commitment of neural crest cells to a sensory neuronal identity requires the expression of Ngn proteins (Greenwood et al., 1999).

The transition from sensory neurogenesis to subtype specification is dependent on pan-sensory expression of the homeobox transcription factors Islet1 and brain-specific homeobox/Pou domain protein 3A (Brn3a, also called Pou4f1) in early postmitotic DRG neurons (Fedtsova and Turner, 1995). Analysis of mice deficient in Islet1 and Brn3a has revealed their requirement for the expression of lineage-specific genes. Islet1 mutants lack molecular markers of cutaneous sensory neurons mediating the sensations of pain and touch, while the expression of proprioceptor markers is preserved (Sun et al., 2008). Conversely, Brn3a mutants do not express the proprioceptor genes TrkC and Runx3.

Emergent somatosensory lineages are marked by their differential expression of the tyrosine receptor kinase (Trk) family of neurotrophin factor receptors (Lallemend and Ernfors, 2012). TrkA, the receptor for nerve growth factor (NGF), is expressed in nociceptive and thermoceptive sensory neurons. TrkB, the receptor for brain-derived neurotrophic factor (BDNF) and neurotrophin-4 (NT-4), is expressed in touch-sensitive neurons. TrkC, the high-affinity receptor for NT-3, is expressed in proprioceptors. As part of their normal development, somatosensory

neurons – including proprioceptors – undergo a period of programmed cell death that is rooted in competition for peripheral trophic support (Ernfors and Lee, 1994; Henderson, 1996). Each of the Trk receptors is required for the survival of the distinct class of neurons that it marks, indicating that neurotrophin signaling plays a permissive role in sensory neuron development (Fariñas et al., 1994; Lallemend and Ernfors, 2012).

Uncoupling Trk signaling from its function in neuronal survival has revealed an instructive role in the specification of somatosensory lineages. Presumptive nociceptive neurons in mice lacking Bax protein, which is required for apoptosis in somatosensory neurons (White et al., 1998), fail to innervate the skin and do not express molecular markers in the absence of the TrkA receptor (Patel et al., 2000). In *Bax*$^{-/-}$, *NT3*$^{-/-}$ mice lacking peripheral NT3, proprioceptive axons express Pv but fail to extend into the dorsal horn, similar to the phenotype observed in mice lacking Er81 (Patel et al., 2003). Furthermore, expression of TrkC from the TrkA locus is sufficient to direct presumptive nociceptors to a proprioceptive fate, confirming that signaling through TrkC does not merely provide a generic survival signal but in fact directs features of generic proprioceptor identity, including Pv and Er81 expression and muscle spindle formation (Moqrich et al., 2004; Patel et al., 2003).

NT3 signaling through the TrkC receptor plays a complex role in regulating proprioceptor identity. Proprioceptors are exposed to multiple sources of NT3 at different points in their maturation. During embryonic development, NT3 is

expressed by intrafusal and extrafusal skeletal muscle fibers, by the mesenchyme surrounding peripheral projection pathways, and by motor neurons in the spinal cord. However, shortly after birth, its expression is restricted to intrafusal muscle fibers (Copray and Brouwer, 1994; Ernfors et al., 1994; Farinas et al., 1996). The level of NT3 expressed by the extrafusal fibers of distinct muscles varies and is correlated with dependence on the transcription factor Er81 (Etv1) for survival in proprioceptors (de Nooij et al., 2013). Thus, in addition to promoting proprioceptor survival and regulating generic features of proprioceptor identity, graded NT3 signaling appears to elicit distinct molecular responses in proprioceptors in a muscle-by-muscle manner (de Nooij et al., 2013). Indeed, altering the level of muscle NT3 expression in transgenic mice has been found to erode the selective connectivity of proprioceptive afferents with target motor neurons (Wang et al., 2007). Furthermore, recent studies have reported changes in gene expression in proprioceptors in response to elevated NT3 signaling (Lee et al., 2012).

Numerous studies have established that expression of the Trk receptors is much broader shortly after neurogenesis than at later stages, indicating that the diversification of somatosensory subtypes involves not only transcriptional activities that induce and maintain expression of the Trk receptors, but also repressor activities that extinguish their expression, thereby driving segregation into functional subtypes (Lallemend and Ernfors, 2012). In proprioceptors, maintenance of *trkC* expression is dependent on expression of the transcription

factor Runx3. Runx3 also represses the expression of TrkB, thereby driving differentiation toward the proprioceptive lineage (Kramer et al., 2006).

Eliminating the function of genes involved in proprioceptor differentiation often impacts the ability of proprioceptors to project into the ventral domain of the spinal cord, where monosynaptic connections with motor neurons are formed. *Er81* mutant mice exhibit severe deficits in motor coordination, yet the induction of muscle spindles occurs normally. The defect in these mutants occurs due to the failure of group Ia proprioceptive afferents to terminate in the ventral horn (Arber et al., 2000). Similarly, altering the level of Runx3 activity in proprioceptors alters the dorsoventral termination zones of proprioceptor axons in chick spinal cord (Chen et al., 2006). Er81 and Runx3 are expressed by all proprioceptors but at varying levels. The effect of these genes on the dorsoventral termination of sensory axons has led to the hypothesis that their graded expression leads to the differentiation of muscle spindle and GTO afferents, which are characterized by distinctions in the dorsoventral extent of their projection (Chen et al., 2006; de Nooij et al., 2013).

In addition to the network of transcription factors and downstream effectors required for generic proprioceptor specification, several terminal features of proprioceptor differentiation have been identified. Proprioceptors are glutamatergic and express vesicular glutamate transporter 1 (vGluT1), which is present peripherally at muscle spindles and GTOs, as well as at proprioceptor

synapses with motor neurons (Wu et al., 2004). The calcium-binding protein Parvalbumin (Pv) is also expressed by all post-mitotic proprioceptors in DRG, although its function in sensory neurons is unclear (Ernfors and Lee, 1994). In the periphery, proprioceptor expression of Neuregulin1 signals through the Erbb2 receptor in intrafusal fibers to regulate the formation of the muscle spindle (Leu et al., 2003). More recently, progress has been made in characterizing the molecular mechanism underlying the conversion of mechanical deformations of the muscle spindle and GTO into afferent firing. Piezo2, a mechanically activated nonselective cation channel, is expressed in sensory endings of proprioceptors innervating both muscle spindles and GTOs, where it is required for stretch-evoked neuronal activity in these cells (Woo et al., 2015). Whirlin (Whrn), a PDZ-scaffold protein involved in vestibular and auditory hair cell transduction, was found to be expressed nearly selectively among DRG neurons by proprioceptors, where it localizes to peripheral sensory endings and facilitates afferent firing in response to muscle stretch (De Nooij et al., 2015). *In vitro* recordings of *piezo2*-deficient *pv*-expressing neurons revealed residual rapidly adapting currents in response to mechanical deformation, suggesting that there may be additional as-yet-unidentified channel proteins involved in proprioceptor mechanotransduction (Woo et al., 2015).

In summary, the neuronal context conferred by Ngn2 and Brn3a results in the expression of Runx3, thereby consolidating proprioceptor identity. Expression of the TrkC receptor by proprioceptors confers survival in response to peripheral NT3 and specifies gross afferent trajectory within the spinal cord via induction of

Er81 and maintenance of Runx3 expression, the graded expression of which may drive the specification of muscle spindle and GTO afferents. In the periphery, formation of the muscle spindle requires proprioceptor expression of Neuregulin1, and proprioceptor mechanosensitivity is dependent on the presence of Whrn and Piezo2 at the end organ. To date, no individual marker distinguishing the proprioceptive lineage from other DRG sensory modalities has been identified, often due to substantial overlap in gene expression between proprioceptors and cutaneous mechanoreceptors. However, the proprioceptor population is demarcated by the intersection of Runx3 and Pv expression (de Nooij et al., 2013).

Characterization of proprioceptor subtype diversity

Despite our knowledge of the transcriptional networks that assign generic proprioceptor identity, our understanding of the molecular correlates of proprioceptor subtype identity is woefully limited. This is perhaps because sensory neurons lack an overt topography within the DRG. Proprioceptors are intermixed with various cutaneous lineages, and although somatosensory cell bodies of distinct modalities can be differentiated to some extent by diameter, fiber type and molecular profile, there is often non-trivial overlap in marker gene expression between the proprioceptive and cutaneous sensory modalities (Lallemend and Ernfors, 2012). Moreover, proprioceptors innervating a given muscle are scattered among several DRG, complicating their identification in the absence of molecular markers. At present, proprioceptors innervating different muscles or end organs

within a muscle can only be accessed by way of distinctions in peripheral termination.

Several molecular screens have taken an unbiased approach to characterizing the diversity of DRG sensory neurons. These efforts have utilized single-cell RNA-Sequencing (RNA-Seq) of individual DRG neurons combined with principal component analysis in an attempt to determine the number of neuronal classes required for function of the somatosensory system (Li et al., 2016; Usoskin et al., 2014). By identifying proprioceptors post-hoc via their co-expression of Runx3 and Pv, these screens have provided some insight into the diversity of the proprioceptor class as a whole. However, salient features of proprioceptor subtype identity were not preserved in these screens; it is impossible to determine from these datasets whether an individual proprioceptor is a muscle spindle or GTO afferent or which muscle it supplies, hence preventing the extraction of associated differences in gene expression.

An RNA-Seq-based approach has been utilized to assess distinctions in gene expression between muscle spindle (groups Ia and II) and GTO (group Ib) afferents. In this study, an Egr3::Wga-mCherry transgenic mouse line was used to direct expression of the transsynaptic neural tracer wheat germ agglutinin to *egr3*-expressing intrafusal muscle fibers, thereby selectively labeling the cell bodies of group Ia and II muscle spindle afferents with WGA-mCherry fusion protein (De Nooij et al., 2015). In combination with YFP expression under control of the *pv*

promoter, dual-labeled group Ia and II proprioceptors can be distinguished from YFP^{+}, $mCherry^{-}$ group Ib cell bodies, enabling the purification and comparison of these populations (De Nooij et al., 2015). While this approach has identified candidate genes expressed in proprioceptor subsets, confirmation of their status as bona fide muscle spindle or GTO afferent markers is pending (Joriene de Nooij, personal communication).

Several studies performed in chick have identified genetic distinctions associated with proprioceptor muscle innervation. Chick proprioceptors have been found to selectively express several members of the type II cadherin family of recognition molecules in association with their limb muscle target (Price et al., 2002). Furthermore, the ETS transcription factors Er81 and Pea3 are expressed in proprioceptors in a manner correlated to muscle innervation (Lin et al., 1998), although these distinctions do not hold in mouse. One chick study took an unbiased approach to profiling differences in proprioceptor gene expression associated with muscle innervation (Chen et al., 2002). This screen identified the transcription factor Lmo4, which was found to be expressed in a majority of proprioceptors innervating adductor muscle, but was nearly absent from proprioceptors innervating several other hindlimb muscles (Chen et al., 2002). However, none of these genes are expressed in an all-or-none manner by an entire cohort of muscle-type proprioceptors, and the logic underlying their specification and function in sensory neurons remain unclear.

In mouse, a fragmented knowledge of proprioceptor muscle-type identity has been gleaned from studies of selective synapse formation between proprioceptors and motor neurons, which have often taken a candidate approach to identifying relevant molecules involved in sensory axon pathfinding and target recognition. Repellant signaling between Semaphorin3e (Sema3e), expressed by motor neurons, and its receptor PlxnD1 in muscle-specific subsets of proprioceptors has been shown to mediate the choice between poly- and monosynaptic connectivity with motor neurons as well as the formation of specific monosynaptic contacts (Fukuhara et al., 2013; Pecho-Vrieseling et al., 2009). Furthermore, type II cadherins are expressed in subsets of mouse DRG neurons, indicating that their expression could be restricted to muscle-type subpopulations of proprioceptors (Demireva et al., 2011), although the function of cadherins in sensory neurons is at present unclear.

Nevertheless, the recognition systems identified by candidate screens are far from sufficient to direct the formation of the complex matrix of connectivity observed between proprioceptors and motor neurons. Despite the importance of proprioceptor subtypes for the formation of spinal circuitry, the molecular identities of proprioceptors innervating distinct limb muscles have never been systematically profiled in mice.

Role of the periphery in proprioceptor subtype specification

During development, proprioceptors innervate targets in the periphery prior to forming synaptic connections with neurons in the CNS (Ramon y Cajal, 1911, 1929; Vaughn and Grieshaber, 1973; Windle and Baxter, 1936). As discussed above, proprioceptors innervating different peripheral targets establish connections with distinct and characteristic subsets of neurons within the spinal cord. One hypothesis regarding how this specificity is achieved holds that developing sensory neurons acquire molecular identities from their peripheral targets that endow them with affinities for the correct subsets of neurons in the CNS (Miner, 1956; Sperry, 1963). In the case of Ia monosynaptic connections with motor neurons, the activity-independent formation of patterned homonymous connectivity (Mendelson and Frank, 1991) lends credence to this theory.

Proprioceptors appear to be uncommitted with respect to specific muscle target and rely on association with motor axons to establish appropriate patterns of peripheral connectivity (Treubert-Zimmermann et al., 2002). When motor neurons are ablated before axonal outgrowth into the limb, sensory axons that normally project to muscles reroute to project along cutaneous nerves, resulting in a lack of sensory muscle innervation (Gallarda et al., 2008; Landmesser and Honig, 1986; Swanson and Lewis, 1986; Wang and Scott, 2000). In addition, transplantation experiments have suggested that the ability of displaced sensory neurons to form segmentally appropriate projections is dependent on the presence of motor axons extending from relocated neural tube segments (Landmesser and Honig, 1986; Landmesser et al., 1983). Together, these studies suggest a model in which

peripheral sensory neurons extend opportunistically along permissive tissue tracts, where they are directed by their interactions with motor axons.

Classical developmental studies performed in several model systems have demonstrated the instructive influence of peripheral elements on developing sensory neurons. In frogs, thoracic sensory axons redirected to project along the brachial nerve into the developing front leg of the tadpole supply spindles in forelimb muscles, which they do not normally contact in wild-type animals (Frank and Westerfield, 1982a). Although proprioceptors in thoracic ganglia do not normally form direct connections with motor neurons (Frank and Westerfield, 1982b), anatomical and physiological evidence demonstrated that rerouted proprioceptors established monosynaptic connections with the motor neurons innervating muscles of the forelimb, indicating that a cue supplied by forelimb motor axons, the brachial nerve pathway, or the target muscles themselves directed the formation of novel but appropriate central connections (Frank and Westerfield, 1982a, 1982b; Smith and Frank, 1987).

Subsequent studies performed in chick attempted to pinpoint the tissue source of this limb-derived cue. At a developmental time point prior to innervation, ventral tissue of the developing hindlimb was surgically removed just distal to the base of the limb and replaced with dorsal tissue (Figure 1.9; Wenner and Frank, 1995). This manipulation resulted in embryos with a duplicate set of dorsal muscles in the ventral half of the limb that are supplied by the motor neurons that normally

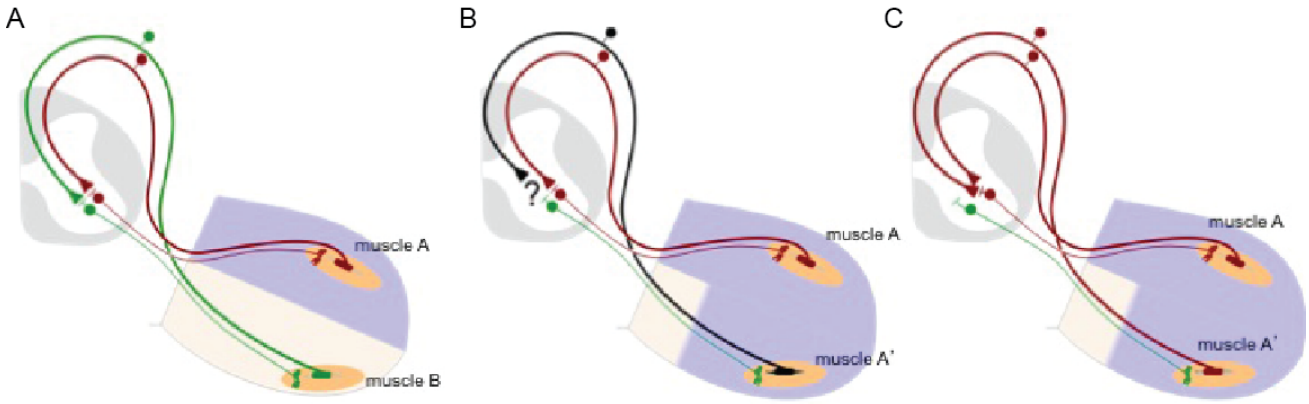

Figure 1.9 Proprioceptor central connectivity is dictated by the periphery

(A-C) Surgical limb duplication experiments in chick reveal the influence of limb dorsoventral identity on synaptic specificity. (A) In wild-type animals, proprioceptors innervating dorsal muscles (muscle A; purple) form connections with laterally situated motor neurons innervating the same dorsal muscle. Likewise, proprioceptors innervating ventral muscle (muscle B; beige) form synapses with medial motor neurons innervating the same ventral muscle. (B) Experimental preparation: dorsodistal limb tissue was grafted in place of dorsoventral tissue, and the central connections formed by proprioceptors innervating the ectopic limb domain (muscle A') were assayed. (C) Proprioceptors innervating muscle A' were found to form synapses with the motor neurons specified to innervate muscle A, rather than those specified to innervate muscle B that in the experimental preparation supply muscle A'.

innervate ventral musculature (Lance-Jones, 1986). In this preparation, sensory axons project along ventral nerve pathways aside the motor axons that normally innervate ventral muscles, only to encounter ectopic dorsal tissue from the proximodistal level of the thigh onward. When the central connections made by proprioceptors supplying ectopic dorsal musculature were assayed, these proprioceptors were found to synapse with the same motor neurons contacted by proprioceptors supplying the corresponding normal dorsal muscles (Wenner and Frank, 1995). Sensory neurons therefore made synaptic connections appropriate for their dorsal target muscle rather than for their proximal ventral environment (Wenner and Frank, 1995), indicating an influence of the dorsoventral identity of peripheral tissue on the patterning of proprioceptor connections with motor neurons.

Because these sensory axons projected to novel muscle targets but did so via their normal proximal pathways in association with their normal motor axon partners, the authors of the study concluded that proprioceptor connectivity was influenced by target muscle (Wenner and Frank, 1995). However, this conclusion overlooks the possibility that transplanted limb mesenchyme – which, like transplanted muscle, is dorsal in character – could influence sensory patterning. Furthermore, in light of more recent studies of motor neuron subtype specification, a role for motor axon in patterning sensory identity cannot be dismissed. Aspects of motor neuron subtype character are retrogradely influenced by peripheral target muscle (Vrieseling and Arber, 2006), raising the possibility that motor axon identity

is altered in the chick dorsal graft preparation and might therefore be capable of instructing the observed pattern of sensory-motor connectivity. Thus, it remains uncertain which tissue in the developing limb supplies the patterning information that instructs proprioceptor connectivity with motor neurons.

In this thesis, I describe the results of a comparative screen designed to detect molecular distinctions in proprioceptors innervating muscles or muscle groups spanning the extent of the dorsoventral and proximodistal axes of the limb. The object of this screen was threefold: (1) to uncover principles of muscle-type diversity for proprioceptors innervating the hindlimb; (2) to establish genetic markers of proprioceptor subtype identity that could be used to assess the role of several peripheral tissues in their specification; and (3) to identify genes with potential roles in establishing selective contacts between proprioceptors and motor neurons. In Chapter 2, I present the results of our characterization of gene expression in proprioceptors innervating different muscles and discuss the implications of these findings for the specification of hierarchical proprioceptor identity. In Chapters 3-5, I assess the expression of several novel molecular markers of proprioceptor muscle-type identity in transgenic mouse lines in which one of three peripheral tissues – motor axon, limb mesenchyme, and target muscle – has been genetically manipulated. Finally, in Chapter 6, I examine whether two of the proprioceptor muscle-type genes identified in our screen are involved in establishing selective contacts with spinal motor neurons.

2 Muscle-specific correlates of proprioceptor identity

2.1 Introduction

Formation of the precise matrix of monosynaptic connections between proprioceptors and spinal motor neurons in the absence of patterned activity implicates molecular recognition between subsets of each cell type. While the molecular identities of motor neurons are comparatively well-characterized (Arber, 2012), little is known about the distinctions between proprioceptors that could mediate selective connectivity with postsynaptic partners. In this chapter, I describe the results of a comparative screen performed to detect molecular distinctions between proprioceptors innervating different muscles – here termed "muscle-type" proprioceptors – of the mouse hindlimb. I validate our findings *in vivo* for a large cohort of these genes and use a genetic reporter to characterize the expression of one gene, *cdh13*, at the level of individual muscles.

2.2 Results

2.2.1 Identifying genetic distinctions between muscle-type proprioceptors

To characterize the molecular diversity of proprioceptors terminating in distinct regions of the mouse hindlimb, we performed an RNA-Sequencing (RNA-Seq)-based screen to identify differences in gene expression between muscle-type proprioceptors. We chose to profile proprioceptors innervating five muscles spanning the proximodistal and dorsoventral extents of the hindlimb: gluteus (GL;

dorsal hip extensor/rotator), quadriceps (Q; dorsal knee extensor), tibalis anterior (TA; dorsal ankle flexor), gastrocnemius (GS; ventral ankle extensor), and intrinsic foot (IF) musculature (Figures 2.1A and B). These muscles or muscle groups were chosen because they lie at distinct proximodistal and dorsoventral limb coordinates representing distinct zones of proprioceptor termination (Figure 2.1B).

We used a combination of genetic and retrograde labeling methods to identify proprioceptors according to muscle innervation. Proprioceptive neurons are marked by the expression of parvalbumin (Pv; Figure 2.1C), which also labels a small population of low-threshold cutaneous mechanoreceptors (Ernfors and Lee, 1994; de Nooij et al., 2013). *Parvalbumin*::Cre (*Pv*::Cre) mice were crossed with a *Thy1*::lox-STOP-lox::YFP reporter line to generate *Pv*::YFP mice (Figure 2.1D; Buffelli et al., 2003; Hippenmeyer et al., 2005; Figure 2.1D). We found that ~96% of YFP^+ sensory neurons in lumbar DRG of these mice expressed Pv at postnatal day 1 (P1). The high coincidence of Pv and YFP protein expression indicated that *Pv*::YFP is a reliable reporter of endogenous *Pv* expression and can be used to distinguish proprioceptors from DRG neurons of other sensory modalities.

To identify proprioceptors on the basis of muscle target, we injected the retrograde tracer cholera toxin B subunit conjugated to Alexa Fluor 555 (ctb^{555}) into the selected hindlimb muscles of P0 *Pv*::YFP mice (Figure 2.1D). To assess specificity of labeling, we dissected out the targeted muscle and examined the localization of Alexa Fluor 555 in surrounding tissue. When targeting TA muscle, ctb^{555} was nearly

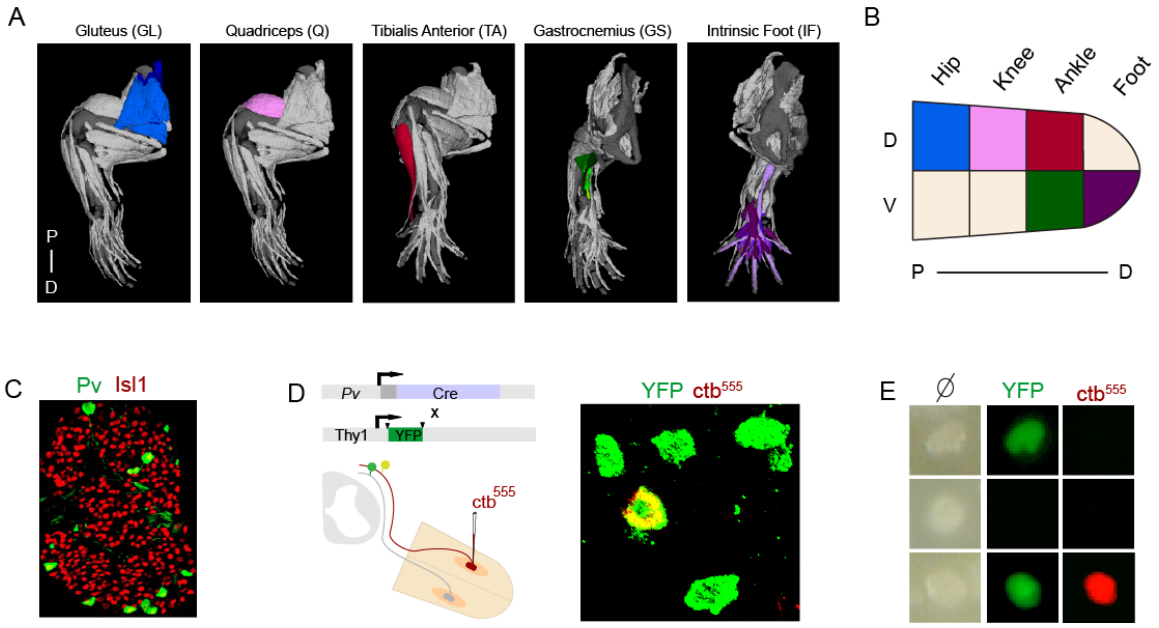

Figure 2.1 Identification and isolation of muscle-specific proprioceptors

(A) Three-dimensional renderings of the muscles or muscle groups injected with ctb^{555}. From left to right: GL = gluteus maximus (light blue) and gluteus medius (dark blue); Q = vastus lateralis (pink) and vastus medialis, vastus intermedius, and rectus femoris (not shown; medial to vastus lateralis); tibialis anterior (red; TA); GS = gastrocnemius lateralis (green) and medialis (dark green), soleus, and plantaris (neon green); and IF = musculature of the intrinsic foot (shades of purple). GL, Q and TA derive from the dorsal muscle mass, whereas GS derives from the ventral muscle mass (Lance-Jones, 1979). Note that the gastrocnemius is partially obscured by the biceps femoris laterally and the semitendinosus medially. P: proximal; D: distal. (B) Schematic of the regions sampled along the proximodistal and dorsoventral limb axes. (C-E) Purification of proprioceptors. (C) Pv immunostaining in P0 L4 DRG distinguishes proprioceptors from other sensory neurons. Scale bar, 25 µm. (D) Left: GL, Q, TA, GS, and IF proprioceptors were retrogradely labeled via muscle injection of ctb^{555} in *Pv*::Cre, *Thy1*::lox-STOP-lox::YFP mice (*Pv*::YFP; arrowheads represent *loxP* sites). Right: ctb^{555}-labeled YFP^{on} proprioceptors innervating TA muscle in PI L4 DRG. Scale bar, 20 µm. (E) Dissociated sensory neurons. Top: generic proprioceptor. Middle: non-proprioceptive DRG sensory neuron. Bottom: proprioceptor identified by muscle innervation; o.i., oblique illumination. Scale bar, 12 µm.

always confined to the TA. However, when targeting GL, Q, and GS, ctb^{555} was frequently detected in adjacent muscles due to their close anatomical apposition to the target (see Figure 2.1A) and the tendency of ctb to diffuse through tissue. For GL, Q, and GS muscles, we therefore elected to isolate proprioceptors labeled via ctb^{555} injections confined to the targeted muscle and its synergists: "GL" samples included proprioceptors innervating gluteus maximus or gluteus medius; "Q" samples included proprioceptors innervating any of the four heads of the quadriceps (rectus femoris, vastus lateralis, vastus medialis, and vastus intermedialis); and "GS" samples included proprioceptors innervating gastrocnemius lateralis, gastrocnemius medialis, soleus, or plantaris. The intrinsic foot (IF) musculature is comprised of ~20 small muscles; our backfills were therefore targeted to all muscles of the ventral footpad rather than to any individual muscle.

While we would have liked to include proprioceptors innervating ventral muscles at the proximodistal positions of hip and thigh in our screen, limb morphology precluded the isolation of these muscle-type proprioceptor populations. The ventral equivalent of the GL, the iliopsoas (IP), is located deep within the hip socket and is inaccessible to retrograde tracing techniques, and the hamstring/adductor group of muscles, which operates at the knee, is largely obscured by muscles of dorsal origin. We therefore omitted proprioceptors innervating these limb domains from our analysis.

Lumbar DRG containing ctb^{555+} neurons labeled by specific injections were removed 24 h after injection and dissociated. Individual YFP^{+}, ctb^{555+} cells were isolated (Figure 2.1E), and 25-30 neurons were pooled to generate samples of muscle target-defined GL, Q, TA, GS, and IF proprioceptors in triplicate. After extraction of total RNA, cDNA libraries were prepared for gene expression profiling by RNA-Seq.

To assess the ability of RNA-Seq to detect differences between 30-cell samples, we performed a pilot screen comparing L2-L6 YFP^{+} proprioceptors from *Pv*::YFP mice to large-diameter YFP^{-} sensory neurons isolated from the same ganglia (see Figure 2.1E). As expected, expression of *pv* was detected in YFP^{+} but not YFP^{-} cells, albeit at ectopically low levels due to the insertion of Cre at the *pv* locus (2.2A; Hippenmeyer et al., 2005). Furthermore, expression of the genes *etv1*, *runx3* and *whirlin* - generic markers of the proprioceptive lineage (Lallemend and Ernfors, 2012; De Nooij et al., 2015) – was significantly upregulated in YFP^{+} cells (Figure 2.2B). We therefore concluded that RNA-Seq is sufficiently sensitive to characterize distinctions between 30-cell samples.

Analysis of our screen data revealed 140 genes with >5-fold enrichment in at least one of the five muscle-specific populations profiled and a minimum RPKM (reads per kilobase per million; $RPKM_{min}$) value of 10 for at least one replicate of the upregulated population ($p<0.001$; Table 2.1). A majority of the differentially expressed genes could be categorized into 5 functional classes: guidance and

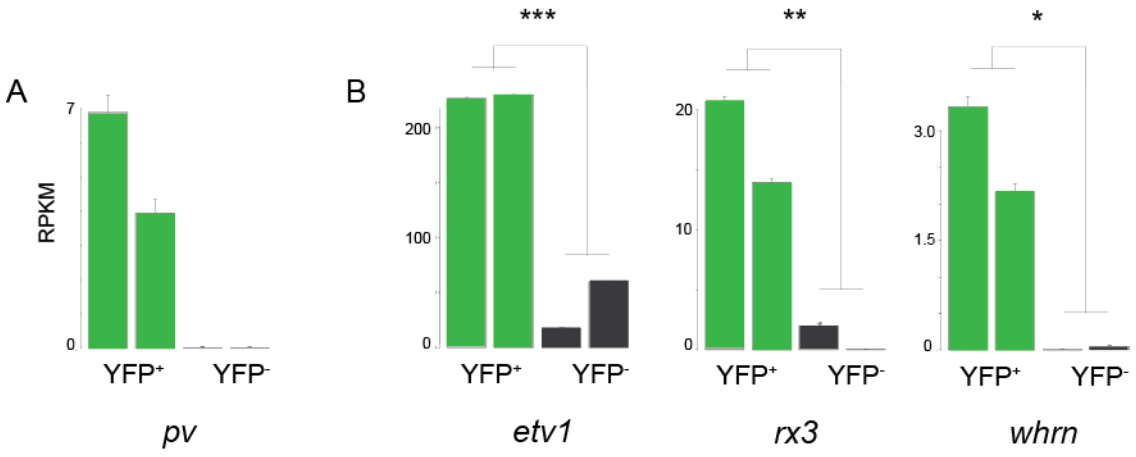

Figure 2.2 Validation of RNA-Seq for small somatosensory samples

(A-B) Proprioceptor marker gene expression in 30-cell samples of proprioceptive and non-proprioceptive DRG neurons. (A) Expression of *pv* in YFP$^+$ and YFP$^-$ DRG neurons isolated from *Pv*::YFP mice. (B) Expression of *etv1*, *trkC*, and *whrn* in YFP$^+$ and YFP$^-$ DRG neurons. *, $p<10^{-4}$. **, $p<10^{-5}$. ***, $p<10^{-6}$.

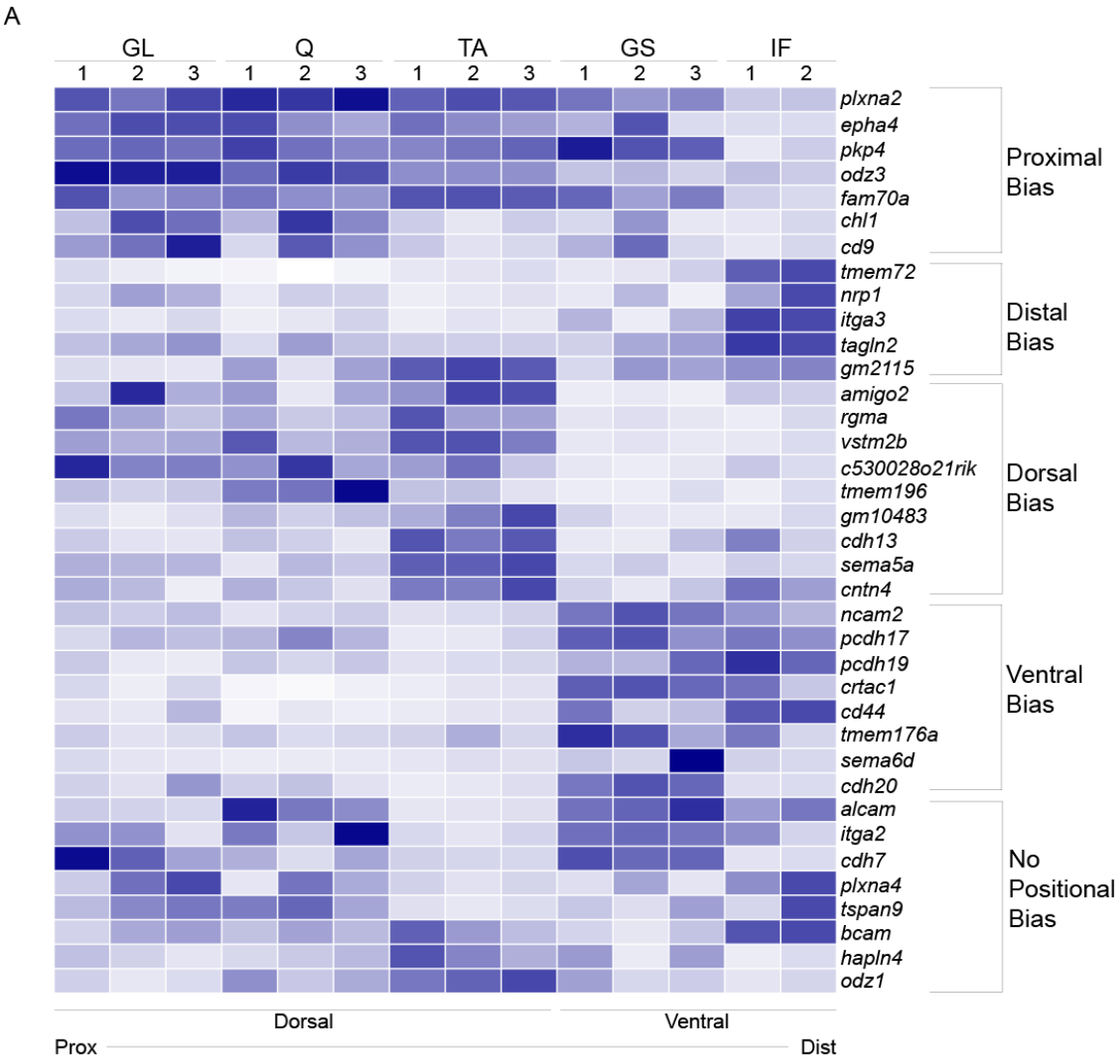
A
GL
Q
TA
GS
IF
1 2 3 1 2 3 1 2 3 1 2 3 1 2
plxna2
epha4
pkp4
odz3
fam70a
chl1
cd9
tmem72
nrp1
itga3
tagln2
gm2115
amigo2
rgma
vstm2b
c530028o21rik
tmem196
gm10483
cdh13
sema5a
cntn4
ncam2
pcdh17
pcdh19
crtac1
cd44
tmem176a
sema6d
cdh20
alcam
itga2
cdh7
plxna4
tspan9
bcam
hapln4
odz1
Proximal Bias
Distal Bias
Dorsal Bias
Ventral Bias
No Positional Bias
Dorsal
Ventral
Prox
Dist

B

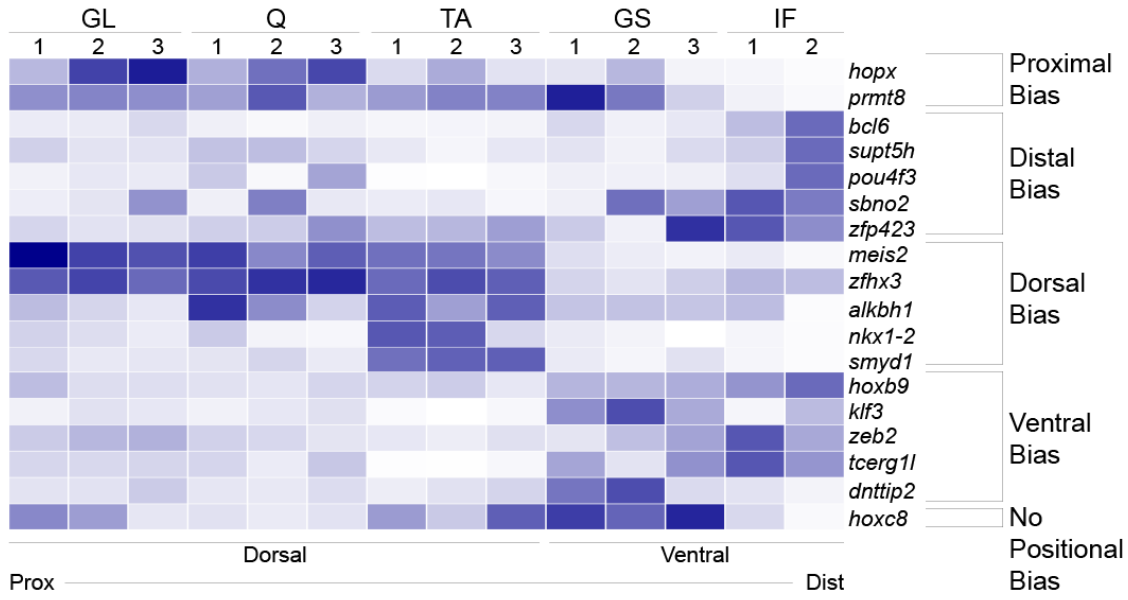
GL
Q
TA
GS
IF
1 2 3 1 2 3 1 2 3 1 2 3 1 2
hopx
prmt8
bcl6
supt5h
pou4f3
sbno2
zfp423
meis2
zfhx3
alkbh1
nkx1-2
smyd1
hoxb9
klf3
zeb2
tcerg1l
dnttip2
hoxc8
Proximal Bias
Distal Bias
Dorsal Bias
Ventral Bias
No Positional Bias
Dorsal
Ventral
Prox
Dist

C

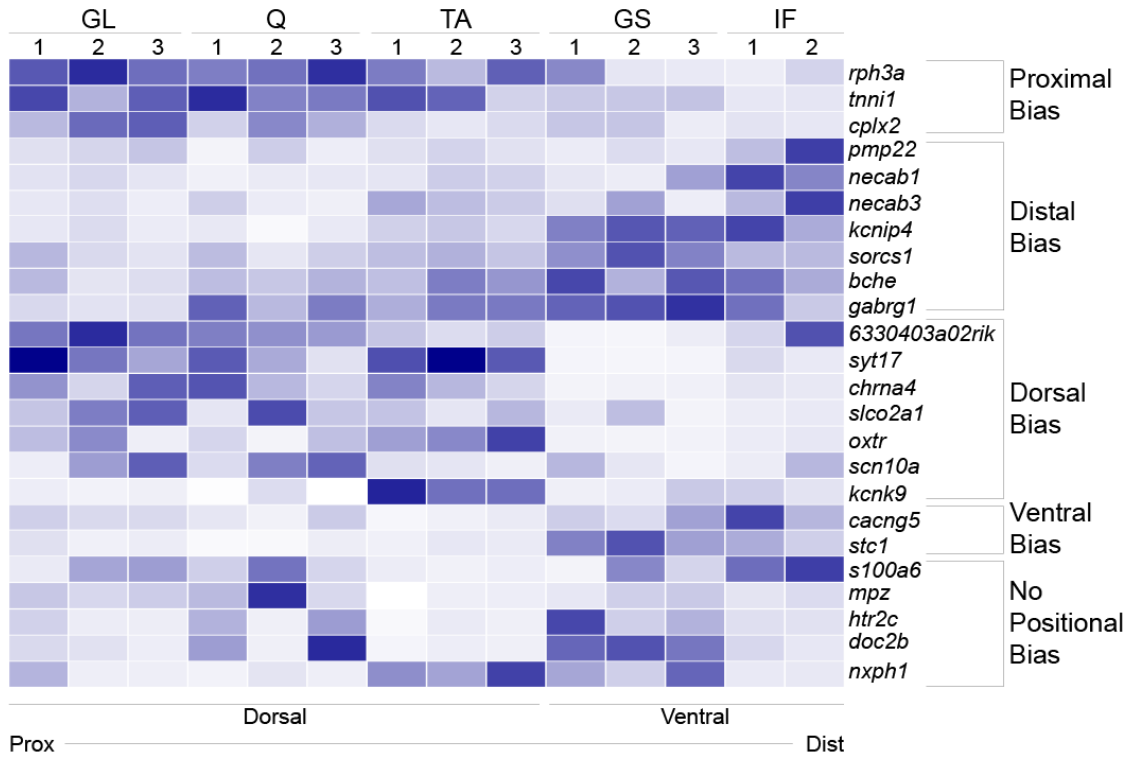
GL
Q
TA
GS
IF
1 2 3 1 2 3 1 2 3 1 2 3 1 2
rph3a
tnni1
cplx2
pmp22
necab1
necab3
kcnip4
sorcs1
bche
gabrg1
6330403a02rik
syt17
chrna4
slco2a1
oxtr
scn10a
kcnk9
cacng5
stc1
s100a6
mpz
htr2c
doc2b
nxph1
Proximal Bias
Distal Bias
Dorsal Bias
Ventral Bias
No Positional Bias
Dorsal
Ventral
Prox
Dist

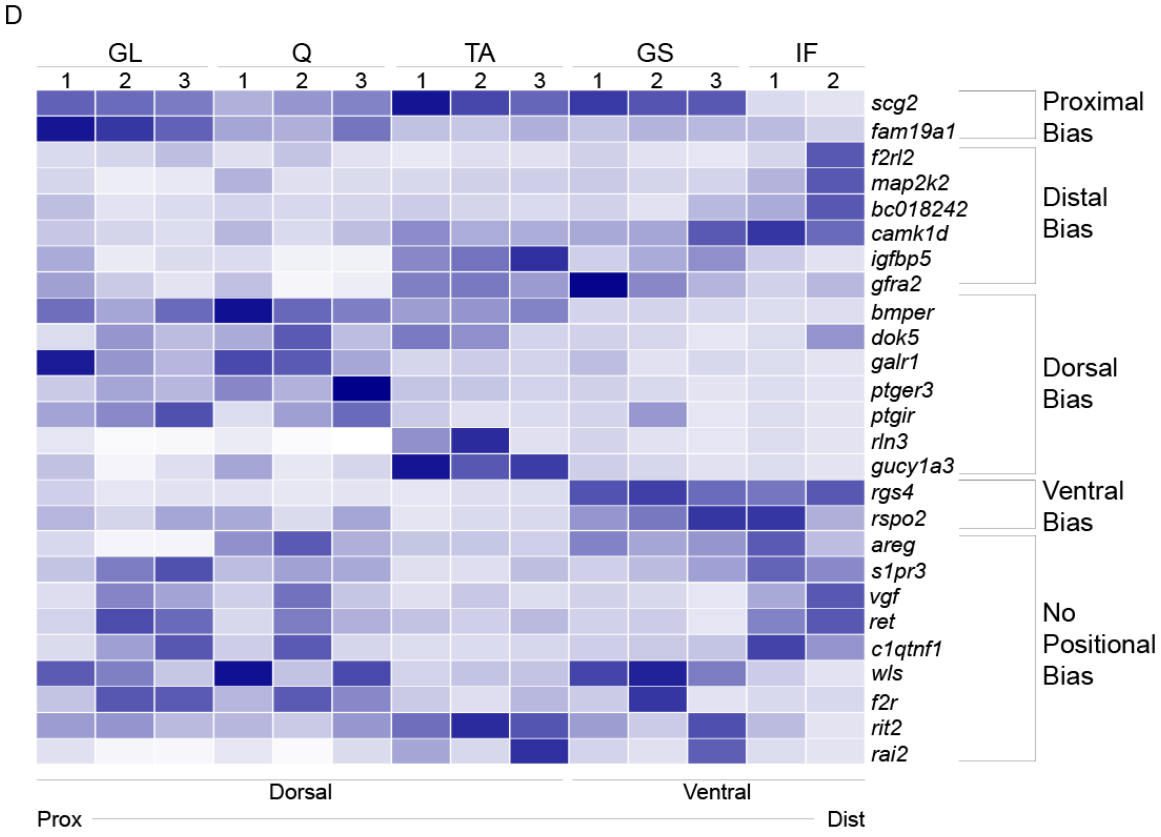
D
GL
Q
TA
GS
IF
1 2 3 1 2 3 1 2 3 1 2 3 1 2
scg2
fam19a1
f2rl2
map2k2
bc018242
camk1d
igfbp5
gfra2
bmper
dok5
galr1
ptger3
ptgir
rln3
gucy1a3
rgs4
rspo2
areg
s1pr3
vgf
ret
c1qtnf1
wls
f2r
rit2
rai2
Proximal Bias
Distal Bias
Dorsal Bias
Ventral Bias
No Positional Bias
Dorsal
Ventral
Prox
Dist

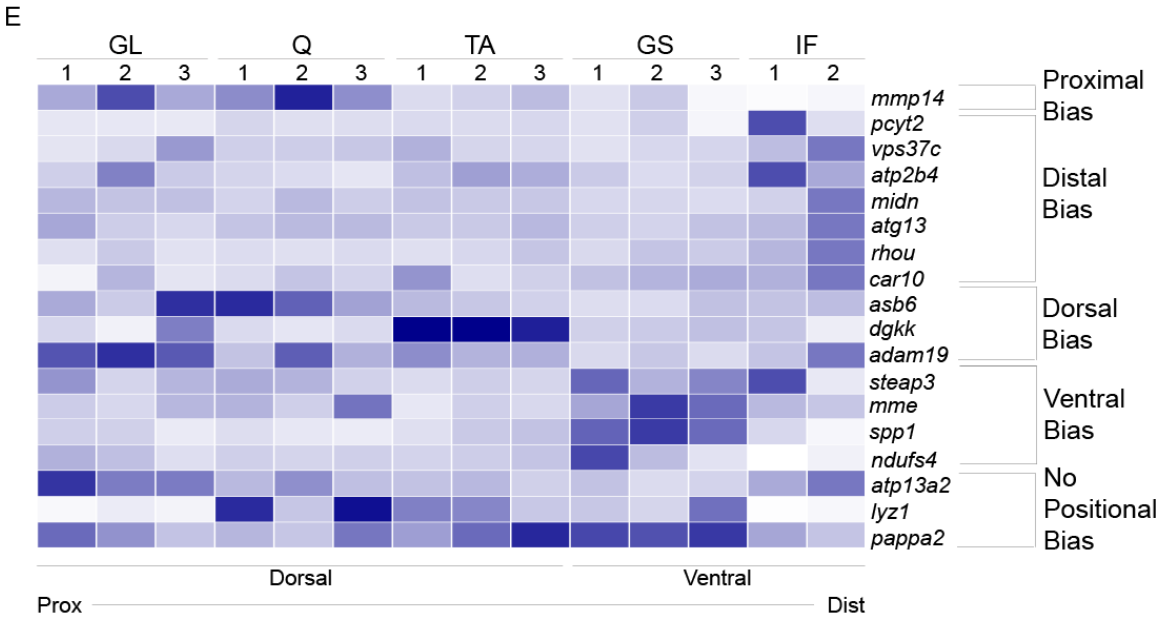
E
GL
Q
TA
GS
IF
1 2 3 1 2 3 1 2 3 1 2 3 1 2
mmp14
pcyt2
vps37c
atp2b4
midn
atg13
rhou
car10
asb6
dgkk
adam19
steap3
mme
spp1
ndufs4
atp13a2
lyz1
pappa2
Proximal Bias
Distal Bias
Dorsal Bias
Ventral Bias
No Positional Bias
Dorsal
Ventral
Prox
Dist

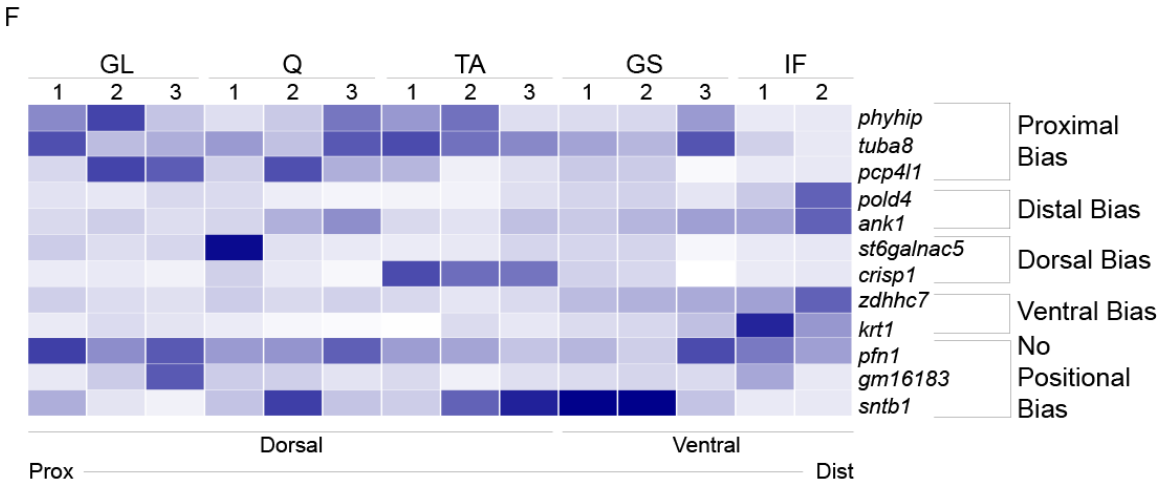

Figure 2.3 Heat map representation of differential gene expression

(A-G) Note that samples are arranged with respect to the proximodistal and dorsoventral limb axes. (A) Guidance, adhesion, and uncharacterized transmembrane proteins. (B) Transcription factors and transcriptional regulators. (C) Neurotransmission. (D) Morphogen, growth factor, and intracellular signaling. (E) Cellular metabolism. (F) Other.

Table 2.1 Genes determined by RNA-Sequencing to exhibit differential expression between muscle-type proprioceptor populations. All values are in reads per kilobase per million (RPKM). (A) Guidance, adhesion, and uncharacterized transmembrane proteins. (B) Transcription factors and transcriptional reguators. (C) Neurotransmission. (D) Morphogen, growth factor, and intracellular signaling. (E) Cellular metabolism. (F) Other; includes markers of non-proprioceptive DRG lineages.

A Guidance and Adhesion Molecules

Gene	GL1	GL2	GL3	Q1	Q2	Q3	TA1	TA2	TA3	GS1	GS2	GS3	FOOT1	FOOT2
plxna2	3.04894234	18.9556422	24.8427865	3.03889599	21.8529431	10.0367832	5.77378325	1.29189583	3.53373738	1.61557965	14.4924306	1.53813822	15.5478192	31.0023151
epha4	7.62380267	11.1236588	11.1323332	11.6453143	8.06336388	4.89357742	11.7990747	8.14887523	6.59375649	3.07911712	14.3333357	1.18758718	1.20359856	0
pkp4	47.437219	56.3178971	53.2208285	75.1522922	62.5257672	41.5074828	59.0466671	61.7877827	72.3665473	68.8700719	87.2097621	52.6114576	1.78828109	9.17687979
odz3	11.3711307	11.3047327	11.461197	7.58028944	11.1727085	8.03011205	7.06539812	6.24064374	6.22674645	1.76737809	3.94446034	1.44558898	1.00545206	1.23444973
fam70a	100.404283	64.2386892	76.9345242	90.8518838	84.8522088	61.0035675	149.165717	137.392959	130.898054	75.9223831	72.9483914	71.7727436	22.6289462	2.14191321
chl1	3.14233151	15.7847381	12.8026994	6.55570214	20.495688	9.53039507	4.49646515	0.30557186	3.29430421	1.58306093	11.6149247	0.72172044	0.79970614	0.70136683
cd9	8.02696192	14.8247546	24.8516393	3.99001294	20.649906	10.7360249	6.1521924	1.15179494	2.21047862	5.33826113	20.8981285	2.34494348	0.65304698	0.75281333
tmem72	0.51167814	0.52135714	0.06270554	0.52444907	0.23076473	0.49463394	0.81642235	0.46281758	1.05838648	0.29893352	0.78603437	2.11451495	11.7452686	15.5757634
nrp1	1.23243204	9.38341353	7.38078223	1.87375925	6.1817888	4.0570534	0.28828095	0.05142655	0.93943137	0.28418449	7.91763438	0.08014036	8.93261668	24.1718671
itga3	0.30446615	0.56034479	1.55404303	0.7651601	1.73858256	2.00798857	0.16058371	0.43890669	0.01593185	2.60390353	0	2.99495283	11.1659664	12.3400959
tagln2	76.0385757	169.361815	223.19219	69.9847695	245.410127	115.015458	106.390402	75.5429148	75.8964196	51.4004371	214.050295	166.777566	471.191201	495.64098
gm2115	0.64957606	1.53432006	1.4763064	9.73541473	3.77291974	8.29990377	21.5351114	22.700699	20.1058736	1.75948373	12.4474768	7.33238526	11.0524443	13.6591978
amigo2	1.77877007	12.5866618	4.35230142	6.01107749	1.78934431	4.56644814	7.89318856	13.4376982	12.875125	0.04176439	0.24709022	0.08244324	2.57081637	1.18358548
rgma	21.3175617	15.2031023	10.0434636	16.6930136	12.1882666	10.9213134	43.3286694	18.6948731	18.5293149	1.17305807	3.75143322	1.81495021	0.06228395	1.00020135
vstm2b	34.1278048	32.4678295	37.6189252	81.926209	38.7902825	33.4260359	108.79858	100.006189	71.69294	1.77180034	6.33824624	3.57888654	3.29187425	0
C530028O21Rik	10.0249601	5.91360652	6.24914297	5.5545676	11.3979727	3.8746026	5.99520311	8.44130475	2.14787667	0.17421803	0	0.49436746	2.22466584	0
tmem196	2.41872031	2.25594092	3.10091756	9.16456098	10.9362989	15.5293036	4.48597362	3.70617888	0.41539195	0	0	1.26655898	0	0
gm10483	0.59353437	1.02809502	3.34686797	10.5805815	8.54498998	7.99141836	14.0483181	21.4612766	33.691676	3.34041339	1.49466959	1.05590245	0.97219813	0.84054103
cdh13	2.16280029	1.50189936	1.44105225	5.45169997	5.11652977	1.68108128	20.6944443	13.8773596	18.4557234	0.2096439	0.18173099	4.17552686	12.017613	1.51764144
sema5a	14.1334286	17.1369272	17.9405679	6.28030351	22.2299056	12.7072156	57.0356424	51.4306162	61.3582098	4.78330787	13.2828087	2.87778989	9.96616081	2.02383292
cntn4	2.46167623	2.62654284	0.30136443	3.46103219	2.9834397	1.10300538	7.57979189	6.44767044	10.1066905	0.9731912	0.29587262	1.78978998	6.60211292	4.23786812
ncam2	4.4497366	5.47825326	8.0575866	3.4848488	7.31407442	5.97447139	2.96287877	2.33257053	4.04314836	14.1317264	31.4161095	16.174127	14.5447648	8.0601214
pcdh17	1.05125513	7.31344709	6.27038205	8.21678735	15.9299821	7.30871195	0.93672828	0.23161011	3.75019124	13.8265269	25.8018384	10.2117926	15.8293711	13.4513231
pcdh19	2.00589858	0.81377204	0.79619945	4.57056525	4.06736292	3.88084831	1.50183353	1.35772686	1.93573781	3.99025005	6.15911403	10.5157967	18.5464835	14.8574938
crtac1	1.70294752	0.7914026	5.22651593	0.97424341	1.59224136	1.61663616	0.75109191	1.07413372	1.26348386	19.8009178	36.8024367	20.7424403	23.8919569	5.3428835
cd44	0.04751736	0.89166511	5.32589371	0.65811948	2.58054511	0.92473474	0.58239185	0.53138769	0.74261909	8.5909011	3.30174949	3.76088995	14.7767363	18.767073
tmem176a	12.8173721	9.50300351	14.7270029	31.5608597	24.2572778	19.610755	24.7582448	44.6570645	13.2242386	91.4025385	126.926915	37.4925	77.9579424	4.58370703
sema6d	3.28263836	6.18513543	6.46579048	7.14453781	11.6502788	7.2494626	6.01049941	6.39401036	4.37091945	13.9164941	15.4811167	99.0243525	14.0545003	2.48346171
cdh20	1.11039649	1.29007303	6.63528341	3.03104734	4.86228919	1.54603929	0.35914624	0.07571701	0.81628868	6.69462734	15.1937654	8.64300857	1.15469552	0
alcam	24.3679546	35.5883539	31.1910241	241.318039	163.040149	109.131348	13.2259681	6.8788065	11.067416	111.898944	213.991479	194.647274	102.490781	168.628336
itga2	9.46295293	11.4337308	2.1272265	15.1372418	7.42980475	25.3796276	3.74569217	0.55867794	3.08705027	11.9934012	21.4035683	13.0592029	12.726312	1.35410526
cdh7	13.8763538	9.39314186	5.23388848	4.81758651	2.57650932	4.85284014	2.65725169	1.59311163	1.39455065	8.27840353	11.7625271	8.10261398	0.69686327	0
plxna4	3.04894234	18.9556422	24.8427865	3.03889599	21.8529431	10.0367832	5.77378325	1.29189583	3.53373738	1.61557965	14.4924306	1.53813822	15.5478192	31.0023151
tspan9	4.70721757	13.1850362	15.6619928	15.6499657	20.4802886	9.24511812	2.61593314	0.06419624	1.59564234	3.76288574	2.51642412	8.99109127	3.36843132	26.7324831
bcam	4.58537306	22.6216684	26.6771966	17.6182957	31.5533559	17.5093303	61.0319586	31.7165969	17.4889232	6.10959859	2.2650746	12.226875	54.5879692	66.8202823
hapln4	4.55773317	4.49998569	2.10161739	4.72419318	8.21179781	7.93682762	29.7622271	18.1577892	10.3198648	9.13709856	0.34007479	10.2925059	0.06587189	0
odz1	3.05513738	1.80287867	4.38524642	19.4651119	11.2971171	12.8046839	30.2030111	32.1201803	39.2940847	11.3034314	5.31637295	5.85834662	1.76974803	1.87499174

B Transcriptional Factors and Transcriptional Regulation

Gene	GL1	GL2	GL3	Q1	Q2	Q3	TA1	TA2	TA3	GS1	GS2	GS3	FOOT1	FOOT2
hopx	5.04400892	23.4807357	27.3508526	7.98131215	15.3972101	13.8456045	4.98287257	10.5273976	3.18681423	1.23693676	8.75555557	1.0682539	0	0
prmt8	44.914486	75.6225279	64.3699941	51.0312255	93.785588	30.3090398	71.7946812	81.520086	94.5776114	121.842358	90.8695082	22.2226979	2.65189985	2.04771306
bcl6	0.66491205	0.77250344	3.23670997	0.53254762	0.66313288	1.353599	1.38810754	1.62089767	0.75582736	3.20344699	0.80922574	2.55241502	9.46919267	27.3683227
supt5h	8.82503911	4.96136173	4.27058825	17.7012052	20.7533165	9.38733181	9.03382274	3.83075399	7.38862606	4.18593069	1.76172118	10.2866679	17.6550938	71.3501057
pou4f3	0	2.29924868	0.75060605	10.0394436	1.15097098	14.0642644	0	0	0.07938119	0	1.32646975	2.99482623	6.98862841	48.1698712
sbno2	0.1678646	0.68538155	5.56550027	0.24106512	6.43503063	0.77781215	1.18530294	1.37440319	0.0870022	0	8.79000651	4.1268746	10.9868094	9.72119435
zfp423	2.21658972	1.5621424	1.60267823	3.87390357	4.91505801	7.6218144	8.18690186	8.29310192	12.6631407	3.77702506	0.65872488	17.4207183	21.4985832	16.4518069
meis2	10.4153417	11.4381286	9.94931696	10.4332016	6.22175822	5.88961034	9.6543654	8.48870418	8.18114315	0.95948686	0.62741393	0.57319475	0.75397572	0.27002444
zfhx3	9.67216247	16.7880872	12.4760955	14.3959565	16.0746964	10.2597994	14.8823759	16.2856381	16.9268681	2.24859424	1.79249482	3.26420566	6.61179895	7.35850127
alkbh1	2.02315017	1.54270433	0.31153521	6.07182904	5.36715205	1.41702964	9.80903846	5.2566083	10.156968	2.07486848	3.0970827	2.2994053	3.55966854	0
nkx1-2	1.73051475	1.49876206	0.13866278	2.98853802	0.72292147	0.41737106	14.6837664	12.8163033	3.06486744	0.3672452	0.17071442	0.01812362	0	0
smyd1	3.40787235	1.42303782	1.40726603	2.73244936	6.84302621	2.39490923	31.0510778	30.9646296	36.6244026	0.90659481	0	4.24207524	0	0
hoxb9	8.96134917	4.66420321	3.71593697	4.3309518	5.03734154	5.98091279	11.5304819	12.5268712	4.94171483	12.7655203	17.0779035	14.4766586	27.802431	45.5310278
klf3	0.04158299	1.98077804	0.74502719	0.33440981	2.55051107	2.44572159	0.50130283	0.08719191	0.0116049	11.5637966	24.8798616	8.2430935	0	0.12268389
zeb2	1.55546583	3.49648194	3.61468358	1.85740191	1.87919293	0.91118473	1.41917664	1.04764193	1.65548614	0.58907272	3.43566713	3.87354745	10.7856737	6.17449317
tcerg1l	1.43710433	1.90357552	1.97249237	2.19057505	1.18823489	2.5956737	0	0.11817037	0.02359202	5.1774573	1.55062112	6.24576494	14.4780133	10.1758653
dnttip2	2.89629611	3.91940708	10.2576958	3.76068275	5.23337439	6.08661383	5.40110477	8.82483121	12.6927242	32.1612574	54.659835	7.91117742	6.34433293	3.12428506
hoxc8	6.55882621	7.94469936	0.66887669	1.47541213	1.46521155	1.50749559	9.75931231	4.8727361	16.678627	14.273266	14.3735792	14.2376413	2.98300406	0.21651195

C Neurotransmission

Gene	GL1	GL2	GL3	Q1	Q2	Q3	TA1	TA2	TA3	GS1	GS2	GS3	FOOT1	FOOT2
rph3a	18.2980783	39.174298	34.9944595	20.4673065	26.9309859	30.8220348	23.3605419	9.03527525	32.1384739	24.5796224	3.70794417	1.99300589	0.01902576	4.97132848
tnni1	15.522337	9.53170888	29.9525397	25.9210677	18.2089766	15.1040007	23.8129558	17.6521254	5.0598534	7.65205256	8.45507971	7.03293208	0.87345821	0.71321864
cplx2	7.14815436	29.94162	43.9037037	7.88057937	25.4569812	13.1572628	7.44717164	1.9429368	5.53521377	11.9662095	12.9738707	1.64604834	2.07259055	0.3905458
pmp22	15.0014089	52.1694893	103.778779	14.6934684	92.3067094	23.5749597	50.2204175	46.6182271	27.9147276	22.64147	54.7394733	23.2270345	96.3312345	355.272247
necab1	0.82991299	3.23446506	1.69440246	1.27921171	2.92957816	2.11756597	2.87643678	3.75587867	4.18057062	2.15220974	1.34490912	9.57037793	23.9591053	14.054528
necab3	1.36460105	6.27858864	0.69296015	12.0600803	7.41079621	3.72528467	25.1647627	13.8297052	12.995834	8.3764479	32.0970279	1.97400275	18.7053424	62.8564662
kcnip4	0.49128723	2.97845402	0.83586904	2.16752116	1.38634187	2.1246522	5.40446573	4.57839679	3.48481608	17.1680904	24.7246164	17.8591115	25.4433287	9.13162003
sorcs1	5.07272585	3.68796413	2.56612754	7.86209382	4.16311229	5.49990791	8.70800398	8.00989133	7.15021535	17.2431256	29.4604326	15.9451314	8.66355722	8.11128974
bche	2.94972758	1.22848788	2.30363076	4.79618378	5.22130451	5.22113605	5.27576052	8.76495386	9.361139	18.178828	7.43417324	13.6412742	13.2903896	6.60073191
gabrg1	1.59420354	1.89353941	2.76138301	15.2930982	8.35214193	11.7598675	8.74459272	11.7473879	16.1946269	19.9800709	23.7690256	22.1389518	17.3957023	4.3809181
6330403A02Rik	4.9434802	13.2204022	11.3844569	6.87213188	7.18118964	5.0485962	3.50327925	1.20231296	2.61474742	0.11057998	0	0.50933347	1.73790018	11.7664978
syt17	11.5577574	9.83533637	7.89554592	10.5376316	6.65452511	1.77266771	12.5562873	15.6866718	13.4834122	0.14830619	0	0	1.69955185	0
chrna4	8.60361204	4.42129438	30.4939887	21.205327	10.8251776	4.83415027	17.2425637	7.50521436	4.7039059	0.61919638	0.82091769	0.63511597	1.43109287	0.15580705
slco2a1	2.12734878	9.95856743	16.9985614	1.66028048	14.7962037	3.68002749	4.64228785	0.95988897	5.57623807	1.17379666	5.70128861	0.01466509	0	0
oxtr	3.2045137	11.1749645	0.22106151	3.45599803	1.68130736	5.19462247	9.363769	9.32985832	21.3864386	0.57376683	0.25731441	0.20803231	0.0306716	0.1502686
scn10a	0	4.56418676	10.6663582	1.46298387	6.64687666	6.33567773	1.54203143	0.6079347	0.00475963	3.84879713	1.01008246	0	0	3.10962361
kcnk9	0	0	0	0	3.78977149	0	20.4774121	10.9299283	15.2495918	0.743831	1.2573485	4.20920815	3.44211966	0.63637322
cacng5	7.73687687	9.96521006	12.4578594	7.48309548	7.2427463	15.8349948	3.38238199	0.87155527	2.44392184	18.99912	12.8197731	31.8247356	80.7720663	24.1976602
stc1	1.70867755	0.42601723	0.92768932	0.60724822	2.24954834	2.69827117	2.69970745	1.7732969 6	1.13433576	26.3409397	39.4551584	15.9883018	14.8357878	5.9577543
s100a6	0.604486	22.773663	33.1836994	10.9378519	39.8764558	9.149696	5.2833414	0.31687409	0.54827116	1.00060271	39.4657035	9.05299012	44.2285323	58.5859437
mpz	4.27213537	4.76988685	8.60001512	9.65843966	35.2205901	5.23102925	0.06205136	0.64755794	0.34474974	2.98201884	8.20915745	7.14792849	1.56220295	2.67270724
htr2c	1.32791862	0.4842451	0.31547714	4.57452759	1.43636284	5.61686323	0.49851632	0.51291615	0.00975245	14.9881947	3.5580617	4.71333739	1.09428693	0.73544837
doc2b	0.797295	1.0789379	0.17648423	4.97585081	1.24166348	10.247123	0.63077254	0.26121586	0	10.2831182	12.5835472	7.59854067	1.51241019	0.1176145
nxph1	2.74327016	0.27718693	0.0762018	0.68941682	2.27851648	0.98864348	7.95092341	5.01713975	15.4010522	7.00058747	3.58205439	10.4826848	0.18171939	0.01348929

D Morphogen, Growth Factor, and Intracellular Signaling

Gene	GL1	GL2	GL3	Q1	Q2	Q3	TA1	TA2	TA3	GS1	GS2	GS3	FOOT1	FOOT2
scg2	33.7118924	32.1509515	39.3341097	14.3877298	33.4956323	25.6413458	52.8442277	44.435736	36.6445911	39.3010369	37.1928239	23.8123281	0.72673795	0.05160129
fam19a1	34.3966736	28.6513215	30.8447842	10.7999727	16.2763794	18.7001914	7.04065789	4.61359851	9.56337951	2.37591696	7.96020351	4.84454301	6.80103059	4.4578971
f2rl2	3.4307963	9.92954056	21.1348229	3.40514594	21.8642358	7.38095851	1.5968058	0	0.48478997	0.7428202	0.1822703	0.0709516	3.16964383	62.3720789
map2k2	4.43733652	3.05929625	5.21823939	14.614414	9.97867328	8.10524559	5.6133728	4.2440582	6.17552349	2.46447479	3.96166121	3.3068555	13.9866451	56.6213586
BC018242	10.0699829	5.34768864	8.84057167	5.91539962	11.9939133	8.92491677	8.34302127	3.1281346	2.24362352	0.52590157	0.01932538	7.47005085	15.8715586	53.4777401
camk1d	6.46642124	7.14625012	7.16254755	10.4221427	9.03875137	11.148078	20.1238832	12.3420758	12.9468393	9.08938049	13.515489	19.9184177	44.4029947	38.9763603
igfbp5	12.1573548	2.88300256	7.47018577	3.09166213	2.60071391	2.34716406	20.3704731	26.3136514	43.6829665	0.95828617	11.8367658	12.029805	4.17043878	0.95008318
gfra2	35.0235148	20.8824671	12.4163738	20.3641066	3.63402478	7.39277215	53.029696	58.6163577	40.4947476	104.009117	47.1248851	16.1780551	7.05891819	32.3217851
bmper	10.5705764	6.69874513	15.5049148	18.4492076	16.8200801	9.303891	6.8896891	7.56838683	9.81739952	0	1.30919382	0.81123887	0.02070111	0.76065307
dok5	1.59788763	16.6067583	14.0070972	11.5322207	39.1871492	10.1262871	20.8932699	17.1819359	3.01864018	0.30518948	2.17817136	0	0.04441137	22.4110996
galr1	10.4076972	4.5233316	4.22614776	7.86259081	10.6635249	3.64988507	1.20907224	1.05808647	0.8766492	1.14852067	0	0.45343782	0	0
ptger3	1.36337802	3.77431964	4.0880974	4.82949808	4.80647827	10.5814868	1.99582102	1.4634097	0.86968909	0.12089962	0.44279064	0.05303485	0.01759339	0.07182904
ptgir	4.49747376	6.80242841	14.1767924	0.96100192	8.12071748	8.23104111	2.23948845	0.02277869	0.45476324	0	5.27381137	0	0	0
rln3	0	0	0	0	0	0	9.51404174	22.0637761	0.12767837	0	0.10667609	0	0	0
gucy1a3	2.00826281	0.24269494	1.75138864	3.61506492	1.3726195	1.89859493	11.415564	8.53616892	10.5705781	0.28346468	0.63161968	0.16532501	0	0
rgs4	17.4313138	14.3982417	22.2421269	7.3804936	19.7195341	17.7161337	6.78630212	1.00507115	3.85652143	102.295155	134.054454	64.1588901	100.366821	164.073778
rspo2	4.6417578	3.22742656	9.61582966	5.98051804	3.96814905	6.95523178	0.88666807	0.50263882	0.85752695	5.95199067	10.5793545	11.1618139	19.936909	7.50318297
areg	1.90307217	0.62788967	0.60414874	11.8427511	28.6024448	8.97478015	5.29861205	3.80037482	2.90843658	11.2505215	8.45223426	7.25481602	22.1347139	8.02100943
s1pr3	3.85289051	12.6760478	23.6362669	5.05047189	13.1288183	7.94348575	1.5628876	0.0169367	4.57829745	0.52144478	4.57667562	5.1862709	17.1082408	15.2994256
vgf	1.02144638	14.2281692	14.2044616	3.59382482	24.2826474	6.42365387	1.87275781	3.45065499	0.7601689	0.2113494	1.3496427	0	8.67310669	28.3028423
ret	1.80477546	14.6442442	16.599218	1.68536626	15.5194649	6.09049607	3.97697288	1.62331281	4.25232418	0.17141026	2.13170641	0	10.4977465	19.6751958
c1qtnf1	0.93699191	7.51397029	18.4361483	2.67455754	19.3121434	3.10666766	1.506118	0.24255559	1.13314043	0.49785125	2.31426817	2.04112189	17.7050855	11.0577723
wls	19.1398307	15.0385657	8.48191051	28.7832819	10.2325603	20.3235565	3.64743327	4.20635009	4.9376827	19.8149015	27.8507258	9.72496491	2.80426056	0.2134566
f2r	16.296811	69.6610075	93.4354187	24.8157208	100.007587	46.5071075	16.4975851	0.04592934	22.9788247	3.64393968	86.0352209	0.876779	2.16064587	8.78255661
rit2	12.3978452	15.2167057	12.8288049	8.32480347	10.6078123	14.2872858	20.7294686	35.1343074	27.7471847	9.22760741	3.87697368	16.8334252	7.090488	0.09982256
rai2	0.31651873	0.2349687	0.03768073	0.39393698	0.05777921	1.85770758	4.36089654	0.41085062	13.0859702	0.02494914	0.10543309	5.66372707	0	0

E Metabolism

Gene	GL1	GL2	GL3	Q1	Q2	Q3	TA1	TA2	TA3	GS1	GS2	GS3	FOOT1	FOOT2
mmp14	2.38483344	8.22557829	4.25364216	9.64547603	20.8238438	6.83954749	1.2105392	1.14047829	2.54545536	0.09234159	2.28283554	0.29620996	2.44900383	0.14812769
pcyt2	1.45008486	1.47242005	1.61467474	3.50181934	2.47592432	3.35181076	3.45108242	1.08341871	0.8861249	0.66215678	3.84755583	1.00755845	54.2010785	10.6808495
vps37c	2.29460633	4.87085735	19.9090463	7.26669748	10.6072944	10.8573686	18.7129185	3.20757929	1.53187609	0.86888085	2.11916587	11.0261433	34.30139	79.300338
atp2b4	1.09535046	4.93094582	2.08637785	1.31486551	1.09973484	0.64548442	3.22143297	4.48412934	3.25843628	2.80935255	0	2.73351124	18.3272578	11.214906
midn	7.64403917	9.22040742	11.3314886	6.18790143	18.7134016	9.4155012	13.4123008	6.85913094	6.19567661	5.79065614	2.22355382	9.39743827	26.5255573	80.5786721
atg13	4.55222382	3.51170081	3.02651825	6.08481541	8.88432768	7.06789777	5.35297429	3.21649931	5.23443314	4.73528129	2.03009393	8.23662325	17.5446045	39.0441487
rhou	4.88182799	12.9561222	6.67324628	3.27163239	5.87330397	9.60546364	5.42064968	4.01071348	11.3693629	7.97060065	18.5456921	23.4766657	62.0356075	132.457466
car10	0.15380737	3.7002581	1.06810466	0.80170518	4.52038274	2.41676681	0.87560448	0.14333594	1.06356804	5.41253461	6.16055278	7.41764509	12.5596294	25.3009652
asb6	1.31849966	1.09001889	6.33444651	11.6476247	7.86243456	3.04110296	2.31202082	1.08910539	0.42929181	0.38579652	0	2.49140697	4.72068573	5.245633
dgkk	1.73048685	0.14461506	11.3531358	1.37334373	0.47522554	2.59962683	35.2089392	29.9511532	25.4814935	4.17106508	3.70937128	7.67984176	13.8763494	2.78564421
adam19	14.7792354	28.799959	26.5518598	10.3220768	43.2879021	13.1339526	24.4460737	10.4614367	21.1808352	3.7335575	7.95980905	7.37007274	24.6374054	62.4303006
steap3	3.25113514	1.63016473	3.8500211	6.65106882	5.9157269	2.29401096	1.295006	1.48831943	0.56243271	17.9071555	5.67445886	9.78461688	22.4223081	2.49054097
mme	2.08429645	2.1490058	5.53123248	8.23128098	4.13771861	13.8427471	0.20939324	2.06379417	0.38086291	12.7326066	32.9553366	17.6345271	14.9902104	12.5037383
spp1	4.28559667	5.88156025	1.86807703	1.19300903	0.29487382	0.997972	2.78195694	6.31331886	6.97369491	59.043301	72.0095996	38.4915881	21.7738581	0.42794941
ndufs4	28.7578107	33.8017178	16.438906	26.3454	27.3342379	29.8360356	25.7882072	19.7038946	24.6700578	276.978711	54.0734442	24.4949534	27.4356861	13.040258
atp13a2	10.0326038	9.86533705	11.7861742	7.67013488	15.7355906	5.81112442	5.78541065	5.26546153	1.50101883	7.42415244	0.1857942	5.18755537	18.7137655	35.3271457
lyz1	0	0.22335039	0	11.8098385	1.97720098	8.99654613	5.28521513	4.02552097	0.8876374	2.08696382	0.48105517	6.03908147	1.30451362	0
pappa2	10.6861375	11.8874883	6.80596762	12.173714	8.8306267	21.3836572	16.6046239	22.9923444	36.0343371	51.7455867	44.3595734	37.4201558	28.3724459	20.6465965

F Other

Gene	GL1	GL2	GL3	Q1	Q2	Q3	TA1	TA2	TA3	GS1	GS2	GS3	FOOT1	FOOT2
phyhip	3.65921758	15.6194837	4.62068684	0.8758147	3.24445167	5.66789305	8.867737	9.26466517	0.63564961	0	0	2.19613492	0.02698258	0
tuba8	26.5658693	19.8360576	31.3759897	25.1016646	17.4724337	30.9818693	70.705396	42.0508769	34.1259893	8.56853198	5.55674572	16.5952128	8.96355106	0
pcp4l1	5.44315304	115.110003	113.255262	13.3907061	89.3634105	25.1488582	46.3076503	6.45308624	4.46105145	6.76702259	3.3095294	1.23825616	0.09958059	0
pold4	2.62685702	3.51600964	21.1441686	9.84239731	5.26384495	5.21539854	7.34122189	6.09222356	4.66517118	1.71293654	1.83752502	4.94197395	21.2260953	128.440571
ank1	1.26568156	5.18257211	3.9051809	2.89359774	9.75507259	9.0141967	6.1275013	3.40416155	5.82596097	1.09173816	2.43194596	3.96555844	10.6398161	29.7978805
st6galnac5	13.2335552	14.6284457	31.9372809	177.264236	17.3727805	12.1037799	18.692653	15.1584638	15.1011793	1.74804003	1.53651254	2.5830544	0.41863003	1.07890283
crisp1	0	0.13291662	0.03197274	1.79987342	0.88247953	0.53096299	15.2174617	9.33212096	8.84438703	0.29637673	0	0.04178929	0	0.09055735
zdhhc7	4.41259982	5.88156025	7.79766446	8.99735277	9.01762592	8.64825847	13.9215059	6.82447491	4.24460708	4.57588893	5.96903746	7.90799736	24.4468199	66.478274
krt1	0.04444023	1.77048194	1.62947193	0	0	0.49969155	0	2.76442943	0	0	0	1.69413271	19.1400819	11.5117834
pfn1	109.82129	149.412267	265.197965	94.9611413	121.251197	111.521634	142.416983	100.518679	45.4263087	21.3866638	6.07461088	65.8061579	150.992759	143.664201
gm16183	0.27323477	8.67690363	45.3492947	6.16478739	8.08853272	3.86005197	9.22313169	2.48266732	1.75383845	0	0.2548423	2.43043431	15.2036524	0
sntb1	1.47702962	0.42640799	0.0315604	1.77666139	8.68678936	1.65423934	2.76225898	6.67059167	10.1254866	4.80625274	5.17485023	0.84563229	0.02736818	0
p2rx3	9.89555938	16.3983551	13.7492172	19.1117185	22.2278949	17.2527751	5.00196514	3.73049461	3.39224351	17.1754286	22.8011066	8.9959202	29.5608679	69.5398606
calca	28.9995011	164.938025	359.189337	41.3289854	209.437834	67.6595732	55.5381721	2.92487631	55.1561928	50.1901979	132.600907	0	0.58358936	0.04332068
lxn	0	6.36518987	5.46403059	0	0.23017813	1.93195883	0.4343184	0.55396931	1.38748626	2.18660665	8.87081042	13.2630562	31.2410991	29.7189037
hspb6	1.51239821	1.96478394	3.741603	5.3845216	1.90237867	6.1113863	16.3809259	2.97302049	4.89345816	7.17138502	5.62033137	10.2955434	16.427917	58.5927703

adhesion molecules, regulators of gene expression, genes involved in neurotransmission, mediators of signal transduction, and genes with roles in metabolic pathways (Figures 2.3A-F).

The largest cohort of differentially expressed genes (DEGs) was comprised of guidance and adhesion molecules (Figure 2.3A), in accord with the requirement for muscle-type proprioceptors to target and synapse with distinct populations of spinal motor neurons during late embryonic development. We identified four members of the Ig superfamily of adhesion molecules (*alcam*, *bcam*, *ncam2*, and *amigo2*). We also identified several classical type II (*cdh7* and *cdh20*) and GPI-anchored (*cdh13*) cadherins - effectors of cell-cell adhesion and cell migration (Basu et al., 2015) – as well as non-clustered protocadherins (*pcdh17* and *pcdh19*) with roles in modulating classical cadherin-mediated cell adhesion and regulating axon extension (Hayashi and Takeichi, 2015). We detected five candidate genes involved in semaphorin signaling (*sema5a*, *sema6d*, *plxna2*, *plxna4*, and *nrp1*) and one in ephrin signaling (*epha4*), both well-characterized axon guidance pathways (Kolodkin et al., 2012). *Crtac1*, a Nogo receptor agonist, has been implicated in the formation of the lateral olfactory tract (Sato et al., 2011), and *rgma* acts as a repulsive guidance molecule (Lah and Key, 2012). Two teneurins (*odz1* and *odz3*), type II transmembrane proteins implicated in the formation of the visual system (Young and Leamey, 2009; Leamey and Sawatari, 2014), were found to be differentially expressed. We also detected two integrins (*itga2* and *itga3*), two CD proteins (*cd9* and *cd44*), *chl1*, *pkp4*, *cntn4,* and *hapln4*. Finally, we identified a

number of transmembrane proteins whose function in neurons has not been characterized but whose localization and predicted domain structures make them candidates for mediating cellular recognition: *vstm2b*, *tagln2*, *gm2115*, *gm10428*, *tmem72*, *tmem176a*, *tmem196*, *tspan9*, *C530028O21Rik (pianp)*, and *fam70a*.

Several differentially expressed genes indicate possible contamination by RNA from non-proprioceptive DRG neurons. The gene *calca*, which is upregulated in GL and Q samples, encodes calcitonin gene-related peptide (CGRPα), a marker of prurinergic nociceptors (McCoy et al., 2012). Likewise, expression of *lxn*, detected in GS and IF samples, is confined to a population of thermosensitive DRG neurons (Takiguchi-Hayashi et al., 1998). The presence of these transcripts may stem from the accidental inclusion of non-proprioceptive DRG neurons in our samples, or could be due to the presence of transcript from lysed cells in the medium following dissociation. Nevertheless, we proceeded to characterize the expression patterns of candidate genes in P1 lumbar DRG tissue.

We performed *in situ* hybridization to assess the expression of candidate genes in lumbar DRG of early postnatal mice (Figure 2.4). If a candidate gene is expressed in a subset of proprioceptors, we would expect to see expression in a subset of large-diameter DRG neurons (*pv* expression is shown in Figure 2.4A to illustrate the density and size of generic proprioceptors in lumbar DRG). Among guidance and adhesion molecules (Figure 2.4B), *alcam*, *cdh7*, *cdh13*, *pcdh17*, *pcdh19*, *sema5a*, *sema6d*, *plxna2*, *amigo2*, *cntn4*, *crtac1*, *cd9*, *tagln2*, *hapln4*, *chl1*, *vstm2b*,

gm2115, and *c530028o21rik* were expressed in a subset of DRG neurons, indicating that they might also be expressed in subsets of proprioceptors. In contrast, *rgma* and *itga2* were ubiquitously expressed in lumbar ganglia, and *bcam*, *ncam2*, *cdh20*, *plxna4*, *nrp1*, *itga3*, and *tspan9* were not detected in DRG neurons (Figure 2.4B). Among transcription factors and transcriptional regulators (Figure 2.4C), *meis2*, *pou4f3*, *smyd1*, *tcerg1l*, and *prmt8* were expressed by a subset of DRG neurons, whereas *zfhx3* was expressed by all neurons in lumbar ganglia and *nkx1-2* was not expressed in DRG. Many candidate genes related to neurotransmission were expressed in sensory subsets (Figure 2.4D): *htr2c*, *chrna4*, *cacng5*, *scn10a*, *kcnk9*, *syt17*, *doc2b*, *sorcs1*, *rph3a*, *6330403a02rik*, *tnni1*, and *s100a6; kcnip4* and *stc1* appear to be expressed throughout the ganglion. Among genes involved in signaling pathways (Figure 2.4E), *rspo2*, *wls*, *vgf*, *gfra2*, *ret*, *ptger3*, *ptgir*, *rgs4*, *fam19a1*, *c1qtnf1*, and *scg2* were expressed in a subset of DRG neurons, while expression of *gucy1a3*, *camk1d* and *bc018242* was not detected in lumbar DRG. Of genes with known roles in metabolic pathways (Figure 2.4F), *steap3* and *spp1* were expressed in DRG subsets, whereas expression of *ndufs4*, *atp2b4*, and *mme* was not detected. Additional genes assessed by *in situ* (Figure 2.4G) include *pcp41l* (expressed in a subset of DRG neurons); *crisp1* and *st6galnac5* (not expressed in lumbar DRG); and *pfn1* and *tuba8* (expressed throughout the DRG). Thus, a majority of the genes identified in our screen are expressed in subsets of DRG neurons, consistent with their predicted expression by proprioceptor subsets.

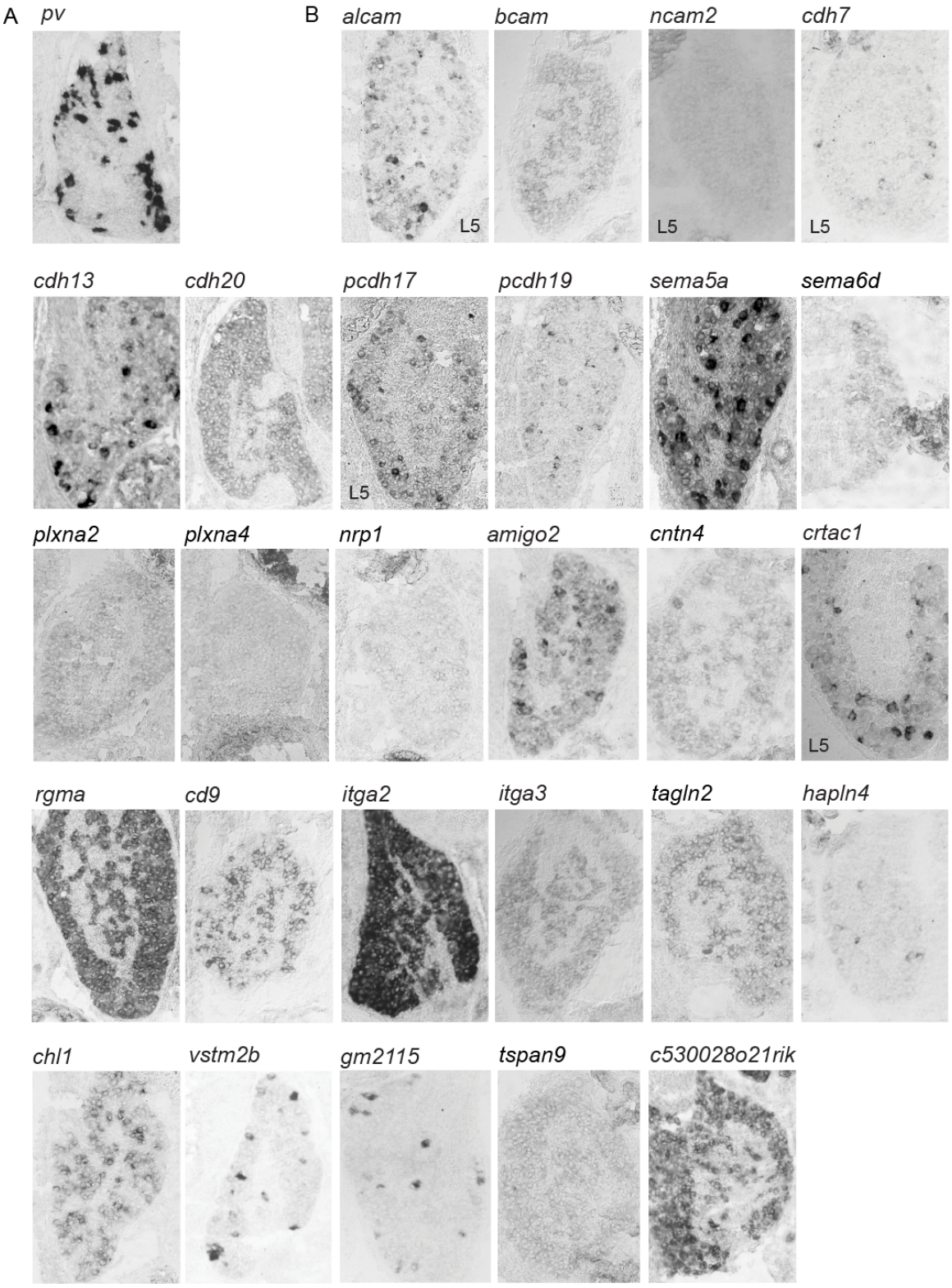
A
pv
B
alcam
bcam
ncam2
cdh7
L5
L5
L5
cdh13
cdh20
pcdh17
pcdh19
sema5a
sema6d
L5
plxna2
plxna4
nrp1
amigo2
cntn4
crtac1
L5
rgma
cd9
itga2
itga3
tagln2
hapln4
chl1
vstm2b
gm2115
tspan9
c530028o21rik

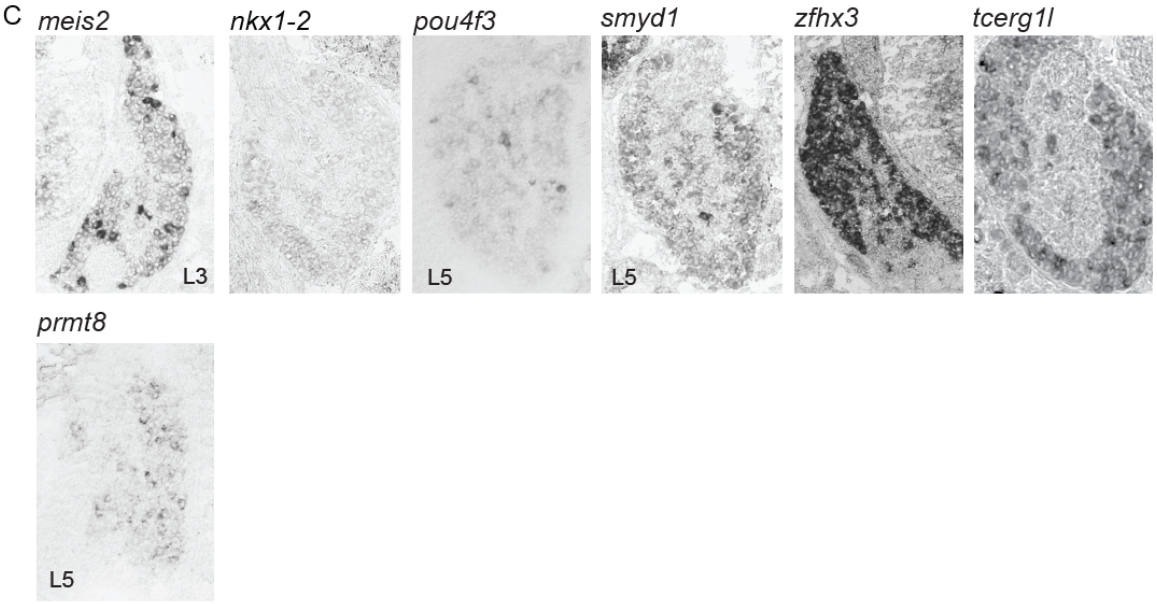
C
meis2
nkx1-2
pou4f3
smyd1
zfhx3
tcerg1l
L3
L5
L5
prmt8
L5

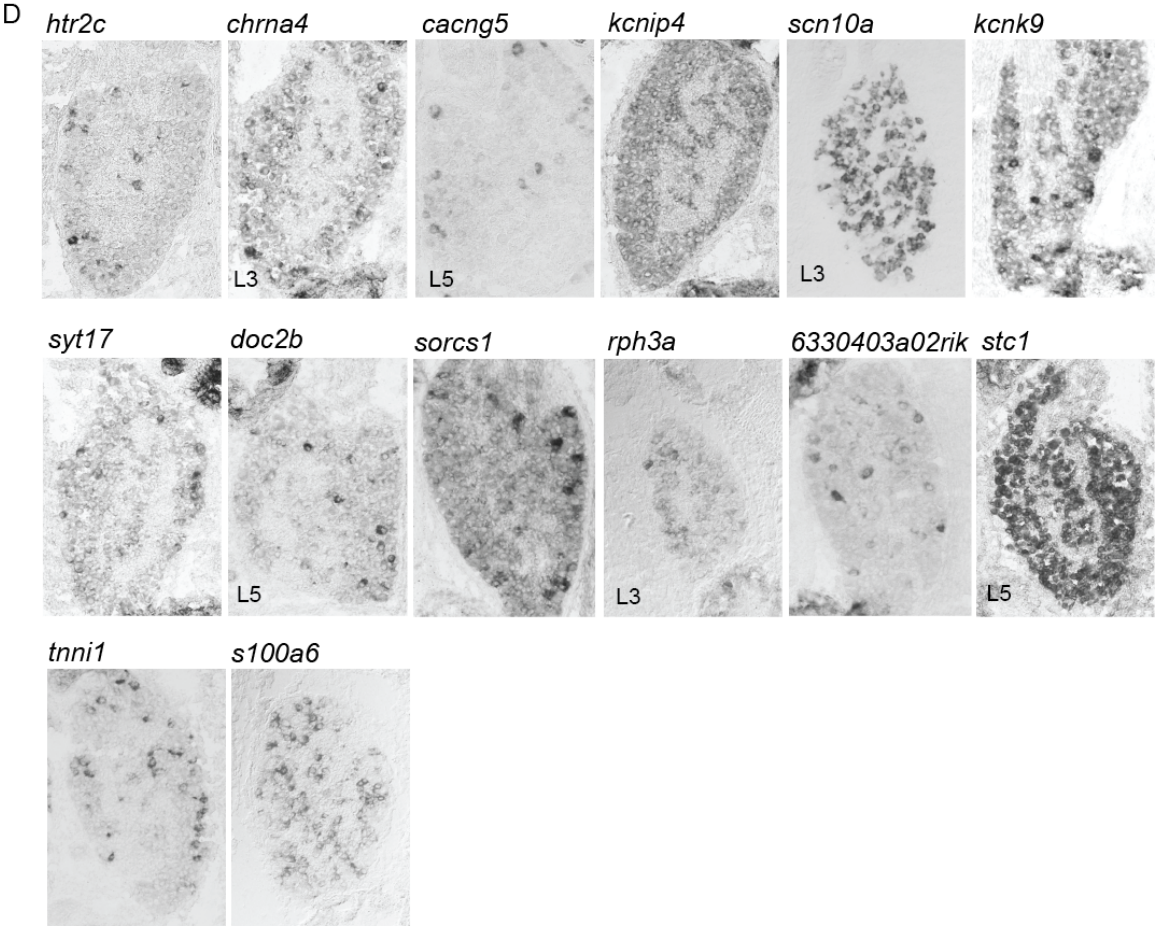
D
htr2c
chrna4
cacng5
kcnip4
scn10a
kcnk9
L3
L5
L3
syt17
doc2b
sorcs1
rph3a
6330403a02rik
stc1
L5
L3
L5
tnni1
s100a6

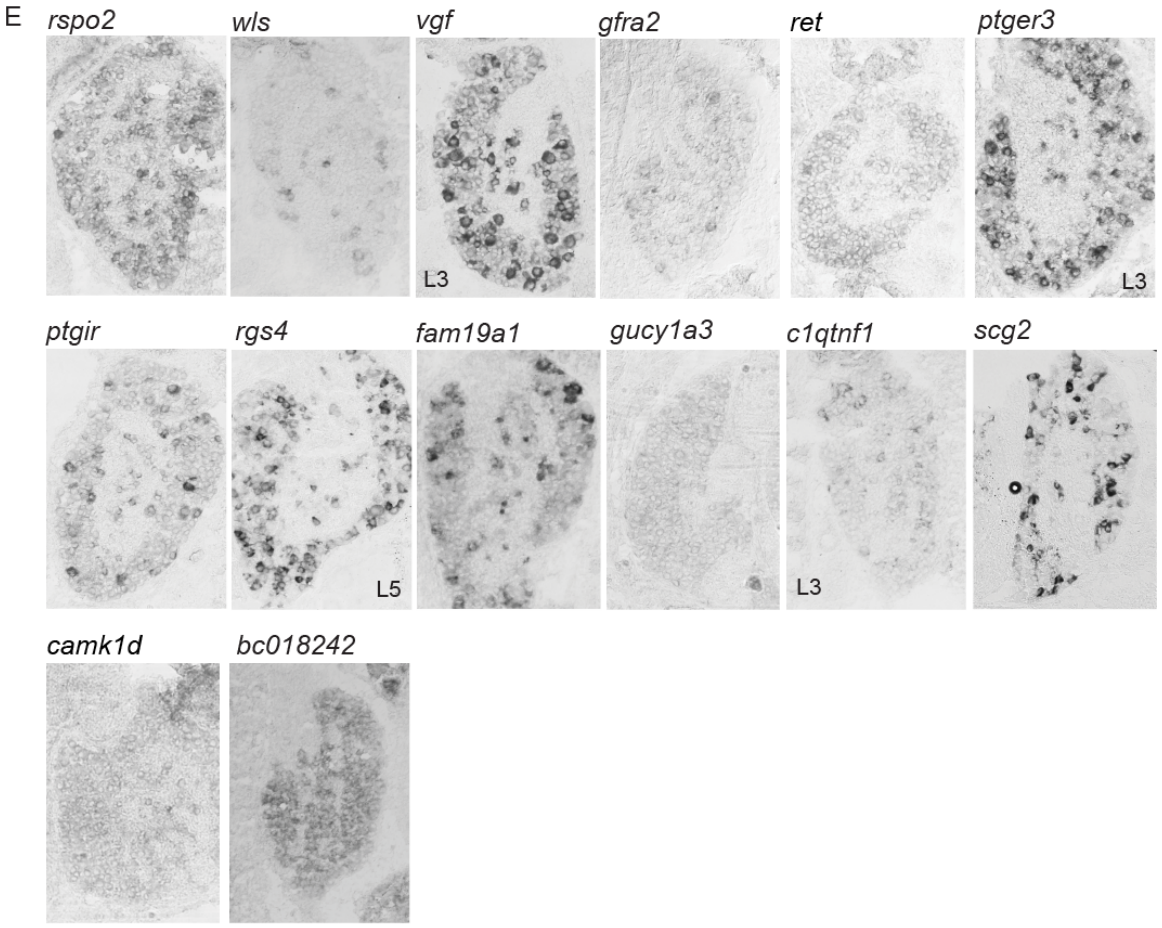
E
rspo2
wls
vgf
gfra2
ret
ptger3
L3
L3
ptgir
rgs4
fam19a1
gucy1a3
c1qtnf1
scg2
L5
L3
camk1d
bc018242
F
ndufs4
atp2b4
steap3
mme
spp1
L5
L5
L5
G
crisp1
pcp41l
st6galnac5
pfn1
tuba8

Figure 2.4 Candidate gene expression in lumbar DRG

(A-G) Candidate gene expression was assessed in P0-P2 lumbar DRG by *in situ* hybridization. All images are representative and show DRG L4 unless otherwise indicated. (A) Expression of the proprioceptor marker *pv*. (B) Guidance, adhesion and transmembrane proteins. (C) Transcription factors and transcriptional regulators. (D) Neurotransmission. (E) Morphogen, growth factor, and intracellular signaling. (F) Cellular metabolism. (G) Other.

2.2.2 Muscle-type proprioceptors are defined by *cdh13*, *vstm2b*, *sema5a*, or *crtac1* expression

Profiling candidate gene expression by chromogenic *in situ* hybridization indicates whether transcript is present in a subset of DRG neurons, but it can neither confirm that these cells are proprioceptors nor characterize their muscle-type selectivity. We therefore chose to analyze the expression of four guidance/adhesion molecules expressed by subsets of DRG neurons: *cdh13*, *vstm2b*, *sema5a*, and *crtac1* (Figure 2.5). We first estimated their incidence in lumbar proprioceptors using double fluorescent *in situ* hybridization (FISH). We found that *cdh13* is expressed by 48% of L2-L6 *pv*^{on} DRG neurons, *vstm2b* by 42%, *sema5a* by 22%, and *crtac1* by 38% (Figures 2.5A, B, E, F, I, J, M, and N). Thus, all four genes are expressed by subsets of proprioceptors. Notably, *cdh13*, *sema5a*, and *crtac1* are also expressed by subsets of *trkA*^{on} and *trkB*^{on} DRG neurons, markers of several cutaneous sensory lineages (Figure 2.6A-C; Lallemend and Ernfors, 2012). In contrast, *vstm2b* expression is confined to *pv*^{on} neurons (Figure 2.5E), suggesting that among DRG neurons, it is expressed exclusively by a subset of proprioceptors.

We next examined whether *cdh13*, *vstm2b*, *sema5a*, and *crtac1* exhibit the muscle-type selectivity predicted in our RNA-Seq screen (refer to Figure 2.3A and Table 2.1) by first assessing their expression in TA and GS proprioceptors. To evaluate the expression of these genes according to muscle innervation, we injected ctb^{555} into TA or GS muscles at P0 and assessed the expression status of these genes

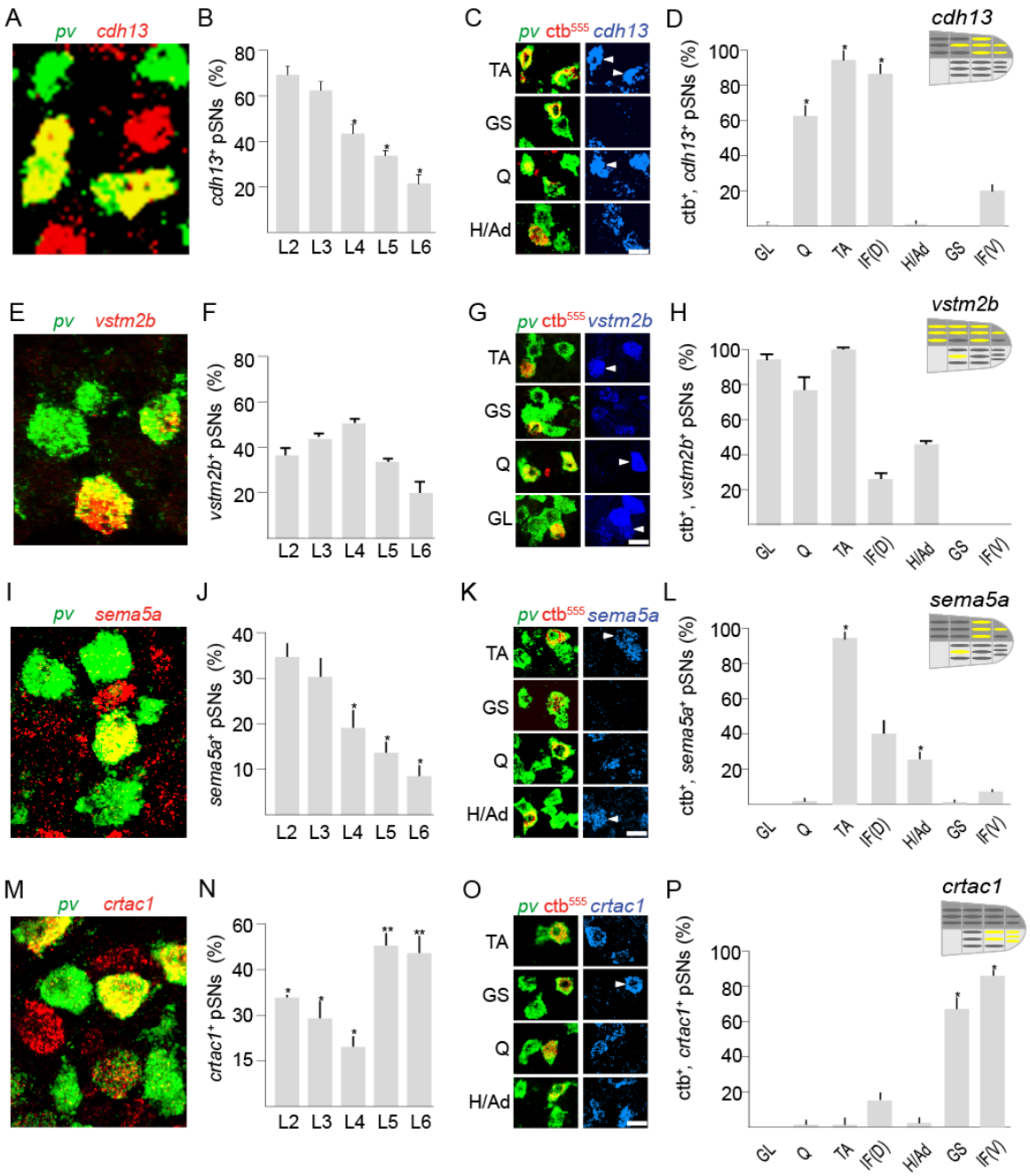

Figure 2.5 Candidate gene expression in muscle-type proprioceptor subpopulations

(A, B, E, F, I, J, M, and N) *cdh13*^{on} (A and B), *vstm2b*^{on} (E and F), *sema5a*^{on} (I and J), and *crtac*^{on} (M and N) proprioceptors at P0 in lumbar DRG (L, lumbar level; n = 6; >300 neurons/level). Data are represented as the mean ± SD. (C, D, G, H, K, L, O, and P) *cdh13*, *vstm2b*, *sema5a*, and *crtac1* status in proprioceptors by muscle. ctb^{555}-labeled TA, GS, Q, and H/Ad or GL proprioceptors (*cdh13*, TA: n=5; GS: n=6; Q: n=3, H/Ad: n=6; *vstm2b*, *sema5a*, and *crtac1*, TA: n=3; GS: n=3; Q: n=3; GL or H/Ad: n=3). Data are represented as the mean ± SD. Scale bar, 20 μm.

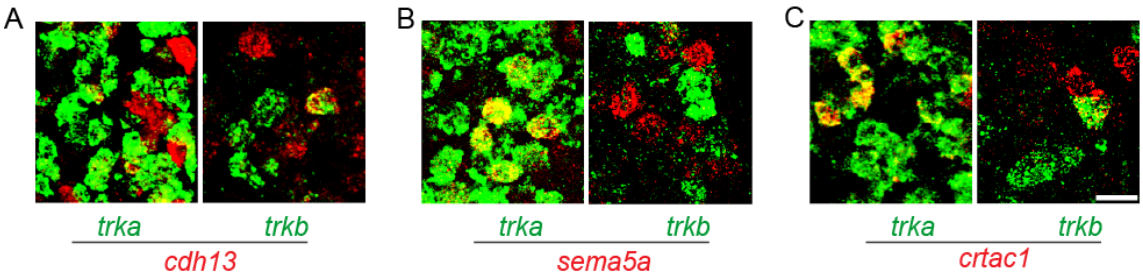

Figure 2.6 Expression of proprioceptor muscle-type genes in cutaneous DRG neurons

Cdh13, *sema5a*, and *crtac1* are co-expressed with the cutaneous sensory markers *trkA* and *trkB*. Note that the expression of *vstm2b* is restricted to *pv*^{on} DRG neurons (Figure 2.5E).

in retrogradely labeled proprioceptors at P1. We found that 96%, 100%, and 95%, respectively, of *pv*^{on}, ctb^{555}-labeled TA neurons expressed *cdh13*, *vstm2b*, and *sema5a*, whereas GS neurons were devoid of *cdh13*, *vstm2b*, and *sema5a* transcript expression. Conversely, 65% of GS neurons expressed *crtac1*, and TA neurons lacked *crtac1* expression (Figures 2.5C, D, G, H, K, L, O, and P).

When we expanded our characterization proximally, we found that 64%, 72%, 2%, and 1% of proprioceptors supplying the dorsal quadriceps (Q) group expressed *cdh13*, *vstm2b*, *sema5a*, and *crtac1*, respectively (Figure 2.5C, D, G, H, K, L, O, and P). Proprioceptors supplying the ventrally positioned hamstring/adductor (H/Ad; comprised of gracilis, semitendinosus, semimembranosus, and adductors muscles) group lacked *cdh13* or *crtac1* expression, although 42% and 25% of these neurons expressed *vstm2b* and *sema5a*, respectively (Figure 2.5C, D, G, H, K, L, O, and P). For the most proximal gluteal (GL) muscle group, we observed that nearly all (89%) backfilled proprioceptors expressed *vstm2b*, while none expressed *cdh13*, *sema5a*, and *crtac1* (Figure 2.5C, D, G, H, K, L, O, and P).

The small size of foot muscles prevented us from targeting dorsal or ventral domains with absolute precision. Nevertheless, dorsally directed ctb^{555} injections revealed that 91%, 25%, 40%, and 14% of retrogradely labeled proprioceptors expressed *cdh13*, *vstm2b*, *sema5a*, and *crtac1*, whereas 24%, 0%, 10% and 89% of proprioceptors expressed *cdh13*, *vstm2b*, *sema5a*, and *crtac1*, respectively, after ventrally directed foot injections (Figure 2.5C, D, G, H, K, L, O, and P).

These findings confirm the selectivity predicted by our RNA-Seq screen and support the notion that proprioceptor gene expression is positionally restricted with respect to limb domain. Whereas dorsal-distal muscles are supplied preferentially by proprioceptors that express *cdh13*, *crtac1* is expressed by proprioceptors that innervate ventral-distal musculature, and *sema5a* is expressed in proprioceptors that supply dorsal or ventral domains at particular proximodistal positions. In contrast, *vstm2b* lacks proximodistal restriction, but is largely confined to proprioceptors innervating dorsal musculature. Thus, there is a clear link between proprioceptor expression of *cdh13*, *vstm2b*, *sema5a*, and *crtac1* and muscle position along the dorsoventral and proximodistal axes of the limb.

2.2.3 Fine-grained analysis of *cdh13* expression using a genetic reporter

To provide a more detailed evaluation of the identity and position of muscles innervated by *cdh13*^{on} proprioceptors, we used a genetic strategy to mark the cell bodies and peripheral and central axons of *cdh13*^{on} neurons. We utilized a knock-in mouse line in which a tamoxifen-inducible Cre recombinase/Estrogen Receptor fusion construct (CreER^{T2}) is expressed under regulatory control of the TA-enriched gene *cdh13* (*Cdh13*::CreER^{T2}). We crossed *Cdh13*::CreER^{T2} mice with a *Tau*::lox-STOP-lox::mGFP line to generate *Cdh13*::GFP tracer mice (Figure 2.7A; Hippenmeyer et al., 2005). Tamoxifen delivery to pregnant females at embryonic day 16.5 (e16.5)

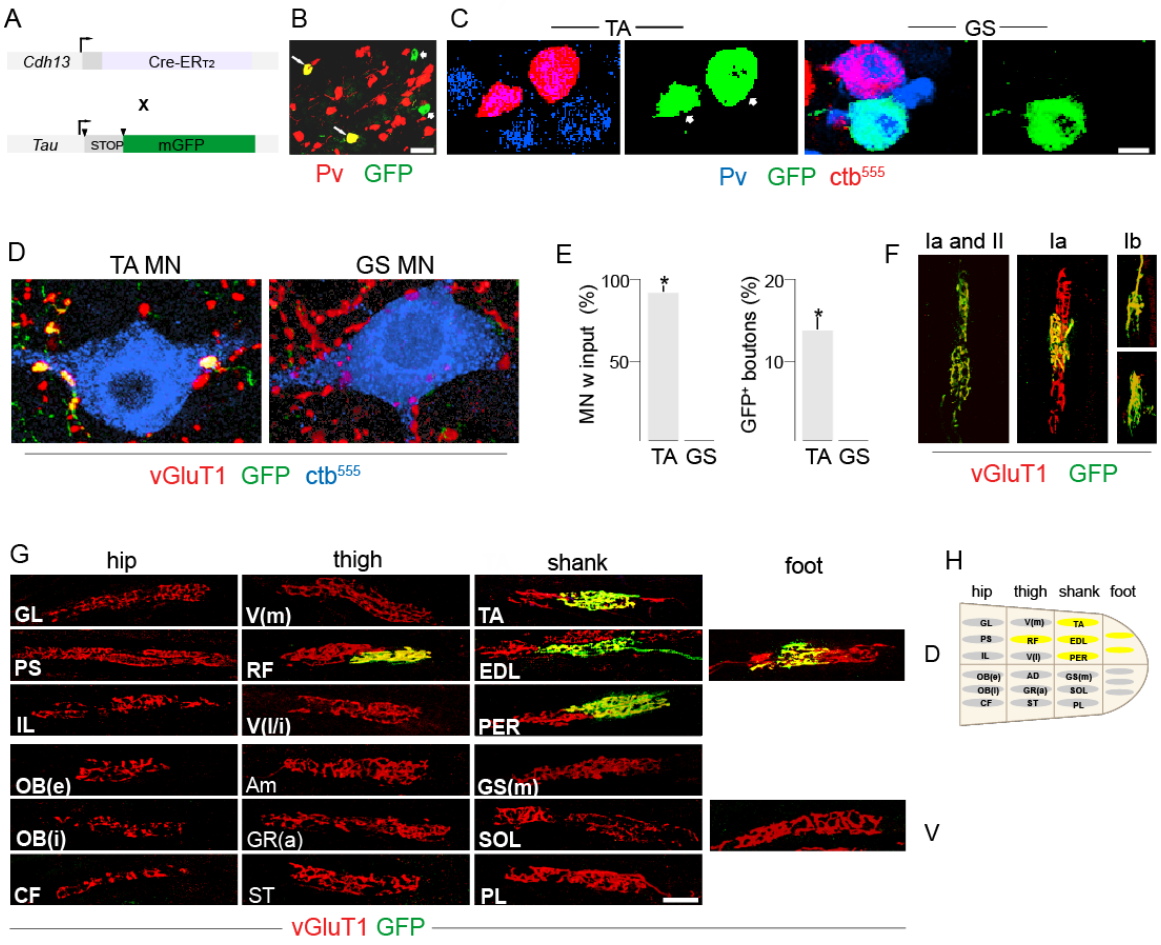

Figure 2.7 *cdh13* expression is restricted to proprioceptors supplying the dorsodistal hindlimb

(A) *Cdh13*::CreER^{T2} and *Tau*::lox-STOP-lox::mGFP mice were crossed to generate *Cdh13*::GFP tracer mice. Tamoxifen was injected into pregnant females at day e16.5 of gestation to induce Cre activity. (B) GFP expression in P2 DRG of *Cdh13*::GFP mice. Long arrows: Pv^{on}, GFP^{+} neurons. Short arrows: Pv^{off}, GFP^{+} neurons. Scale bar, 50 μm. (C) GFP expression in TA proprioceptors in *Cdh13*::GFP mice. TA or GS proprioceptors in P0 *Cdh13*::GFP mice were retrogradely labeled by ctb^{555} muscle injection. At P1, DRG were removed and the expression of Pv and GFP was assessed by immunostaining. Arrows: Pv^{on}, GFP^{+}, ctb^{555+} TA proprioceptors. Scale bar, 10 μm. (D) TA but not GS motor neurons receive *cdh13*^{on} input from TA synergist afferents. Immunostaining for GFP and vGluT1 demarcates GFP^{+} proprioceptive boutons on TA (left) but not GS (right) motor neurons. Scale bar, 20 μm. (E) TA and GS retrogradely labeled motor neurons receiving GFP^{+}, vGlut1^{+} input (left), and GFP^{+} proprioceptive inputs to

TA and GS motor neurons (n = 3 mice; TA: n = 36 MNs, 836 boutons; GS: n = 61 MNs, 1287 boutons). Data is represented as the mean ± SD. (F) GFP labels TA muscle spindle (Ia and II) and GTO (Ib) terminals in *Cdh13*::GFP mice. P7 TA muscles immunostained for vGluT1 and GFP. (G) *Cdh13*^{on} proprioceptors supply dorsal-distal hindlimb muscles. Hindlimb muscles along the rostrocaudal and proximodistal axes of the limb in *Cdh13*::GFP mice (tamoxifen induction at e14.5-16.5) were assessed for GFP expression at spindle terminals by immunostaining at P7 (n ≥ 3 mice; additional muscles innervated by *cdh13*^{off} proprioceptors include: pectineus, flexor digitorum longus, tibialis posterior, semimembranosus, semitendinosus, quadratus femoris, biceps femoris, and body wall). Scale bar, 50 μm.

resulted in GFP expression in Pv^{on} lumbar DRG neurons (Figure 2.7B). The fraction of GFP^{on} proprioceptors in DRG L3-5 was ~8%, whereas ~45% of proprioceptors express *cdh13* at these levels (see Figures 2.4A and B), indicating a tamoxifen induction efficiency of ~18% (Figure 2.7B). The low induction efficiency likely reflects a high level of Hsp-90 expression in DRG neurons, which retains the $CreER^{T2}$ fusion protein in the cytoplasm (Zhao et al., 2006).

We determined the fidelity of GFP expression in *Cdh13*::GFP mice by analyzing TA and GS proprioceptors. At P1, 15% of ctb^{555}-labeled TA proprioceptors, but no GS proprioceptors, expressed GFP (Figure 2.7C), mirroring endogenous *cdh13* expression. The central connectivity of *cdh13*^{on} proprioceptors (TA/EDL/PER) was assessed by monitoring GFP expression in $vGlut1^{+}$ proprioceptor terminals in the ventral spinal cord of *Cdh13*::GFP mice. 92% of TA motor neurons received inputs from GFP-labeled $vGluT1^{+}$ proprioceptor terminals and, inversely, 14% of all $vGluT1^{+}$ proprioceptor terminals on TA motor neuron somata and the proximal 100 μm of the dendritic tree co-expressed GFP (Figures 2.7D-F). This low fraction presumably reflects mosaicism in GFP expression after tamoxifen induction. In contrast, none of the $vGluT1^{+}$ terminals on the somata and proximal dendrites of GS motor neurons expressed GFP (Figures 2.7E and F). Thus, the pattern of sensory-motor contacts in *Cdh13*::GFP mice conforms to the agonist-antagonist rules of synaptic patterning.

We next assessed the peripheral terminations of *cdh13*^{on} proprioceptors in *Cdh13*::GFP mice. After retrograde tracer injection, we detected *cdh13* transcript expression in most TA proprioceptors, suggesting that all three classes of proprioceptors – group Ia, group II, and group Ib afferents – express *cdh13*. In support of this view, analysis of TA muscle revealed annulospiral GFP$^+$, vGluT1$^+$ type Ia and type II sensory endings in muscle spindles, as well as more broadly arborized type Ib endings associated with GTOs (Figures 2.7F and G). In contrast, GFP expression was not observed in sensory endings in GS muscle (Figure 2.7G), consistent with the TA group specificity of *Cdh13*::GFP expression.

To further investigate the relationship between proprioceptor *cdh13* status and the limb position of muscle targets, we assayed the status of GFP expression in individual hip, thigh, shank, and foot muscle spindles of P7 *Cdh13*::GFP mice exposed to tamoxifen in utero at ~e15.5. At the dorsal shank level, GFP$^+$ endings were observed in the TA, EDL, and PL muscles (Figures 2.7G and H). In contrast, none of the spindles of the ventrally derived GS, SOL, PL, tibialis posterior (TP), or flexor digitorius longus (FDL) shank muscles were innervated by GFP$^+$ proprioceptors (Figures 2.7G and H).

At more proximal levels, none of the spindles of dorsally or ventrally derived hip muscles – GL, iliacus (IL), psoas (PS), obterator externus/internus (Oe/i), and caudoemoralis (CF) – contained GFP$^+$ sensory terminals (Figures 2.7G and H). For dorsally derived thigh muscles, the RF, but not the V group (Vl, Vi, and Vm) or

pectineus (Pec) muscles, contained GFP$^+$ proprioceptors, providing an explanation for the mosaic *cdh13* status of RF/V proprioceptors detected in retrograde tracing experiments. The ventrally derived muscles AD/GR/ST/SM and biceps femoris (BF) did not contain any GFP$^+$ sensory terminals. Finally, we observed that spindles in the most dorsally located intrinsic foot muscles, but not the ventral foor muscles, contained GFP$^+$ terminals (Figures 2.7G and H). This muscle-by-muscle analysis consolidates the view that *cdh13*^{on} proprioceptors supply dorsally derived limb muscles with a distal positional bias.

2.3 Discussion

Using high-throughput RNA-sequencing, I identified 140 genes exhibiting differential expression – in many cases binary – between muscle-type proprioceptor subsets. I then validated these results and expanded our characterization to additional muscle groups using a combination of fluorescence *in situ* hybridization and intramuscular backfill with the retrograde tracer ctb^{555}. Using a genetic reporter line, we were able to characterize the status of *cdh13* expression in proprioceptors at the resolution of individual muscles by assaying for GFP expression at the muscle spindle, providing insight into the organization of proprioceptor subtype identity.

2.3.1 Screening muscle-type proprioceptors: general considerations

Given recent advances in single-cell sequencing, why did we assay pooled samples rather than individual neurons? Isolating neurons by virtue of *pv* expression status likely resulted in the inclusion of a small number of non-proprioceptive low threshold mechanoreceptors – a second class of *pv*-expressing DRG neurons - in our samples. Moreover, each muscle receives innervation by Group Ia, II and Ib proprioceptors, which are presumed to differ at the molecular level (de Nooij et al., 2013). We surmised that pooling neurons would allow us to detect genetic distinctions in proprioceptors that are primarily associated with muscle innervation by neutralizing any differences corresponding to pv^{on} LTMRs or proprioceptor functional subclass.

We chose to focus our characterization of candidate gene expression patterns on transmembrane proteins due to their potential involvement in establishing selective monosynaptic connectivity with spinal motor neurons. Of the ~40 genes encoding transmembrane proteins identified by our screen, we were able to provide a thorough characterization of the muscle-type expression pattern of four. Our ability to examine the expression patterns of the remaining genes was limited by expression levels below the threshold for detection by double FISH or by the lack of available antibody or transgenic reagents to facilitate characterization.

While we primarily aimed to detect binary on-off differences in gene expression between muscle-type proprioceptors, we identified several examples of graded expression between muscle-type proprioceptor subsets. Most notably,

vstm2b is predicted to be expressed in a proximal^{low} to distal^{high} gradient among dorsally-innervating proprioceptors (see Figure 2.3A). Indeed, our FISH results appear to validate this prediction; proximal GL-innervating proprioceptors consistently express lower levels of *vstm2b* than do more distally innervating TA proprioceptors (see Figure 2.5G). Graded expression of recognition molecules has been shown to underlie differential responses to axon guidance cues in motor neurons (Bonanomi and Pfaff, 2010). Thus, when examining functional roles for genes exhibiting muscle-type selectivity, it may be important to consider not only binary distinctions but also differences in relative levels of gene expression.

2.3.2 The grain of proprioceptor muscle-type identity

Our assessment of *cdh13*, *vstm2b*, *sema5a*, and *crtac1* by fluorescent *in situ* hybridization combined with ctb injection revealed that expression of these genes is confined to proprioceptors supplying muscles located in distinct domains along the dorsoventral and proximodistal limb axes. However, this approach was unable to address several emergent questions regarding muscle-type identity: 1) What is the most basic meaningful unit of proprioceptor muscle-type identity? and 2) Do all proprioceptors innervating a given muscle share a common gene expression profile?

The availability of a *Cdh13*::CreER^{T2} line enabled us to address these questions through the examination of *cdh13* expression at higher resolution than is achievable using FISH combined with backfill. Our analysis of *Cdh13*::GFP

expression at proprioceptor terminals in individual muscles revealed a shared *cdh13*^{on} identity for proprioceptors innervating TA muscle and its synergists extensor digitorum longus (EDL) and peroneus longus (PL), as well as for all proprioceptors innervating dorsal intrinsic foot muscles. This finding demonstrates that synergy group is a relevant unit of proprioceptor identity; because proprioceptors innervating synergist muscles generally target the same cohort of motor neuron, this unit of identity could conceivably facilitate afferent targeting of these motor neurons during late embryonic development. The expression of *cdh13* by proprioceptors innervating the RF head of the quadriceps but not its synergist vastii muscles indicates that proprioceptors also possess subtype identities on the level of individual muscles. Subtle differences in heteronymous connectivity patterns between the RF and vastii muscles could necessitate this distinction.

Intriguingly, we found that all proprioceptors innervating the TA, including Group Ia, II and Ib proprioceptors, express *cdh13*. Because Group Ia, II and Ib proprioceptors innervating a given muscle project to distinct dorsoventral termination zones and therefore have distinct sets of postsynaptic partners in the spinal cord, it is difficult to envision how *cdh13* could play a role in establishing synaptic specificity for each of these subpopulations. As a consequence, we speculate that the shared *cdh13* expression profile of Group Ia, II and Ib TA proprioceptors is likely a reflection of the mode of peripheral induction of this gene.

The chimeric profiles obtained for *vstm2b* expression in Q, H/Add, and IF proprioceptors; *sema5a* in H/Add and IF proprioceptors; and *crtac1* in GS proprioceptors (Figures 2.5H, L and P) might be explained by binary distinctions in expression among muscles of the synergy groups receiving innervation by afferents expressing these genes, as we observed for the dorsal thigh muscles of *Cdh13*::GFP mice. Alternatively, these phenotypes might be explained by differences in expression status among Group Ia, II and Ib proprioceptors in all muscles of the synergy group. Resolving this issue requires peripheral representation of *vstm2b*, *sema5a* and *crtac1* expression status at muscle spindle and GTO sensory terminals using tools analogous to the *Cdh13*::GFP tracer line; unfortunately, no such reporter lines for these genes exist at this time.

2.3.3 Proprioceptor muscle-type identity conforms to limb organization

Our screen results and *in vivo* characterization of several differentially expressed genes have revealed a positional logic for hindlimb-innervating proprioceptors. Many of the genes differentially expressed among muscle-type proprioceptors are predicted to exhibit a bias along the proximodistal or dorsoventral limb axis, or both (see Figure 2.3). This patterning is exemplified by the genes *cdh13*, *vstm2b*, *sema5a*, and *crtac1*, whose expression along these axes we characterized *in vivo*. *Cdh13* and *vstm2b* exhibit a marked dorsal bias in their expression, whereas *crtac1* expression is confined to proprioceptors innervating ventral limb musculature. Furthermore, whereas *cdh13*, *sema5a*, and *crtac1*

expression is restricted to proprioceptors innervating distal musculature, *vstm2b* is expressed by proprioceptors innervating the extent of the proximodistal axis.

The expression pattern of *sema5a* diverges from those observed for *cdh13*, *vstm2b* and *crtac1* in an interesting way Whereas expression of *cdh13*, *vstm2b* and *crtac1* was confined to proprioceptors innervating either dorsal or ventral territory, *sema5a* is expressed by proprioceptors supplying both dorsal and ventral domains at distinct proximodistal positions. Interestingly, all of the muscles receiving *sema5a*^{on} innervation are joint flexors, suggesting that this gene may be involved in differential targeting of flexor versus extensor synergy groups. There is precedence for this biomechanically-restricted pattern of connectivity: vestibular input preferentially targets extensor over flexor motor neurons (Basaldella et al., 2015), implying a mechanism by which flexor and extensor motor neurons could be differentially targeted.

How might positionally restricted patterns of proprioceptor gene expression arise? Molecular processes governing limb morphogenesis rely heavily on proximodistally and dorsoventrally restricted patterning cues. The morphogens retinoic acid (RA) and FGF are distributed in opposing gradients along the proximodistal limb axis and confer proximal and distal limb morphology, respectively (Mariani et al., 2008; Mercader et al., 2005; Yashiro et al., 2004). Expression of the morphogen Wnt7a in dorsal limb ectoderm induces expression of

the transcription factor Lmx1b in dorsal but not ventral limb anlagen, which in turn specifies many features of limb dorsoventral identity (Chen and Johnson, 2002).

The restriction of a cohort of proprioceptor genes with respect to the dorsoventral limb axis is particularly intriguing in light of the finding that limb dorsoventral identity influences synaptic specificity between proprioceptors and motor neurons in chick (Wenner and Frank, 1995), which implies that the limb is capable of inducing molecular distinctions in proprioceptors that are reflective of peripheral termination. In Chapters 3-5, I describe experiments designed to establish a role for the periphery in assigning proprioceptor muscle-type identity in mouse and to assess the impact of three dorsoventrally distinct peripheral tissues – motor axon, limb mesenchyme, and muscle - on proprioceptor expression of the dorsoventrally restricted genes *cdh13*, *vstm2b*, *sema5a*, and *crtac1*.

3 Motor axon is dispensable for proprioceptor *cdh13* expression

3.1 Introduction

To explore the involvement of limb inductive signaling in specifying proprioceptor muscle-type identity, we employed genetic strategies designed to disrupt putative tissue sources of patterning information. We considered the involvement of three tissues that are encountered by sensory axons as they project into the limb: the motor axons that fasciculate with sensory axons during invasion of the embryonic limb, the muscle targets innervated by sensory afferents, and the limb mesenchymal tissues traversed by axons during limb innervation (Figure 3.1).

In this chapter, I examine whether the motor axon plays a role - either instructive or permissive - in inducing expression of the proprioceptor muscle-type marker *cdh13*. I first demonstrate that patterned expression of the proprioceptor muscle-type genes *cdh13* and *vstm2b* begins after hindlimb innervation, consistent with specification by a peripheral cue. I proceed to examine the induction of proprioceptor *cdh13* expression in mice genetically manipulated to lack motor neuron subtype character or to lack motor neurons altogether. I find that neither of these manipulations affects proprioceptor expression of *cdh13*, indicating that motor axon plays neither an instructive nor permissive role in specifying proprioceptor *cdh13* subtype character.

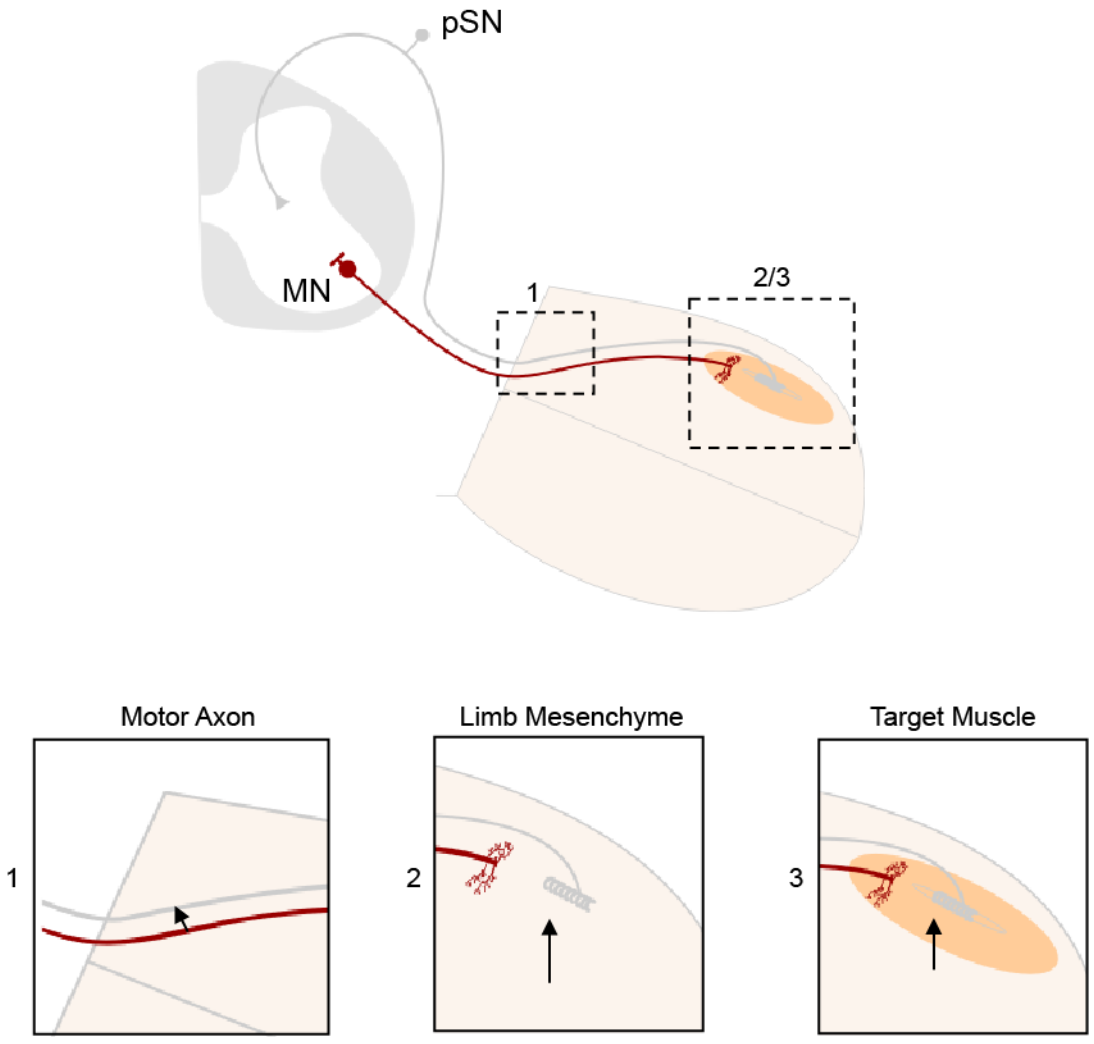

Figure 3.1 Putative sources of proprioceptor muscle-type inductive cues

Three tissues contacted by sensory axons during limb innervation – motor axon (1), limb mesenchyme (2), and muscle (3) – were examined for a role in patterning proprioceptor muscle-type gene expression.

3.1.1 Interactions between peripheral sensory and motor axons

As motor and sensory axons project into the limb bud mesenchyme, they are bundled together within peripheral nerves. Motor axons emanating from a single lumbosacral spinal segment and sensory axons from the corresponding DRG meet and intermix as they project toward the lumbar plexus, where several spinal nerves converge and then diverge into the peripheral nerve branches that grow toward muscle targets. Axonal tracing experiments have revealed that proprioceptor axons innervating the chick hindlimb are situated adjacent to motor axons innervating the same muscle for much of their course through the limb (Honig et al., 1998). This intranerve fasciculation provides a physical basis for axon-axon signaling between sensory and motor subtypes beginning early in their projection into the periphery.

Indeed, molecular axon-axon interactions have been found to drive the selective fasciculation of sensory and motor axons within peripheral nerves. Mouse molecular genetic studies have demonstrated that the segregation of motor and sensory axons within nerves projecting to axial muscle requires repulsive transaxonal signaling between the receptor tyrosine kinases EphA3 and EphA4 on motor axon growth cones and their cognate ephrin-A ligands on sensory axons (Gallarda et al., 2008), revealing an influence of sensory axon-derived signals on motor axons. The converse influence of motor axon on sensory axon is also rooted in molecular interactions; at thoracic levels, removal of EphA3 and EphA4 from axial

motor axons prompts sensory axons to project exclusively to hypaxial muscle (Wang et al., 2011), revealing that motor axon-derived signals are required for establishing normally patterned peripheral sensory projections. These studies provide precedent for molecular signaling between sensory and motor axons, supporting the hypothesis that axon-axon interactions might specify proprioceptor subtype identity.

3.1.2 Motor neuron projection patterns are intrinsically specified

Developing motor axons possess a high degree of autonomous targeting specificity, allowing them to actively seek and innervate discrete muscle targets from the outset (Landmesser, 2001). This ability is intrinsically programmed by transcriptional networks that specify molecular and organizational features of motor neuron subsets (Dasen, 2009). Among limb-innervating motor neurons, three levels of organization have been defined based on settling position and termination within the limb, with each successive level governing a distinct aspect of motor axonal projection pattern (Figure 3.2). Motor neurons at limb levels acquire lateral motor columnar (LMC) identities that direct their axons toward the limb. Once motor axons reach the base of the limb, the specification of divisional identities within the LMC sets motor axons on a dorsal or ventral trajectory upon entering the limb mesenchyme. Finally, the specification of motor pool identity enables motor neurons to project toward and form precise connections with individual muscle targets (Landmesser, 1978b, 2001).

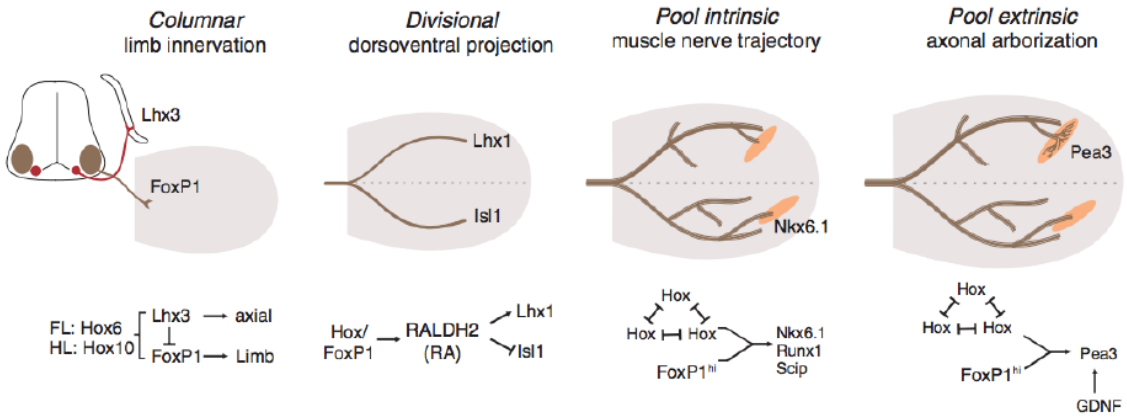

Figure 3.2 Transcriptional control of motor neuron projection pattern

Sequential steps in the transcriptional control of limb innervation patterns. Molecular determinants of motor nerve branching are noted with respect to hierarchical motor neuron subtype identity. Adapted from Dasen, 2009.

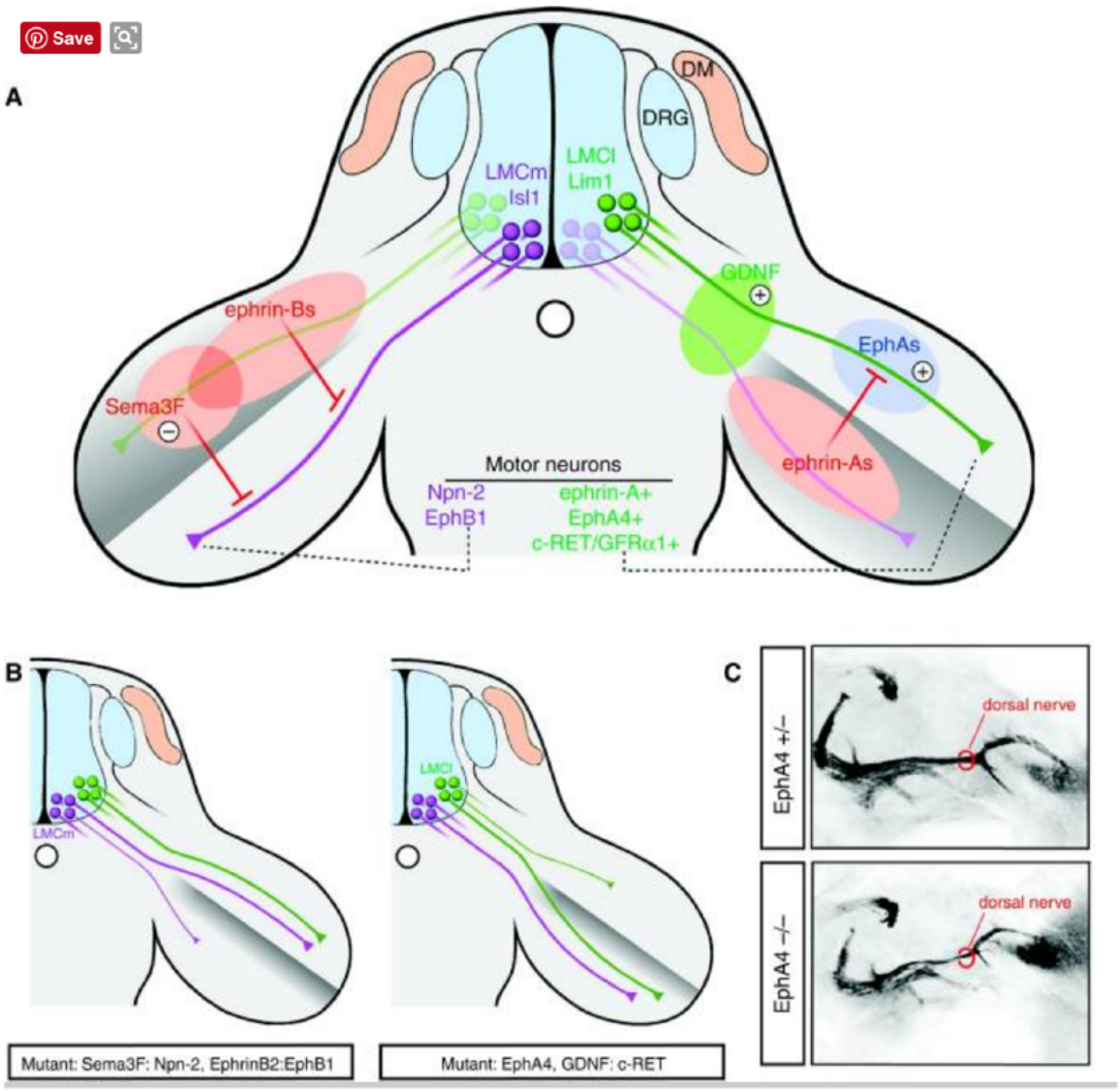

Figure 3.3 Motor neuron transcriptional identity directs dorsoventral projection

(A) Left: Isl1-positive LMC_M axons (purple) expressing Npn2 and EphB1 are repelled by Sema3F and EphrinB in the dorsal limb mesenchyme and select a ventral trajectory. Right: A combination of repulsive and attractive signals direct Lim1-positive LMC_L axons (green) to dorsal limb muscles. Ephrin-As in the ventral mesenchyme trigger "forward" repulsive signaling through axonal EphA4, whereas EphAs localized in the dorsal limb may elicit attractive "reverse" signaling through axonal ephrin-As. GDNF localized at the base of the limb controls the dorsal trajectory of LMC_L axons expressing c-Ret. Additional studies have identified a role for Netrin signaling in dorsoventral choice by motor axons (not shown). (B) Left: Disruption of Sema3F:Npn2 or ephrin-B:EphB1 signaling

leads to dorsal projection of ventrally fated LMC_M axons. Right: Ablation of EphA4 or interference with GDNF:c-Ret signaling causes dorsally projecting LMC_L axons to select a ventral trajectory. (C) Dorsal view of hindlimb innervating motor axons visualized with the Hb9::GFP transgene in e12.5 mouse embryos. The dorsal (peroneal) nerve becomes thinner in *EphA4* mutants because of the misprojection of LMC_L axons into the ventral limb (the ventral nerve is out of the plane of focus). Adapted from Bonanomi and Pfaff, 2010.

Each of these sequential phases of limb innervation is linked to a genetic program defined by transcriptional networks involving members of the Hox gene family (Figure 3.2). Expression of the transcription factor FoxP1 specifies limb innervating motor neurons, and Hox10 expression distinguishes hindlimb- from forelimb-innervating motor neurons (Dasen et al., 2003). The dorsoventral choice made by hindlimb motor axons at the base of the limb is a consequence of the pattern of LIM homeodomain transcription factor expression specified downstream of this Hox/FoxP1 network: dorsally-projecting motor neurons in the lateral portion of the LMC (LMC_L) are characterized by selective expression of the LIM homeobox transcription factor Lhx1, whereas ventrally projecting motor neurons situated medially (LMC_M) express Isl1 (Kania and Jessell, 2003; Tsuchida et al., 1994).

Downstream of Lhx1 and Isl1, a cohort of guidance receptors enables LMC_L and LMC_M axons to follow mesenchymal cues into the dorsal and ventral compartments of the limb, respectively (Figure 3.3). Expression of ephrinA in ventral mesenchyme repels EphA4-expressing LMC_L axons away from ventral and into dorsal limb (Eberhart et al., 2002; Helmbacher et al., 2000), while expression of c-Ret and GFRα1 by LMC_L axons allows them to follow GDNF at the base of the limb bud into dorsal limb mesenchyme (Bonanomi et al., 2012; Dudanova et al., 2010; Kramer et al., 2006). Conversely, in LMC_M axons, expression of EphB2 and Unc5c mediates a repellent response to ephrinB and Netrin1 in dorsal mesenchyme, preventing these axons from entering dorsal limb (Luria et al., 2008; Poliak et al.,

2015). LMC_M axons also express Npn2, which repels them from Sema3F-expressing dorsal mesenchyme (Huber et al., 2005).

Finally, the guidance of motor axons to specific muscles is directed by a Hox network operating in the presence of high levels of the accessory factor FoxP1 to establish the transcriptional identities of motor pools (Dasen et al., 2005). The Hox/FoxP1 network appears to direct motor innervation patterns by activating a diverse array of downstream transcription factors and cell surface receptors. In one notable example, Hox/FoxP1 programs direct the expression of Nkx6.1, a homeodomain transcription factor, in select motor pools. At hindlimb levels, the motor nerve branch supplying TA muscle is derived from Nkx6.1-expressing motor neurons. In *Nkx6.1* mutants, axons that normally project to TA are rerouted to different muscle targets (de Marco Garcia and Jessell, 2008), implicating Nkx6.1 and by extension the Hox/FoxP1 program in establishing motor axonal trajectory.

FoxP1 gates the entirety of the output of the Hox program in LMC motor neurons (Dasen et al., 2008). Genetic inactivation of the *Foxp1* gene erases all Hox-dependent steps of LMC motor neuron differentiation, resulting in the loss of motor neuron topography and all known identifying molecular features of motor pools (Dasen et al., 2008). Remarkably, the overall pattern of axonal projections into the limb is preserved in these mutants (Dasen et al., 2008; Rousso et al., 2008), although motor neurons appear to select projection pathways in the limb in a stochastic manner. These findings are consistent with the view that the overall pattern of

motor nerve branching within the limb is determined by preestablished permissive or inhibitory domains within the limb mesenchyme; the FoxP1/Hox program thus provides LMC neurons with identities that enable axons to respond to local cues, which promote the selection of one of many available paths.

3.1.3 Extrinsically specified facets of motor neuron subtype identity

While many aspects of motor pool identity are programmed through the cell-intrinsic activities of the Hox transcriptional network, evidence has emerged for the peripheral specification of certain features of subtype identity. Expression of the ETS transcription factor Pea3 in motor pools is dependent on muscle- and mesenchyme-derived GDNF (Haase et al., 2002; Lin et al., 1998), which provides a permissive environment for Pea3 specification in competent motor neurons. Pea3 has been shown to instruct muscle-specific patterns of axonal arborization, motor pool settling position, and pool-specific dendritic arborization (Haase et al., 2002; Livet et al., 2002; Vrieseling and Arber, 2006). Peripherally-specified programs of gene expression therefore provide an additional layer of motor neuron subtype diversity that might contribute to proprioceptor subtype specification.

3.2 Results

3.2.1 *cdh13* and *vstm2b* expression initiate after hindlimb innervation

Certain features of proprioceptor subtype identity appear to be acquired in a neuron-autonomous manner, whereas others are dependent on limb signaling (Chen et al., 2002). If cell-autonomous signals instruct the expression of *cdh13* and *vstm2b*, then these genes might be expressed in proprioceptors prior to limb innervation. Thus, prior to assessing the effect of limb tissues on proprioceptor gene expression, we sought to establish when these genes are first expressed.

To determine the onset of *cdh13* expression, we assessed lumbar DRG for the expression of *cdh13* in proprioceptors at embryonic timepoints before and after limb innervation. Expression of the proprioceptor marker gene *pv* does not begin until e14.5 (Arber et al., 2000; Hippenmeyer et al., 2005), several days after limb innervation. We therefore assessed the coexpression of *cdh13* with *trkC*, which is expressed by proprioceptors beginning at e10.5. We detected no *cdh13* transcript in lumbar DRG at e10.5 or e11.5 (Figure 3.4A), times at which sensory axons have arrived at the lumbar plexus (e10.5) and established dorsal and ventral nerve branches within the limb mesenchyme (e11.5). By e12.5, however, ~25% of *trkC*^{on} neurons had initiated *cdh13* expression (Figure 3.4A). Thus, the onset of *cdh13* expression in proprioceptors occurs after sensory axonal innervation of the hindlimb.

We also examined the GFP status of dorsal and ventral shank muscle spindles in *Cdh13*::mGFP mice following tamoxifen injection of pregnant females at several gestational timepoints. Injections at e10.5 did not result in proprioceptor GFP

expression (data not shown), consistent with a ~24 h delay between tamoxifen injection and recombination (Hayashi and McMahon, 2002). At every developmental time point examined, dorsal (TA, EDL) but not ventral (GS, SOL) shank muscles received GFP^+ proprioceptor innervation (Figure 3.4B). Thus, the restriction of *cdh13* expression to dorsodistal muscles is established early and maintained throughout development.

It is possible that *cdh13* expression in limb-innervating proprioceptors is initially more widespread and that its restricted pattern is established through the death of $cdh13^{on}$ proprioceptors innervating other limb territories. To rule out this possibility, we examined the expression of *cdh13* in retrogradely labeled TA and GS proprioceptors of $bax1^{-/-}$ mice, in which neurons are blocked from undergoing programmed cell death (White et al., 1998). As in wild-type mice, TA but not GS proprioceptors expressed *cdh13* in $bax1^{-/-}$ animals (Figure 3.4C), indicating that the dorsodistal selectivity of *cdh13* expression arises independently of programmed sensory neuron death.

To determine the onset of *vstm2b* expression, we performed *in situ* hybridization at several embryonic time points. While we did not observe *vstm2b* expression in lumbar DRG at e12.5, by e13.5, a subset of lumbar DRG neurons expressed the gene (Figure 3.5A). We also examined the subtype specificity of *vstm2b* expression at the time of its induction. Although we were unable to examine the muscle specificity of *vstm2b* expression at its onset, double FISH for *vstm2b* and

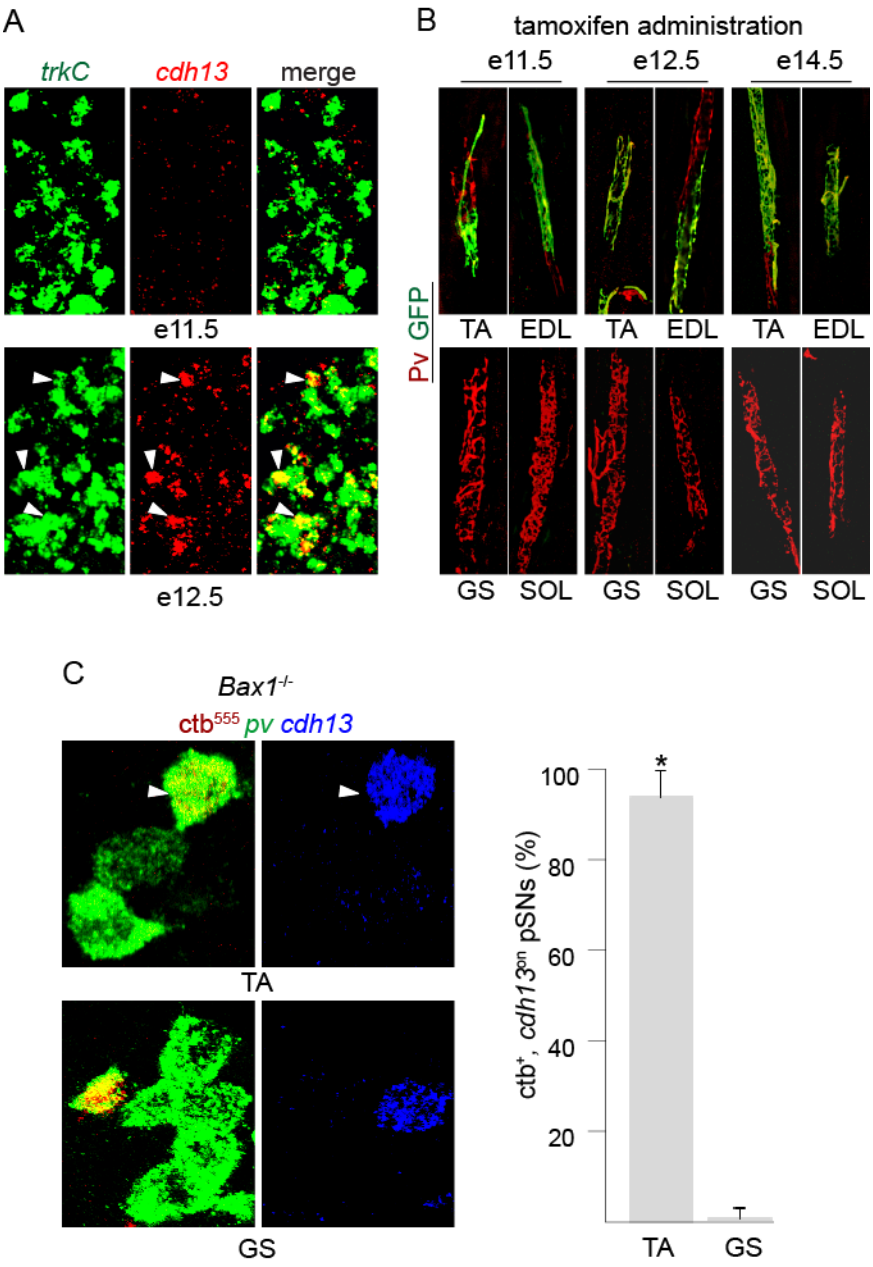

Figure 3.4 Early specificity of *cdh13* expression

(A) Double FISH for *trkC* and *cdh13* at e11.5 and e12.5 in L5 DRG. Arrowheads demarcate double-labeled *trkC*^{on}, *cdh13*^{on} neurons at e12.5. (B) The GFP status of dorsal and ventral shank muscle spindles was assessed following tamoxifen injection of pregnant *Cdh13*::GFP females at the indicated gestational times. At every time point examined, dorsal (TA, EDL) but not ventral (GS, Sol) shank muscles received GFP^{+} proprioceptor innervation. (C) TA and GS proprioceptors of *Bax1*$^{-/-}$ mice were retrogradely labeled by ctb^{555} injection at P0 and assessed by FISH for *pv* and *cdh13* expression. Similar to wild-type mice, TA but not GS proprioceptors expressed *cdh13*.

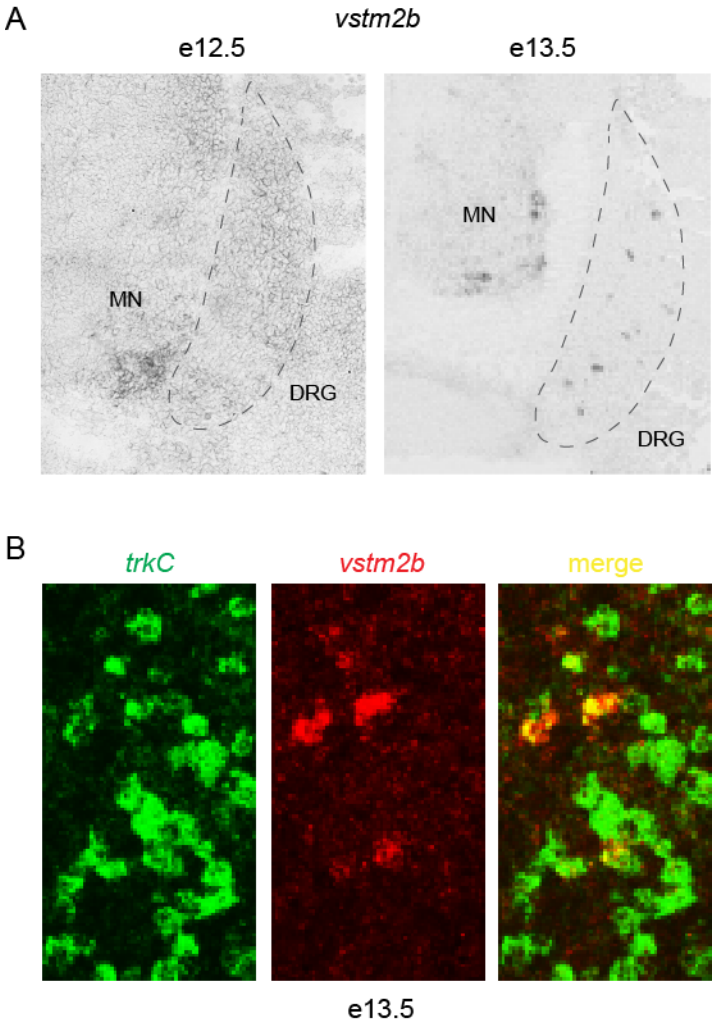

Figure 3.5 Proprioceptor *vstm2b* expression initiates after limb innervation

(A) *In situ* hybridization for *vstm2b* reveals that its expression in lumbar DRG begins around e13.5. (B) Double FISH for *trkC* and *vstm2b* in lumbar DRG of e13.5 wild-type mice reveals that a subset of *trkC*^{on} neurons express *vstm2b*, and all *vstm2b*-expressing neurons express *trkC*, consistent with the restriction of *vstm2b* to a subset of proprioceptors from its onset.

trkC at e13.5 revealed that a subset of *trkC*^{on} DRG neurons coexpressed *vstm2b* and all *vstm2b*^{on} neurons coexpressed *trkC* (Figure 3.5B), consistent with restriction of *vstm2b* to a subset of proprioceptors from its induction. Together, these findings indicate that restricted *vstm2b* expression is initiated following limb innervation.

It is worth noting that the onset of *vstm2b* expression lags that of *cdh13* by ~1 day. This may be reflective of differing modes of induction for the proprioceptor expression of these genes – a possibility that we explore in Chapters 4 and 5.

3.2.2 Motor neuron subtype identity does not instruct proprioceptor *cdh13* expression

We set out to determine whether the subtype identities of limb-innervating motor axons might impose proprioceptor subtype identities. To this end, we inactivated FoxP1, a Hox cofactor required for the emergence of pool identities in limb-innervating motor neurons (Dasen et al., 2008). Combinatorial expression of Hox transcription factors in motor neurons directs the differential expression of surface labels such as type II cadherins. In the absence of FoxP1, limb-innervating motor neurons appear to select their muscle targets at random, indicating that they are unable to follow instructive mesenchymal cues to the muscle targets encoded by their Hox transcriptional identities. We selectively abolished FoxP1 activity in motor neurons by crossing an *Olig2*::Cre driver line with mice carrying a floxed *foxP1* allele to generate FoxP1$^{MN\Delta}$ mice (Figure 3.6A; Feng et al., 2010). We first examined

generic proprioceptor development in FoxP1$^{MN\Delta}$ mice. We found that at P1, the density of *pv*^{on} neurons expressing *cdh13* was unchanged in L2 and L5 DRG when compared to wild-type littermates (Figures 3.6B and C).

We examined the effect of abolishing motor neuron subtype character on proprioceptor *cdh13* expression. If motor neuron pool identity instructs proprioceptor subtype character, we would expect to see a reduction in the percentage of proprioceptors expressing *cdh13*. Instead, we found that at P1, the percentage of *cdh13*^{on} proprioceptors was unchanged between wt and FoxP1$^{MN\Delta}$ mice (Figure 3.6C). Furthermore, the postnatal viability of FoxP1$^{MN\Delta}$ mice permitted us to examine the muscle specificity of *cdh13* expression in the absence of motor pool surface markers. We found that 100% of ctb^{555}-labeled TA proprioceptors expressed *cdh13* in FoxP1$^{MN\Delta}$ mice, mimicking the endogenous pattern observed in wild-type mice (Figures 3.6C and D). Conversely, <4% of backfilled GS proprioceptors expressed *cdh13*, as observed in wild-type animals (Figures 3.6C and D). Thus, motor neuron identity is not involved in establishing the restricted pattern of proprioceptor *cdh13* expression.

3.2.3 Motor axon does not provide a permissive environment for the induction of proprioceptor *cdh13* expression

We next considered whether a generic signal provided by motor neurons might act with other inductive signals to direct the selectivity of proprioceptor

cdh13 expression. To assess this issue, we used a genetic strategy to ablate motor neurons by crossing an *Olig2*::Cre driver line with *Rosa*::DTA mice (Wu et al., 2006) to generate MN^{DTA} mice (Figure 3.7A). More than 95% of lateral motor column (LMC) motor neurons in MN^{DTA} mice were ablated by e11.5, as assessed by the expression of the transcription factors FoxP1 and Isl1 (Figure 3.7B). Limb muscles in MN^{DTA} mice exhibited atrophy at e18.5 (data not shown). Nevertheless, proprioceptor endings were present in limb muscle in association with muscle spindles (Figure 3.7C), and the density of pv^{on} neurons in e18.5 lumbar DRG was similar in wild-type and MN^{DTA} mice (Figure 3.7D).

Because MN^{DTA} mice die shortly after birth, we were unable to identify the muscle target of proprioceptors by retrograde labeling. Nevertheless, we were able to quantify the fraction of neurons at rostrocaudal levels containing $cdh13^{on}$ proprioceptors. We found that the proportion of $cdh13^{on}$ proprioceptors was unchanged in MN^{DTA} mice compared with wild-type littermates; as assessed by fluorescence *in situ* hybridization, *cdh13* was expressed in ~70% of wild-type and ~69% of MN^{DTA} proprioceptors in L2 DRG and in ~32% of wild-type and ~34% of MN^{DTA} proprioceptors in L5 DRG (Figures 3.8A and B). Thus, motor axons do not create a permissive environment for the specification of proprioceptor *cdh13* expression.

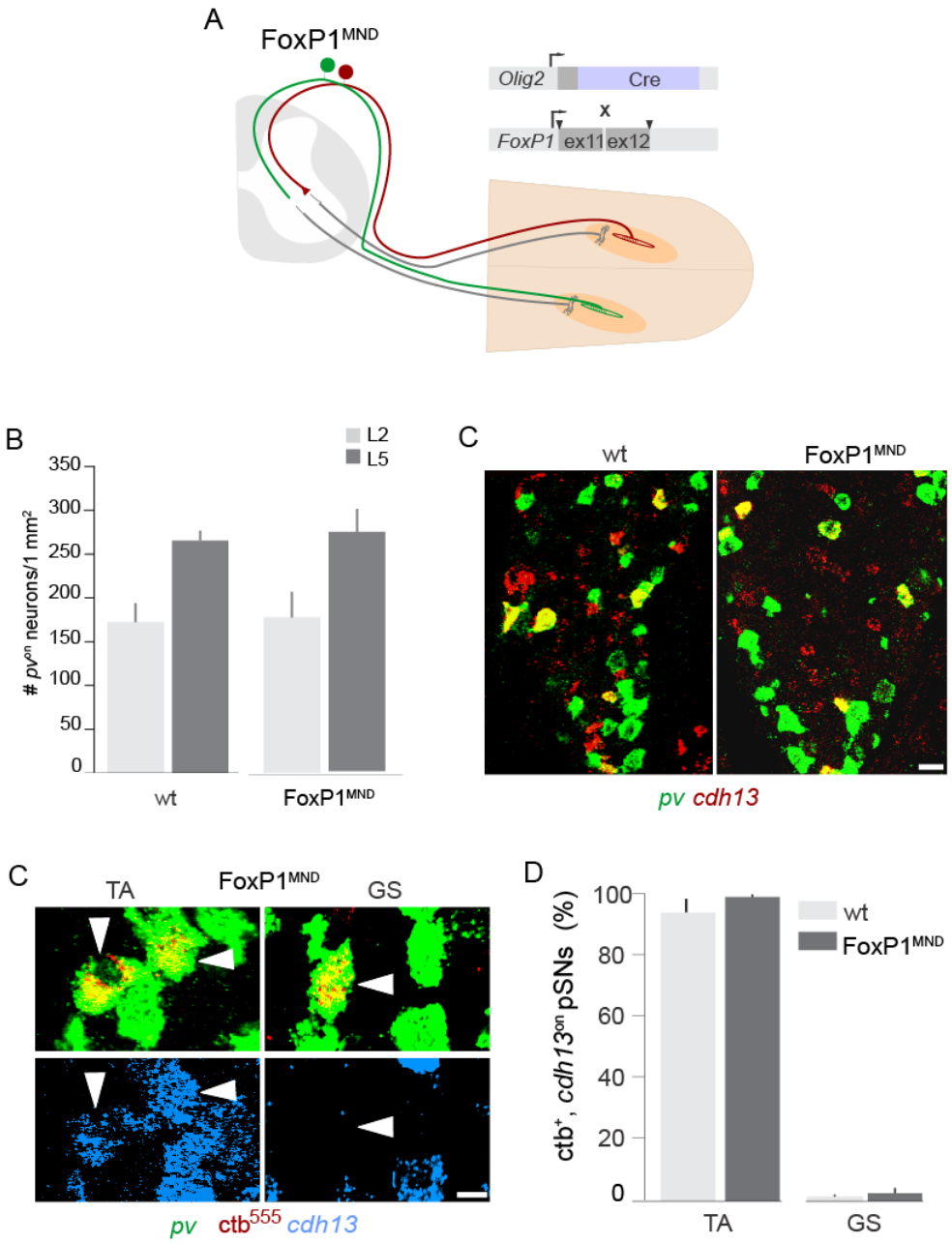

Figure 3.6 *Cdh13* expression is unaffected in the absence of motor neuron subtype character

(A) Erosion of motor neuron identity was achieved by crossing *Olig2*::Cre with floxed *FoxP1* mice (FoxP1$^{MN\Delta}$). (B) The density of proprioceptors in DRG L2 and L5 was unchanged in FoxP1$^{MN\Delta}$ mice, as assessed by FISH (see 3.6C). (C) *Cdh13* and *pv* expression in P0 FoxP1$^{MN\Delta}$ L4 DRG. The percentage of proprioceptors expressing *cdh13* does not differ between FoxP1$^{MN\Delta}$ and wild-type (wt) mice. Scale bar, 30 µm. (D) TA or GS propricoeptors in wt and FoxP1$^{MN\Delta}$ mice identified

by ctb^{555} and examined for *cdh13* expression by double FISH. Arrowheads indicate *pv*^{on}, ctb^{555+}, *cdh13*^{on} or *pv*^{on}, ctb^{555+}, *cdh13*^{off} TA or GS proprioceptors, respectively. Scale bar, 10 μm. (E) The *cdh13* of TA and GS proprioceptors does not differ between wt and FoxP1$^{MN\Delta}$ mice (TA: n = 3 mice; GS: n = 3 mice). Data are represented as the mean ± SD (D and E).

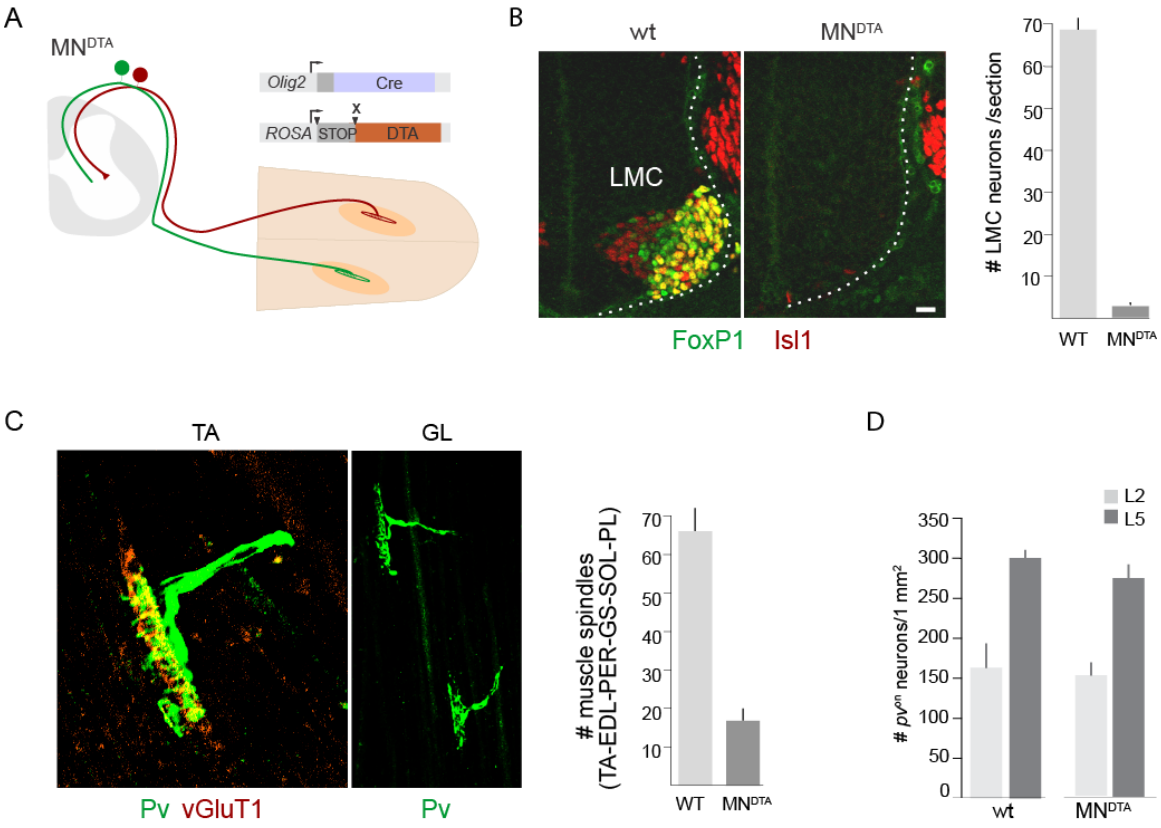

Figure 3.7 Cellular phenotypes of MN^{DTA} mice

(A) Post-mitotic motor neurons were killed by crossing *Olig2*::Cre with *Rosa26*::lox-stop-lox:DTA mice (MN^{DTA}). (B) LMC neurons are killed in MN^{DTA} mice, as shown by immunostaining for FoxP1 and Isl1 in e11.5 wt and MN^{DTA} lumbar spinal cords. Note the lack of FoxP1^{on} neurons in the ventrolateral spinal cord in MN^{DTA} mice. Quantification reveals that more than 95% of ventrolaterally located FoxP1^{on} motor neurons are ablated in MN^{DTA} mice. (C) Muscle spindles develop in MN^{DTA} mice. Right: Representative TA and GL muscle spindles in MN^{DTA} mice are visualized by Pv and vGluT1 immunostaining. Left: Quantification of shank muscle spindles in wild-type and MN^{DTA} mice. The number of spindles formed in MN^{DTA} mice is reduced by ~80% compared to the wild-type. (D) The density of proprioceptors in DRG L2 and L5 was unchanged in MN^{DTA} mice, as assessed by FISH.

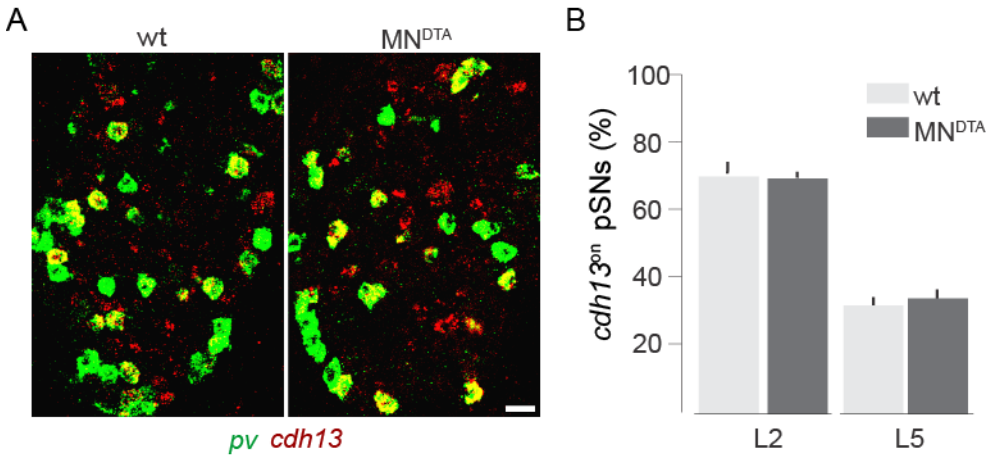

Figure 3.8 Loss of motor neurons does not affect *cdh13* induction

(A and B) The percentage of proprioceptors expressing *cdh13* is similar in wt and MN^{DTA} mice. (A) Images show double FISH for *pv* and *cdh13* in e18.5 L4 DRG. Scale bar, 30 µm. (B) Quantification of proprioceptors expressing *cdh13* in wt and MN^{DTA} L2 and L5 DRG at e18.5 (n = 3 mice). Data are represented as the mean ± SD.

3.3 Discussion

While there is ample evidence for the involvement of axo-axonal interactions in fasciculation and pathfinding (Wang and Marquardt, 2013), the specification of neuronal subtype character via signaling between axons has not been described. Nevertheless, the abundance of molecular distinctions between motor neuron subpopulations combined with the close association between motor and proprioceptor axons during limb innervation led us to consider the motor axon as a source of patterning information.

Our results corroborate previous findings arguing against a role for motor axon in the specification of proprioceptor muscle-type identity. In chick double-dorsal limb preparations, sensory-motor connectivity was shown to be influenced by an ectopic peripheral element (Wenner and Frank, 1995). Motor axons were dismissed as a source of sensory patterning information because they were argued to be unaffected by surgical manipulation (Wenner and Frank, 1995), which we can attribute in retrospect to the preservation of dorsoventral guidance cues located in the retained proximal portion of limb bud. In FoxP1$^{MN\Delta}$ mice, afferents have been shown to target appropriate domains of the LMC in the absence of motor axon subtype character (Sürmeli et al., 2011), providing additional evidence against a role for motor axon in proprioceptor subtype specification.

However, concluding that motor axon subtype does not specify any facet of proprioceptor identity based on these studies and our findings is erroneous for two reasons: (1) it assumes that the only function of proprioceptor muscle-type identity is to establish patterned monosynaptic connectivity with motor neurons; and (2) it dismisses a role for peripherally specified features of motor neuron subtype identity in assigning proprioceptor subtype. Because we performed our proprioceptor muscle-type screen at P1, the differential expression of some of these genes could be specified by late-onset features of motor neuron subtype identity. Thus, while our experiments indicate that motor axon is not the tissue substrate of *cdh13* induction, it remains possible that expression of one or more of the genes identified in our screen is assigned by motor axon.

4 Limb mesenchyme influences proprioceptor muscle-type identity

4.1 Introduction

The limb mesenchyme plays a critical role in diverse aspects of limb development ranging from motor axon guidance to muscle cleavage patterning (Kardon et al., 2003; Stifani, 2014). Despite the known roles of mesenchyme in shaping elements of spinal motor circuitry, direct assessment of its contribution to patterning proprioceptor subtype identity has been prevented by the lack of proprioceptor genetic markers. In this chapter, I assess the involvement of the mesenchyme in specifying proprioceptor muscle-type identity by assaying proprioceptor gene expression in mice in which the dorsoventral identity of the mesenchyme has been genetically altered to a double-ventral or double-dorsal fate.

To achieve these phenotypes, we manipulated expression of the transcription factor Lmx1b, which is expressed by dorsal mesenchyme and patterns dorsal limb morphology (Figure 4.1A). I first demonstrate that the dorsoventral morphology of the shank in *Lmx1b* loss- or gain-of-function mutants is converted to a double-ventral or double-dorsal phenotype. I next show that generic features of proprioceptor development are maintained in these genetic backgrounds. Finally, I demonstrate that the proprioceptor expression of several muscle-type markers is

altered in these mutant backgrounds in accord with the nature of the dorsoventral conversion, indicating that proprioceptor identity is imposed by spatially confined signals from the limb mesenchyme.

4.1.1 Mesenchymal signals pattern dorsoventral limb morphology

The developing limb is often viewed as a Cartesian coordinate system, with patterning cues distributed along the orthogonal anterior-posterior, proximodistal, and dorsoventral axes (Wolpert, 1969). The final form of the limb is a consequence of inductive events occurring along these axes and the interactions between them (Capdevila and Izpisua Belmonte, 2001; Johnson and Tabin, 1997). The limb mesenchyme supplies much of the positional information that instructs mature limb morphology along the cardinal limb axes (Bénazet and Zeller, 2009).

When considering the role of limb mesenchyme in specifying proprioceptor muscle-type gene expression, two findings led us to narrow our focus to the dorsoventral axis, which delineates the flexor and extensor compartments of the mature limb typified by the TA (dorsal ankle flexor) and GS (ventral ankle extensor) synergist groups. First, dorsoventral limb character patterned by the mesenchyme has been reported to influence proprioceptor connectivity with motor neurons (Wenner and Frank, 1995). Second, many of the candidate genes identified in our screen of muscle-type proprioceptors segregate with respect to proprioceptor innervation along the dorsoventral axis: *cdh13*, *vstm2b*, *sema5a*, and *crtac1* exhibit

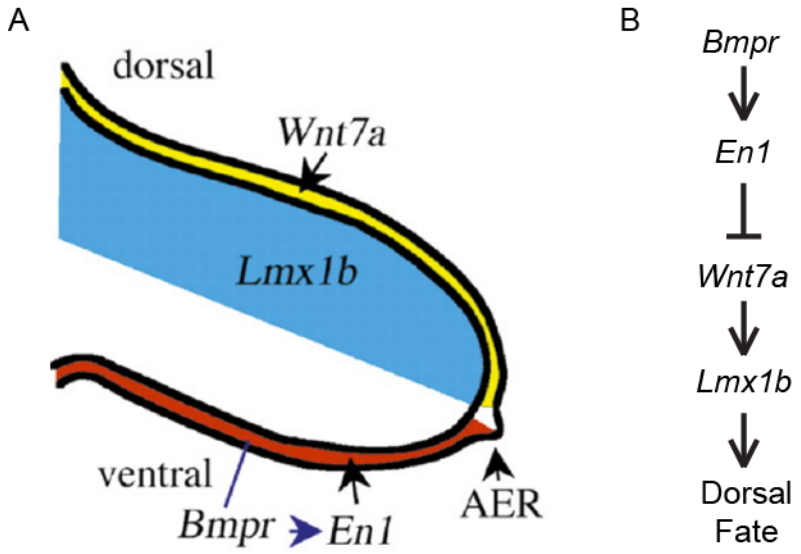

Figure 4.1 Specification of the dorsoventral limb axis

(A) The expression patterns of genes that regulate dorsoventral patterning of the limb mesenchyme. This schematic depicts a transverse section of the limb bud, with proximal to the left and distal to the right ending in the AER (apical ectodermal ridge). Dorsal is at top and ventral is at bottom. (B) Model for the genetic pathway regulating dorsoventral patterning of the hindlimb. Bmpr signaling in the limb ectoderm is required for En1 expression (red in A) in the ventral ectoderm. En1 suppresses the expression of Wnt7a (yellow) in ventral ectoderm, thereby restricting its expression to dorsal ectoderm. Wnt7a has been shown to induce the expression of Lmx1b (blue), which is necessary and sufficient for limb dorsalization, in the mesenchyme underlying the dorsal ectoderm. Adapted from Ahn et al., 2001.

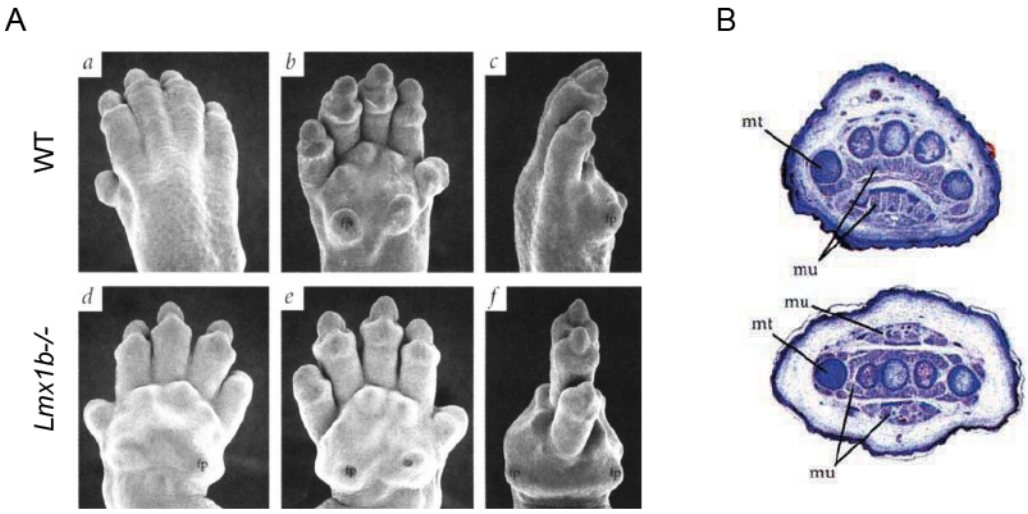

Figure 4.2 Ventralization of dorsal limb in *Lmx1b*$^{-/-}$ mice

(A) Scanning electron micrographs of wild-type (a-c) and mutant (d-f) e16.5 forelimbs. Dorsal (a, d), ventral (b, e) and posterior (c, f) views are shown. External dorsal features (hair follicles) are lost in mutants and are replaced by ventral features (foot pads, fp). In addition, the characteristic ventral flexure of digits is absent in mutants (compare panels c and f). (B) Limb histology of *Lmx1b* homozygous mutants stained with Mallory's trichrome. Transverse sections of wild-type (upper) and mutant (lower) newborn hindlimbs at the level of the metatarsals (mt), with dorsal limb toward the top of the figure. Note the duplication of ventral musculature (mu) in mutant animals. Adapted from Chen et al., 1998.

all-or-none distinctions between proprioceptors innervating the dorsal TA group versus ventral GS group. We therefore sought a genetic method by which to manipulate the dorsoventral identity of the limb mesenchyme.

The dorsoventral limb axis is specified through a series of epithelial-mesenchymal interactions. A simplified model holds that the morphogen Wnt7a, expressed in dorsal ectoderm, induces expression of the LIM-homeodomain transcription factor Lmx1b in dorsal limb mesenchyme (Figures 4.1A and B; Riddle et al., 1995; Vogel et al., 1995). In ventral ectoderm, the transcription factor En1 is induced by BMP signaling to repress expression of Wnt7a and Lmx1b in ventral ectoderm and mesenchyme, respectively (Figures 4.1A and B; Ahn et al., 2001; Davis et al., 1991; Gardner and Barald, 1992; Loomis et al., 1996).

In reality, the situation in the embryo is far more complex. In *wnt7a* mutants, *lmx1b* expression is only lost from the distal anterior mesenchyme, indicating that additional signals must act to regulate its dorsoventral expression (Cygan et al., 1997; Loomis et al., 1998). Likewise, in *en1* mutants, *lmx1b* is expressed only in proximal ventral mesenchyme, despite the disinhibition of *wnt7a* expression throughout the ventral ectoderm (Loomis et al., 1998). Nevertheless, epistasis analyses of double mutants indicate that Lmx1b is the only relevant target of Wnt7a and En1 with respect to dorsoventral patterning (Chen and Johnson, 2002). Furthermore, Lmx1b loss- and gain-of-function studies have demonstrated that its

expression by the mesenchyme is both necessary and sufficient to instruct dorsal fate during limb development (Riddle et al., 1995; Vogel et al., 1995).

In *Lmx1b*$^{-/-}$ mice, dorsal mesenchyme acquires a ventral mesenchymal identity. As a result, characteristic features of dorsoventral polarity, including the shape of the phalanges, tendon morphology, and muscle arrangement, are lost at the level of the digits, which acquire a mirror-symmetric ventral-ventral appearance (Figures 4.2A and B; Chen et al., 1998). Lineage tracing studies have shown that *lmx1b*-expressing mesenchymal cells contribute to dorsal bone, tendon, cartilage, and muscle connective tissue (Li et al., 2010). However, *lmx1b* is not expressed in muscle progenitors, indicating that its role in muscle patterning is non-cell autonomous (Li et al., 2010). Thus, Lmx1b expression by the mesenchyme patterns the dorsoventral axis of the developing limb through both cell-autonomous and non-cell autonomous mechanisms.

4.2 Results

4.2.1 Generation of *Vstm2b*::LacZ mice

To facilitate our analysis of *vstm2b* expression, we generated a LacZ reporter allele from targeted embryonic stem cells acquired from the International Knockout Mouse Consortium (Ringwald et al., 2011). Homologous recombination was used to generate ES cells carrying a transgenic allele with reporter, constitutive null and conditional null potential (Skarnes et al., 2011) at the *vstm2b* locus (Figure 4.3A). A

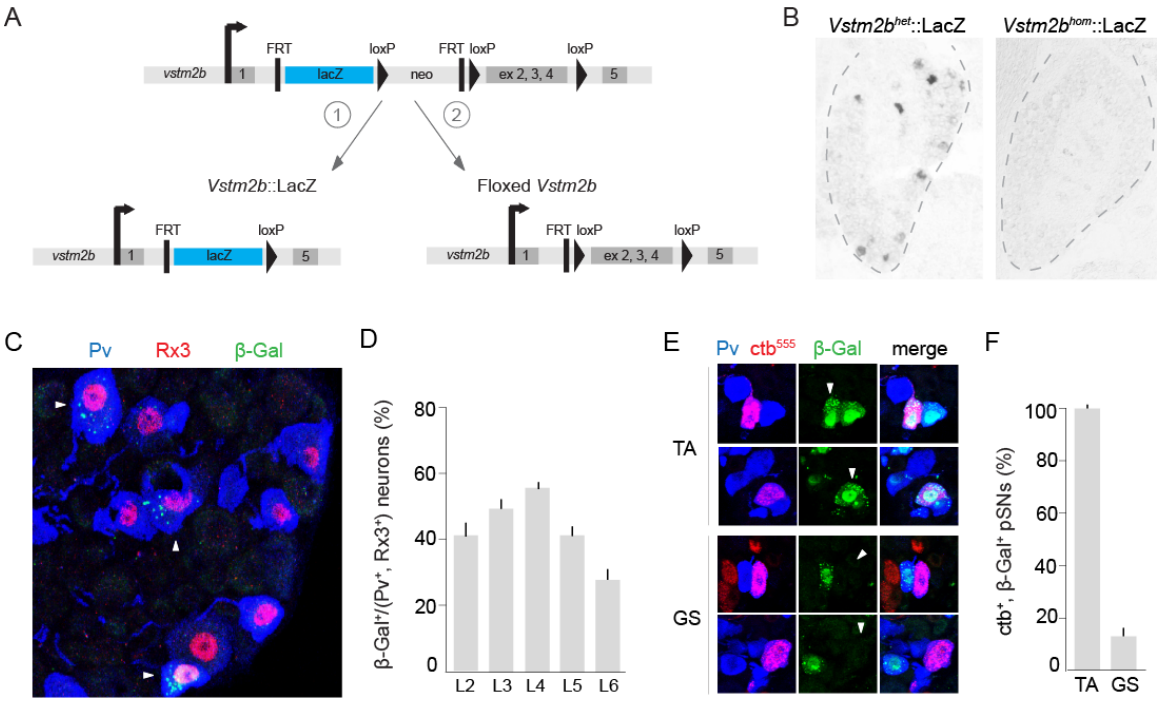

Figure 4.3 Generation of transgenic *vstm2b* reporter and knockout mouse lines

(A) Exons 2-4 of the *vstm2b* locus were replaced with a cassette containing an IRES-LacZ reporter and neomycin selection element flanked by FRT sites for downstream excision with Flp recombinase, as well as exons 2-4 flanked by loxP sites for downstream excision with Cre recombinase. *Vstm2b*::LacZ mice were generated by crossing the targeted allele to a *Protamine*::Cre deleter line, which initiates recombination in the male germline (1). A floxed *Vstm2b* allele was generated by crossing the targeted allele to *Rosa26*::FlpO deleter mice (2). (B) *Vstm2b*::LacZ is a null allele. Expression of *vstm2b* was examined in L4 DRG of P0 mice heterozygous or homozygous (*Vstm2b*^{het}::LacZ or *Vstm2b*^{hom}::LacZ) for the *Vstm2b*::LacZ allele using *in situ* hybridization with a probe specific to deleted exons 2-4. (C-D) β-gal expression was assessed by antibody staining of DRG neurons co-expressing Pv and Runx3 in P1 *Vstm2b*^{het}::LacZ mice. (C) *Vstm2b*::LacZ expression is restricted to proprioceptors. The punctate appearance of β-gal antibody staining is indicative of vesicular packaging and has been observed in proprioceptors of other LacZ driver lines (Joriene De Nooij, personal communication). (D) β-gal expression in L2-L6 proprioceptors was observed in proportions similar to those of endogenous *vstm2b* expression. (E-F) *Vstm2b*::LacZ is expressed in TA but not GS proprioceptors. (E) TA or GS proprioceptors of *Vstm2b*^{het}::LacZ mice were retrogradely labeled with ctb^{555} and assessed at P1 for expression of β-gal protein. (F) Muscle-type specificity of β-gal expression in *Vstm2b*^{het}::LacZ mice mimics that of *vstm2b* in wild-type mice.

Protamine::Cre deleter line (O'Gorman et al., 1997) was used to excise the Neo selection cassette as well as *vstm2b* exons 2-4 in the male germline to yield a *Vstm2b*::LacZ reporter allele with constitutive null potential (Figure 4.3A1). We also utilized the *Rosa26*::FlpO deleter line (Raymond and Soriano, 2007) to produce a floxed *Vstm2b* allele for the generation of conditional mutants (Figure 4.3A2).

We first sought to establish that *Vstm2b*::LacZ is a null allele. To this end, we examined *vstm2b* RNA expression in homozygous *Vstm2b*::LacZ mice using a probe complementary to deleted exons 2-4. We observed no *vstm2b* signal in *Vstm2b*::LacZ homozygotes, in contrast to the population of large-diameter DRG neurons strongly expressing *vstm2b* in heterozygotes (Figure 4.3B). We also noted the absence of *vstm2b* expression in spinal motor neurons and interneurons of *Vstm2b*::LacZ homozygotes (data not shown). We were therefore satisfied that *Vstm2b*::LacZ is a null allele.

We next assessed the expression pattern of the *Vstm2b*::LacZ allele in heterozygous mice. Notably, we observed that *Vstm2b*::LacZ reporter expression was confined to DRG neurons expressing both Pv and Runx3 (Figure 4.3C), the coincidence of which defines the proprioceptive sensory lineage (de Nooij et al., 2013). *Vstm2b* is therefore the first gene identified whose expression among DRG neurons is definitively restricted to a proprioceptor subset. The proportion of LacZ^{on} proprioceptors in DRG L2-L5 is similar to the proportion of *vstm2b*^{on}/*pv*^{on} neurons observed by *in situ* hybridization (Figure 4.3D; refer to Figure 2.5F), suggesting that

the *Vstm2b*::LacZ allele recapitulates endogenous *vstm2b* expression. To confirm the muscle-type specificity of LacZ reporter expression, we injected ctb^{555} into TA or GS muscle in *Vstm2b*::LacZ heterozygotes and immunostained for β-gal and Pv protein (Figure 4.3E). We observed that 100% (23/23) of backfilled TA neurons expressed β-gal, whereas ~14% (6/44) of backfilled GS neurons expressed the protein (Figure 4.3F; β-gal^{on} GS proprioceptors are likely the result of ctb diffusion into apposing muscles receiving *vstm2b*^{on} proprioceptor innervation). Thus, muscle-type specificity of *vstm2b* expression is preserved in *Vstm2b*::LacZ mice.

β-gal protein does not readily diffuse into axons (Callahan and Thomas, 1994) and is not present at the muscle spindle. We were therefore unable to use the *Vstm2b*::LacZ allele assess the expression status of proprioceptors innervating individual muscles or to examine the specificity of central connections with motor neurons.

4.2.2 Manipulation of mesenchymal *Lmx1b* expression results in dorsoventral conversion of shank tissues

In order to examine the role of limb mesenchyme in establishing proprioceptor gene expression profiles, we analyzed *cdh13*, *vstm2b*, *sema5a* and *crtac1* expression in mice in which the normal dorsoventral character of the limb mesenchyme was genetically manipulated to either a double-ventral or double-dorsal fate.

We decided to focus this analysis on proprioceptors innervating the shank, where all muscle-type proprioceptor genes exhibit a clear all-or-none distinction in expression along the dorsoventral axis: all muscles of the dorsally derived anterior crural group (TA, EDL, PL) are innervated by *cdh13*^{on}, *vstm2b*^{on}, *sema5a*^{on} and *crtac1*^{off} proprioceptors, whereas all muscles of the ventrally derived posterior crural group (GS, Sol, Plan) are innervated by *cdh13*^{off}, *vstm2b*^{off}, *sema5a*^{off} and *crtac1*^{on} proprioceptors. This clear distinction is lost at the more proximal level of the thigh: *vstm2b*, for example, is expressed primarily by proprioceptors innervating the dorsal quadriceps group, but a cohort of ventral hamstring/adductor proprioceptors also expresses the gene (refer to Figure 2.5H).

To induce dorsoventral mesenchymal conversion, we manipulated expression of Lmx1b in the limb mesenchyme. We assessed the affect of double-ventral limb mesenchyme (d/v → v'/v) on proprioceptor subtype identity by examining proprioceptor gene expression in an *Lmx1b*$^{-/-}$ background (Chen et al., 1998). To generate mice with double-dorsal limb mesenchyme (d/v → d/d'), *lmx1b* was expressed in ventral limb mesenchyme by crossing *Rosa26*::lsl.Lmx1b to *Prx1*::Cre mice, such that Cre expression is directed throughout the limb mesenchyme from ~e9.5 (termed *Prx1*^{Lmx1b}; Li et al., 2010), prior to hindlimb innervation by motor and sensory axons.

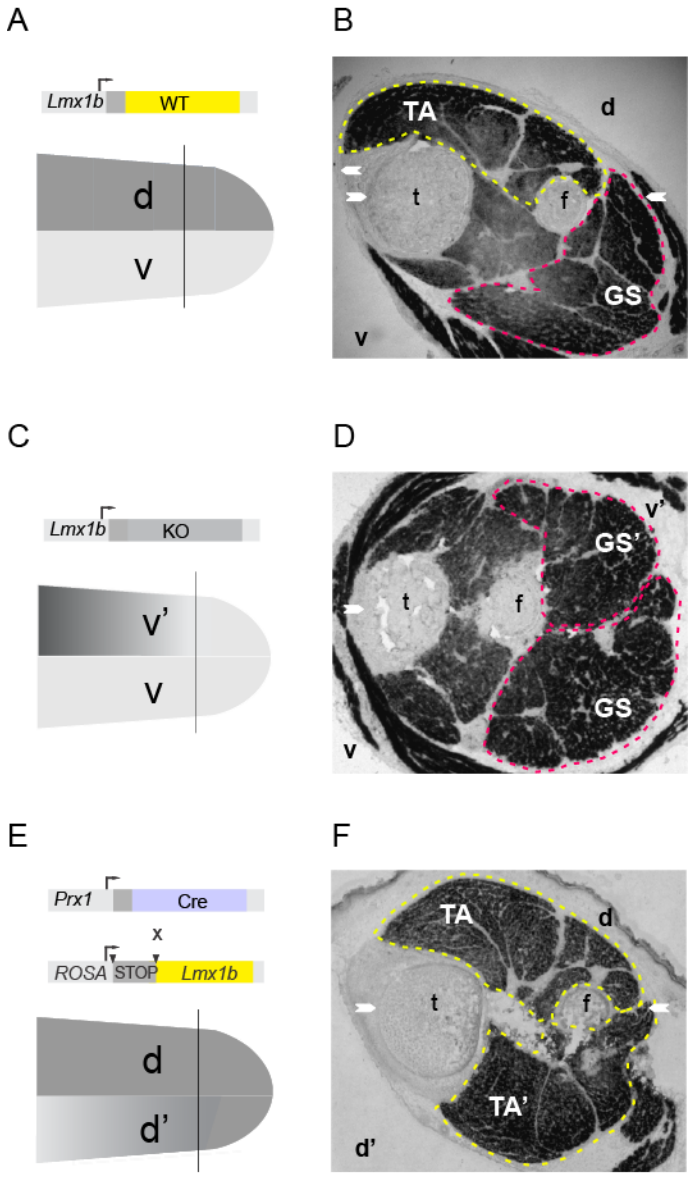

Figure 4.4 Dorsoventral conversion of the shank in *Lmx1b*$^{-/-}$ and *Prx1*^{Lmx1b} mice

(A, C, and E) Illustrations depicting the dorsal or ventral status of the limbs of WT, *Lmx1b*$^{-/-}$ and *Prx1*^{Lmx1b} mice (dorsal, dark gray; ventral, light gray) and the genetic strategies used to alter mesenchymal *Lmx1b* expression. Vertical lines indicate the proximodistal locations of the cross sections shown in B, D, and F. (B, D, and F) Anatomical changes in the shanks of *Prx1*^{Lmx1b} and *Lmx1b*$^{-/-}$ mice are illustrated by *in situ* hybridization for myosin in cross sections of p0 WT (B), *Lmx1b*$^{-/-}$ (D) and *Prx1*^{Lmx1b} (F) hindlimbs. In WT mice, yellow and pink dotted lines demarcate dorsal TA and ventral GS muscle synergist groups, respectively. Note the near mirror image duplication of dorsal muscles in *Prx1*^{Lmx1b} mice (F) or ventral muscles in *Lmx1b*$^{-/-}$ mice (D; t: tibia, f: fibula, d: dorsal, v: ventral, d': duplicated dorsal, v': duplicated ventral).

Manipulating the expression of Lmx1b in limb mesenchyme by genetic loss- or gain-of-function results in the transformation of muscle, bone, and connective tissue to double-ventral or double-dorsal character, respectively. While this transformation has been characterized for the digits (Chen and Johnson, 2002; Chen et al., 1998), it has been reported that limb ventralization in *Lmx1b*$^{-/-}$ mice is incomplete at proximal limb levels (Chen et al., 1998; Feenstra et al., 2012). We therefore examined the ventralization and dorsalization of shank tissues in *Lmx1b*$^{-/-}$ and *Prx1*^{Lmx1b} mice, respectively, by generating cross-sections of the hindlimb from ankle to knee and staining for myosin to delineate muscle morphology (Figure 4.4A-C). Whereas wild-type hindlimbs exhibit asymmetric morphology in which the antagonist TA and GS muscle groups are easily delineated (Figure 4.4A), *Lmx1b*$^{-/-}$ and *Prx1*^{Lmx1b} mice display near mirror-symmetric morphology. In *Lmx1b*$^{-/-}$ mice, we observed a clear duplication of ventral musculature (termed v'), including the GS, Sol, and Plan, in place of the dorsal TA synergist group (Figure 4.4B). Likewise, in *Prx1*^{Lmx1b} mice, we observed duplicated dorsal musculature (termed d'), including the TA, EDL, and PL, in place of the ventral GS group (Figure 4.4C). Thus, the dorsoventral conversion of limb mesenchyme is fully penetrant at the level of the shank.

4.2.3 Proprioceptor gene expression following innervation of double-ventral shank

Prior to examining the impact of mesenchymal transformation on proprioceptor muscle-type gene expression, we sought to determine whether generic proprioceptor development is affected in *Lmx1b*$^{-/-}$ and *Prx1*^{Lmx1b} mice. We found that the incidence of *pv*^{on} neurons in L2 and L5 DRG did not differ significantly between wild-type, *Lmx1b*$^{-/-}$ and *Prx1*^{Lmx1b} mice (Figure 4.5A). Furthermore, the number of dorsal and ventral shank muscle spindles was unchanged in altered dorsoventral backgrounds (Figure 4.5B). Thus, dorsoventral manipulation of the limb mesenchyme does not significantly alter generic aspects of hindlimb-innervating proprioceptor development.

We first examined the expression of proprioceptor genes in *Lmx1b*$^{-/-}$ mice. *Lmx1b*$^{-/-}$ mice die within 24 h of birth (Chen et al., 1998), precluding the identification of muscle-type proprioceptors by ctb^{555} retrograde labeling. We therefore compared the proportion of proprioceptors expressing *cdh13* or *vstm2b* in wild type and *Lmx1b*$^{-/-}$ mice at ~e18, just prior to birth. For *cdh13*, we observed statistically significant decreases of ~18% and ~14% in the number of *cdh13*^{on} proprioceptors in L4 and L5 DRG, respectively (Figure 4.6B; $p<0.001$) - ganglia which contain the bulk of proprioceptors innervating the TA group muscles of the dorsal shank in wild-type mice. For *vstm2b*, we observed a similar decrease of ~15% in the number of *vstm2b*^{on} proprioceptors in DRG L4, where a large portion of TA group proprioceptors are located (Figures 4.6A and C; $p<0.001$). The lack of a significant decrease in *vstm2b*-expressing proprioceptors across lumbar ganglia might be attributed to the incomplete ventralization of thigh and hip musculature in

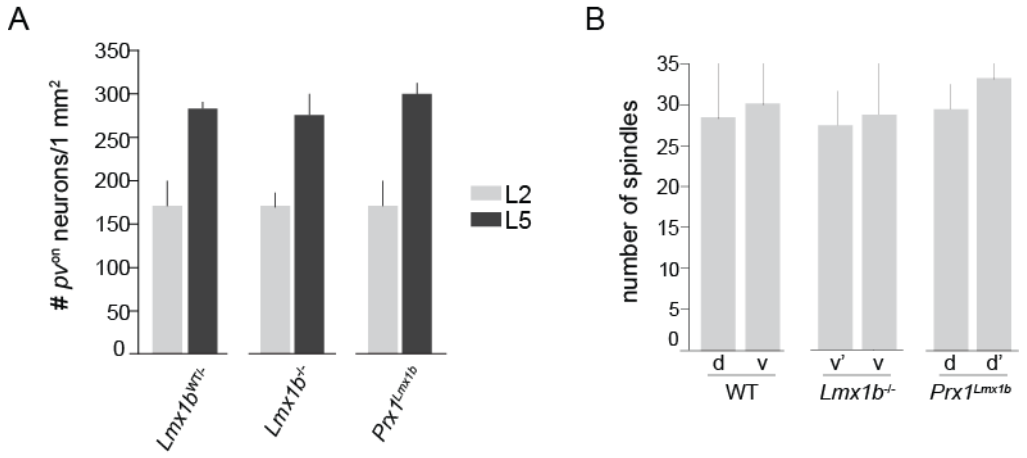

Figure 4.5 Generic features of proprioceptor development are unperturbed in *Lmx1b*$^{-/-}$ and *Prx1*^{Lmx1b} mice

(A) The density of proprioceptors, assessed by *pv* labeling, was unchanged in DRG L2 and L5 of *Lmx1b*$^{-/-}$ and *Prx1*^{Lmx1b} compared to wild-type mice. *(B)* *Lmx1b*$^{-/-}$ and *Prx1*^{Lmx1b} mice possess a normal complement of muscle spindles. Spindles were identified by Pv immunostaining of 25 µm cryosections of dorsally or ventrally located shank muscles in P0 wild-type, *Prx1*^{Lmx1b} and *Lmx1b*$^{-/-}$ mice.

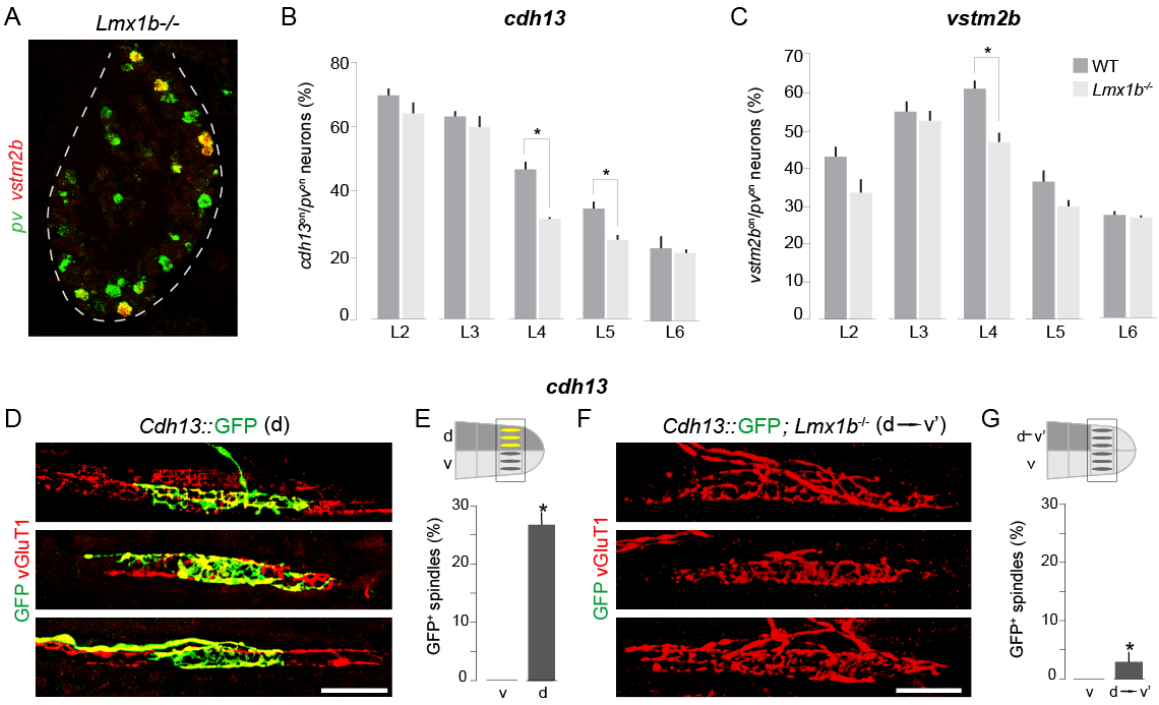

Figure 4.6 Proprioceptor gene expression in *Lmx1b*$^{-/-}$ mice

(A-C) *vstm2b* and *cdh13* expression in lumbar DRG of e18 *Lmx1b*$^{-/-}$ mice. (A) Gene expression in proprioceptors was examined by double FISH for *cdh13* or *vstm2b* and *pv*. Shown here is the expression of *vstm2b* in DRG L4. (B) The proportion of *cdh13*^{on} proprioceptors decreased in each lumbar DRG of *Lmx1b*$^{-/-}$ mice compared to the respective ganglion in wild-type mice, with significant differences observed for DRG L4 and L5 (n=3; *p < 0.001, Student's t test). Data are represented as the mean ± SEM. (C) The proportion of *vstm2b*^{on} proprioceptors decreased in each lumbar DRG of *Lmx1b*$^{-/-}$ mice compared to the respective ganglion in wild-type mice, with a significant difference observed for DRG L4 (n=5; p < 0.001, Student's t test). Data are represented as the mean ± SEM. (D-G) Proprioceptors supplying duplicated ventral shank in *Lmx1b*$^{-/-}$ mice lack *cdh13* expression. Shank muscles of wild-type *Cdh13*::GFP (D and E) and *Lmx1b*$^{-/-}$, *Cdh13*::GFP (F and G) mice analyzed for GFP^{+} spindle afferents. (E and G) Percentage of GFP^{+} muscle spindles in dorsally or ventrally innervating proprioceptors in *Cdh13*::GFP (E) and *Lmx1b*$^{-/-}$, *Cdh13*::GFP (G) mice (*p < 0.001, Student's t test, when comparing dorsally located muscles in *Lmx1b*$^{-/-}$ to wild-type dorsal muscles; n=3 mice/genotype). (D and F) GFP status of vGluT1^{+} endings in muscle spindles supplying dorsally located muscles in *Cdh13*::GFP (D) and *Lmx1b*$^{-/-}$, *Cdh13*::GFP (F) mice. Data are represented as the mean ± SD. Scale bars, 50 µm.

Lmx1b$^{-/-}$ mice. Alternatively, this phenotype might be explained by the wild-type cohort of *vstm2b*^{on} proprioceptors innervating ventral thigh musculature; these neurons would be unaffected by the d → v' conversion of limb tissues in *Lmx1b*$^{-/-}$ hindlimbs. Nevertheless, these results imply that dorsal mesenchymal character is required to induce *cdh13* and *vstm2b* expression in TA group proprioceptors.

Our inability to examine *vstm2b* status at the muscle spindle precluded an analysis of its expression in proprioceptors supplying v' muscles of *Lmx1b*$^{-/-}$ mice. However, we used our ability to genetically label *cdh13*^{on} proprioceptors at the muscle spindle to assess *cdh13* expression in the muscles of v' shank. We crossed *Lmx1b*$^{-/-}$ mice to *Cdh13*::GFP homozygotes and assayed muscle spindles for the presence of GFP+ afferents at e18, following tamoxifen activation of Cre recombinase at e14.5 (Figures 4.6D-G). We dissected v and v' shank muscles from *Lmx1b*$^{-/-}$, *Cdh13*::GFP mice as well as v and d shank muscles from *Lmx1b*^{WT}, *Cdh13*::GFP littermates and examined the GFP status of spindles in these muscles (Figures 4.5D-G). In the dorsal limb of wild-type mice, we found that ~28% of muscle spindles received GFP^{+} afferent innervation, consistent with the efficiency of tamoxifen-mediated Cre induction. In contrast, in *Lmx1b*$^{-/-}$ mutants, only ~2% of v' muscle spindles were associated with GFP^{+} sensory axon terminals (Figures 4.6D-G; $p<0.001$). In both wild-type and *Lmx1b*$^{-/-}$ mutant mice, spindles supplying ventral shank muscles lacked GFP^{+} proprioceptor terminals (Figures 4.6D-G). These results indicate that *cdh13* expression in proprioceptors is influenced by limb mesenchyme.

4.2.4 Proprioceptor gene expression following innervation of double-dorsal shank

We next examined the expression of proprioceptor genes in *Prx1*^{Lmx1b} mice. The postnatal viability of this line allowed us to examine gene expression in muscle-type proprioceptors identified by retrograde labeling. The expression of proprioceptor genes was assessed at P1 after injection of ctb^{555} into d' shank muscles at P0 (Figures 4.6A-P). We found that ~66% of *pv*^{on} neurons innervating d' muscles in *Prx1*^{Lmx1b} mice exhibited *cdh13* expression, in contrast to wild-type mice, where none of the proprioceptors innervating ventral shank muscles expressed *cdh13* (Figures 4.7A-D). All proprioceptors innervating dorsal shank muscles in *Prx1*^{Lmx1b} mice expressed *cdh13*, indicating no deviation from the normal *cdh13* profile (Figures 4.7B and D).

To assess the expression of *vstm2b* in shank-innervating proprioceptors of *Prx1*^{Lmx1b} mice, we crossed *Prx1*^{Lmx1b} animals to *Vstm2b*::LacZ mice and examined retrogradely labeled shank proprioceptors for β-gal expression at P1 (Figure 4.7E-H). We found that ~96% of Pv^{on} neurons supplying ventrally located d' muscles in *Prx1*^{Lmx1b} mice expressed β-gal, whereas only ~5% of ventral shank muscles in wild-type mice expressed β-gal. As expected, all proprioceptors supplying dorsal shank muscles in *Prx1*^{Lmx1b} mice expressed β-gal, in line with the endogenous profile of *vstm2b* expression (Figures 4.7 F and H).

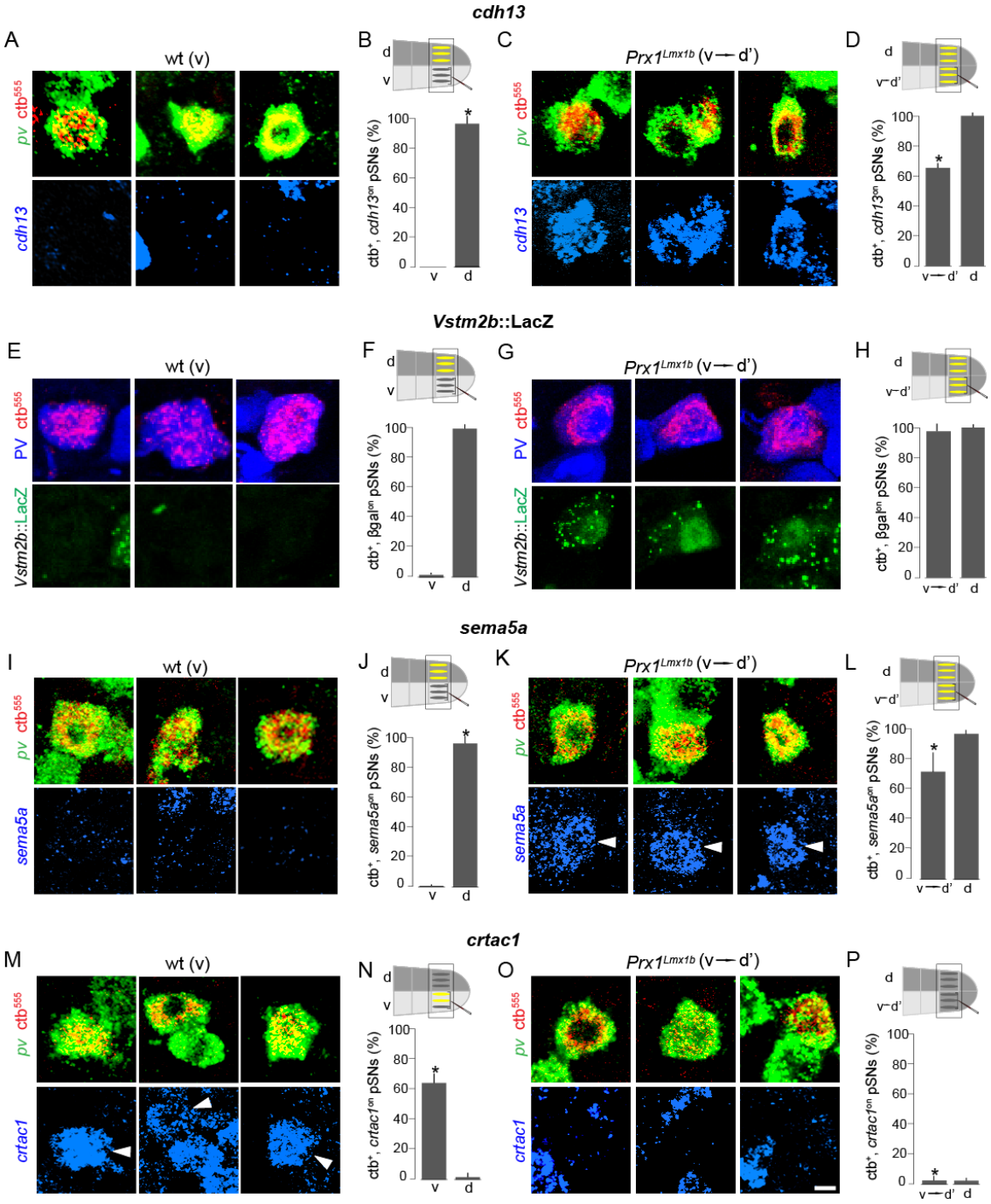
cdh13
A
wt (v)
pv ctb555
cdh13
B
d
v
ctb+, cdh13on pSNs (%)
v
d
C
Prx1Lmx1b (v→d')
D
v→d'
Vstm2b::LacZ
E
PV ctb555
Vstm2b::LacZ
F
ctb+, βgalon pSNs (%)
G
H
sema5a
I
sema5a
J
ctb+, sema5aon pSNs (%)
K
L
crtac1
M
crtac1
N
ctb+, crtac1on pSNs (%)
O
P

Figure 4.7 Proprioceptor gene expression in *Prx1^{Lmx1b}* mice

(A-P) Proprioceptors supplying duplicated dorsal shank in *Prx1^{Lmx1b}* mice express *cdh13*, *vstm2b*, and *sema5a*, but not *crtac1*. Shank proprioceptors of wild-type and *Prx1^{Lmx1b}* mice were identified by ctb^{555}, and their *cdh13* (A-D), *sema5a* (I-L), and *crtac1* (M-P) expression was assessed by double FISH with *pv*. *Vstm2b*::LacZ expression (E-H) was assessed by immunostaining for β-gal and Pv. (A-P) Retrogradely labeled proprioceptors supplying ventrally located muscles in wild-type and *Prx1^{Lmx1b}* mice. Scale bar, 10 μm. Dorsally or ventrally innervating shank proprioceptors expressing *cdh13* (B, D), *Vstm2b*::LacZ (F, H), *sema5a* (J, L), or *crtac1* (N, P) in wild-type and *Prx1^{Lmx1b}* mice (*p<0.001, Student's t test, when comparing ventrally located shank muscles in *Prx1^{Lmx1b}* to wild-type ventral muscles; n=3 mice/genotype/gene).

We also examined the expression of proprioceptor muscle-type genes *sema5a* and *crtac1* in *Prx1^{Lmx1b}* mice in proprioceptors supplying d' shank muscles after retrograde labeling. We found that ~72% of *pv*^{on} neurons innervating d' muscles in *Prx1^{Lmx1b}* mice exhibited *sema5a* expression, in contrast to wild-type mice, where none of the proprioceptors innervating ventral shank muscles expressed *sema5a* (Figures 4.6I-L; $p<0.001$). Conversely, the expression of *crtac1* in *pv*^{on} neurons was reduced from ~67% in wild-type mice to ~2% in *Prx1^{Lmx1b}* mice (Figures 4.7M-P). No deviation from the normal *sema5a* and *crtac1* expression profile was observed in proprioceptors innervating dorsal shank in *Prx1^{Lmx1b}* mice (Figure 4.7K, L, O and P).

Thus, we conclude that expression of the muscle-type proprioceptor genes *cdh13*, *vstm2b*, *sema5a*, and *crtac1* is influenced by the dorsoventral character of the limb mesenchyme.

4.3 Discussion

Genetic manipulation of the dorsoventral identity of limb mesenchyme to a double-dorsal or double-ventral character allowed me to assess the role of mesenchymal character in patterning the expression of dorsally or ventrally restricted proprioceptor genes. Before assessing proprioceptor gene expression in these mutants, I confirmed that double-dorsal and double-ventral transformations were fully penetrant at the shank level of the hindlimb and established that generic

features of proprioceptor development were unperturbed. I found that proprioceptor muscle-type gene expression is respecified when confronted with ectopic limb morphology, demonstrating that the dorsoventral character of the limb mesenchyme is involved in patterning proprioceptor gene expression.

4.3.1 Regionally restricted limb mesenchymal signals induce proprioceptor gene expression

The dorsoventral restriction of *cdh13*, *vtsm2b*, *sema5a*, and *crtac1* proprioceptor expression could have its basis in inductive and/or repressive mesenchymal signals. The simplest scheme holds that inductive signals expressed selectively by dorsal and distal limb mesenchyme induce *cdh13* expression in proprioceptors that innervate this mesenchymal domain, whereas a dorsal inductive signal unrestricted along the proximodistal axis may induce *vstm2b* expression. Conversely, an inductive signal expressed selectively by ventral-distal limb mesenchyme may induce *crtac1* proprioceptor expression (Figure 4.8). Under this model, in *Lmx1b*$^{-/-}$ mice with ventralized limbs, dorsal cues specifying *cdh13* and *vstm2b* expression are absent, resulting in the loss or reduction of proprioceptors expressing these genes (refer to Figure 4.6). Similarly, loss of ventral inductive signals in the dorsalized limbs of *Prx1*^{Lmx1b} mice would result in the loss of *crtac1*-expressing proprioceptors. In contrast, dorsalization results in the ectopic expression of dorsal inductive cues, leading to the expression of *cdh13*, *vstm2b*, and *sema5a* in proprioceptors innervating ventrally situated musculature (Figure 4.7).

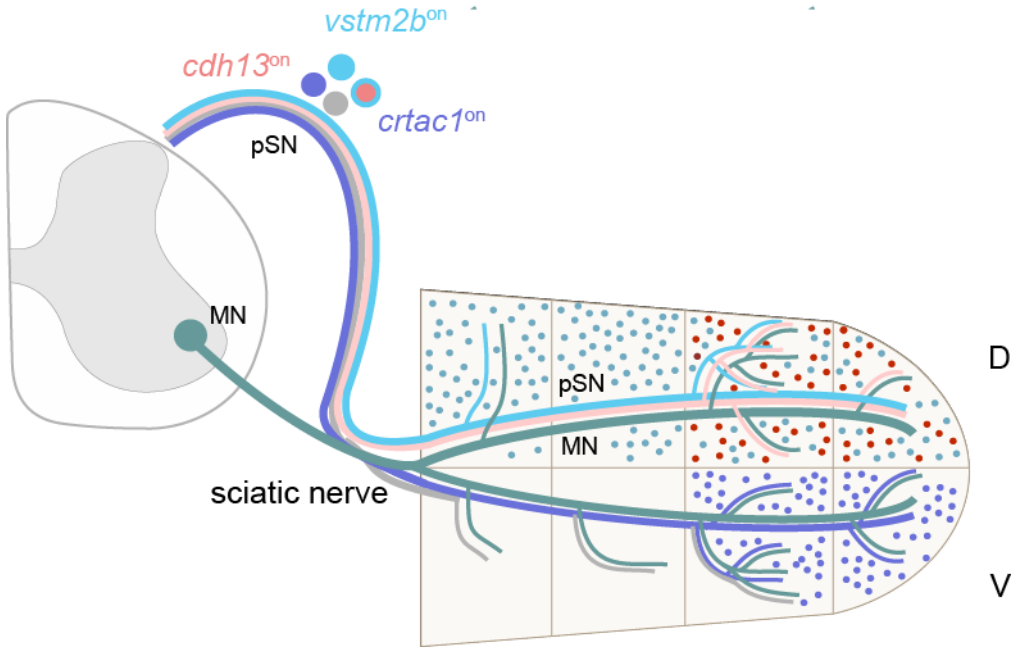

Figure 4.8 A model for the induction of proprioceptor gene expression by limb mesenchyme

Patterning mechanisms for proprioceptor gene expression include *cdh13*, *vstm2b*, or *crtac1* inductive signals in dorsodistal, dorsal, or ventrodistal hindlimb, respectively. Inhibitory and inductive signals may pattern proprioceptor gene expression along these limb axes. Note that the *cdh13*^{on} population is a subset of the *vstm2b*^{on} population.

More complex scenarios are also possible. In the case of *cdh13*, the intersection of repressive and inductive signals could form a grid-like system of positional information such that *cdh13* expression is shaped by the presence of both an inductive signal along the entire proximodistal axis of the dorsal limb mesenchyme and an independent proximal repressive signal.

4.3.2 Proprioceptor gene expression along the proximodistal limb axis

Our experiments in *Lmx1b*$^{-/-}$ and *Prx1*^{Lmx1b} mice have produced insight into the induction of proprioceptor genes along the dorsoventral limb axis. However, the expression of *cdh13*, *sema5a*, and *crtac1* is similarly restricted along the proximodistal limb axis, indicating that the inductive or repressive signals patterning their expression must mimic this compartmentalization. How might the proximodistal restriction of proprioceptor patterning cues be achieved?

The limb proximodistal axis is specified by opposing gradients of the morphogens retinoic acid (RA) and fibroblast growth factor (FGF) (Mercader et al., 2005). Together, these gradients result in the definition of mesenchymal domains of Hox gene expression that correspond to the thigh, shank and foot of the mature limb (Bénazet and Zeller, 2009). These molecular programs likely with dorsoventral patterning information interact to give rise to the restricted patterns of proprioceptor *cdh13*, *sema5a*, and *crtac1* expression observed in wild-type mice.

Experimental strategies for assessing the role of RA and FGF signaling in inducing proprioceptor gene expression are discussed in Chapter 7.

We had hoped that the expanded expression profile of *vstm2b* would yield insight into the role of dorsoventral mesenchyme at more proximal limb levels. However, due to the incomplete dorsalization and ventralization of the limbs of $Prx1^{Lmx1}$ and *Lmx1b* mice at levels proximal to the shank (Sebastian Poliak, personal communication), we could not assess the role of thigh or hip dorsoventral mesenchymal character on inducing *vstm2b* expression. The incomplete penetrance of limb ventralization and dorsalization in *Lmx1b* and $Prx1^{Lmx1b}$ animals at levels proximal to the shank is likely the result of interaction between proximodistal and dorsoventral patterning systems, emphasizing the spatial and temporal complexity of limb development.

Notably, the proprioceptor genes examined in this chapter, with the exception of *vstm2b*, exhibit a distal bias in expression. It is interesting to consider how a proximal bias in proprioceptor gene expression might be achieved in light of the fact that all limb-innervating neurons must pass through the proximal limb mesenchyme. Two putative mechanisms involving temporal regulation of inductive cues might resolve this phenomenon. The first is to delay the expression of proximal mesenchyme-derived patterning cues until after most sensory axons have projected through the proximal limb and into more distal domains. Segregation of axons at the lumbar plexus occurs at e10.5 and the proximal portion of the limb is traversed by

axons by e11.5 (Luria et al., 2008); if molecular correlates of proprioceptor muscle-type identity function to establish selective connectivity, the expression of a proximal cue by e12.5 would provide ample time for the induction of proprioceptor subtypes prior to the formation of sensory-motor synapses at ~e16.5. A second possible mechanism involves muscle-derived inductive cues. Myoblasts migrate into the limb and differentiate concomitant with innervation, and might therefore represent a temporally delayed source of inductive cues compared to mesenchyme.

4.3.3 Possible involvement of muscle in proprioceptor gene induction

Based on our experiments in *Lmx1b*$^{-/-}$ mice, we proposed a model for proprioceptor gene induction in which positionally restricted mesenchymal cues induce the expression of *cdh13*, *vstm2b*, *sema5a*, and *crtac1* in proprioceptor subsets. However, in addition to its ability to pattern proprioceptor gene expression, the dorsoventral identity of the mesenchyme has a marked effect on the pattern of muscle cleavage (see Figures 4.2 and 4.5). It is therefore possible that mesenchyme does not alter proprioceptor gene expression directly but rather acts through muscle to specify neuronal subtype identity. In Chapter 5, I examine whether the restriction of *vstm2b* to proprioceptors is the consequence of direct patterning by the mesenchyme or whether it arises indirectly due to the influence of mesenchyme on muscle patterning.

5 Limb muscle contributes to proprioceptor subtype specification

5.1 Introduction

In Chapter 4, I provide evidence that the limb mesenchyme contains cues that pattern proprioceptor gene expression. However, it is unclear whether these cues affect proprioceptors directly or indirectly through the non-cell autonomous influence of *lmx1b*-expressing mesenchyme on muscle patterning. This led me to examine the possibility that muscle is involved in patterning *cdh13* and *vstm2b* expression, the latter of which is restricted among DRG neurons to proprioceptors. In this chapter, I examine the role of myogenic precursors in patterning proprioceptor muscle-type identity by assaying proprioceptor *cdh13* and *vstm2b* expression in mutant mice devoid of limb muscle.

5.1.1 Sequential phases of limb muscle formation

During embryogenesis, skeletal muscle forms in the vertebrate limb from somites: round, epithelial structures derived from paraxial mesoderm (Christ and Ordahl, 1995). Muscle precursor cells, or myoblasts, delaminate from the dorsal part of the somite, called the dermomyotome, and migrate into the periphery, where they proliferate and differentiate into skeletal muscle (Figure 5.1). Migrating muscle precursors are generated at the occipital, cervical, and fore- and hindlimb levels of

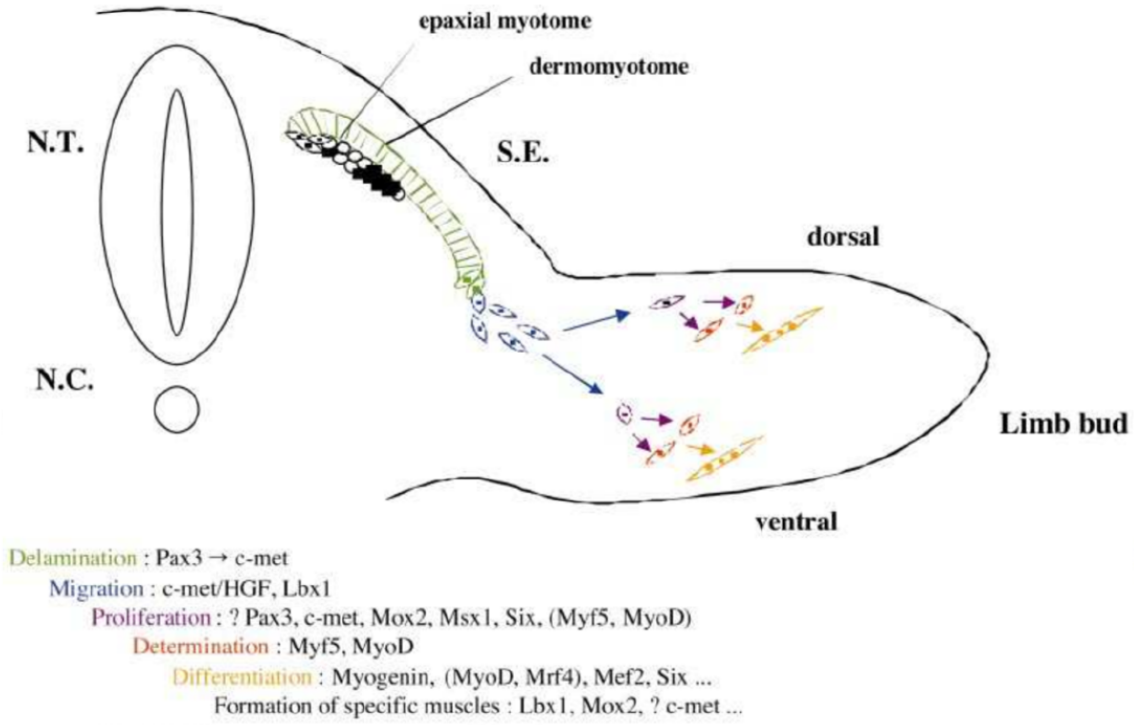

Figure 5.1 Factors involved in the formation of limb skeletal muscle

Schematic representation of skeletal muscle formation in the limb illustrating the different stages and genes involved at each stage. N.C., notochord; N.T., neural tube; S.E., surface ectoderm. Adapted from Buckingham et al., 2003.

the rostrocaudal body axis, where they give rise to skeletal muscles of the hypoglossal cord, diaphragm, and limbs, respectively. Myoblasts contributing to limb muscle migrate to the limb bud, where they segregate into separate dorsal and ventral streams of cells that aggregate to form the dorsal and ventral muscle masses (Schramm and Solursh, 1990). These masses subsequently subdivide into dorsal and ventral thigh, shank and foot muscle masses, which in turn cleave to form the individual muscles characteristic of the adult limb (Kardon, 1998; Lance-Jones, 1979).

The delamination of muscle progenitors from the dermomyotome requires an epithelial-mesenchymal transition involving the expression of several factors. Both delamination and migration are dependent on the expression of c-Met, a tyrosine kinase receptor, in muscle progenitors. The c-Met ligand HGF, also called scatter factor (SF), is expressed by the limb mesenchymal cells that delineate the migratory route traversed by myoblasts (Dietrich et al., 1999), thereby restricting the activation of c-Met and consequent delamination and migration of myoblasts to appropriate axial levels. Mutant mouse embryos lacking functional c-Met (Bladt et al., 1995) or HGF (Schmidt et al., 1995) are characterized by the absence of limb skeletal muscle. Transcription of the *c-met* gene depends on the expression of Pax3, a paired- and homeobox transcription factor, in muscle precursors (Epstein et al., 1996). Similar to mice deficient in c-Met or HGF, *Pax3* mutant mice lack limb muscle (Tajbakhsh et al., 1997); visualization of cells of the *pax3* lineage in *pax3* mutant mice has revealed that they do not delaminate from the hypaxial dermomyotome

(Buckingham et al., 2003) and are therefore unable to migrate away from their somite of origin.

The migration of delaminated muscle precursors into the limb bud requires expression of the homeodomain transcription factor Lbx1 (Figure 5.2), which is specified by Pax3 (Mennerich et al., 1998). Lbx1 expression is restricted to migratory precursors (Jagla et al., 1995; Figure 5.2A) and is induced before delamination, maintained during migration, and downregulated upon differentiation (Dietrich et al., 1998, 1999; Mennerich et al., 1998), coincident with its role in myoblast migration. In mice lacking Lbx1, myoblasts delaminate from the dermomyotome but fail to migrate laterally into the limb bud, resulting in limbs largely devoid of muscle (Figures 5.2B and C; Brohmann et al., 2000; Gross et al., 2000). Lbx1-deficient myoblasts retain the ability to migrate ventrally to give rise to tongue and diaphragm muscles, demonstrating that Lbx1 is necessary for the lateral, but not ventral, migration of hypaxial muscle precursors and suggesting that Lbx1 regulates responsiveness to a lateral migration signal emanating from the developing limb (Gross et al., 2000).

Migrating myoblasts retain proliferative capacity, allowing for the amplification of the precursor population at locations far from the somite. In vertebrates, the transcription factor Six1 is expressed during myogenesis and has been found to regulate myoblast proliferation. Mice deficient in *six1* exhibit appendicular and body wall muscles that are severely reduced in size, a phenotype

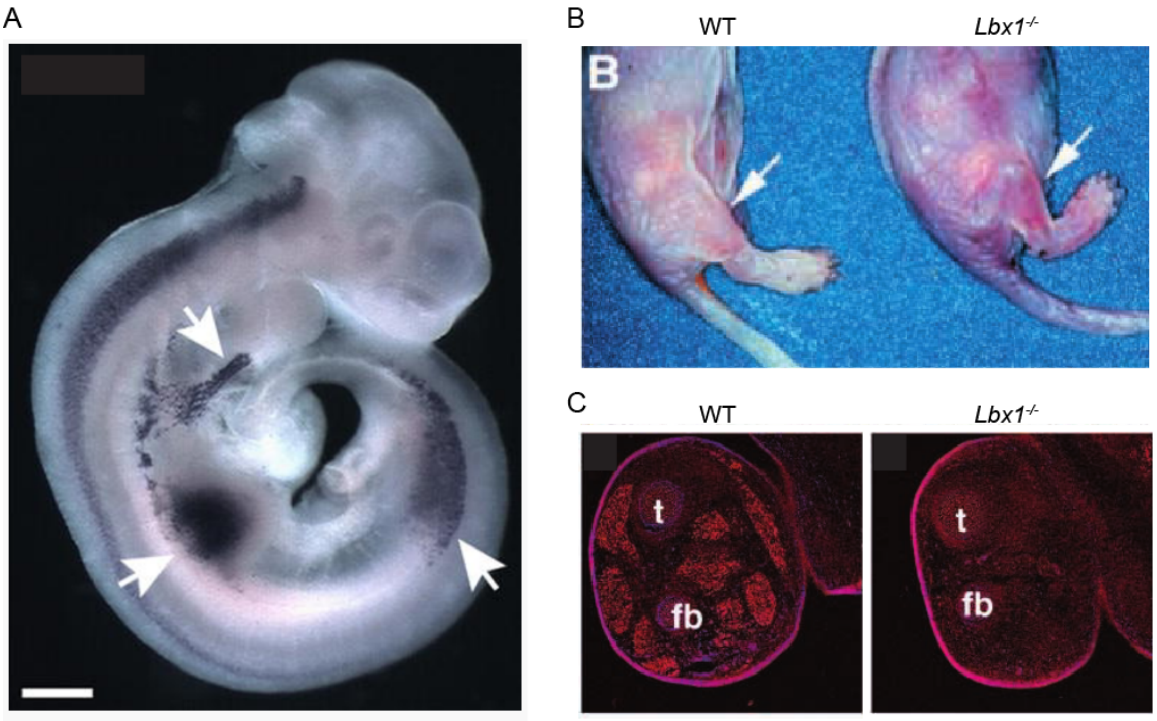

Figure 5.2 *Lbx1* is required for muscle precursor migration

(A) *Lbx1* expression is restricted to the hypaxial migrating myoblast lineage. Here, *lbx1* expression is demarcated by whole-mount *in situ* hybridization of muscle precursor cells in e10.5 mouse embryo with a probe specific to *Lbx1*. Arrows, counterclockwise from top, point toward muscle precursor cells migrating along the hypoglossal cord and into the fore- and hindlimbs. An additional stream of cells moves towards the diaphragm (not shown). Bar: 500 microns. Adapted from Vasyutina and Birchmeier, 2006. (B) Loss of *Lbx1* results in the failure of muscle precursors to migrate into the limb bud, leading to the development of muscleless limbs. Arrows point to the shanks of wild-type (left) and *Lbx1*$^{-/-}$ (right) mice. (C) Longitudinal sections through the shanks of e13.5 wild-type and *Lbx1*$^{-/-}$ embryos stained with an antibody against MyoD (red). Left: Section through the tibia (t) and fibula (f) showing muscles in the lower hindlimb of a wild-type embryo. Right: Same, but for an *Lbx1*$^{-/-}$ embryo. Note the complete absence of MyoD-expressing cells. (B and C) are adapted from Gross et al., 2000.

resulting not from a deficit in migration but rather in the proliferation and/or differentiation of muscle precursors (Laclef et al., 2003; Li et al., 2003).

The commitment and differentiation of myoblasts to a muscle cell fate, a process known as myogenesis, is initiated by the upregulation of several muscle-specific factors. Two basic helix-loop-helix transcription factors, Myf5 and MyoD, cooperate in the determination of muscle precursors, whereas Myogenin, which accumulates during muscle development, is essential for muscle differentiation (Arnold and Braun, 2000; Olson, 1993). These genes are necessary and sufficient for commitment to a myogenic fate; in their absence, cells that would normally form muscle adopt other fates (Kablar et al., 1999). Conversely, when overexpressed, they convert non-muscle to muscle cells and transactivate many genes expressed in skeletal muscle. Migrating precursors do not express myogenic determination genes; it is only after reaching the limb bud that MyoD, Myf5 and Myogenin expression is initiated (Tajbakhsh and Buckingham, 1994). In the absence of MyoD, the onset of myogenesis is delayed, suggesting that Myf5 alone is initially insufficient to drive the formation of skeletal muscle (Kablar et al., 1997). Myf5 expression in limb myoblasts is directly activated by Pax3 (Bajard et al., 2006), whereas the initiation of MyoD expression in limb skeletal muscles is directly and positively regulated by the transcription factor Pitx2 in a Myf5-independent manner (L'Honore et al., 2010).

Finally, the terminal differentiation of myoblasts involves the synthesis of muscle-specific proteins such as myosin heavy chain and the fusion of postmitotic myocytes into multinucleate myotubes (Buckingham, 2001).

5.1.2 Limb muscle patterning

Experiments in avian embryos have demonstrated that early stages of limb muscle differentiation are cell autonomous and occur independent of the influence of limb tissue (Buckingham, 2001). In contrast, the overall pattern of limb musculature is specified by the limb environment. Somites from any axial level possess the ability to give rise to normal limb muscle, indicating that early-stage myoblasts are undetermined with respect to the pattern of muscles to which they will contribute (Chevallier et al., 1977; Christ et al., 1977). Furthermore, single-cell lineage analysis of muscle precursors has revealed that individual myogenic cells in the somites or within the proximal limb are not predetermined to form particular muscles or muscles situated at particular proximodistal or dorsoventral limb coordinates (Kardon et al., 2002). These studies suggest that myoblasts are patterned by extrinsic signals after the cells have migrated through the proximal limb.

As myoblasts differentiate, they are immediately oriented in a highly ordered array that prefigures the pattern of the mature adult musculature (Kardon, 1998). Remarkably, the pattern of muscle cleavage holds even in the absence of myoblasts,

indicating that the limb contains cues that direct subdivision of the dorsal and ventral muscles masses (Grim and Wachtler, 1991). On a tissue level, previous studies have found that the limb ectoderm and tendons negatively regulate muscle differentiation, thereby defining regions in the limb where muscle does not form (Amthor et al., 1998; Kardon, 1998; Robson and Hughes, 1996). On a molecular level, SHH, BMP, FGF and Notch signaling have been found to regulate muscle differentiation in the limb (Christ and Brand-Saberi, 2002; Duprez, 2002; Francis-West et al., 2003). However, the generalized expression of these molecules within the limb suggests that they cannot straightforwardly determine the pattern of individual limb muscles; generalized patterning information must be integrated and refined by myoblasts to specify muscle pattern.

Descriptions of the precise molecular mechanisms regulating muscle cleavage patterning are scarce. Expression of the homeobox transcription factor Mox2 is known to be required for the normal morphogenesis of limb musculature. *Mox2* mutant mice exhibit an overall reduction in forelimb and hindlimb muscle mass that is associated with the absence of specific forelimb muscles (Mankoo et al., 1999). These defects are prefigured by defects in muscle patterning in the embryo: at e13.5, when the identification of individual muscles is feasible, several forelimb muscles were found to be absent, and abnormal cleavage of the hindlimb extensor digitorum longus (EDL) muscle – a TA synergist - was observed (Mankoo et al., 1999). However, Mox2 is expressed in both muscle precursor cells and distal limb mesenchyme (Mankoo et al., 1999); a conditional Mox2 allele for tissue-specific

deletion of the gene is lacking, so whether Mox2 plays a cell autonomous or non-cell autonomous role in muscle patterning remains unclear.

5.1.3 Influence of the mesenchyme on muscle patterning

Several lines of evidence implicate the limb mesenchyme in positively regulating the pattern of muscle cleavage. First, muscle connective tissue forms normally in the absence of muscle (Grim and Wachtler, 1991; Jacob and Christ, 1980), indicating that it does not depend on muscle for its patterning and hence could be a source of muscle-patterning information. Second, muscle connective tissue can organize even nonmuscle cells to form muscle-like structures (Grim and Wachtler, 1991). Finally, manipulating the pattern of mesenchyme-derived cues alters the pattern of musculature formed in the limb. For example, the deletion or overexpression of Lmx1b has been shown to alter the dorsoventral polarity of hindlimb musculature at the level of the foot (Chen et al., 1998; Li et al., 2010) and shank (Chapter 4).

In both mouse and chick, a subpopulation of limb mesenchymal cells expressing the transcription factor *tcf4* has been shown to establish a prepattern for muscle cleavage (Kardon et al., 2003). These mesenchymal cells establish patterned expression of *tcf4* in the absence of muscle tissue, and altering mesenchymal *tcf4* expression changes the resultant pattern of muscle cleavage (Kardon et al., 2003). In chick, *tcf4*-expressing mesenchymal cells remain adjacent to muscle and appear to

express collagen I, an early marker of muscle connective tissue, suggesting that these cells give rise to the connective tissue surrounding select limb muscles (Kardon et al., 2003). From this study, a model of muscle patterning in the vertebrate limb has emerged: patterning signals that define the cardinal axes of the limb are integrated to induce the expression of transcriptional determinants such as Tcf4 in select mesenchymal cells, which signal locally to instruct patterned myogenesis. Each local region of myogenesis then serves as the nucleus for a future anatomical muscle.

The influence of the mesenchyme on muscle patterning led us to question whether two of the proprioceptor genes impacted by our manipulations of mesenchymal identity – *cdh13* and *vstm2b* – are in fact patterned by muscle. To this end, we examined the expression of *cdh13* and *vstm2b* by proprioceptors in mice deficient in *lbx1*, one of the factors required for muscle precursor migration into the limb.

5.2 Results

5.2.1 Muscleless hindlimbs of *Lbx1*$^{-/-}$ mice receive proprioceptor innervation

We set out to determine the influence of limb muscle in patterning proprioceptor muscle-type gene expression (Figure 5.3A) by examining proprioceptor *cdh13* and *vstm2b* expression following innervation of limbs devoid of muscle. Staining for myosin, a marker of muscle tissue, in wild-type and *Lbx1*$^{-/-}$

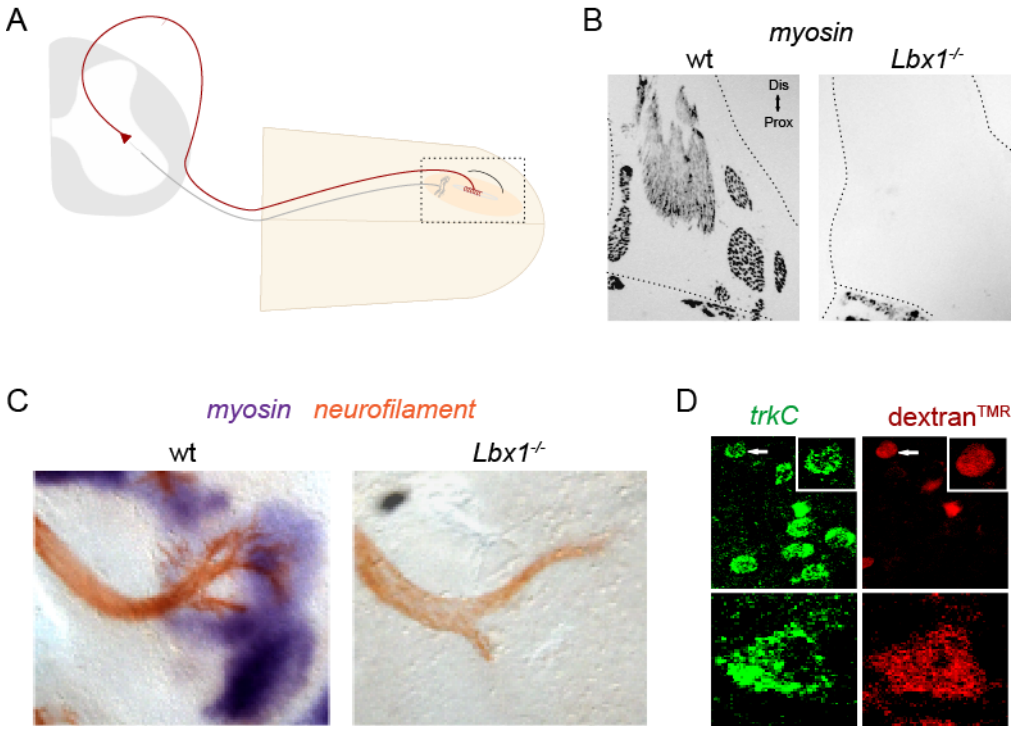

Figure 5.3 *Lbx1*$^{-/-}$ hindlimbs receive proprioceptor innervation

(A) Motor neuron and proprioceptive sensory neuron innervating a hindlimb muscle. The boxed area highlights putative signaling from muscle to proprioceptive sensory axons. (B) Developing muscles are absent from *Lbx1*$^{-/-}$ hindlimbs, as indicated by *in situ* hybridization for the muscle marker *myosin*. Prox-dis: proximodistal. (C) *In situ* hybridization for *myosin* and *neurofilament* reveals that the major branches of the nerve innervating the hindlimb form correctly in *Lbx1*$^{-/-}$ mice. (D) *trkC*^{on} sensory neurons innervate the limb in *Lbx1*$^{-/-}$ mice. Images show two representative *trkC*^{on} DRG neurons retrogradely labeled by hindlimb injection of dextran-tetramethylrhodamine in e13.5 *Lbx1*$^{-/-}$ embryos.

mice revealed the near absence of differentiated hindlimb muscle in mutant animals (Figure 5.3B). In some *Lbx1*$^{-/-}$ embryos, we observed residual gluteus muscle in the proximal compartment of the limb (data not shown), a finding reported previously for *Lbx1* mutants (Gross et al., 2000). This is presumably due to the ability of delaminated muscle precursors to passively invade the most proximal portion of the limb bud, where they differentiate under the influence of proximal positional cues.

Whole mount *in situ* hybridization labeling for neurofilament revealed that the major peripheral nerve trajectories in *Lbx1*$^{-/-}$ mice are grossly similar to those in wild-type limbs (Figure 5.3C; see also Phelan and Hollyday, 1990). To determine whether these nerves supply the developing limb with proprioceptive sensory innervation, we injected the tracer dextran-tetramethylrhodamine into the hindlimbs of e13.5 *Lbx1*$^{-/-}$ embryos and examined retrogradely labeled DRG neurons for expression of the generic proprioceptor marker *trkC* (Figure 5.3D). Indeed, we observed dextran^{TMR}-labeled DRG neurons that expressed *trkC*, indicating that the limbs of *Lbx1*$^{-/-}$ embryos receive proprioceptor innervation. We therefore proceeded to examine the status of *cdh13* and *vstm2b* expression in hindlimb-innervating proprioceptors of *Lbx1*$^{-/-}$ mice.

5.2.2 Proprioceptor *cdh13* expression is unaffected by loss of muscle

We first examined whether limb muscles might be the source of a *cdh13* inductive signal for proprioceptors. In the absence of limb muscle, we were unable

to identify proprioceptor subpopulations by peripheral target innervation. Nevertheless, we reasoned that quantifying the proportion of *cdh13*-expressing proprioceptors in lumbar DRG of wild-type and *Lbx1*$^{-/-}$ mice would allow us to assess whether the absence of hindlimb muscle impacts expression of the gene.

We chose to assess the expression of proprioceptor muscle-type genes in *Lbx1*$^{-/-}$ mice and wild-type littermates at e15.5, a timepoint after the onset of wild-type proprioceptor *cdh13* and *vstm2b* expression, but before proprioceptor survival is affected by the absence of muscle-derived NT3. Indeed, in *Lbx1*$^{-/-}$ mice examined at e15.5, the density of *pv*^{on} neurons in L2 and L5 DRG was unchanged when compared to wild-type DRG (203 *pv*^{on} neurons/1 mm^2 in wild-type versus ~198 *pv*^{on} neurons/1 mm^2 in *Lbx1*$^{-/-}$ mice at L2, p = 0.68; 334 *pv*^{on} neurons/1 mm^2 in wild-type versus 320 *pv*^{on} neurons/1 mm^2 in *Lbx1*$^{-/-}$ mice at L5, p = 0.12).

We compared the proportion of proprioceptors expressing *cdh13* in e15.5 wild-type and *Lbx1*$^{-/-}$ mice at different lumbar rostrocaudal levels. If muscle supplies *cdh13* patterning information, we would expect the proportion of *cdh13*^{on} proprioceptors to decrease in *Lbx1*$^{-/-}$ mice, in which hindlimbs are nearly devoid of muscle. We found that in both L2 and L5 DRG, proprioceptor *cdh13* expression was similar in *Lbx1*$^{-/-}$ and wild-type embryos (~69% in wild-type versus ~63% in *Lbx1*$^{-/-}$ at L2, p = 0.18; ~34% in wild-type versus ~35% in *Lbx1*$^{-/-}$ at L5, p = 0.89). These data argue against the idea that muscle is the source of signals required for the induction of proprioceptor *cdh13* expression.

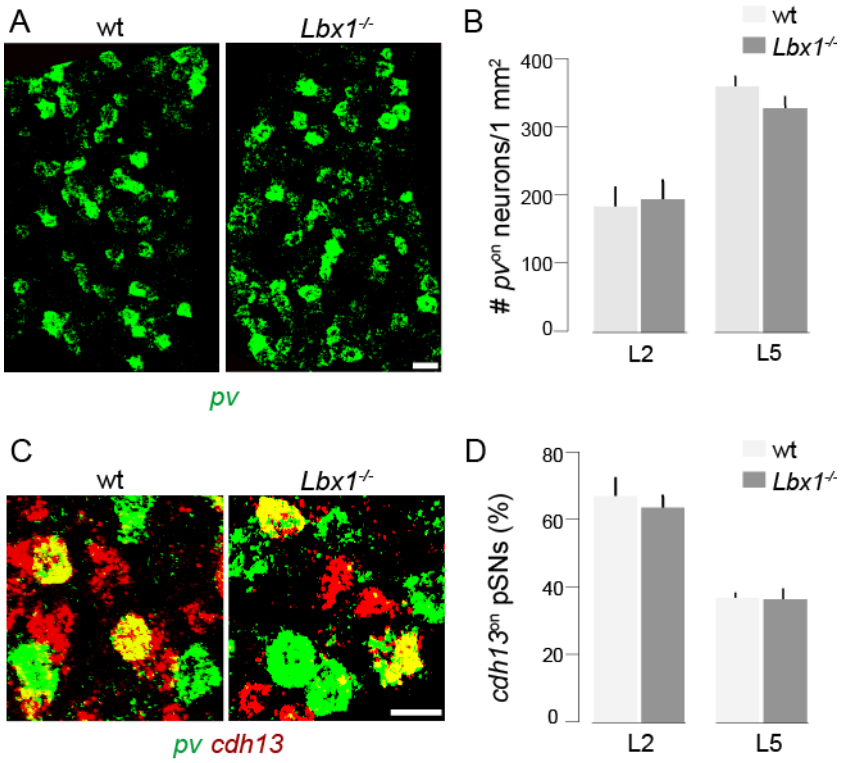

Figure 5.4 Proprioceptor *cdh13* expression is unperturbed by the absence of muscle

(A and B) The density of proprioceptors is similar in wild-type (wt) and *Lbx1*$^{-/-}$ DRG. (A) *In situ* hybridizations for *pv* in e15.5 L4 DRG of wt and *Lbx1*$^{-/-}$ mice. Scale bar, 20 µm. (B) Proprioceptor density in L2 and L5 DRG of wt and *Lbx1*$^{-/-}$ mice. (C and D) *cdh13*^{on} proprioceptors are conserved in *Lbx1*$^{-/-}$ DRG. (C) Double FISH for *pv* and *cdh13* in e15.5 wt and *Lbx1*$^{-/-}$ DRG. Scale bar, 10 µm. (D) Percentage of proprioceptors expressing *cdh13* in L2 and L5 DRG of e15.5 wt and *Lbx1*$^{-/-}$ mice (n = 3 mice/genotype).

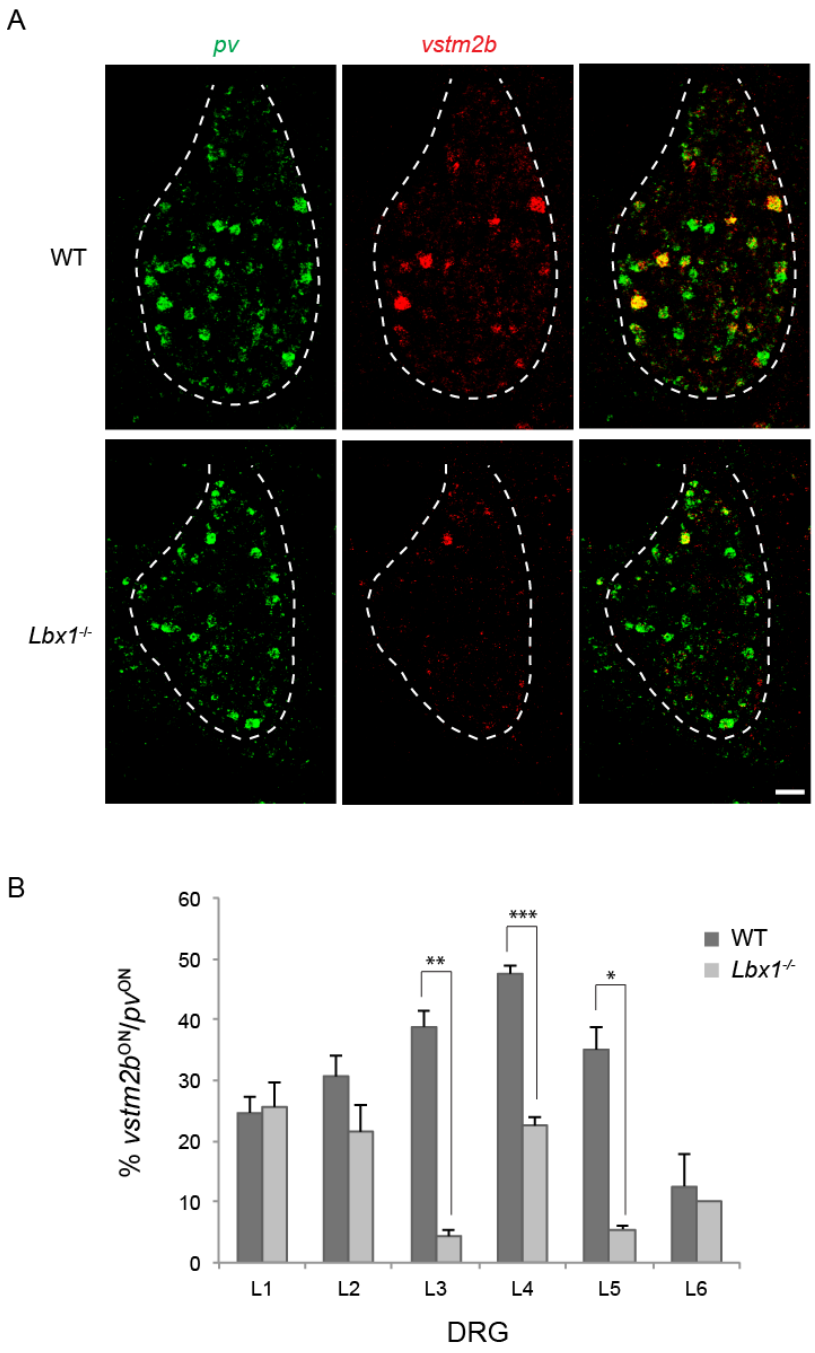

Figure 5.5 Proprioceptor *vstm2b* expression is dependent on the presence of muscle

(A) Double FISH for *pv* and *vstm2b* in e15.5 L4 DRG reveals a marked reduction in the density of *vstm2b*^{on} proprioceptors in *Lbx1*$^{-/-}$ embryos. Scale bar, 50 µm. (B) Quantification of the proportion of *vstm2b*^{on} proprioceptors in DRG L1-L6 of wt and *Lbx1*$^{-/-}$ embryos (n = 4 mice/genotype; ***p<0.0001, **p<0.001, *p<0.01). Data are represented as the mean ± SEM.

5.2.3 Proprioceptor *vstm2b* expression requires the presence of muscle

We next examined the status of *vstm2b* expression in the proprioceptors of e15.5 *Lbx1*$^{-/-}$ embryos. As with *cdh13*, we reasoned that if the expression of *vstm2b* in hindlimb-innervating proprioceptors is induced by muscle, we would see a decrease in the proportion of *vstm2b*^{on} proprioceptors in lumbar ganglia. Because *vstm2b* is expressed by a larger proprioceptor subpopulation than *cdh13*, we examined its expression in DRG L2-L6, thereby surveying the entire complement of hindlimb-innervating proprioceptors. We also examined expression of the gene in DRG L1; proprioceptors in this ganglion innervate only axial and hypaxial musculature (de Nooij et al., 2013), the development of which is unaffected in *Lbx1*$^{-/-}$ animals.

Remarkably, fluorescent *in situ* hybridization revealed the near absence of *vstm2b*-expressing *pv*^{on} neurons in lumbar DRG of *Lbx1*$^{-/-}$ embryos (Figure 5.5A). Quantification of the number of *vstm2b*^{on} proprioceptors in DRG L2-L6 indicated a marked decrease in the proportion of cells expressing the gene in *Lbx1*$^{-/-}$ compared to wild-type mice (Figure 5.5B). While the proportion of *vstm2b*^{on} proprioceptors decreased in all lumbar ganglia, this difference was significant in DRG L3-L5, with the most dramatic differences observed in L3 and L5 (Figure 5.5B; ~31% in wild-type versus ~21% in *Lbx1*$^{-/-}$ at L2, p = 0.08; ~39% in wild-type versus ~4% in *Lbx1*$^{-/-}$ at L3, p = 0.0002; ~47% in wild-type versus ~23% in *Lbx1*$^{-/-}$ at L4, p = 0.00001; ~35% in wild-type versus ~6% in *Lbx1*$^{-/-}$ at L5, p = 0.002; ~13% in wild-type versus

~10% in *Lbx1*$^{-/-}$ at L6, p = 0.39). Thus, we conclude that proprioceptor expression of *vstm2b* requires the presence of limb muscle.

5.3 Discussion

Examining the expression of *cdh13* and *vstm2b* in *Lbx1* mutant mice devoid of limb muscle enabled us to determine that while *cdh13* expression in proprioceptors is influenced by limb mesenchyme alone, the induction of *vstm2b* is dependent on the presence of limb muscle. Here I discuss our experimental findings and propose an updated model for the induction of *vstm2b* expression in proprioceptors.

5.3.1 Residual *vstm2b* expression in proprioceptors of *Lbx1*$^{-/-}$ mice

We observed a marked decrease in the number of lumbar proprioceptors expressing *vstm2b* in *Lbx1*$^{-/-}$ mice. Nevertheless, a cohort of these cells continued to express the gene in DRG L3-L5, despite the near absence of limb muscle. What might explain the persistence of *vstm2b*^{on} proprioceptors in these animals?

The most likely source of cues inducing *vstm2b* expression in the L3-L5 proprioceptors of *Lbx1*$^{-/-}$ mutants is the gluteal muscle reported to persist in *Lbx1*$^{-/-}$ embryos (Gross et al., 2000), which in wild-type mice receives *vstm2b*^{on} proprioceptor innervation. Backfill experiments indicate that proprioceptors innervating the gluteal group are located in DRG L3-L5, with the bulk of this cohort

located in DRG L4 (data not shown). Indeed, most of the *vstm2b*^{on} proprioceptors observed in DRG L3-L5 in *Lbx1*$^{-/-}$ mice are found at L4, consistent with the hypothesis that *vstm2b* expression is induced by the gluteus in these animals.

Another possible source of *vstm2b* inductive cues in *Lbx1*$^{-/-}$ embryos is the axial musculature surrounding the spinal column. This musculature is derived from a non-migratory population of myoblasts that does not express *lbx1* and is therefore unaffected in *Lbx1* mutants. Axially innervating proprioceptors are found in DRG at all rostrocaudal levels. At thoracic levels, DRG do not contain limb-innervating proprioceptors; rather, they contain proprioceptors innervating axial and hypaxial (body wall) musculature. We observed *vstm2b* expression in a subset of thoracic DRG neurons (data not shown), consistent with the notion that proprioceptors supplying axial muscles express *vstm2b*. Further, expression of *vstm2b* in L1 proprioceptors, which innervate axial and hypaxial musculature, is unchanged between wild-type and *Lbx1*$^{-/-}$ mice (Figure 5.5B; ~25% in wild-type versus ~26% in *Lbx1*$^{-/-}$, p = 0.43). Nevertheless, the peripheral muscle targets of *vstm2b*-expressing proprioceptors in wild-type thoracic DRG and *Lbx1*$^{-/-}$ lumbar DRG must be confirmed by retrograde labeling experiments.

Similarly, *vstm2b* expression by axial proprioceptors could explain the lack of significant difference between *Lbx1*$^{-/-}$ and wild-type mice in the proportion of *vstm2b*^{on} cells in L2 and L6 ganglia (Figure 5.5). DRG L2 and L6 each contain small cohorts of limb-innervating proprioceptors that normally express *vstm2b* in wild-

type mice (some quadriceps proprioceptors at L2 and intrinsic foot proprioceptors at L6; data not shown), which accounts for the overall decrease in the proportion of *vstm2b*^{on} proprioceptors present in these ganglia in *Lbx1*$^{-/-}$ mice. However, the proprioceptors found in these ganglia are overwhelmingly those innervating axial and hypaxial musculature (de Nooij et al., 2013), whose *vstm2b* expression status would be unchanged in *Lbx1*$^{-/-}$ embryos.

5.3.2 A revised model for proprioceptor *vstm2b* induction

In wild-type animals, *vstm2b* is expressed in nearly all proprioceptors innervating dorsal musculature and is mostly absent from those supplying ventral muscles. Furthermore, the expression of *vstm2b* by wild-type proprioceptors is not restricted with respect to the proximodistal limb axis, as is the case for *cdh13*. In light of our finding that muscle influences proprioceptor *vstm2b* expression, how might this pattern be established in wild-type embryos?

The simplest way to achieve this expression pattern would be through the presence of an inductive cue restricted to the dorsal muscle mass or, conversely, a repressive cue restricted to the ventral muscle mass (Figure 5.6A). Indeed, myoblasts are first visible in the hindlimb in the form of dorsal and ventral muscle masses beginning at e12.5 (Martin, 1990), just prior to the onset of proprioceptor *vstm2b* expression at e13.5. However, migratory muscle precursors are not prespecified with respect to dorsal or ventral trajectory, calling into question

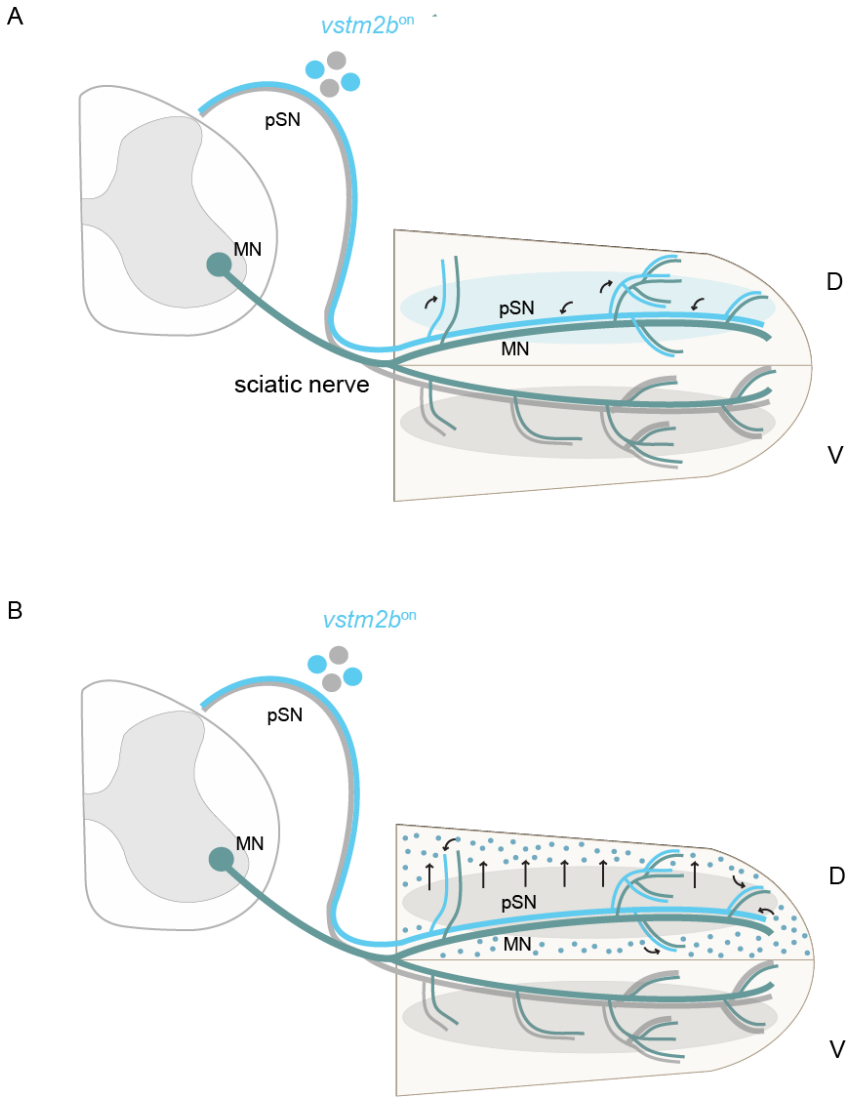

Figure 5.6 Models for muscle-dependent induction of *vstm2b*

Two models for the induction of proprioceptor *vstm2b* expression are equally plausible. (A) An inductive cue supplied by dorsal muscle mass (shown here) or a repressive cue supplied by ventral muscle mass acts on proprioceptors to specify dorsally restricted *vstm2b* expression in proprioceptors. (B) The presence of generic muscle is required to induce expression of a mesenchymal cue required for *vstm2b* expression in proprioceptors; dorsoventral restriction of this mesenchymal cue could be achieved via differential competence of dorsal and ventral mesenchyme to respond to the presence of muscle.

whether they possess distinct dorsoventral gene expression profiles this early in development. Distinctions among individual limb muscles in the level of NT3 expression (de Nooij et al., 2013) and in binary expression of the transcription factor Engrailed1 (Jay Bikoff, personal communication) indicate that individual limb muscles must at some point acquire distinct molecular identities. However, when and how this occurs is unknown.

In an alternative scenario, proprioceptor expression of *vstm2b* might be specified by a mesenchymal cue, the expression of which is dependent on the presence of, and feedback from, differentiating muscle (Figure 5.6B). This model represents a permissive rather than instructive role for the muscle in specifying proprioceptor subtype identity and is equally consistent with the observed influence of both mesenchyme and muscle on proprioceptor *vstm2b* expression.

One point in favor of an instructive role for muscle is the unprecedented restriction of *vstm2b* expression to proprioceptors within the DRG. In contrast to *vstm2b*, *cdh13*, which is specified in proprioceptors by a mesenchymal cue, is also expressed by cutaneous sensory neurons. Proprioceptors and cutaneous sensory neurons fasciculate together in peripheral nerves and traverse the same route through the mesenchyme on their way to peripheral targets (Honig et al., 1998), resulting in the exposure of both subpopulations to the same regionally restricted mesenchymal cues. Although it is unknown whether *cdh13*-expressing cutaneous sensory neurons exhibit topographically restricted expression corresponding to

dorsodistal epidermis, it is possible that exposure to mesenchymal cues induces *cdh13* in both proprioceptors and cutaneous modalities.

The easiest way to restrict *vstm2b* expression to proprioceptors, it seems, would be through a target-derived signal bound to the muscle cell surface. However, in the model involving a permissive role for muscle, generic proprioceptors might be competent to respond to a mesenchymal cue that generic neurons of various cutaneous sensory modalities lack the ability to respond to. Thus, an element of intrinsic proprioceptor identity may be required for muscle-type specification.

Remarkably, each model of *vstm2b* induction results in novel implications for limb development. An instructive role for muscle in patterning proprioceptor gene expression would require molecular distinctions between the dorsal and ventral muscle masses early in development, which thus far have not been reported (Buckingham et al., 2003). Alternatively, a permissive role for muscle would depend on reverse signaling from muscle to mesenchyme, a patterning mechanism not previously described in the literature. Thus, our study of proprioceptor specification has also yielded novel insight into the complex developmental process of limb patterning.

6 Involvement of muscle-type genes in synaptic specificity

6.1 Introduction

Thus far, we have used our insight into proprioceptor muscle-type identity to examine the role of discrete peripheral elements in inducing the expression of proprioceptor subtype genes. I now turn to the question of whether two of the genes characterized as proprioceptor muscle-type markers – *cdh13* and *vstm2b* – might play a functional role in establishing selective monosynaptic connections between proprioceptors and motor neurons.

The formation of connections between defined neuronal populations and their postsynaptic target cells is crucial for the generation of functional neuronal circuitry. A combination of molecular and activity-dependent mechanisms is generally employed by presynaptic neurons to locate appropriate postsynaptic partners and to refine synaptic contacts. Although the feedback circuits formed by Ia proprioceptive afferents and spinal motor neurons are some of the best characterized within the nervous system, the developmental mechanisms underlying selective connectivity within this system are poorly defined. The formation of specific monosynaptic connections in the absence of patterned activity (Mears and Frank, 1997; Mendelson and Frank, 1991) has implicated the involvement of molecular recognition between sensory and motor subsets. Until now, the lack of known distinctions between muscle-type proprioceptor

subpopulations has posed a major obstacle to identifying recognition systems with putative roles in patterning sensory-motor connectivity.

The expression of *cdh13* and *vstm2b* by TA but not GS proprioceptors suggests that these genes might be capable of mediating target discrimination by Ia afferent subpopulations. TA and GS muscles are functional antagonists and as such avoid supplying each other with sensory feedback. The requisite antagonist avoidance and homonymous specificity between these reflex arcs likely arise from distinctions in gene expression between TA and GS proprioceptive afferents. In this chapter, I assess whether Cdh13 and Vstm2b act as molecular determinants of monosynaptic specificity by examining mutant mice for misprojections within the TA and GS reflex arcs.

6.1.1 Molecular mechanisms of sensory-motor circuit assembly

Prior to the work presented in Chapter 2 of this thesis, few molecular distinctions capable of mediating selective target recognition by muscle-type proprioceptors had been reported. Nevertheless, studies of motor neuron transcription factor expression and known molecular recognition systems have yielded a partial mechanistic understanding of how sensory-motor specificity arises in the embryo.

In motor neurons, expression of the ETS transcription factor Pea3 contributes to pool positioning and dendritic arborization (Livet et al., 2002; Vrieseling and Arber, 2006), two features of postsynaptic populations known to impact target selectivity. Pea3 is expressed by forelimb-innervating motor neurons projecting to the cutaneous maximus and latissimus dorsi muscles. In Pea3 mutant mice, cutaneous maximus motor neurons receive errant sensory contacts from triceps proprioceptors (Vrieseling and Arber, 2006), indicating that Pea3 is required for sensory-motor specificity for several muscles of the forelimb. The precise mechanism by which Pea3 restricts sensory-motor contacts is unclear due to its effect on both motor pool positioning and arborization. However, Pea3 has been shown to regulate the downstream expression of several surface recognition molecules, including Cadherin7, Cadherin8, and Sema3E, in motor neurons (Livet et al., 2002).

Mouse genetic studies of motor neuron Sema3E and its cognate receptor PlexinD1 in sensory neurons have established their involvement in sensory-motor circuit formation. In the forelimb, the cutaneous maximus (Cm) muscle represents an atypical reflex arc in that it does not receive homonymous monosynaptic input. Expression of Sema3E by Cm motor neurons and PlxnD1 by Cm afferents results in a repellant interaction that prevents monosynaptic connections from forming (Figure 6.1A; Pecho-Vrieseling et al., 2009). In the hindlimb, Sema3e is expressed by gluteus but not hamstring motor neurons while PlxnD1 is expressed by hamstring but not gluteus proprioceptors, suggesting that repulsive signaling may mediate antagonist

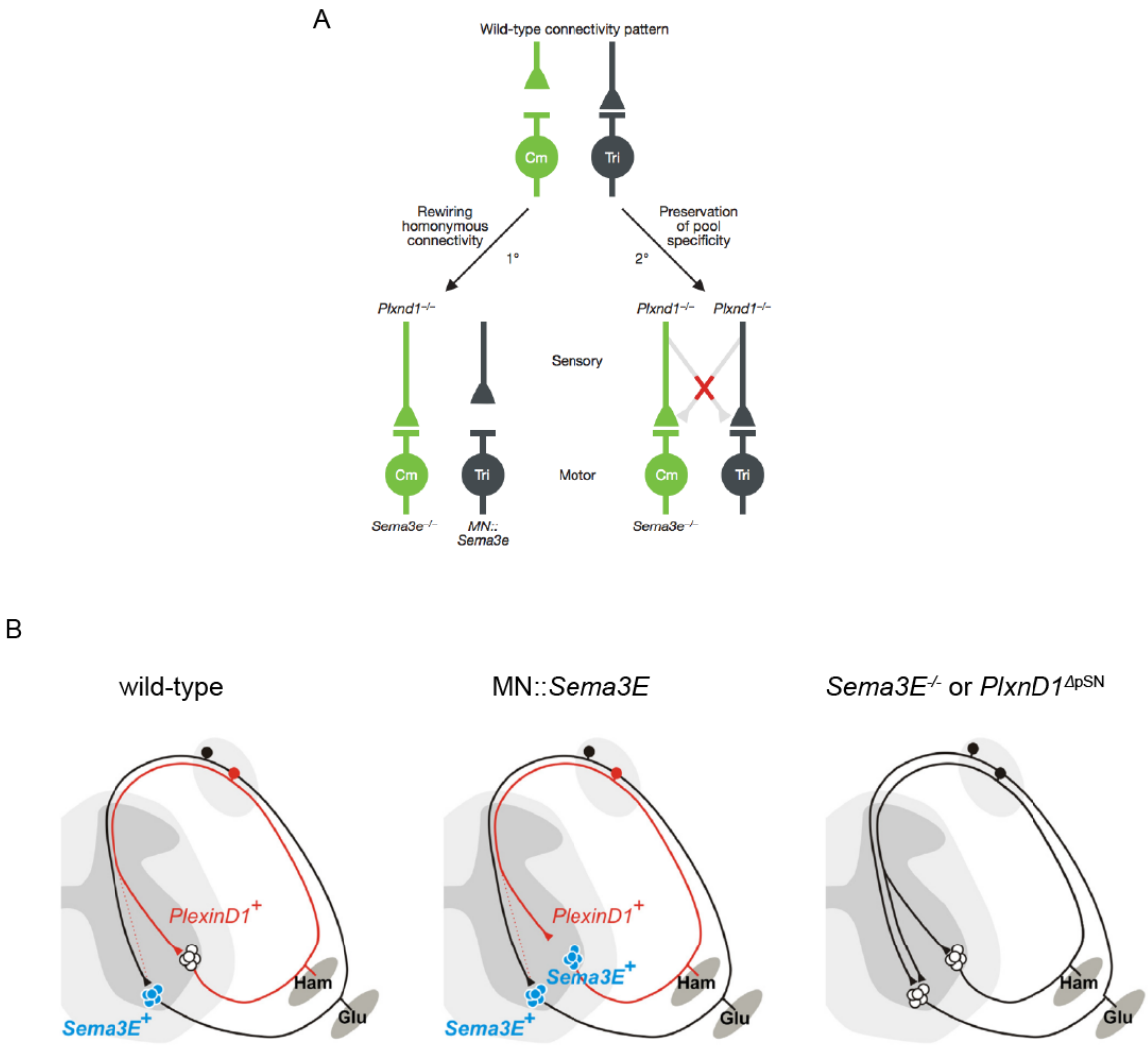

Figure 6.1 Molecular recognition in sensory-motor circuit formation

(A-B) Sema3e-PlxnD1 repulsion has been implicated in the formation of specific sensory-motor connections. (A) Connectivity patterns in cutaneous maximus (Cm) and triceps (Tri) reflex arcs in wild-type mice (top) and in mice with altered Sema3E-PlxnD1 signaling (bottom). Top: In wild-type mice, triceps but not cutaneous maximus motor neurons receive direct homonymous proprioceptive inputs. Bottom left: Changing the profile of Sema3E-PlxnD1 expression rewires homonymous connectivity. Loss of Sema3E-PlxnD1 signaling results in monosynaptic connections between Cm afferents and Cm motor neurons; ectopic Sema3E expression reduces monosynaptic connections between Tri afferents and Tri motor neurons. Bottom right: changing Sema3E-PlxnD1 signaling does not erode pool specificity; no aberrant heteronymous connections were observed, suggesting that additional recognition systems, likely also downstream of Pea3 in

motor neurons, are involved in the formation of monosynaptic connections. Adapted from Pecho-Vrieseling et al., 2009. (B) Left: At lumbar levels of the spinal cord, Sema3E-PlxnD1 signaling suppresses inappropriate synaptic connections between hamstring (Ham) and gluteus (Glu) motor neurons. Middle: Ectopic expression of Sema3E in Ham motor neurons reduces the strength of homonymous connections between Ham afferents and Ham motor neurons. Right: In the absence of Sema3E-PlxnD1 signaling, strong aberrant monosynaptic connections between Ham sensory afferents and Glu motor neurons were observed. Adapted from Fukuhara et al., 2013.

avoidance between these reflex arcs (Figure 6.1B). Indeed, ectopic pan-motor neuronal expression of *sema3e* leads to a reduction in monosynaptic connectivity between hamstring motor neurons and proprioceptors, and deletion of either *sema3e* or *plxnd1* results in aberrant contacts between hamstring proprioceptors and gluteus motor neurons (Fukuhara et al., 2013). Together, these studies indicate that Sema3E-PlxnD1 signaling regulates both the formation of polysynaptic versus monosynaptic contacts with motor neurons and the specificity of monosynaptic connections within a small subset of limb-innervating reflex arcs.

Beyond Sema-Plexin signaling, type II cadherins have been suggested to play a role in sensory-motor selectivity. In chick, motor pools are defined by combinatorial expression of type II cadherins (Price et al., 2002). Retrogradely identified muscle-type proprioceptors were found to express a cohort of cadherins at similar cellular proportions to their cognate motor neuron populations. However, the analysis of cadherin expression by muscle-type proprioceptors conducted in this study was limited to two genes, and no role was established for these cadherins in the formation of monosynaptic sensory-motor connections (Price et al., 2002).

Thus, our understanding of the molecular mechanisms underlying formation of the complex matrix of monosynaptic connectivity between ~50 subsets of limb-innervating proprioceptors and their cognate motor neurons remains incomplete. Insight into the spatial organization of motor neurons and the function of this

topography in gating afferent input suggests that an overarching spatial and molecular logic may underlie the construction of spinal sensory-motor circuitry.

6.1.2 Motor neuron topography mirrors limb organization

Spinal motor neurons are topographically segregated into columns that innervate distinct peripheral domains. In tetrapods, limb-innervating motor neurons are found at rostrocaudal levels corresponding to limb position and are located within the lateral motor column (LMC) in the ventral horn of the spinal cord (Romanes, 1951). Within the LMC, motor neurons innervating an individual muscle are clustered together in a unit referred to as a motor pool (Figure 6.2A; Hollyday, 1980; Romanes, 1964), each of which occupies a stereotyped position within the LMC. Upon examination, a higher order of pool organization becomes apparent: pools that innervate synergist muscles are grouped together in clusters termed columels (Figure 6.2A; Romanes, 1951; Sürmeli et al., 2011).

Motor columels are spatially organized within the spinal cord in a topographic map that reflects the anatomical arrangement of muscles in the limb (Figure 6.2B-E; Hollyday and Jacobson, 1990; Landmesser, 1978a; McHanwell and Biscoe, 1981; Romanes, 1964; Vanderhorst and Holstege, 1997). At both fore- and hindlimb levels of the spinal cord, motor pools – and by extension, columels – that are located more ventrally in the spinal cord innervate muscles located more proximally within the limb, whereas those located more dorsally innervate muscles

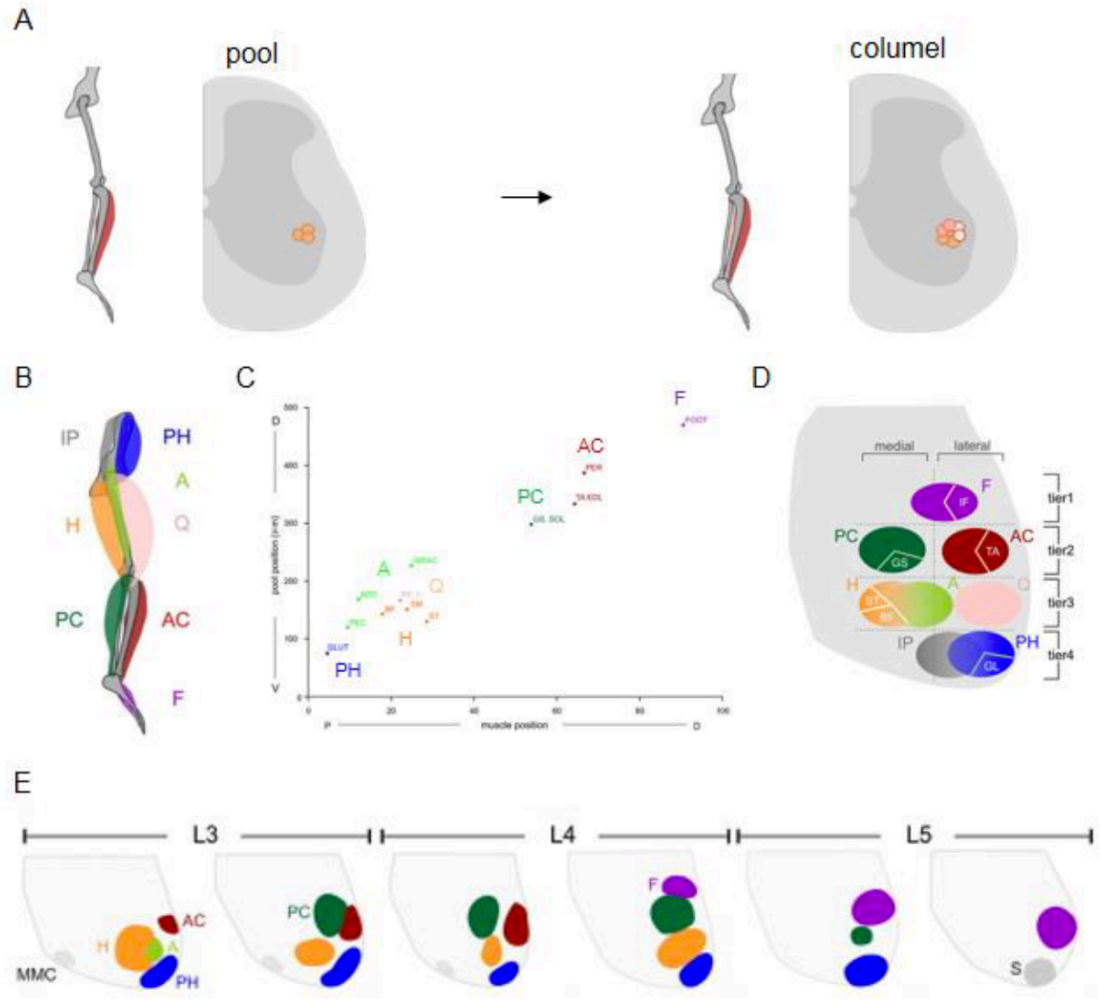

Figure 6.2 Motor neuron position is correlated with intralimb termination

(A) Motor neurons that innervate a single muscle are clustered in motor pools. Motor pools innervating synergist muscles are arranged in higher order clusters termed columels. (B) The proximodistal and dorsoventral organization of muscles of the mammalian hindlimb. Abbreviations: proximal hip (PH; includes GL), iliopsoas (IP), adductors (A), quadriceps (Q), hamstrings (H), anterior crural (AC; includes TA), posterior crural (PC; includes GS), intrinsic foot (F). (C) The dorsoventral (μm) positions of motor pools in the cat lumbar spinal cord and the proximodistal (cm) positions of muscles in the cat hindlimb. (D) Columelar organization along the dorsoventral and mediolateral axes after rostrocaudal compression. Columels are assigned to dorsoventral tiers that correspond to muscles at individual joints and mediolateral divisions corresponding to dorsoventral position within a joint. (E) Columelar positions from L3 to L5 in mouse. Adapted from Sürmeli et al., 2011.

located more distally (McHanwell and Biscoe, 1981; Romanes, 1964; Vanderhorst and Holstege, 1997). Likewise, motor pools situated laterally within the LMC innervate muscles of dorsal origin, whereas motor pools situated medially innervate ventral musculature (Landmesser, 1978b; Tosney and Landmesser, 1985).

At hindlimb levels, the LMC is divided into four dorsoventral domains, or tiers, that contain motor neurons projecting to the foot, shank, thigh, and hip (Figure 6.2D; Sürmeli et al., 2011). Each of these tiers can in turn be subdivided according to the mediolateral, or divisional, settling position of the motor neurons within it. The most dorsally positioned tier is occupied by motor neurons projecting to the intrinsic foot (IF) muscles. The second tier is occupied by motor neurons projecting to the crural muscles of the shank, with posterior crural muscles (ankle extensors; GS, Sol, Plan) located in the medial division and anterior crural muscles (ankle flexors; TA, EDL, PL) located laterally. The third tier is occupied by motor neurons projecting to the thigh, with the medial division containing motor neurons projecting to the adductor and hamstring muscles (knee flexors) and the lateral division containing those projecting to the quadriceps (knee extensors). Finally, the most ventrally positioned tier is occupied by motor neurons projecting to proximal hip muscles, with the iliopsoas hip flexor muscles located more medially than the gluteal extensor muscles.

Thus, the settling position of motor columels within the LMC is linked to intralimb termination along two spatial axes. While the positional organization of

motor neurons has long been appreciated, an understanding of why this topography exists has emerged only recently.

6.1.3 Motor neuron columelar organization provides a connectivity template

One explanation proposed for the positional correlation between motor neuron and muscle is that it might facilitate motor axon projection to prescribed muscle targets. Recent evidence from molecular genetic studies, however, argues against this theory.

Motor neurons can be stripped of the cadherin code that enables them to sort and settle within subdomains of the LMC by deleting the genes encoding β- and γ-catenin (Demireva et al., 2011), proteins that anchor cadherins within the cell membrane and mediate intracellular signaling. In these mice, motor neuron position is scrambled while expression of upstream transcriptional programs, including the motor pool markers Nkx6.1, Nkx6.2, and Er81, remains intact. Under these conditions, motor neurons retain the ability to follow limb mesenchymal cues to the limb muscle targets dictated by their transcriptional identities (Demireva et al., 2011; Garcia and Jessell, 2008), indicating that motor neuron topography in and of itself is dispensable for the fidelity of peripheral motor projection, so long as other aspects of motor pool molecular identity remain in tact.

Elimination of the Hox cofactor FoxP1 in motor neurons scrambles motor neuron position within the LMC and strips motor pools of identifying surface markers (Dasen et al., 2008; Sürmeli et al., 2011). In this context, incoming proprioceptive afferents retain the ability to target the dorsoventral tier of the LMC in which their motor neuron targets would typically be clustered in wild-type mice (Sürmeli et al., 2011). Taken together, these studies suggest that the topographical organization of motor neurons within the LMC exists to facilitate pathfinding and recognition by incoming sensory afferents.

In light of this view, the compartmental molecular organization of limb-innervating proprioceptors and the ability of the limb to impose proprioceptor positional identities possess an elegant logic. Expression of *cdh13*, for example, is shared among proprioceptors innervating the TA muscle and its synergists: a "columelar" group of proprioceptors. These proprioceptors in turn share postsynaptic targets in the motor neurons of the TA columelar group, which reside at spinal coordinates topographically aligned with the limb coordinates innervated by this group of proprioceptors. The ability of limb mesenchyme and muscle to direct gene expression in proprioceptors in accord with intralimb termination therefore presents an attractive model for the coordination of peripheral and central targeting in these neurons. Under this model, proprioceptor genes such as *cdh13*, with columelar expression patterns and known roles in cell-cell recognition, are especially attractive candidates for mediating target selectivity between Ia proprioceptive afferents and motor neurons.

6.2 Results

6.2.1 Transient erosion of sensory-motor target specificity in *cdh13* mutant mice

The recognition functions proposed for many type II cadherins (Duan et al., 2014) led us to examine whether elimination of Cdh13 function has any impact on the selectivity of monosynaptic sensory-motor connections. TA and GS motor neurons are situated within the same dorsoventral tier of the LMC but differ in mediolateral settling position. Its expression by TA but not GS proprioceptors therefore suggests that Cdh13 might gate the mediolateral trajectory of TA afferents.

We analyzed homozygous *Cdh13*::CreER^{T2} mice in which expression of *cdh13* is eliminated, henceforth termed *Cdh13^{mut}*::GFP mice. In *Cdh13^{mut}*::GFP animals, the number of muscle spindles present in dorsal and ventral shank muscles was similar to the number observed in *Cdh13^{het}*::GFP and wild-type mice (Figure 6.3A). In addition, TA but not GS proprioceptors of *Cdh13^{mut}*::GFP mice express GFP (data not shown), arguing against a role for *cdh13* in peripheral sensory targeting and muscle spindle formation.

To assess connectivity in *Cdh13^{mut}*::GFP mice, we utilized our ability to detect GFP expression at the proprioceptor central synapse (see Figure 2.7D). GFP expression was induced in *Cdh13^{mut}*::GFP mice and *Cdh13^{het}*::GFP control littermates

by tamoxifen injection at e16.5, and TA and GS motor neurons were labeled postnatally by intramuscular injection of ctb^{555}. The incidence of GFP$^+$ sensory boutons on TA and GS motor neurons was then assessed at both P7 and P18. In addition to their distinct mediolateral settling positions, TA and GS motor pools occupy different rostrocaudal positions within the LMC. We therefore restricted our analysis to the rostrocaudal extent of the LMC containing both TA and GS motor pools (L4-L5; see Figure 6.2E).

Comparison of the fraction of GFP$^+$ TA/EDL/PER sensory terminals in contact with antagonist GS group motor neurons in *Cdh13^{mut}*::GFP mice at P7 revealed a ~5-fold increase in GFP$^+$/vGluT1$^+$ proprioceptor terminals on retrogradely labeled GS/SOL/PL motor neurons compared with *Cdh13^{het}*::GFP littermates (Figures 6.3B and C; $p<0.001$). We were concerned that this difference might reflect the increased dosage of Cre protein in homozygous compared to heterozygous *Cdh13*::GFP mice. We therefore adjusted our data to reflect a 1.7-fold difference in active Cre protein and recombination efficiency between homozygous and heterozygous mice. Even with this correction, we found a ~3-fold increase in the incidence of ectopic GFP$^+$/vGluT1$^+$ boutons in *Cdh13^{mut}*::GFP mice at P7 ($p<0.01$).

Interestingly, by P18, the mistargeting of GS motor neurons by TA afferents in *Cdh13^{mut}*::GFP mice was far less pronounced (Figure 6.3C). This shift in phenotype is indicative of a restricted developmental period during which ectopic sensory

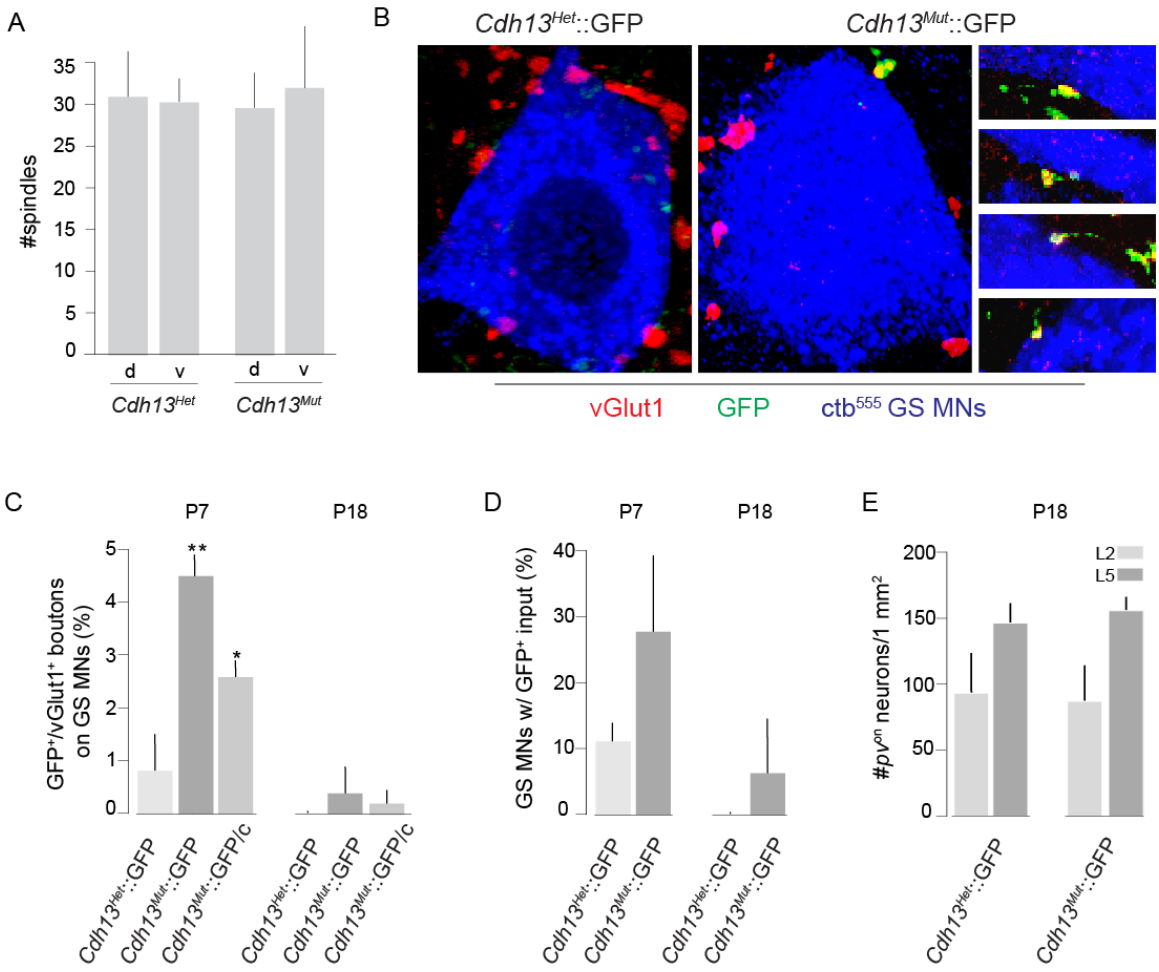

Figure 6.3 Deletion of *cdh13* results in transient ectopic connectivity between TA afferents and GS motor neurons

(A) *Cdh13*^{Mut}::GFP mice possess a normal complement of muscle spindles. Spindles were identified by Pv immunostaining of 25 µm cryosections of dorsal (d) or ventral (v) shank muscles at P0. (B) Transient erosion of sensory-motor specificity in *Cdh13*^{Mut}::GFP mice is revealed by the presence of GFP^{+} TA group boutons on retrogradely labeled GS motor neurons. Left: Retrogradely labeled GS motor neurons in the *Cdh13*^{Het}::GFP background lack GFP^{+} sensory boutons. Middle and Right: GFP^{+} inputs to GS motor neurons were observed in *Cdh13*^{Mut}::GFP mice. Pregnant *Cdh13*::GFP females were injected with tamoxifen at e16.5 of gestation. GFP^{+} proprioceptor input, demarcated by vGluT1, to the soma and proximal 100 µm dendrites of retrogradely labeled GS motor neurons

was analyzed in progeny at P7 and P18 in *Cdh13*^{Het}::GFP and *Cdh13*^{Mut}::GFP mice (n = 3 mice/genotype; P7 *Cdh13*^{Het}::GFP mice: n = 104 MNs, 1868 boutons; P7 *Cdh13*^{Mut}::GFP mice: n = 114 MNs, 1758 boutons; P18 *Cdh13*^{Het}::GFP mice: n = 75 MNs, 1572 boutons; P18 *Cdh13*^{Mut}::GFP mice: n = 45 MNs, 832 boutons). (C) Percentage of vGluT1^{+} inputs labeled by GFP on GS motor neurons of *Cdh13*^{Het}::GFP and *Cdh13*^{Mut}::GFP mice. *Cdh13*^{Mut}::GFP/c: value that corrects for the ~1.7-fold higher efficiency of tamoxifen-induced Cre recombination in *Cdh13*^{Mut}::GFP mice versus *Cdh13*^{Het}::GFP mice. Significant differences between *Cdh13*^{Mut}::GFP and *Cdh13*^{Het}::GFP mice were determined by Student's t-test (**p<0.001; *p<0.01). (D) Percentage of GS motor neurons receiving vGlut1^{+}, GFP^{+} input. (E) The density of Pv^{on} neurons in P18 DRG was unchanged between *Cdh13*^{Mut}::GFP and *Cdh13*^{Het}::GFP mice.

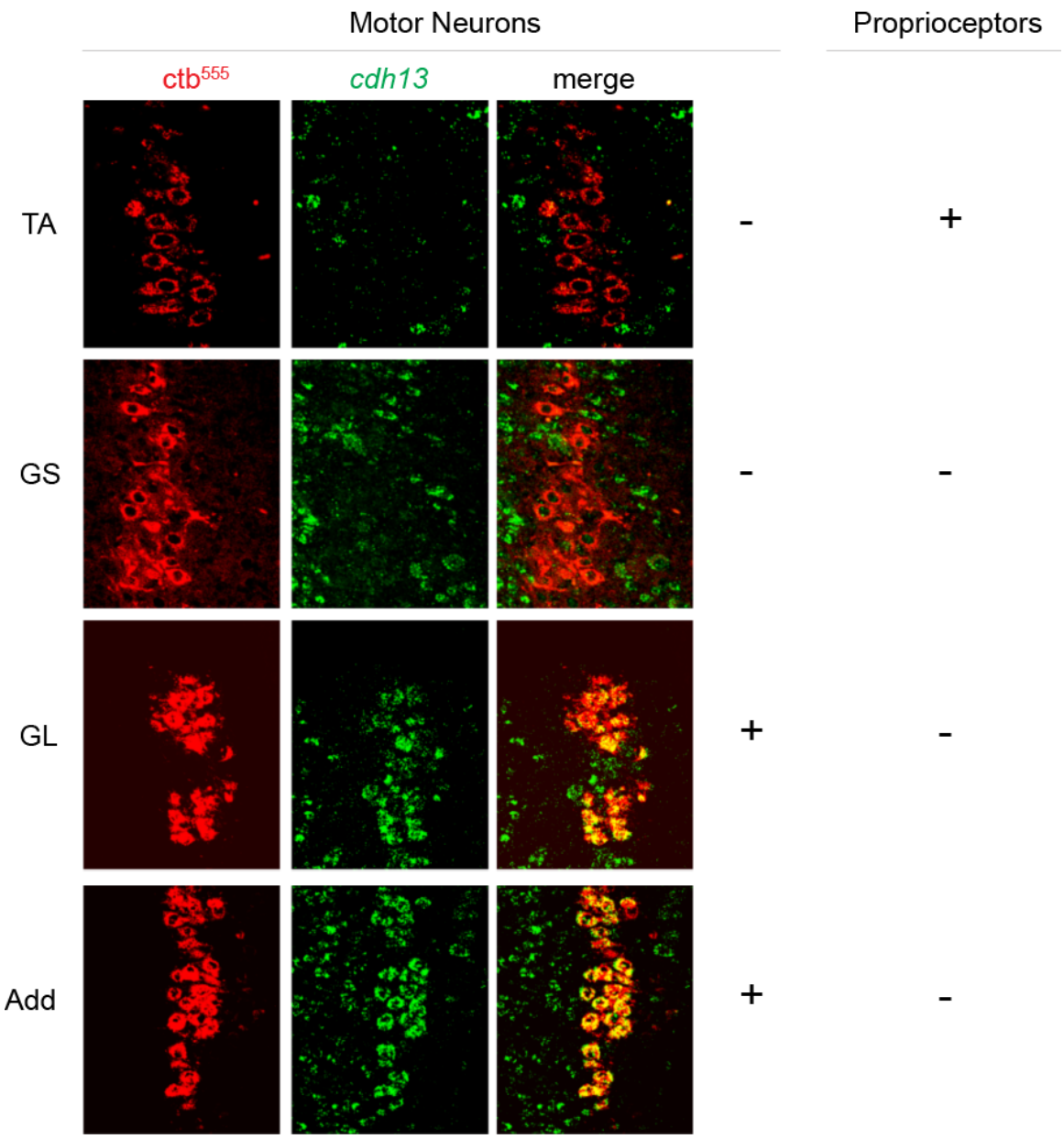

Figure 6.4 *Cdh13* expression in hindlimb motor pools

Cdh13 expression was examined by fluorescence *in situ* hybridization at P1 in backfilled motor neurons. Neither GS nor TA motor neurons expressed *cdh13*, while GL and Add motor neurons expressed the gene. The *cdh13* status of proprioceptors innervating these muscles is not correlated.

boutons are present on antagonist motor pools. The density of *pv*^{on} neurons in lumbar DRG did not differ significantly between *Cdh13*^{het}::GFP and *Cdh13*^{mut}::GFP mice (Figure 6.3E), arguing against cell death as the mechanism underlying the late correction of misprojections.

The formation of Cdh13 dimers in *trans* has been shown to inhibit neurite outgrowth *in vitro* (Ciatto et al., 2010). We therefore examined the *cdh13* expression status of motor pools receiving *cdh13*^{on} and *cdh13*^{off} homonymous proprioceptor innervation and found that neither TA nor GS motor neurons express *cdh13*, indicating that Cdh13 likely does not establish synaptic specificity within the TA and GS reflex arcs via inhibitory dimerization in *trans*. However, we did observe expression of *cdh13* in the GL and Add motor pools, both of which are situated ventrally with respect to the TA motor pool. It is therefore possible that *cdh13* expression by GL and Add motor neurons might repel TA afferents from projecting too far ventrally within the LMC, analogous to the reported Sema3E/PlxnD1-mediated repulsion of hamstring afferents by GL motor neurons within the LMC (Fukuhara et al., 2013).

6.2.2 *vstm2b* knockout mice lack TA afferent misprojections to GS motor neurons

The near-complete restriction of *vstm2b* expression to proprioceptors innervating dorsal limb musculature (see Figure 2.5H) led us to consider a role for

this gene in targeting laterally situated LMC motor neurons. *vstm2b* is predicted to encode a transmembrane protein belonging to the Ig superfamily (IgSF), a large class of molecules with diverse roles in neuronal circuit formation (Figures 6.5A and B; Rougon and Hobert, 2003). The murine VSTM gene family includes *vstm2a*, *vstm2b*, *vstm2l*, *vstm3*, *vstm4*, and *vstm5* (Figures 6.5B, C and D), all of which encode IgSF proteins of various complexity and domain structure. Of these, the best-studied is Vstm3 (TIGIT), which interacts with two nectin IgSF proteins at the immunological synapse between natural killer and T cells to regulate T cell activation (Levin et al., 2011).

Because β-galactosidase protein is not transported axonally in *Vstm2b*::LacZ mice, we were unable to utilize reporter expression to assay for the presence of *vstm2b*^{on} TA group boutons on GS motor neurons. Instead, we took advantage of the differential transport properties of the neuronal tracers ctb and rhodamine-dextran. While both rhodamine-dextran and ctb are retrogradely transported to motor neuron and proprioceptor cell bodies, only ctb is transported transganglionically to central synapses (Figure 6.6A; Sürmeli et al., 2011), thereby allowing two populations of motor neurons and one population of sensory terminals to be labeled in one experimental animal.

Using this method, we assayed for misprojections by TA proprioceptors onto GS motor neurons at P7 in *Vstm2b*^{mut}::LacZ mice. Comparison of the fraction of ctb^{+} TA sensory terminals in contact with antagonist GS group motor neurons in

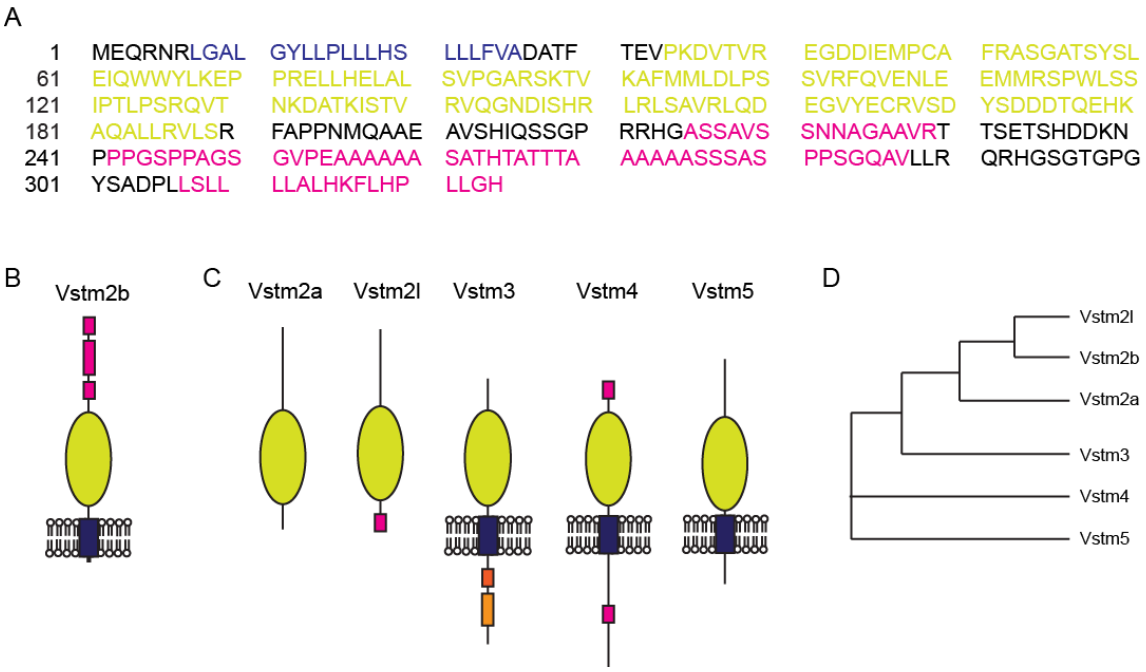

Figure 6.5 Structure of Vstm2b and other VSTM family members

(A) Primary amino acid sequence of Vstm2b. Note that Vstm2b is a Type II transmembrane protein, with its transmembrane domain near the N terminus. Blue: transmembrane domain. Green: IgV domain. Pink: putative low complexity domains. (B) Structure of Vstm2b, with domains colored as in (A). (C) Predicted structures of other murine VSTM proteins based on primary amino acid sequence. Vstm2a and 2l lack transmembrane domains. Vstm3 (TIGIT) is unique in the presence of an ITIM domain, which signals intracellularly. (D) Cladogram illustrating the relationship between primary amino acid sequences of murine VSTM proteins.

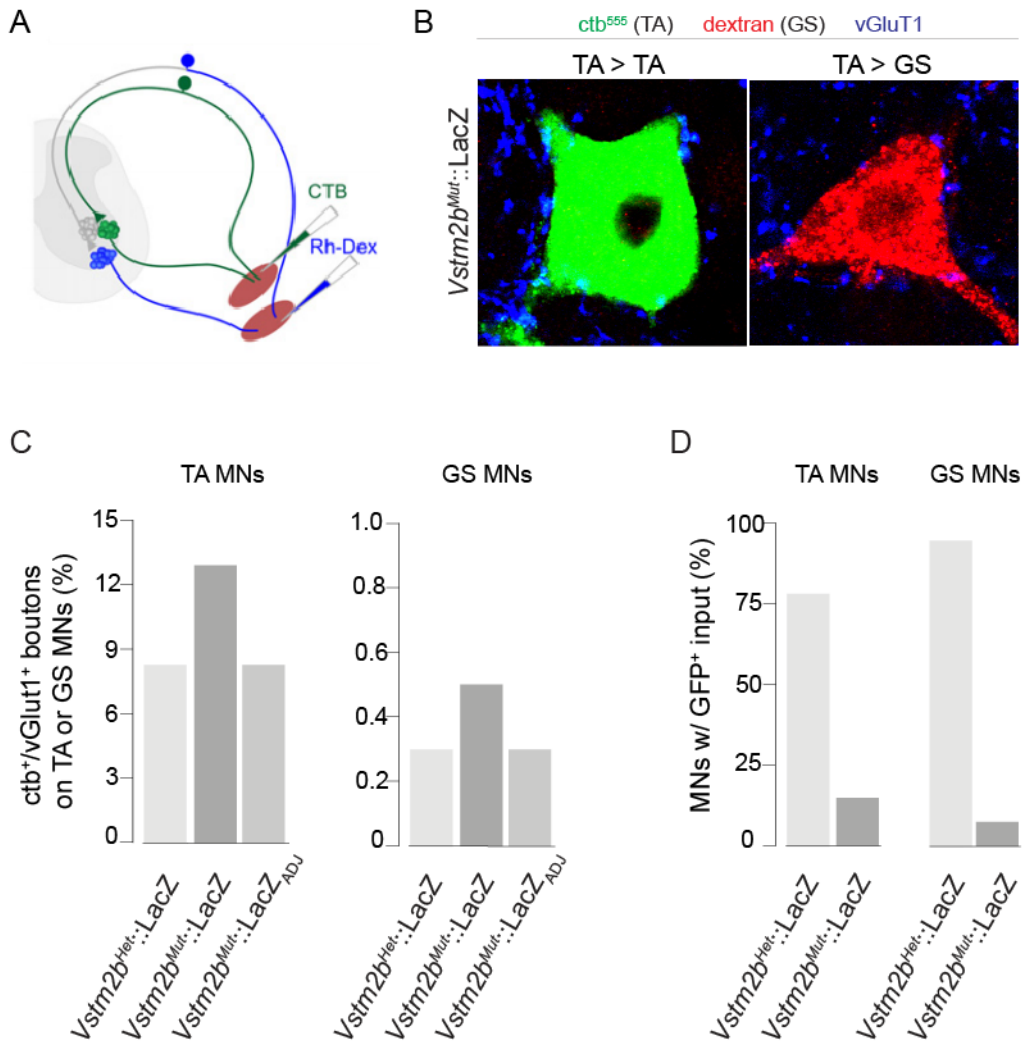

Figure 6.6 Antagonist specificity is preserved in the absence of *vstm2b*

(A) Retrograde labeling with ctb and dextran identifies motor neurons innervating one of two muscles and proprioceptors innervating one muscle. (B) Sensory-motor specificity is maintained in *Vstm2b*^{mut}::LacZ mice, as indicated by examination of TA boutons on GS motor neurons at P7. Left: TA boutons on TA motor neurons are identified by coincidence of ctb and vGluT1. Right: GS motor neurons lacked ctb^{+}, vGluT1^{+} boutons, indicating that antagonist avoidance is preserved in *Vstm2b*^{mut}::LacZ mice. ctb^{+} proprioceptor input, demarcated by vGluT1, to the soma and proximal 100 µM dendrites of retrogradely labeled TA or GS motor neurons was analyzed in *Vstm2b*^{het}::LacZ and *Vstm2b*^{mut}::LacZ mice at P7 following tracer injection at P3 (*Vstm2b*^{het}::LacZ mice: n = 18 TA and 16 GS MNs, 878 TA and 597 GS boutons; *Vstm2b*^{mut}::LacZ mice: n = 19 TA and 16 GS MNs, 533 TA and 372 GS boutons). (C) Percentage of vGluT1^{+} inputs labeled by ctb on TA and GS motor neurons of *Vstm2b*^{het}::LacZ and *Vstm2b*^{mut}::LacZ mice. *Vstm2b*^{mut}::LacZ$_{ADJ}$: values normalized for the efficiency of ctb transport between individual mice. (D) Percentage of GS motor neurons receiving vGlut1^{+}, ctb^{+} input.

Vstm2b^{mut}::LacZ mice revealed no difference in the proportion of ctb^{+}/vGluT1^{+} proprioceptor terminals on retrogradely labeled GS/SOL/PL motor neurons compared with *Vstm2b*^{het}::LacZ littermates after adjusting for efficiency of retrograde labeling (Figures 6.6B and C). Thus, Vstm2b does not appear to influence selectivity within the TA and GS reflex arcs.

6.3 Discussion

6.3.1 Involvement of Cdh13 and Vstm2b in sensory-motor circuit formation

In this chapter, we have identified a role for *cdh13* in motor neuron target discrimination by Group Ia proprioceptive afferents. While its effect is clear, the molecular mechanism by which Cdh13 mediates recognition is less so. Cdh13 is an atypical GPI-anchored cadherin and as such lacks an intracellular domain with signal transduction capacity, suggesting that it must act in *cis* with an as yet unknown coreceptor in its role mediating target recognition. Furthermore, motor neuron *cdh13* expression does not match proprioceptor expression of the gene in a manner corresponding to homophilic or homophobic recognition, raising the question of what Cdh13 binds in *trans*.

Studies of afferent trajectory in FoxP1 mutant mice hold clues to the cellular source of Cdh13 ligand. Afferents in FoxP1 mutants maintain the ability to target appropriate dorsoventral tier domains of the LMC when motor neurons are scrambled or even absent, suggesting that guidance cues directing dorsoventral

afferent trajectory are supplied by the neuropil surrounding motor neurons (Sürmeli et al., 2011). However, mediolateral targeting is disrupted in these mice, indicating that along this axis, guidance cues are supplied by motor neurons themselves (Sürmeli et al., 2011). Thus, a heterotypic binding partner for Cdh13 is likely to be located on the motor neuron surface.

We also lack a mechanistic explanation for the transience of misprojections observed in *Cdh13*^{mut}::GFP mice. While activity-dependent refinement does not appear to sculpt the initial pattern of homonymous monosynaptic connections in wild-type mice, it could act to eliminate errant contacts in a mutant context. As mice become ambulatory over the first few weeks of postnatal life, rhythmic locomotor activity might act to strengthen appropriate monosynaptic contacts and prune the rare ectopic TA boutons present on GS motor neurons in *Cdh13*^{mut}::GFP mutants.

We were unable to observe an effect of *vstm2b* deletion on specificity within the TA and GS reflex arcs, despite its expression by dorsal proprioceptors and suspected role in mediolateral targeting. It is possible that the lack of misprojection phenotype observed in *Vstm2b*^{mut}::LacZ mice was due to low efficiency of bouton labeling by ctb. To circumvent this problem, the *Cdh13*::GFP reporter allele could be used in place of ctb to label central synapses. Because all TA group proprioceptors express both *vstm2b* and *cdh13*, *Cdh13*::GFP expression could be used to examine the termination pattern of *vstm2b*^{on} TA group afferents in the *vstm2b* knockout background. Alternatively, physiological methods could be used to assay for

misprojections in *Vstm2b*^{mut}::LacZ mice; short-latency monosynaptic input to antidromically identified motor neurons can be assessed via intracellular recording following stimulation of individual muscle nerves (refer to Fukuhara et al., 2013).

The relatively late onset of *vstm2b* at e13.5 (Figure 3.5) argues against a role in peripheral sensory targeting, although Vstm2b might be involved in the formation of muscle spindles. Complicating our assessment of Vstm2b function is our inability to determine its subcellular localization. Attempts to generate a Vstm2b antibody have yielded non-specific staining or cross-reactivity with Vstm2a; the effort to produce a specific reagent is ongoing. Determining whether Vstm2b protein is present on the axon or at peripheral or central axon terminals would greatly aid our characterization of its function in proprioceptors.

6.3.2 Completing the monosynaptic connectivity matrix

Sensory-motor circuit assembly requires the contribution of several distinct developmental mechanisms. Sensory afferents utilize positional targeting, molecular recognition, and activity-dependent mechanisms during sequential stages of circuit formation that require increasingly subtle forms of target discrimination.

The small but significant misprojection phenotype observed in *Cdh13*^{mut}::GFP mice is consistent with the view that formation of the complete matrix of monosynaptic connectivity is a highly redundant and combinatorial process

(Schwabe et al., 2013). Indeed, the lack of overt behavioral deficits in *Cdh13*^{mut}::GFP mice (data not shown) supports a role for functional redundancy in the formation of this crucial circuitry. Furthermore, the large number of differentially expressed guidance and adhesion molecules identified in our screen of muscle-type proprioceptors suggests that combinatorial gene expression is likely to define proprioceptor muscle-type subsets. Future studies will focus on characterizing the large number of differentially expressed genes whose functions in the assembly of spinal circuitry have not yet been ascertained, including known recognition molecules Sema5a and Crtac1.

Expression of *cdh13* demarcates a proprioceptor columelar group, and our analysis of *Cdh13*^{mut}::GFP mice implicates Cdh13 in maintaining the fidelity of columelar targeting. While such a mechanism would restrict afferents to small regions of the LMC that contain biomechanically appropriate motor neuron target populations, the connectivity within these columelar domains must be weighted according to the homonymous or heteronymous status of the motor neurons contained within. How might these fine distinctions be achieved?

One possibility is suggested by the *cdh13*^{on} "pool" identity of rectus femoris proprioceptors (Figure 2.5D). The *cdh13* expression status of rectus femoris muscle deviates from that of its vastii synergists within the quadriceps group - a difference that could conceivably mediate discrimination between homonymous and heteronymous motor neuron targets. Alternatively, proprioceptor activity could

account for the synaptic weighting observed in mature animals. Indeed, following blockade of sensory transmission by tetanus toxin expression in proprioceptors, an increase in the incidence of heteronymous connections was observed within the TA synergist group, suggesting that connections within a columelar group are initially promiscuous and are later pruned by activity-mediated feedback (Mendelsohn et al., 2015).

6.3.3 Beyond monosynaptic connectivity: proprioceptor input to local interneuron circuits

The *cdh13*^{on} status of all proprioceptors innervating a given muscle raises the question of why its expression is required in Group Ib and II afferents. While we have identified a role for Cdh13 in mediating monosynaptic contacts between Ia afferents and motor neurons, the reason for its presence in Ib and II afferents, which do not contact motor neurons directly, is less clear.

Recent work has characterized the topographical and molecular organization of various local interneuron populations in the spinal cord (Bikoff et al., 2016; Gabitto et al., 2016; Tripodi et al., 2011). Genetic studies have identified a number of subpopulations within the Engrailed1-defined V1 cardinal interneuron population that are marked by combinatorial transcription factor expression (Bikoff et al., 2016; Gabitto et al., 2016). These transcriptionally defined subpopulations occupy discrete spatial domains and are likely to express different combinations of surface

recognition molecules based on transcription factor profile. Moreover, several of these subpopulations, such as Renshaw cells, are integrated into distinct spinal microcircuits with respect to motor neurons. It is highly likely that these interneurons receive differential input from muscle-type proprioceptor subsets, invoking a need for molecular distinctions encompassing Group Ib and II afferents. Although we lack tools for the representation of *vstm2b* at end organs within muscle, our backfill studies of *vstm2b* strongly imply that it is expressed by Group Ia, II and Ib proprioceptors: *vstm2b* expression is consistently detected in 100% of TA proprioceptors identified by retrograde labeling. Thus, although we were unable to demonstrate a need for Vstm2b in the formation of monosynaptic specificity, its expression might be required for differential connectivity with spinal interneuron populations.

7 General discussion

In this thesis, I have described efforts to characterize proprioceptor subtype identity as it relates to limb muscle innervation. I employed RNA-Sequencing to identify genetic determinants of proprioceptor subpopulations terminating in distinct muscles or muscle groups located at distinct positions along the proximodistal and dorsoventral axes of the mouse hindlimb, resulting in the identification of proprioceptor genes whose expression is correlated with peripheral innervation. Detailed characterization of the expression of several of these genes – *cdh13*, *vstm2b*, *sema5a*, and *crtac1* – revealed hierarchical principles of proprioceptor organization with respect to limb biomechanics and the pattern of spinal connectivity between limb-innervating sensory afferents and motor neurons.

The identification of proprioceptor muscle-type genes enabled me to assess the impact of three peripheral tissues – motor axon, limb mesenchyme and target muscle – on the specification of proprioceptor subtype identity. I first found that motor axon plays neither an instructive nor permissive role in inducing proprioceptor gene expression. I next observed that the dorsoventral identity of the limb mesenchyme instructs patterned expression of *cdh13*, *vstm2b*, *sema5a*, and *crtac1* in proprioceptors. Lastly, I found that muscle is dispensable for proprioceptor *cdh13* expression but is required for *vstm2b* induction, in which it may play either an instructive role by directly patterning *vstm2b* or a permissive one via an effect on mesenchyme.

Finally, I examined whether *cdh13* or *vstm2b* plays a role in establishing selective connections between muscle-specific afferent populations and their motor neuron targets. While I detected no role for Vstm2b in the formation of specific contacts between TA afferents and GS motor neurons, I observed a subtle targeting defect between these populations in *Cdh13* mutant mice, thereby providing a direct molecular link between peripheral specification of proprioceptor subtype identity and the ability of these afferents to form patterned connections in the spinal cord.

Here, I discuss these findings in the context of the development of neuronal circuits underlying coordinated limbed movement. I elaborate alternative limb-based and intrinsic strategies for specifying proprioceptor subtype diversity, and describe how these mechanisms might contribute to the formation of mature circuitry in the spinal cord. I also propose several experiments rooted in our findings that are designed to uncover the transcriptional logic and molecular mechanisms of proprioceptor subtype specification.

7.1.1 Proprioceptor diversity assigned in limb motor coordinates

The distinct molecular character of muscle-type proprioceptors, exemplified by *cdh13*, *vstm2b*, *sema5a*, and *crtac1* expression, reveals molecular differences that correlate with muscle positional character. Genes that mark defined subsets of proprioceptors had been identified previously, but without examining the link

between gene expression and the domain of limb innervation. For example, *plexinD1* and *lmo4* are expressed by proprioceptors supplying both dorsal and ventral muscles, but the status of molecular expression with regard to the proximodistal limb axis has not been analyzed (Chen et al., 2002; Fukuhara et al., 2013).

Our muscle-by-muscle analysis of proprioceptor *cdh13* expression indicates that the muscle-type identity of proprioceptors is assigned in a positional manner that conforms to the common biomechanical function exhibited by synergist muscle groups (Eccles et al., 1957; Nichols, 1994). It also implies that proprioceptor and motor pool identities adhere to the same positional logic. This is perhaps not surprising, since the peripheral and central terminals of both sets of neurons occupy the same local microdomains in the limb and spinal cord. The expression of *cdh13* by proprioceptors innervating each of the ankle flexor muscles further suggests that functionally related proprioceptors share a common molecular profile. Nevertheless, in some instances, proprioceptor identity segregates with individual muscles. This is apparent in the expression of *cdh13* by proprioceptors innervating the rectus femoris but not vastii muscles, potentially a reflection of the distinct biomechanical features and activity profiles of these muscles (Eccles et al., 1957; Nichols, 1994).

Other proprioceptor subtype genes identified in our screen – notably *vestm2b*, *sema5a*, and *crtac1* – exhibit patterns of expression distinct from that of *cdh13*, yet conform to the core principle of positional distinctions for individual limb

domains. The fact that *cdh13* and *vstm2b* are expressed by proprioceptors supplying partially overlapping muscle groups suggests that the logic of proprioceptor pool identity may emerge through combinatorial programs of specification supplied by both limb mesenchyme and muscle, as discussed in Chapter 5. Thus, the limb mesenchyme may coordinate multiple aspects of motor circuit assembly by regulating muscle cleavage and motor axon guidance, as well as the specification of proprioceptor muscle-type identity.

7.1.2 Linking peripheral specification and central connectivity

A number of the genes identified and characterized in proprioceptors as a result of our screen are known to function as guidance and adhesion molecules. The role of limb peripheral tissue in instructing proprioceptor connectivity with motor neurons prompted us to examine whether these genes might be involved in establishing specific monosynaptic contacts with motor neurons. Some support for a role for muscle-type identity in establishing sensory-motor specificity is provided by our analysis of *cdh13* mutant mice, which exhibit a modest incidence of aberrant sensory-motor connections. The nature of the observed changes in connectivity in *cdh13* mutants could reflect the combinatorial or redundant roles of other molecules in establishing final patterns of sensory-motor connectivity. Moreover, because *cdh13* is not expressed by GS or TA motor neurons, heterophilic interactions may link Cdh13 to other type II cadherins. Limb inductive signals that specify dorsoventral proprioceptor identity are likely to instruct the recognition of

motor neurons in medial and lateral divisions of the LMC, whereas proximodistal limb signaling may confer recognition of the tier domains that appear to contribute to the dorsoventral patterning of sensory-motor connections (Sürmeli et al., 2011).

To this end, we surmised that *vstm2b* might play a role in discriminating between medial and lateral LMC motor neurons. Vstm2b is predicted to encode a type II transmembrane Ig-domain protein, placing it physically within the membrane where it could be involved in cellular recognition. However, we did not observe a connectivity defect in *vstm2b* mutant animals. This may be due to limitations of the technical approach used to assay misprojections; below, I discuss an alternative strategy for labeling TA afferents that may improve our ability to detect aberrant synapses. Vstm2b may also be involved in establishing selective connectivity with interneuron populations in the spinal cord. However, prior to assaying the putative functional involvement of Vstm2b in any aspect of circuit formation, it is critical to determine whether it is present at central and/or peripheral proprioceptor terminals. Unfortunately, in the absence of a specific antibody, we are unable to assess the subcellular localization of Vstm2b in proprioceptors at different stages of circuit formation.

7.1.3 A role for intrinsic specification in defining proprioceptor muscle-type identity

The abundance of evidence pointing to a peripheral influence in sensory patterning led us to focus our examination of proprioceptor subtype specification on the role of limb elements. However, studies performed in chick have suggested that some aspects of proprioceptor subtype identity might be intrinsically specified. Lmo4, which marks a subset of proprioceptors in a manner correlated with muscle innervation, is expressed in the same proportion of proprioceptors following limb ablation, indicating that its expression is patterned in the absence of limb-derived cues (Chen et al., 2002).

One of our proposed models for *vstm2b* induction raises the possibility that intrinsic features of proprioceptor identity might be required for the acquisition of muscle-type identity. In the model of *vstm2b* induction involving a permissive role for muscle, we propose that generic features of proprioceptor identity might create a cellular environment that is competent to respond to dorsoventrally restricted mesenchymal cues. One interpretation of our study of *vstm2b* expression holds that the expression of muscle-type markers by proprioceptors but not cutaneous sensory neurons requires the activation of as-yet-unidentified surface effector molecules downstream of pan-proprioceptor transcription factors such as Runx3 or Er81 to mediate a selective response to restricted mesenchymal cues. Such intrinsically specified determinants of proprioceptor muscle-type identity would be characterized by several properties: (1) expression prior to innervation of the limb bud and in the absence of the limb bud; (2) restricted expression by proprioceptors; and (3) protein localization to the cell membrane.

7.1.4 Alternative modes of peripheral specification

As discussed in Chapter 6, the topographic alignment between limb coordinate and motor neuron settling position suggests a scheme for simplifying the connectivity problem faced by proprioceptors. Limb positional coordinates imposed by cues distributed along the cardinal limb axes might induce gene expression profiles in proprioceptors that instruct the targeting of discrete spinal coordinates containing appropriate motor neuron targets. Our screen of muscle-type identity was designed with this possibility in mind; we surveyed genetic distinctions in proprioceptors correlated with termination along the proximodistal and dorsoventral hindlimb axes, with the ultimate goal of exploring the influence of the cues assigning limb positional values on the generation of neuronal diversity.

Beyond this model, NT3 signaling has been proposed to play a role in specifying proprioceptor subtype identity, providing an alternative pathway for generating proprioceptor diversity. NT3 is expressed at distinct levels by different muscles of the embryonic hindlimb (Figure 7.1A and B). Interestingly, the level of muscle NT3 expression is uncorrelated with the position of the muscle along the three cardinal limb axes. While the need for mosaic muscle-by-muscle NT3-dependent programs of gene expression in limb-innervating proprioceptors is unclear, NT3 appears to play a broader role in the specification of proprioceptor

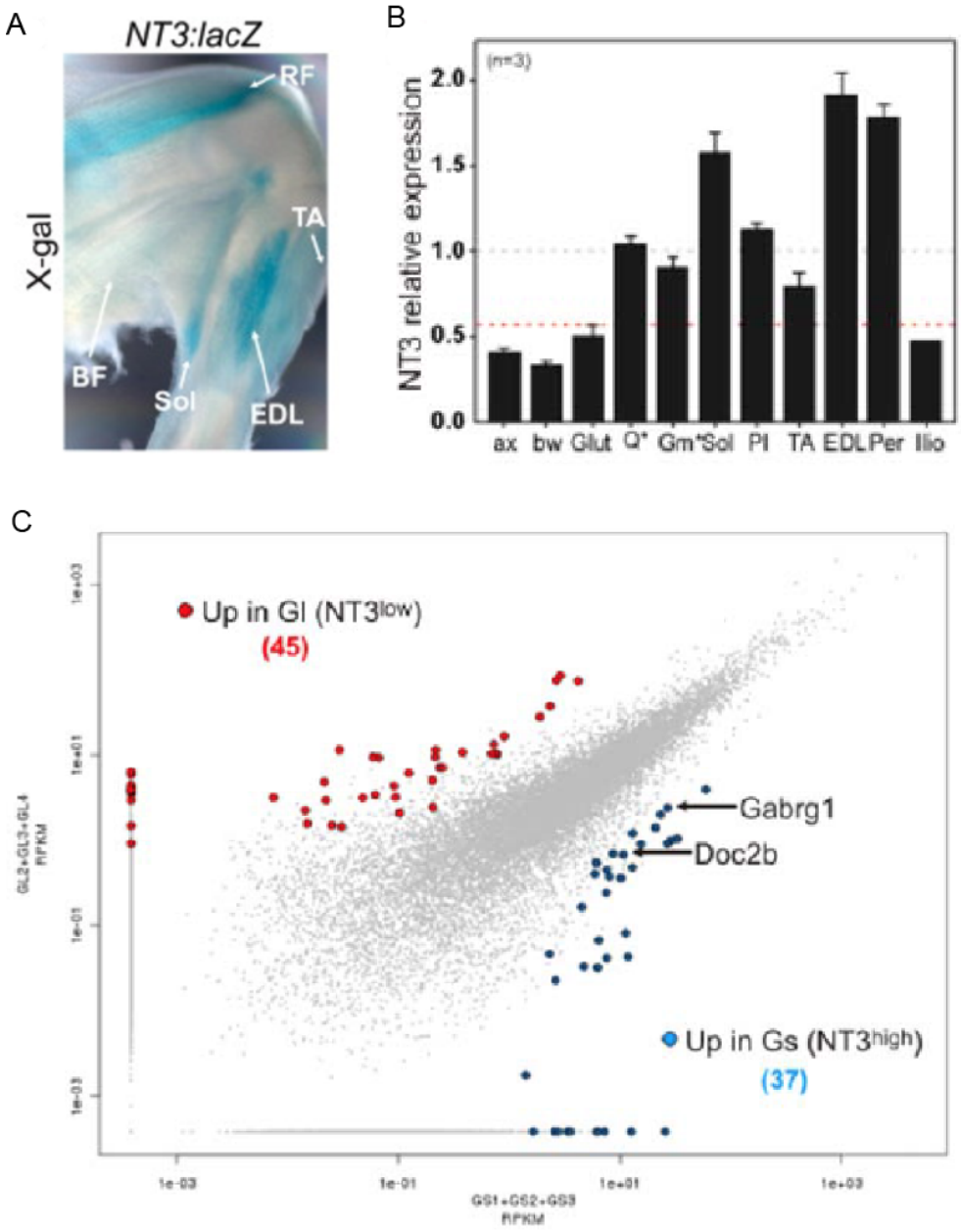

Figure 7.1 Muscle NT3 level directs proprioceptor subtype identity

(A) β-gal activity levels in e15.5 embryonic hindlimb muscles of *NT3*::LacZ mice. Muscles indicated are rectus femoris (RF), soleus (Sol), extensor digitorum longus (EDL), tibialis anterior (TA), and biceps femoris (BF). (B) *NT3* expression levels in e16.5 hindlimb muscles relative to *MyoD*. Asterisk denotes that NT3 expression in Quadrieps (Q) and medial Gastrocnemius (Gm) is asymmetrically distributed, with the highest MT3 levels observed near sensory endings. ax: axial; bw: body wall; Glut: gluteus; Pl: plantaris; Per: peroneus; Ilio: iliacus. (A and B) are adapted from de Nooij et al., 2013. (C) Pairwise comparison of GL and GS samples reveals 45 and 37 upregulated transcripts, respectively, that may be regulated by muscle NT3 level. Taken from the RNA-Seq dataset presented in Chapter 2.

subtypes. The expression level of NT3 differs uniformly between axial and hypaxial musculature, suggesting that NT3 signaling through the TrkC receptor could direct class-defining features of axial and hypaxial proprioceptors (de Nooij et al., 2013). Muscle NT3 level is correlated with proprioceptor sensitivity to loss of the transcription factor Er81 (de Nooij et al., 2013). Notably, several muscles low in NT3 expression and deprived of proprioceptor innervation in Er81 mutants - limb gluteus and adductor muscles, hypaxial muscles, and axial muscles - share one organizational feature: lack of group Ia reciprocal inhibitory circuitry in the spinal cord (refer to Figure 1.1; Eccles and Lundberg, 1958; Jankowska and Odutola, 1980; Sears, 1964). Thus, the proprioceptor NT3-Er81 signaling cassette may confer gene expression profiles that help to organize spinal circuitry appropriate to the biomechanical demands of the target muscle group.

Our muscle-type RNA-Seq data has been used to probe the role of differential NT3 signaling by limb muscles in assigning proprioceptor subtype identity. The gluteus muscle expresses low levels of NT3 during embryonic development, while the gastrocnemius muscle is marked by comparatively high NT3 expression. It is therefore possible that distinctions in gene expression between GL and GS proprioceptors are reflective of differential exposure to NT3. Our comparison of GL and GS proprioceptors yielded 45 genes upregulated in GL proprioceptors and 37 upregulated in GS. While the investigation of these genes with respect to NT3 signaling is ongoing, one GS gene – *spp1* – appears to be directly regulated by the level of NT3 supplied by muscle (Joriene de Nooij, unpublished data).

7.2 Future directions

7.2.1 Patterning proprioceptor proximodistal identity

In this thesis, I focused my investigation of proprioceptor subtype specification by the periphery on the influence of the dorsoventral hindlimb axis. However, many of the genes identified in our RNA-Seq screen are predicted to differ in expression along the proximodistal axis of the hindlimb; in one of many examples, *cdh13* is restricted to proprioceptors innervating distal segments of the limb (Figure 2.5). Given what is known about limb development, how might the proximodistal restriction of proprioceptor muscle-type gene expression be achieved?

During embryonic development, the outgrowth and segmental morphology of the limb is established by opposing gradients of retinoic acid (RA) and FGF (Mariani et al., 2008; Vogel et al., 1996; Yashiro et al., 2004) . RA is produced at the proximal end of the limb by the synthetic enzyme RALDH2, and FGFs are expressed at the distal end of the limb by cells of the apical ectodermal ridge (Figure 7.2A). These gradients direct the expression of Hox transcription factors and cofactors by limb mesenchyme in discrete proximodistal domains that give rise to the thigh, shank and foot of the mature hindlimb (Figure 7.2A; Cooper et al., 2011; Mercader et al., 2005). Intriguingly, we examined response to RA signaling in a mouse line expressing LacZ under control of a RA response element (RARE::LacZ) and observed signal in a subset of DRG neurons at e14.5, raising the possibility that

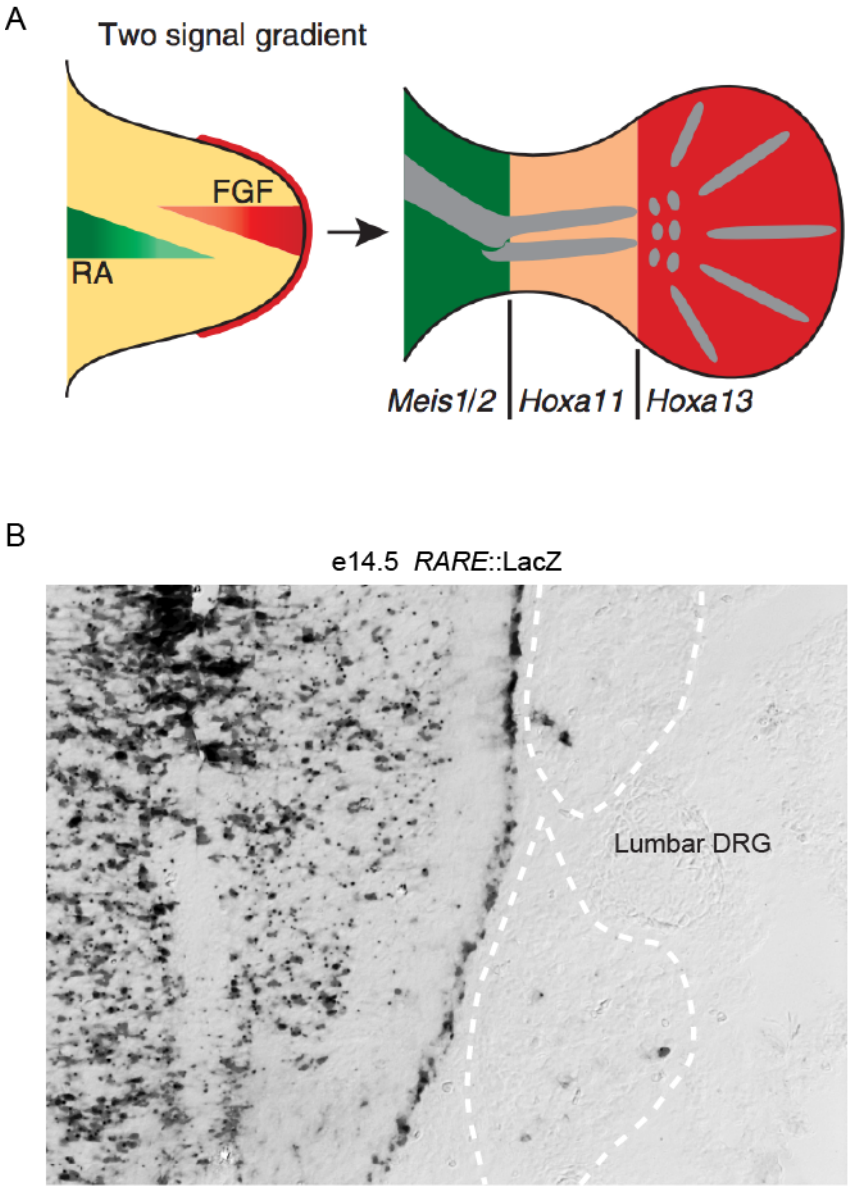

Figure 7.2 Retinoic acid and FGFs pattern the proximodistal limb axis

(A) Proximodistal RA and FGF gradients direct specification of limb proximodistal patterning, including the induction of mesenchyme transcriptional domains. Adapted from Bénazet and Zeller, 2009. (B) X-Gal staining in *RARE*::LacZ embryos reveals a subset of lumbar DRG neurons responsive to retinoic acid at e14.5.

proprioceptors are influenced by RA signaling around the time muscle-type gene expression is initiated (Figure 7.2B).

Assessing the impact of proximodistal ectodermal or mesenchymal character on proprioceptor gene expression poses a practical challenge. Whereas manipulation of the dorsoventral limb axis results in the duplication of limb tissues, altering the expression of genes involved in proximodistal patterning often results in limb truncation or segmental deletion (Sun et al., 2002), rendering an assessment of gene expression by proprioceptors innervating ectopic limb territory impossible. Thus, rather than examining mice deficient in proximodistal patterning genes, a more fruitful strategy may be to adopt a genetic gain-of-function approach. The generation of a *Rosa26*::lox-STOP-lox.RALDH2 or similar FGF transgenic line, when combined with a *Prx1*::Cre driver, would drive the overexpression of proximodistal patterning genes throughout the limb mesenchyme. Although this approach comes with potential complications regarding the timing and tissue source of ectopically expressed patterning cues, these modifications have not yet been attempted in mice and may provide a suitable system for examining proprioceptor muscle-type gene expression in an altered proximodistal context.

It is interesting to note that the extent of the truncation or deletion phenotypes observed following deletion of proximodistal patterning genes differs between the forelimb and hindlimb (Sun et al., 2002), with forelimb defects often

being less severe. To this end, characterizing the expression patterns of muscle-type genes in forelimb-innervating proprioceptors may be useful.

7.2.2 Probing the transcriptional logic of proprioceptor muscle-type identity

The Hox code that specifies motor neuron pool identity is directed by opposing gradients of RA and FGF signaling (Dasen and Jessell, 2009). Likewise, we expected that the RA and FGF gradients present in the developing hindlimb would direct a transcription factor code underlying the specification of proprioceptor muscle-type identity. However, we failed to identify a transcriptional logic in muscle-type proprioceptors resembling that of motor neurons.

This may be due to the developmental timing of our screen. Prior to this study, the only method permitting the identification of proprioceptors by muscle innervation was neuronal tracer backfill, which must be performed postnatally. However, any transcription factors specifying proprioceptor muscle-type identity would presumably be induced soon after hindlimb innervation around e11.5 and might be required only transiently to direct muscle-type programs of gene expression. Transcription factor expression might therefore have been downregulated prior to our characterization of muscle-type distinctions at P1.

The markers identified in our screen now permit the isolation of proprioceptors innervating distinct muscles by genetic reporter expression. It is

now possible to isolate muscle-type proprioceptors as early as e12.5 using *Cdh13*::GFP mice. Likewise, isolation of *vstm2b*-expressing proprioceptors should be possible as early as e13.5 using the *Vstm2b*::LacZ allele in combination with a commercially available substrate designed to fluorescently label live β-gal-expressing cells. In combination with a fluorescent reporter of proprioceptor status driven by the *pv* or *runx3* promoter, these tools will permit the isolation and comparison of *cdh13*^{on}/*vstm2b*^{on}, *cdh13*^{off}/*vstm2b*^{on}, and *cdh13*^{off}/*vstm2b*^{off} proprioceptors – overlapping but distinct muscle-type cohorts with unique proximodistal and dorsoventral termination patterns - at e13.5. This approach will yield an unprecedented view into the early steps of proprioceptor muscle-type specification and should result in the identification of transcription factors that assign muscle-type identity.

7.2.3 Identifying proprioceptor patterning cues

Our experiments have identified requirements for limb mesenchyme and muscle in patterning proprioceptor muscle-type gene expression. However, the molecular agents acting within these tissues to directly influence proprioceptor gene expression remain unknown. How might we identify the molecules involved in patterning proprioceptor muscle-type gene expression?

Our studies of *cdh13* induction indicate definitively that its patterning cue is supplied by limb mesenchyme. Due to the dorsodistal restriction in *cdh13*^{on}

proprioceptor innervation, we expect that the *cdh13* patterning cue(s) will be similarly compartmentalized along the proximodistal and dorsoentral axes in one of several possible patterns depending on the inductive or repressive nature of the patterning cue(s) involved. Interestingly, studies examining the altered transcriptional profile of the mesenchyme in double-ventral limbs have identified genes regulated by *lmx1b* whose expression is restricted along the dorsoventral and proximodistal axes (Feenstra et al., 2012; Gu and Kania, 2010; Krawchuk and Kania, 2008). We can therefore adopt a candidate approach to identifying *cdh13* inductive molecules. The secreted cerebellin (Cbln) family of proteins contains candidates for *cdh13* induction, given their restricted expression by dorsal limb mesenchyme and downregulation from limb mesenchyme in *Lmx1b*$^{-/-}$ mice (Feenstra et al., 2012; Haddick et al., 2014). Alternatively, it is possible that mesenchymal cues responsible for guiding motor axons have a dual role in specifying proprioceptor muscle-type identity: ephrins, glial-derived neurotrophic factor (GDNF), and netrin1 are expressed in a restricted manner by dorsal or ventral limb mesenchyme and regulate the dorsoventral choice of motor axons (Poliak et al., 2015; Stifani, 2014). An *in vitro* culture system could be used to test the ability of these proteins to induce *cdh13* expression in explanted *Cdh13*::GFP lumbar DRG.

Proprioceptor *vstm2b* expression presents a more complicated scenario in that it might be patterned directly by muscle or through a permissive effect of muscle on mesenchymal gene expression. We must therefore consider two possible tissue sources of patterning information. Regardless of tissue source, a *vstm2b*

pattering cue must meet several criteria. The muscle-type expression pattern of *vstm2b* dictates that its patterning cue will be restricted to the dorsal or ventral limb and will span its proximodistal extent, regardless of tissue source. Unlike putative *cdh13* inductive cues, the expression of a *vstm2b* patterning gene would be downregulated in *Lbx1* mutants due to the requirement of muscle for its expression. Furthermore, because of the patterning defect observed following *lmx1b* manipulation, we would expect the expression of this cue to be either absent or ectopically expressed, depending on the inductive or repressive nature of the signal, in the double-ventral limbs of *Lmx1b* mutants.

To identify putative muscle-derived patterning cues, we must first identify differences in gene expression between the dorsal and ventral muscle masses at the time when *vstm2b* expression initiates in proprioceptors. To this end, I propose a comparative screen of dorsal and ventral hindlimb myoblasts at e12.5. The *Lbx1* null allele used in this study harbors a GFP knockin allele, allowing the fluorescent labeling of all migratory muscle precursors *in situ* within the limb bud. Following the separation of dorsal from ventral limb bud, dissociation and FACS sorting of muscle cells will permit the isolation and genetic profiling of these populations. Dorsoventrally segregated secreted or surface proteins identified in this screen present attractive targets for *vstm2b* patterning cues.

In cases of proprioceptor patterning by the mesenchyme, the precise mesenchymal cell type that represents the source of inductive signals is also

uncertain. Based on the timing of onset of *cdh13* expression, undifferentiated limb mesechymal cells or one of their derivative tissues could be sources of patterning information. For example, TCF4-positive limb connective tissue, which has been proposed to set the pattern of muscle cleavage (Kardon et al., 2003), could specify proprioceptor positional identity.

7.2.4 Characterizing the role of *vstm2b* in circuit formation

Our analysis of the role of Vstm2b in spinal circuit formation was based on an assumption that the dorsoventral selectivity of this gene confers mediolateral targeting specificity within the spinal cord. This led us to search for misprojections between TA afferents and GS motor neurons in *Vstm2b* mutant mice, which we were unable to detect. This may have been due to the low efficiency of bouton labeling by the retrograde tracer ctb; rare misprojections by TA afferents may not have been detected in this scenario. To circumvent this possible technical issue, ctb could be replaced by the *Cdh13*::GFP reporter, which would allow visualization of TA group sensory boutons via native fluorescence.

While this assay might be used to reveal misprojections between other pairwise combinations of sensory and motor neurons, it is labor intensive and low-yield in light of the complexity of sensory-motor connectivity. We therefore considered taking a viral tracing approach to compare the overall spinal trajectory of TA proprioceptors in wild-type and *Vstm2b* mutant backgrounds. In this

paradigm, an AAV virus carrying Cre protein is injected into individual muscles of mice carrying both *Pv*::Flp and *Rosa26*::dual.stop-tdTomato alleles, resulting in the sparse labeling of a muscle-specific population of proprioceptive afferents with tdTomato. This approach will allow us to detect gross deviations in both the trajectory and termination of a muscle-specific afferent population deficient in a single putative determinant of synaptic specificity. In this manner, we will be able to determine wholesale if the pattern of connectivity between muscle-type proprioceptors and interneuronal or motor neuron populations might be altered by allowing us to examine many postsynaptic target populations in parallel. This approach could in theory be utilized to assess the role of any candidate gene in establishing specific synaptic contacts, so long as a null allele is available.

If Vstm2b is found to regulate synaptic specificity, it will be necessary to determine its binding partners in both *cis* and *trans.* We observed *vstm2b* expression in spinal motor neurons and interneuronal populations, although the subtype specificity of its expression – if any – has not yet been characterized. Defining the motor pool expression pattern of *vstm2b* may therefore provide insight into the mode of recognition underlying target recognition by *vstm2b*-expressing afferents.

7.3 Conclusion

Proprioceptive feedback represents a significant mechanism by which movement is coordinated and refined. Limbed motion is dependent on the

specification of proprioceptor subtypes linking muscle to motor neuron, and the work presented in this thesis addresses two intrinsically linked sides of this problem by way of characterizing the molecular identities of muscle-type proprioceptors. First, I have determined that the induction of proprioceptor muscle-type genes occurs in a manner dependent on both mesenchyme and muscle, suggesting that cues from multiple tissue sources are integrated to specify the ~50 proprioceptor subtypes presumably required to establish the complete matrix of sensory-motor connections. Second, I have established a molecular link between the peripheral specification of proprioceptor subtype identity and the formation of specific sensory-motor contacts within the spinal cord. Despite these advances, this work only begins to characterize the subtype diversity of proprioceptive sensory neurons; continued efforts in this field will provide additional insight into the mechanisms through which proprioceptors diversify to generate the spinal circuits required for motor control.

8 Experimental procedures

All experiments and procedures were performed in accordance with NIH guidelines and were approved by the Institutional Animal Care and Use Committee of Columbia University.

8.1 Mouse strains

The following mouse strains were used in this work: *Pv*::Cre (Hippenmeyer et al., 2005), *Thy1*::lox-STOP-lox.YFP (Buffelli et al., 2003), *Cdh13*::CreER^{T2} (Poliak et al., 2016), *Tau*::lox-STOP-lox.mGFP (Hippenmeyer et al., 2005), *Bax*$^{-/-}$ (Knudson et al., 1995), *Olig2*::Cre (Dessaud et al., 2007), floxed *FoxP1* (Feng et al., 2010), *Rosa26*::lox-STOP-lox.DTA (Wu et al., 2006), *Lbx1*$^{-/-}$ (Gross et al., 2000), *Lmx1b*$^{-/-}$ (Chen et al., 1998), *Prx1*::Cre (Logan et al., 2002), *Rosa26*::lsl.Lmx1b (Li et al., 2010), and *RARE-hsp68*::LacZ (Rossant et al., 1991; JAX strain 008477).

The *Vstm2b*::LacZ reporter/null allele was generated from targeted ES cells obtained from the EUCOMM division of the IKMC project (Ringwald et al., 2011). Chimeras were produced from *vstm2b* ES cell clone F02 with the help of Monica Mendelsohn and Natalia Zabello at Columbia University, and offspring carrying the targeted allele were crossed to *Protamine*::Cre (O'Gorman et al., 1997; JAX strain 003328) mice to achieve male germline deletion of the Neo cassette and *vstm2b* exons 2-4. We also utilized *Rosa26*::FlpO mice (Raymond and Soriano, 2007; JAX

strain 007844) to excise the LacZ reporter and Neo cassette to generate a conditional *Vstm2b* allele.

Cre activity and subsequent expression of GFP in *Cdh13*::mGFP mice were induced by intraperitoneal injection of tamoxifen (5 mg in sesame oil; Sigma) into pregnant females at the gestational times indicated in the text.

8.2 Isolation of muscle-specific proprioceptors

Muscles of P0 mice anesthetized by hypothermia were injected with ctb^{555} (List Biological Laboratories) using a hand-pulled capillary attached to an aspirator tube. The specificity of muscle injections was confirmed at P1 by muscle dissection and examination under a fluorescence microscope. Following ventral laminectomy, DRG containing ctb^{555}-filled neurons were identified under a microscope (MVX10 MacroView, Olympus) and removed from the spinal column using a fine forceps. Isolated DRG were transferred to a microcentrifuge tube containing ACSF and dissociated by sequential treatments in papain and collagenase/dispase solutions as described previously (Malin et al., 2007). Dissociated cells were sparsely plated on a transparent Sylgard-lined 3 cm dish and allowed to settle for 10 minutes at 4C.

Cells positive for both YFP and ctb^{555} were manually isolated essentially as described in Hempel et al., 2007. Isolated neurons were transferred directly into an RNase-free microcentrifuge tube (SafeSeal Microcentrifuge Tubes; Sorenson

BioScience, Inc.) containing 100 µL lysis buffer (Arcturus PicoPure RNA Isolation Kit; Applied Biosystems) on ice. At the end of collection, the cells were lysed by incubation for 30 minutes at 42C. Lysed cell samples were stored at -80C until use.

8.3 RNA-sequencing

8.3.1 cDNA library preparation and sequencing

When necessary, individual collections were pooled to generate 25-30 cell samples. These samples were concentrated to a uniform volume suitable for input to subsequent processing steps using a Speedvac vacuum concentrator (ThermoFisher). RNA was extracted from pooled samples using a PicoPure RNA isolation kit (Arcturus) according to the manufacturer's instructions, and cDNA was synthesized using the Ovation RNA-Seq System V2 Kit (Nugen). cDNA libraries were constructed at the Columbia Genome Center using the Nextera DNA Sample Prep Kit (Illumina), and 100 bp paired-end reads were generated on an Illumina HiSeq sequencer to a depth of 25-30 million reads per sample. RNA-Seq data for TA and GS samples was published in Poliak et al., 2016, and the corresponding FASTQ files have been deposited in the GEO repository under the accession number GSE71028.

8.3.2 Data processing

Raw FASTQ sequencing files were processed using the ExpressionPlot framework (Friedman and Maniatis, 2011). Illumina adapter sequences, low quality

bases, and primers were removed from the dataset. Reads were then aligned to the mm9 mouse genome assembly and to a database of splice junctions using bowtie (Langmead et al., 2009). Aligned reads were then mapped to genes annotated in the UCSC Genome Browser (Karolchik et al., 2014) and Ensembl (Aken et al., 2016) databases.

8.3.3 Identification of differentially expressed genes

Differentially expressed genes (DEGs) between proprioceptor subpopulations were extracted by multiple pairwise comparisons in ExpressionPlot using the DESeq package (Anders et al., 2010), which normalizes samples using median fold change and models read counts using the negative binomial distribution. *P*-values were derived using Fisher's exact test.

DEGs identified in ExpressionPlot were filtered using the following parameters: $P<10^{-4}$, FC>5 (for any pairwise comparison), and $RPKM_{min}=10$ (for at least one replicate of the subpopulation exhibiting upregulated expression. Refer to Table 2.1 for a complete list of genes meeting these criteria.

8.3.4 Data visualization

Heat maps illustrating normalized DEG expression levels were generated from .txt files using the following R code:

```
> setwd("/Users/username/desktop/foldername")
> genes <- read.table("filename.txt", header = TRUE)
> genes
> row.names(genes) <- genes$gene
> genes <- genes[,2:15]
> genes
> genes_matrix <- data.matrix(genes)
> my_palette <- colorRampPalette(c("white", "darkblue"))(n=299)
> genes_heatmap <- heatmap(genes_matrix, Rowv=NA, Colv=NA, col=my_palette,
scale="column", margins=c(5,10))
```

where entities in **bold** must be specified by the user. Heatmaps were scaled to uniform row heights using Adobe Illustrator.

8.4 *In situ* hybridization

For chromogenic *in situs,* 10-16 μM cryostat sections were hybridized with digoxigenin (DIG)-labeled probes as described previously (Schaeren-Wiemers and Gerfin-Moser, 1993). Fluorescence *in situ* hybridization (FISH) was performed on 12-16 μM cryostat sections hybridized with DIG- and fluorescein isothiocyanate (FITC)-labeled probes using the FITC/Cy5 TSA Plus Fluorescence System for signal amplification according to the manufacturer's instructions (PerkinElmer). All *in situs* were performed on fresh-frozen tissue.

Probe templates were isolated by polymerase chain reaction (PCR) from P1 lumbar DRG or e13.5 whole embryo cDNA libraries. cDNA libraries were synthesized using the SuperScript III First-Strand Synthesis System for RT-PCR (Invitrogen) from RNA purified using an Absolutely RNA Miniprep Kit (Agilent). Primers were sourced from the Allen Mouse Brain Atlas (Lein et al., 2007) or were

designed using the web-based Primer3 program (http://bioinfo.ut.ee/primer3/). Reverse primers were appended with the T7 polymerase binding sequence to facilitate probe synthesis. PCR products were gel purified, sequenced, and used directly for the transcription of DIG- or FITC-labeled (Roche) probes.

8.5 Immunohistochemistry

Tissue used for immunohistochemistry was fixed for 2 h or overnight in 4% paraformaldehyde in phosphate buffered saline (PBS). The tissue was then embedded in low-melt agarose for vibratome sectioning (30-100 μM; Leica) or dehydrated in a 30% sucrose solution in 0.1M PB and embedded in OCT (Tissue-Tek) for cryosectioning (10-20 μM; Bright). For cryosections, immunohistochemistry was performed by overnight incubation of the tissue at 4C in primary antibody diluted in PBS containing 0.1% Triton X-100 detergent (0.1% PBT). The tissue was then washed 3x in PBS and incubated with secondary antibody diluted in 0.1% PBT for 1 h at room temperature. Sections were then washed in PBS and mounted in Vectashield (Vector Laboratories). For vibratome sections, tissue was incubated with primary antibodies at 4C for 24-72 h in 0.3% PBT. The sections were washed for 5 h in 0.3% PBT and then incubated overnight at 4C with secondary antibodies diluted in 0.3% PBT. Sections were then washed in PBS and mounted in Vectashield.

The following primary antibodies were used in this work: rabbit anti-Pv

(1:5000, Swant), guinea pig anti-Islet1/2 (1/16000; Dasen et al., 2005), rabbit anti-GFP (1:1500, Life Technologies), guinea pig anti-vGluT1 (1:8000; Betley et al., 2009), rabbit anti-FoxP1 (1/16000; Dasen et al., 2008), chick anti-β-galactosidase (1:5000, Abcam ab9361), goat anti-cholera toxin B subunit (1:8000, List Biological Laboratories), and rabbit anti-tetramethylrhodamine (1:1000, Invitrogen).

Secondary antibodies were generated in donkey and conjugated to FITC, Cy3, or Cy5 (Jackson Immunoresearch Laboratories). Those conjugated to FITC or Cy5 were diluted 1:500 and those conjugated to Cy3 were diluted 1:1000.

8.6 X-gal staining

Sections of β-gal-expressing tissue were post-fixed in 4% formaldehyde (Sigma) and immersed in X-Gal staining solution (0.02% Igepal, 0.01% sodium deoxychoate, 5 mM potassium ferricyanide, 5 mM potassium ferrocyanide, and 2 mM $MgCl_2$ diluted in 0.1M PBS, pH 7.5 and supplemented with 1 mg/mL X-Gal just prior to use) overnight at 37C in the dark.

8.7 Connectivity assays

The presence of misprojections from TA proprioceptors to GS motor neurons in genetic knockout lines was assessed essentially as described by Sürmeli et al. (2011). For *vstm2b* knockout mice, unconjugated ctb was injected into TA muscle

and rhodamine-dextran (rh-dex) was injected into GS muscle at P3-P4, the earliest timepoint GS injection specificity could be achieved. After four days, the animals were sacrificed and prepared for vibratome sectioning (70 μM). Sections were immunostained for ctb, rh-dex (TMR), and vGluT1. This procedure was repeated for *cdh13* knockout (*Cdh13*::mGFP) mice, but mGFP labeling of TA/EDL/PL sensory boutons was used in place of ctb backfill. Correspondingly, sensory endings were immunostained for GFP rather than ctb protein.

Quantification of vGluT1^{+} sensory boutons with and without ctb or *Cdh13*::mGFP expression on retrogradely labeled motor neuron somata and ~75 μM of the proximal dendritic arbor was performed for Z-stack images using Zen software (Zeiss).

8.8 Imaging

Fluorescence images were collected on a Zeiss LSM 510 Meta confocal microscope. Bright field images were captured on an Olympus microscope.

8.9 Statistical Analysis

Statistical analyses were performed using Microsoft Excel. Comparisons of gene expression between DRG and experimental conditions were made using the

one-tailed Student's t-test for unequal variance; error bars were represented as the standard error of the mean (SEM).

Bibliography

Ahn, K., Mishina, Y., Hanks, M.C., Behringer, R.R., and Crenshaw 3rd, E.B. (2001). BMPR-IA signaling is required for the formation of the apical ectodermal ridge and dorsal-ventral patterning of the limb. Development *128*, 4449–4461.

Akay, T., Tourtellotte, W.G., Arber, S., and Jessell, T.M. (2014). Degradation of mouse locomotor pattern in the absence of proprioceptive sensory feedback. *111*, 16877–16882.

Aken, B.L., Ayling, S., Barrell, D., Clarke, L., Curwen, V., Fairley, S., Fernandez-Banet, J., Billis, K., Garcia-Giron, C., Hourlier, T., et al. (2016). The Ensembl Gene Annotation System. 1–19.

Amthor, H., Christ, B., Weil, M., and Patel, K. (1998). The importance of timing differentiation during limb muscle development. Curr. Biol. *8*, 642–652.

Anders, S., Huber, W., S, A., and W, H. (2010). Differential expression analysis for sequence count data. Genome Biol *11*, R106.

Anderson, D.J. (1999). Lineages and transcription factors in the specification of vertebrate primary sensory neurons. Curr. Opin. Neurobiol. *9*, 517–524.

Arber, S. (2012). Motor Circuits in Action: Specification, Connectivity, and Function. Neuron *74*, 975–989.

Arber, S., Ladle, D.R., Lin, J.H., Frank, E., and Jessell, T.M. (2000). ETS Gene Er81

Controls the Formation of Functional Connections between Group Ia Sensory Afferents and Motor Neurons. Cell *101*, 485–498.

Arnold, H., and Braun, T. (2000). Genetics of muscle determination and development. Curr. Top. Dev. Biol. *48*, 129–164.

Aziz Moqrich, Taryn J Earley, James Watson, Mary Andahazy, Carey Backus, Dionisio Martin-Zanca, Douglas E Wright, Louis F Reichardt, and A.P. (2004). Expressing TrkC from the TrkA locus causes a subset of dorsal root ganglia neurons to switch fate. Nat. Neurosci *7*, 812–818.

Bajard, L., Relaix, F., Lagha, M., Rocancourt, D., Daubas, P., and Buckingham, M.E. (2006). A novel genetic hierarchy functions during hypaxial myogenesis : Pax3 directly activates Myf5 in muscle progenitor cells in the limb. 2450–2464.

Basaldella, E., Takeoka, A., Sigrist, M., and Arber, S. (2015). Multisensory Signaling Shapes Vestibulo-Motor Circuit Specificity. Cell *163*, 301–312.

Basu, R., Taylor, M.R., and Williams, M.E. (2015). The classic cadherins in synaptic specificity. Cell Adhes. Migr. *9*, 193–201.

Bénazet, J.D., and Zeller, R. (2009). Vertebrate limb development: moving from classical morphogen gradients to an integrated 4-dimensional patterning system. Cold Spring Harb. Perspect. Biol. *1*, 1–15.

Betley, J.N., Wright, C.V.E., Kawaguchi, Y., Erdélyi, F., Szabó, G., Jessell, T.M., and Kaltschmidt, J.A. (2009). Stringent Specificity in the Construction of a GABAergic

Presynaptic Inhibitory Circuit. Cell *139*, 161–174.

Biewener, A.A. (2016). Locomotion as an emergent property of muscle contractile dynamics. 285–294.

Bikoff, J.B., Gabitto, M.I., Rivard, A.F., Drobac, E., MacHado, T.A., Miri, A., Brenner-Morton, S., Famojure, E., Diaz, C., Alvarez, F.J., et al. (2016). Spinal Inhibitory Interneuron Diversity Delineates Variant Motor Microcircuits. Cell *165*, 207–219.

Bladt, F., Riethmacher, D., Isenmann, S., Aguzzi, A., and Birchmeier, C. (1995). Essential role for the c-met receptor in the migration of myogenic precursor cells into the limb bud. Nature *376*, 768–771.

Bonanomi, D., and Pfaff, S.L. (2010). Motor axon pathfinding. Cold Spring Harb. Perspect. Biol. *2*, 1–19.

Bonanomi, D., Chivatakarn, O., Bai, G., Abdesselem, H., Lettieri, K., Marquardt, T., Pierchala, B.A., and Pfaff, S.L. (2012). Ret is a multifunctional coreceptor that integrates diffusible- and contact-axon guidance signals. Cell *148*, 568–582.

Brohmann, H., Jagla, K., and Birchmeier, C. (2000). The role of Lbx1 in migration of muscle precursor cells. Development *127*, 437–445.

Brown, A.G. (1981a). Organization in the Spinal Cord (New York: Springer Verlag).

Brown, A.G. (1982). The dorsal horn of the spinal cord. Q. J. Exp. Physiol. *67*, 193–212.

Brown, B.Y.A.G., and Fyffe, R.E.W. (1981). Printed in Great Britain 121. 121–140.

Buckingham, M. (2001). Skeletal muscle formation in vertebrates. Curr. Opin. Genet. Dev. *11*, 440–448.

Buckingham, M., Bajard, L., Chang, T., Daubas, P., Hadchouel, J., Meilhac, S., Montarras, D., Rocancourt, D., and Relaix, F. (2003). The formation of skeletal muscle: from soma to limb. J. Anat. *202*, 59–68.

Buffelli, M., Burgess, R.W., Feng, G., Lobe, C.G., Lichtman, J.W., and Sanes, J.R. (2003). Genetic evidence that relative synaptic efficacy biases the outcome of synaptic competition. Nature *424*, 430–434.

Burke, R., and Nelson, P. (1966). Synaptic activity in motoneurons during natural stimulation of muscle spindles. Science (80-.). *151*, 1088–1091.

Burke, R.E., and Glenn, L.L. (1996). Horseradish peroxidase study of the spatial and electrotonic distribution of group Ia synapses on type-identified ankle extensor motoneurons in the cat. J. Comp. Neurol. *372*, 465–485.

Callahan, C.A., and Thomas, J.B. (1994). Tau-beta-galactosidase, an axon-targeted fusion protein. Proc. Natl. Acad. Sci. U. S. A. *91*, 5972–5976.

Capdevila, J., and Izpisua Belmonte, J.C. (2001). Patterning mechanisms controlling vertebrate limb development. Annu. Rev. Cell Dev. Biol. *17*, 87–132.

Chen, H., and Johnson, R.L. (2002). Interactions between dorsal-ventral patterning

genes lmx1b, engrailed-1 and wnt-7a in the vertebrate limb. Int. J. Dev. Biol. *46*, 937–941.

Chen, A.I., De Nooij, J.C., and Jessell, T.M. (2006). Graded activity of transcription factor Runx3 specifies the laminar termination pattern of sensory axons in the developing spinal cord. Neuron *49*, 395–408.

Chen, H., Lun, Y., Ovchinnikov, D., Kokubo, H., Oberg, K.C., Pepicelli, C. V, Gan, L., Lee, B., and Johnson, R.L. (1998). Limb and kindney defects in Lmx1b mutant mice suggest an involvement of LMX1B in human nail patella syndrome. Nat. Genet. *19*, 51–55.

Chen, H., Yip, J.W., Stewart, A.F.R., and Frank, E. (2002). Differential expression of a transcription regulatory factor , the LIM domain only 4 protein Lmo4 , in muscle sensory neurons. *4889*, 4879–4889.

Chevallier, a, Kieny, M., and Mauger, a (1977). Limb-somite relationship: origin of the limb musculature. J. Embryol. Exp. Morphol. *41*, 245–258.

Christ, B., and Brand-Saberi, B. (2002). Limb muscle development. Int. J. Dev. Biol. *46*, 905–914.

Christ, B., and Ordahl, C. (1995). Early stages of chick somite development. Anat. Embryol. (Berl). *191*, 381–396.

Christ, B., Jacob, H.J., and Jacob, M. (1977). Experimental analysis of the origin of the wing musculature in avian embryos. Anat. Embryol. (Berl). *150*, 171–186.

Ciatto, C., Bahna, F., Zampieri, N., VanSteenhouse, H.C., Katsamba, P.S., Ahlsen, G., Harrison, O.J., Brasch, J., Jin, X., Posy, S., et al. (2010). T-cadherin structures reveal a novel adhesive binding mechanism. Nat. Struct. Mol. Biol. *17*, 339–347.

Cooper, K.L., Hu, J.K.-H., ten Berge, D., Fernández-Terán, M.A., Ros, M.Á., and Tabin, C.J. (2011). Initiation of proximal-distal patterning in the vertebrate limb by signals and growth. Science (80-.). *332*, 1083–1086.

Copray, J.C.V.M., and Brouwer, N. (1994). SELECTIVE EXPRESSION OF NEUROTROPHIN-3 MESSENGER RNA IN MUSCLE SPINDLES OF THE RAT. *63*.

Cygan, J., Johnson, R., and McMahon, A. (1997). Novel regulatory interactions revealed by studies of murine limb pattern in Wnt-7a and En-1 mutants. Development *124*, 5021–5032.

Dasen, J.S. (2009). Transcriptional Networks in the Early Development of Sensory-Motor Circuits (Elsevier Inc.).

Dasen, J.S., and Jessell, T.M. (2009). Hox Networks and the Origins of Motor Neuron Diversity (Elsevier Inc.).

Dasen, J.S., Liu, J.-P., and Jessell, T.M. (2003). Motor neuron columnar fate imposed by sequential phases of Hox-c activity. Nature *425*, 926–933.

Dasen, J.S., Tice, B.C., Brenner-Morton, S., and Jessell, T.M. (2005). A Hox regulatory network establishes motor neuron pool identity and target-muscle connectivity. Cell

123, 477–491.

Dasen, J.S., De Camilli, A., Wang, B., Tucker, P.W., and Jessell, T.M. (2008). Hox Repertoires for Motor Neuron Diversity and Connectivity Gated by a Single Accessory Factor, FoxP1. Cell *134*, 304–316.

Davis, C. a, Holmyard, D.P., Millen, K.J., and Joyner, a L. (1991). Examining pattern formation in mouse, chicken and frog embryos with an En-specific antiserum. Development *111*, 287–298.

Demireva, E.Y., Shapiro, L.S., Jessell, T.M., and Zampieri, N. (2011). Motor neuron position and topographic order imposed by β- And γ-catenin activities. Cell *147*, 641–652.

Dessaud, E., Yang, L.L., Hill, K., Cox, B., Ulloa, F., Ribeiro, A., Mynett, A., Novitch, B.G., and Briscoe, J. (2007). Interpretation of the sonic hedgehog morphogen gradient by a temporal adaptation mechanism. Nature *450*, 717–720.

Dietrich, S., Schubert, F.R., Healy, C., Sharpe, P.T., and Lumsden, A. (1998). Specification of the hypaxial musculature. Development *125*, 2235–2249.

Dietrich, S., Abou-rebyeh, F., Brohmann, H., Bladt, F., and Sonnenberg-, E. (1999). The role of SF / HGF and c-Met in the development of skeletal muscle. Development *126*, 1621–1629.

Duan, X., Krishnaswamy, A., De La Huerta, I., and Sanes, J.R. (2014). Type II cadherins guide assembly of a direction-selective retinal circuit. Cell *158*, 793–807.

Dudanova, I., Gatto, G., and Klein, R. (2010). GDNF acts as a chemoattractant to support ephrina-induced repulsion of limb motor axons. Curr. Biol. *20*, 2150–2156.

Duprez, D. (2002). Signals regulating muscle formation in the limb during embryonic development. Int. J. Dev. Biol. *46*, 915–925.

Eberhart, J., Swartz, M.E., Koblar, S.A., Pasquale, E.B., and Krull, C.E. (2002). EphA4 Constitutes a Population-Specific Guidance Cue for Motor Neurons. Dev. Biol. *247*, 89–101.

Eccles, R.M., and Lundberg, A. (1958). Integrative pattern of Ia synaptic actions on motoneurones of hip and knee muscles. J. Physiol. 271–298.

Eccles, J.C., Eccles, R., and Lundberg, A. (1957). The convergence of monosynaptic excitatory afferents on to many different species of alpha motoneurones. J. Physiol. *137*, 22–50.

Epstein, J.A., Shapiro, D.N., Cheng, J., Lam, P.Y., and Maas, R.L. (1996). Pax3 modulates expression of the c-Met receptor during limb muscle development. Proc. Natl. Acad. Sci. U. S. A. *93*, 4213–4218.

Ernfors, P., and Lee, K. (1994). Lack of Neurotrophin-3 Leads to Deficiencies in the Peripheral Nervous System and Loss of Limb Proprioceptive Afferents. *77*, 503–512.

Ernfors, P., Lee, K., and Jaenisch, R. (1994). Target derived and putative local actions of neurotrophins in the peripheral nervous system. *103*.

Farinas, I., Jones, K., Backus, C., Wang, X., and Reichardt, L. (1994). Severe sensory and sympathetic deficits in mice lacking neurotrophin-3. Nature *369*.

Farinas, I., Yoshida, C.K., Backus, C., and Reichardt, L.F. (1996). Lack of Neurotrophin-3 Results in Death of Spinal Sensory Neurons and Premature. *17*, 1065–1078.

Fedtsova, N.G., and Turner, E.E. (1995). Brn-3.0 expression identifies early post-mitotic CNS neurons and sensory neural precursors. Mech. Dev. *53*, 291–304.

Feenstra, J.M., Kanaya, K., Pira, C.U., Hoffman, S.E., Eppey, R.J., and Oberg, K.C. (2012). Detection of genes regulated by Lmx1b during limb dorsalization. Dev. Growth Differ. *54*, 451–462.

Feng, X., Ippolito, G.C., Tian, L., Wiehagen, K., Oh, S., Willen, J., Bunte, R.M., Maika, S.D., Harriss, J. V, Caton, A.J., et al. (2010). Foxp1 is an essential transcriptional regulator for the generation of quiescent naive T cells during thymocyte development Foxp1 is an essential transcriptional regulator for the generation of quiescent naive T cells during thymocyte development. Blood *115*, 510–518.

Francis-West, P.H., Antoni, L., and Anakwe, K. (2003). Regulation of myogenic differentiation in the developing limb bud. J. Anat. *202*, 69–81.

Frank, E., and Jackson, P.C. (1986). Normal electrical activity is not required for the formation of specific sensory-motor synapses. Brain Res. *378*, 147–151.

Frank, E., and Westerfield, M. (1982a). The formation of appropriate central and peripheral connexions by foreign sensory neurones of the bullfrog. J. Physiol. 495–505.

Frank, E., and Westerfield, M. (1982b). Synaptic organization of sensory and motor neurones innervating triceps brachii muscles in the bullfrog. J. Physiol. *324*, 479–494.

Frank, E., and Westerfield, M. (1983). Development of sensory-motor synapses. 593–610.

Friedman, B.A., and Maniatis, T. (2011). ExpressionPlot : a web-based framework for analysis of RNA-Seq and microarray gene expression data ExpressionPlot : a web-based framework for analysis of RNA-Seq and microarray gene expression data. Genome Biol. *12*, R69.

Fukuhara, K., Imai, F., Ladle, D.R., Katayama, K. ichi, Leslie, J.R., Arber, S., Jessell, T.M., and Yoshida, Y. (2013). Specificity of Monosynaptic Sensory-Motor Connections Imposed by Repellent Sema3E-PlexinD1 Signaling. Cell Rep. *5*, 748–758.

Gabitto, M.I., Pakman, A., Bikoff, J.B., Abbott, L.F., Jessell, T.M., and Paninski, L. (2016). Bayesian Sparse Regression Analysis Documents the Diversity of Spinal Inhibitory Interneurons. Cell *165*, 220–233.

Gallarda, B.W., Bonanomi, D., Müller, D., Brown, A., Alaynick, W.A., Andrews, S.E., Lemke, G., Pfaff, S.L., and Marquardt, T. (2008). Segregation of axial motor and

sensory pathways via heterotypic trans-axonal signaling. *320*, 233–236.

Garcia, N.V.D.M., and Jessell, T.M. (2008). Early Motor Neuron Pool Identity and Muscle Nerve Trajectory Defined by Postmitotic Restrictions in Nkx6.1 Activity. Neuron *57*, 217–231.

Gardner, C.A., and Barald, K.F. (1992). Expression Patterns of Engrailed-Like Proteins in the Chick-Embryo. Dev. Dyn. *193*, 370–388.

Greenwood, A.L., Turner, E.E., and Anderson, D.J. (1999). Identification of dividing, determined sensory neuron precursors in the mammalian neural crest. Development *126*, 3545–3559.

Grillner, S., and Zangger, P. (1984). The effect of dorsal root transection on the efferent motor pattern in the cat ' s hindlimb during locomotion.

Grim, M., and Wachtler, F. (1991). Muscle morphogenesis in the absence of myogenic cells. Anat. Embryol. (Berl). *183*, 67–70.

Gross, M.K., Moran-rivard, L., Velasquez, T., Nakatsu, M.N., and Jagla, K. (2000). Lbx1 is required for muscle precursor migration along a lateral pathway into the limb. *424*, 413–424.

Gu, W.X.W., and Kania, A. (2010). Identification of genes controlled by LMX1B in E13.5 mouse limbs. Dev. Dyn. *239*, 2246–2255.

Haase, G., Dessaud, E., Garce, A., Filippi, P., Schmalbruch, H., Arber, S., Mediterranee,

C., Luminy, C. De, and Cedex, M. (2002). GDNF Acts through PEA3 to Regulate Cell Body Positioning and Muscle Innervation of Specific Motor Neuron Pools. *35*, 893–905.

Haddick, P.C.G., Tom, I., Luis, E., Quiñones, G., Wranik, B.J., Ramani, S.R., Stephan, J.P., Tessier-Lavigne, M., and Gonzalez, L.C. (2014). Defining the ligand specificity of the Deleted in Colorectal Cancer (DCC) receptor. PLoS One *9*, 1–12.

Hayashi, S., and McMahon, A.P. (2002). Efficient Recombination in Diverse Tissues by a Tamoxifen-Inducible Form of Cre: A Tool for Temporally Regulated Gene Activation/Inactivation in the Mouse. Dev. Biol. *244*, 305–318.

Hayashi, S., and Takeichi, M. (2015). Emerging roles of protocadherins: from self-avoidance to enhancement of motility. J. Cell Sci. *128*, 1455–1464.

Helmbacher, F., Schneider-Maunoury, S., Topilko, P., Tiret, L., and Charnay, P. (2000). Targeting of the EphA4 tyrosine kinase receptor affects dorsal/ventral pathfinding of limb motor axons. Development *127*, 3313–3324.

Hempel, C.M., Sugino, K., and Nelson, S.B. (2007). PROTOCOL A manual method for the purification of fluorescently labeled neurons from the mammalian brain. *2*, 2924–2929.

Henderson, C.E. (1996). Role of neurotrophic factors in neuronal development. Curr. Opin. Neurobiol. 64–70.

Hiebert, G.W., and Pearson, K.G. (1999). Contribution of Sensory Feedback to the

Generation of Extensor Activity During Walking in the Decerebrate Cat.

Hippenmeyer, S., Vrieseling, E., Sigrist, M., Portmann, T., Laengle, C., Ladle, D.R., and Arber, S. (2005). A developmental switch in the response of DRG neurons to ETS transcription factor signaling. PLoS Biol. *3*, 0878–0890.

Hollyday, M. (1980). Organization of motor pools in the chick lumbar lateral motor column. J. Comp. Neurol. *194*, 143–170.

Hollyday, M., and Jacobson, R.D. (1990). Location of motor pools innervating chick wing. J. Comp. Neurol. *302*, 575–588.

Hongo, T. (1984). The pattern of monosynaptic Ia-connections to hindlimb motor nuclei in the baboon: a comparison with the cat. Proc. R. Soc. London *221*, 261–289.

Honig, M.G., Frase, P. a, and Camilli, S.J. (1998). The spatial relationships among cutaneous, muscle sensory and motoneuron axons during development of the chick hindlimb. Development *125*, 995–1004.

Horstadius, S. (1950). The Neural Crest: Its Properties and Derivatives in the Light of Experimental Research (Oxford University Press).

Huber, A.B., Kania, A., Tran, T.S., Gu, C., De Marco Garcia, N., Lieberam, I., Johnson, D., Jessell, T.M., Ginty, D.D., and Kolodkin, A.L. (2005). Distinct roles for secreted semaphorin signaling in spinal motor axon guidance. Neuron *48*, 949–964.

Humeau, Y., Doussau, F., Grant, N.J., and Poulain, B. (2000). How botulinum and

tetanus neurotoxins block neurotransmitter release *. *82*.

Hunt, C. (1974). Muscle Receptors, Volume II, Handbook of Sensory Physiology (Springer-Verlag).

Jacob, H.J., and Christ, B. (1980). On the formation of muscular pattern in the chick limb. In Teratology of the Limbs, (Berlin: Walter de Gruyter and Co.), pp. 89–97.

Jagla, K., Dollé, P., Mattei, M.G., Jagla, T., Schuhbaur, B., Dretzen, G., Bellard, F., and Bellard, M. (1995). Mouse Lbx1 and human LBX1 define a novel mammalian homeobox gene family related to the Drosophila lady bird genes. Mech. Dev. *53*, 345–356.

Jankowska, E., and Odutola, A. (1980). Crossed and uncrossed synaptic actions on motoneurones of back muscles in the cat. Brain Res. *193*, 427–438.

Johnson, R.L., and Tabin, C.J. (1997). Molecular models for vertebrate limb development. Cell *90*, 979–990.

Kablar, B., Krastel, K., Ying, C., Asakura, a, Tapscott, S.J., and Rudnicki, M. a (1997). MyoD and Myf-5 differentially regulate the development of limb versus trunk skeletal muscle. Development *124*, 4729–4738.

Kablar, B., Krastel, K., Ying, C., Tapscott, S.J., Goldhamer, D.J., and Rudnicki, M.A. (1999). Myogenic determination occurs independently in somites and limb buds. Dev. Biol. *206*, 219–231.

Kania, A., and Jessell, T.M. (2003). Topographic motor projections in the limb imposed by LIM homeodomain protein regulation of ephrin-A:EphA interactions. Neuron *38*, 581–596.

Kardon, G. (1998). Muscle and tendon morphogenesis in the avian hind limb. Development *125*, 4019–4032.

Kardon, G., Campbell, J.K., and Tabin, C.J. (2002). Local extrinsic signals determine muscle and endothelial cell fate and patterning in the vertebrate limb. Dev. Cell *3*, 533–545.

Kardon, G., Harfe, B.D., and Tabin, C.J. (2003). A Tcf4-positive mesodermal population provides a prepattern for vertebrate limb muscle patterning. Dev. Cell *5*, 937–944.

Karolchik, D., Barber, G.P., Casper, J., Clawson, H., Cline, M.S., Diekhans, M., Dreszer, T.R., Fujita, P.A., Guruvadoo, L., Haeussler, M., et al. (2014). The UCSC Genome Browser database: 2014 update. Nucleic Acids Res. *42*, 764–770.

Kiehn, O. (2016). Decoding the organization of spinal circuits that control locomotion. Nat. Publ. Gr. *17*, 224–238.

Knudson, C.M., Tung, K.S.K., Tourtellotte, W.G., Brown, G.A.J., Korsmeyer, S.J., Tourttellotte, W.G., Brown, G.A.J., and Korsmeyer, S.J. (1995). Bax-deficient mice with lymphoid hyperplasia and male germ cell death. Science (80-.). *270*, 96–99.

Kolodkin, A.L., Tessier-lavigne, M., Chédotal, A., Richards, L.J., Dent, E.W., Gupton,

S.L., Frank, B., Adams, R.H., Eichmann, A., Engle, E.C., et al. (2012). Mechanisms and Molecules of Neuronal Wiring : A Primer.

Kramer, E.R., Knott, L., Su, F., Dessaud, E., Krull, C.E., Helmbacher, F., and Klein, R. (2006). Cooperation between GDNF/Ret and ephrinA/EphA4 Signals for Motor-Axon Pathway Selection in the Limb. Neuron *50*, 35–47.

Krawchuk, D., and Kania, A. (2008). Identification of genes controlled by LMX1B in the developing mouse limb bud. Dev. Dyn. *237*, 1183–1192.

Kuno, M., and Miyahara, J.T. (1969). Analysis of synaptic efficacy in spinal motoneurones from "quantum" aspects. 479–493.

L'honore, A., Ouimette, J.-F., Lavertu-Jolin, M., and Drouin, J. (2010). Pitx2 defines alternate pathways acting through MyoD during limb and somitic myogenesis. Development *137*, 3847–3856.

Laclef, C., Hamard, G., Demignon, J., Souil, E., Houbron, C., and Maire, P. (2003). Altered myogenesis in Six1-deficient mice. Development *130*, 2239–2252.

Lah, G.J., and Key, B. (2012). Dual roles of the chemorepellent axon guidance molecule RGMa in establishing pioneering axon tracts and neural fate decisions in embryonic vertebrate forebrain. Dev. Neurobiol. *72*, 1458–1470.

Lallemend, F., and Ernfors, P. (2012). Molecular interactions underlying the specification of sensory neurons. Trends Neurosci. *35*, 373–381.

Lance-Jones, C. (1979). The morphogenesis of the thigh of the mouse with special reference to tetrapod muscle homologies. J. Morphol. *162*, 275–309.

Lance-Jones, C.C. (1986). Motoneuron projection patterns in chick embryonic limbs with a double complement of dorsal thigh musculature. Dev. Biol. *116*, 387–406.

Landmesser, L. (1978a). The distribution of motoneurones supplying chick hind limb muscles. J. Physiol. *284*, 371–389.

Landmesser, L.T. (1978b). The development of motor projection patterns in the chick hind limb. J. Physiol. *284*, 391–414.

Landmesser, L.T. (2001). The acquisition of motoneuron subtype identity and motor circuit formation. Int. J. Dev. Neurosci. *19*, 175–182.

Landmesser, L., and Honig, M.G. (1986). Altered sensory projections in the chick hind limb following the early removal of motoneurons. Dev. Biol. *118*, 511–531.

Landmesser, L., O-Donovan, M., and Honig, M. (1983). The response of avian hindlimb motor and sensory neurons to an altered periphery. Prog. Clin. Biol. Res. *110*, 207–216.

Langmead, B., Trapnell, C., Pop, M., and Salzberg, S. (2009). Ultrafast and memory-efficient alignment of short DNA sequences to the human genome. Genome Biol. *10*, R25.

Leamey, C.A., and Sawatari, A. (2014). The teneurins: New players in the generation

of visual topography. Semin. Cell Dev. Biol. *35*, 173–179.

Lee, M.T., and O'Donovan, M.J. (1991). Organization of Hindlimb Muscle Afferent Projections to Lumbosacral Motoneurons in the Chick Embryo. *11*, 2564–2573.

Lee, J., Friese, A., Mielich, M., Sigrist, M., and Arber, S. (2012). Scaling Proprioceptor Gene Transcription by Retrograde NT3 Signaling. *7*.

Lein, E.S., Hawrylycz, M.J., Ao, N., Ayres, M., Bensinger, A., Bernard, A., Boe, A.F., Boguski, M.S., Brockway, K.S., Byrnes, E.J., et al. (2007). Genome-wide atlas of gene expression in the adult mouse brain. Nature *445*, 168–176.

Leu, M., Bellmunt, E., Schwander, M., Fariñas, I., Brenner, H.R., and Müller, U. (2003). Erbb2 regulates neuromuscular synapse formation and is essential for muscle spindle development. 2291–2301.

Levin, S.D., Taft, D.W., Brandt, C.S., Bucher, C., Howard, E.D., Chadwick, E.M., Johnston, J., Hammond, A., Bontadelli, K., Ardourel, D., et al. (2011). Vstm3 is a member of the CD28 family and an important modulator of T-cell function. Eur. J. Immunol. *41*, 902–915.

Li, C., Li, K., Wu, D., Chen, Y., Luo, H., Zhao, J., and Wang, S. (2016). Somatosensory neuron types identified by high-coverage single-cell RNA-sequencing and functional heterogeneity. 2016.

Li, X., Oghi, K. a, Zhang, J., Krones, A., Bush, K.T., Glass, C.K., Nigam, S.K., Aggarwal, A.K., Maas, R., Rose, D.W., et al. (2003). Eya protein phosphatase activity regulates

Six1-Dach-Eya transcriptional effects in mammalian organogenesis. Nature *426*, 247–254.

Li, Y., Qiu, Q., Watson, S.S., Schweitzer, R., and Johnson, R.L. (2010). Uncoupling skeletal and connective tissue patterning: conditional deletion in cartilage progenitors reveals cell-autonomous requirements for Lmx1b in dorsal-ventral limb patterning. Development *137*, 1181–1188.

Lin, J.H., Saito, T., Anderson, D.J., Lance-jones, C., Jessell, T.M., Arber, S., and Hughes, H. (1998). Functionally Related Motor Neuron Pool and Muscle Sensory Afferent Subtypes Defined by Coordinate ETS Gene Expression. *95*, 393–407.

Livet, J., Sigrist, M., Stroebel, S., De Paola, V., Price, S.R., Henderson, C.E., Jessell, T.M., and Arber, S. (2002). ETS gene Pea3 controls the central position and terminal arborization of specific motor neuron pools. Neuron *35*, 877–892.

Logan, M., Martin, J.F., Nagy, A., Lobe, C., Olson, E.N., and Tabin, C.J. (2002). Expression of Cre Recombinase in the developing mouse limb bud driven by a Prxl enhancer. Genesis *33*, 77–80.

Loomis, C. a, Harris, E., Michaud, J., Wurst, W., Hanks, M., and Joyner, a L. (1996). The mouse Engrailed-1 gene and ventral limb patterning. Nature *382*, 360–363.

Loomis, C. a, Kimmel, R. a, Tong, C.X., Michaud, J., and Joyner, a L. (1998). Analysis of the genetic pathway leading to formation of ectopic apical ectodermal ridges in mouse Engrailed-1 mutant limbs. Development *125*, 1137–1148.

Luria, V., Krawchuk, D., Jessell, T.M., Laufer, E., and Kania, A. (2008). Specification of Motor Axon Trajectory by Ephrin-B:EphB Signaling: Symmetrical Control of Axonal Patterning in the Developing Limb. Neuron *60*, 1039–1053.

Ma, Q., Fode, C., Guillemot, F., and Anderson, D.J. (1999). NEUROGENIN1 and NEUROGENIN2 control two distinct waves of neurogenesis in developing dorsal root ganglia. Genes Dev. *13*, 1717–1728.

Machado, T.A., Paninski, L., Jessell, T.M., Miri, A., Machado, T.A., Pnevmatikakis, E., Paninski, L., Jessell, T.M., and Miri, A. (2015). Primacy of Flexor Locomotor Pattern Revealed by Ancestral Reversion of Motor Neuron Identity. Cell *162*, 338–350.

Malin, S.A., Davis, B.M., and Molliver, D.C. (2007). Production of dissociated sensory neuron cultures and considerations for their use in studying neuronal function and plasticity. *2*, 152–160.

Mankoo, B.S., Collins, N.S., and Ashby, P. (1999). Mox2 is a component of the genetic hierarchy controlling limb muscle development. *400*, 69–73.

Mariani, F. V, Ahn, C.P., and Martin, G.R. (2008). Genetic evidence that FGFs have an instructive role in limb proximal-distal patterning. Nature *453*, 401–405.

Martin, P. (1990). Tissue patterning in the developing mouse limb. Int. J. Dev. Biol. *34*, 323–336.

Matthews, P.B.C. (1972). Mammalian Muscle Receptors and Their Central Actions

(London: Edward Arnold Publishers).

McCoy, E.S., Taylor-Blake, B., and Zylka, M.J. (2012). CGRPα-expressing sensory neurons respond to stimuli that evoke sensations of pain and itch. PLoS One *7*.

McHanwell, S., and Biscoe, T.J. (1981). The localization of motoneurons supplying the hindlimb muscles of the mouse. Trans. R. Soc. *293*, 477–508.

Mears, S.C., and Frank, E. (1997). Formation of specific monosynaptic connections between muscle spindle afferents and motoneurons in the mouse. J. Neurosci. *17*, 3128–3135.

Mendell, L.M., and Henneman, E. (1968). Terminals of single Ia fibers: distribution within a pool of 300 homonymous motor neurons. Science (80-.). *160*, 96–98.

Mendelsohn, A.I., Simon, C.M., Abbott, L.F., Mentis, G.Z., and Jessell, T.M. (2015). Activity Regulates the Incidence of Heteronymous Sensory-Motor Connections. Neuron *87*, 111–123.

Mendelson, B., and Frank, E. (1991). Specific monosynaptic sensory-motor connections form in the absence of patterned neural activity and motoneuronal cell death. J. Neurosci. *11*, 1390–1403.

Mennerich, D., Scha, K., and Braun, T. (1998). Pax-3 is necessary but not sufficient for lbx1 expression in myogenic precursor cells of the limb. *73*, 147–158.

Mercader, N., Tanaka, E.M., and Torres, M. (2005). Proximodistal identity during

vertebrate limb regeneration is regulated by Meis homeodomain proteins. Development *132*, 4131–4142.

Miner, N. (1956). Integumental specification of sensory fibers in the development of cutaneous local sign. J. Comp. Neurol. *105*, 161–170.

Nelson, S.G., and Mendell, L.M. (1978). Projection of single knee flexor Ia fibers to homonymous and heteronymous motoneurons. J. Neurophysiol. *41*, 778–787.

Nichols, T. (1994). A biomechanical perspective on spinal mechanisms of coordinated muscular action: an architecture principle. Acta Anat 1–13.

Nichols, T., Wilmink, R., and Burkholder, T. (2002). The multidimensional and temporal regulation of limb mechanics by spinal circuits. In Progress in Motor Control, pp. 179–193.

Nichols, T., Bunderson, N., and Lyle, M. (2016). Neural Regulation of Limb Mechanics: Insights from the Organization of Proprioceptive Circuits. In Neuromechanical Modeling of Posture and Locomotion, B. Prilutsky, and D. Edwards, eds. (Springer), pp. 69–102.

de Nooij, J.C., Doobar, S., and Jessell, T.M. (2013). Etv1 Inactivation Reveals Proprioceptor Subclasses that Reflect the Level of NT3 Expression in Muscle Targets. Neuron *77*, 1055–1068.

De Nooij, J.C., Simon, C.M., Simon, A., Doobar, S., Steel, K.P., Banks, X.W., Mentis, G.Z., Bewick, G.S., and Jessell, T.M. (2015). Cellular/Molecular The PDZ-Domain Protein

Whirlin Facilitates Mechanosensory Signaling in Mammalian Proprioceptors. *35*, 3073–3084.

O'Gorman, S., Dagenais, N. a, Qian, M., and Marchuk, Y. (1997). Protamine-Cre recombinase transgenes efficiently recombine target sequences in the male germ line of mice, but not in embryonic stem cells. Proc. Natl. Acad. Sci. U. S. A. *94*, 14602–14607.

Okawa, H., Hoon, M., Yoshimatsu, T., Santina, L. Della, and Wong, R.O.L. (2014). Illuminating the multifaceted roles of neurotransmission in shaping neuronal circuitry. Neuron *83*, 1303–1318.

Olson, E.N. (1993). Regulation of muscle transcription by the MyoD family. The heart of the matter. Circ. Res. *72*, 1–6.

Patel, T.D., Jackman, A., Rice, F.L., Kucera, J., and Snider, W.D. (2000). Development of sensory neurons in the absence of NGF/TrkA signaling in vivo. Neuron *25*, 345–357.

Patel, T.D., Kramer, I., Kucera, J., Niederkofler, V., Jessell, T.M., Arber, S., and Snider, W.D. (2003). Peripheral NT3 signaling is required for ETS protein expression and central patterning of proprioceptive sensory afferents. Neuron *38*, 403–416.

Pecho-Vrieseling, E., Sigrist, M., Yoshida, Y., Jessell, T.M., and Arber, S. (2009). Specificity of sensory-motor connections encoded by Sema3e-Plxnd1 recognition. Nature *459*, 842–846.

Perez, S.E., Rebelo, S., and Anderson, D.J. (1999). Early specification of sensory

neuron fate revealed by expression and function of neurogenins in the chick embryo. Development *126*, 1715–1728.

Phelan, K., and Hollyday, M. (1990). Axon guidance in muscleless chick wings: the role of muscle cells in motoneuronal pathway selection and muscle nerve formation. J. Neurosci. *10*, 2699–2716.

Poliak, S., Morales, D., Croteau, L.-P., Krawchuk, D., Palmesino, E., Morton, S., Jean-François, C., Charron, F., Dalva, M.B., Ackerman, S.L., et al. (2015). Synergistic integration of Netrin and ephrin axon guidance signals by spinal motor neurons. Elife 1–26.

Poliak, S., Norovich, A.L., Yamagata, M., Sanes, J.R., and Jessell, T.M. (2016). Muscle-type Identity of Proprioceptors Specified by Spatially Restricted Signals from Limb Mesenchyme. Cell *164*, 512–525.

Price, S.R., De Marco Garcia, N. V., Ranscht, B., and Jessell, T.M. (2002). Regulation of motor neuron pool sorting by differential expression of type II cadherins. Cell *109*, 205–216.

Ramon y Cajal, S. (1911). Histologie du Systeme Nerveux de l'Homme et des Vertebres (Madrid: Instituto Ramon y Cajal).

Ramon y Cajal, S. (1929). Studies on Vertebrate Neurogenesis (Springfield, IL: Charles Thomas).

Raymond, C.S., and Soriano, P. (2007). High-efficiency FLP and ??C31 site-specific

recombination in mammalian cells. PLoS One *2*, 1–4.

Riddle, R.D., Ensini, M., Nelson, C., Tsuchida, T., Jessell, T.M., and Tabin, C. (1995). Induction of the LIM homeobox gene Lmx1 by WNT6a establishes dorsoventral pattern in the vertebrate limb. Cell *83*, 631–640.

Ringwald, M., Iyer, V., Mason, J.C., Stone, K.R., Tadepally, H.D., Kadin, J.A., Bult, C.J., Eppig, J.T., Oakley, D.J., Briois, S., et al. (2011). The IKMC web portal: A central point of entry to data and resources from the International Knockout Mouse Consortium. Nucleic Acids Res. *39*, 849–855.

Robson, L.G., and Hughes, S.M. (1996). The distal limb environment regulates MyoD accumulation and muscle differentiation in mouse-chick chimaeric limbs. Development *122*, 3899–3910.

Romanes, G.J. (1951). Motor cell columns of the lumbo-sacral spinal. J. Comp. Neurol. *94*, 313–363.

Romanes, G.J. (1964). The Motor Pools of the Spinal Cord. Prog. Brain Res. *11*, 93–119.

Rossant, J., Zirngibl, R., Cado, D., Shago, M., and Goguere, V. (1991). Expression of retinoic acid response element-hsp lacZ transgene defines specific domains of transcriptional activity during mouse embryogenesis. Genes Dev. *5*, 1333–1344.

Rossignol, S. Neural control of stereotypic limb movements. In Handbook of Physiology, pp. 173–216.

Rougon, G., and Hobert, O. (2003). New Insights into the Diversity and Function of Neuronal Immunoglobulin Superfamily Molecules. Annu. Rev. Neurosci. *26*, 207–238.

Rousso, D.L., Gaber, Z.B., Wellik, D., Morrisey, E.E., and Novitch, B.G. (2008). Coordinated Actions of the Forkhead Protein Foxp1 and Hox Proteins in the Columnar Organization of Spinal Motor Neurons. Neuron *59*, 226–240.

Sato, Y., Iketani, M., Kurihara, Y., Yamaguchi, M., Yamashita, N., Nakamura, F., Arie, Y., Kawasaki, T., Hirata, T., Abe, T., et al. (2011). Cartilage acidic protein-1B (LOTUS), an endogenous Nogo receptor antagonist for axon tract formation. Science *333*, 769–773.

Schaeren-Wiemers, N., and Gerfin-Moser, A. (1993). A Single Protocol to Detect Transcripts of Various Types and Expression Levels in Neural Tissue and Cultured-Cells - in-Situ Hybridization Using Digoxigenin-Labeled Crna Probes. Histochemistry *100*, 431–440.

Schmidt, C., Bladt, F., Goedecke, S., Brinkmann, V., Zschiesche, W., Sharpe, M., Gherardi, E., and Birchmeier, C. (1995). Scatter factor/hepatocyte growth factor is essential for liver development. Nature *373*, 699–702.

Schoultz, T.W., and Swett, J.E. (1972). The fine structure of the Golgi tendon organ. J. Neurocytol. *1*, 1–25.

Schramm, C., and Solursh, M. (1990). The formation of premuscle masses during

chick wing bud development. Anat. Embryol. (Berl). *182*, 235–247.

Schwabe, T., Neuert, H., and Clandinin, T.R. (2013). XA network of cadherin-mediated interactions polarizes growth cones to determine targeting specificity. Cell *154*, 351–364.

Scott, J. (2005). The Golgi tendon organ. In Peripheral Neuropathy, P. Dyck, and P. Thomas, eds. (Philadelphia: WB Saunders), pp. 151–161.

Scott, J.G., and Mendell, L.M. (1976). Individual EPSPs produced by single triceps surae Ia afferent fibers in homonymous and heteronymous motoneurons. J. Neurophysiol. *39*, 679–692.

Sears, T. (1964). The slow potentials of thoracic respiratory motoneurones and their relation to breathing. J. Physiol. 404–424.

Sherrington, C. (1906). The integrative action of the nervous system (New Haven: Yale Univeristy Press).

Shneider, N.A., Mentis, G.Z., Schustak, J., and Donovan, M.J.O. (2009). Functionally Reduced Sensorimotor Connections Form with Normal Specificity Despite Abnormal Muscle Spindle Development : The Role of Spindle-Derived Neurotrophin 3. *29*, 4719–4735.

Skarnes, W.C., Rosen, B., West, A.P., Koutsourakis, M., Bushell, W., Iyer, V., Mujica, A.O., Thomas, M., Harrow, J., Cox, T., et al. (2011). A conditional knockout resource for the genome-wide study of mouse gene function. Nature *474*, 337–342.

Smith, C.L., and Frank, E. (1987). Peripheral specification of sensory neurons transplanted to novel locations along the neuraxis. J. Neurosci. *7*, 1537–1549.

Sommer, L., Ma, Q., and Anderson, D.J. (1996). neurogenins,a Novel Family ofatonal-Related bHLH Transcription Factors, Are Putative Mammalian Neuronal Determination Genes That Reveal Progenitor Cell Heterogeneity in the Developing CNS and PNS. Mol. Cell. Neurosci. *8*, 221–241.

Sonner, M.J., Walters, M.C., and Ladle, D.R. (2017). Analysis of Proprioceptive Sensory Innervation of the Mouse Soleus : A Whole- Mount Muscle Approach. 1–18.

Sperry, R.W.W. (1963). Chemoaffinity in the orderly growth of nerve fiber patterns and connections. Proc. Natl. Acad. Sci. U. S. A. *50*, 703.

Stapley, P.J., Ting, L.H., Hulliger, M., and Macpherson, J.M. (2002). Automatic Postural Responses Are Delayed by Pyridoxine-Induced Somatosensory Loss. *22*, 5803–5807.

Stifani, N. (2014). Motor neurons and the generation of spinal motor neuron diversity. *8*, 1–22.

Sun, X., Mariani, F. V, and Martin, G.R. (2002). Functions of FGF signalling from the apical ectodermal ridge in limb development. Nature *418*, 501–508.

Sun, Y., Dykes, I.M., Liang, X., Eng, S.R., Evans, S.M., and Turner, E.E. (2008). A central role for Islet1 in sensory neuron development linking sensory and spinal gene regulatory programs. Nat. Neurosci. *11*, 1283–1293.

Sürmeli, G., Akay, T., Ippolito, G.C., Tucker, P.W., and Jessell, T.M. (2011). Patterns of spinal sensory-motor connectivity prescribed by a dorsoventral positional template. Cell *147*, 653–665.

Swanson, G.J., and Lewis, J. (1986). Sensory nerve routes in chick wing buds deprived of motor innervation. J. Embryol. Exp. Morphol. *95*, 37–52.

Tajbakhsh, S., and Buckingham, M.E. (1994). Mouse limb muscle is determined in the absence of the earliest myogenic factor myf-5. Proc. Natl. Acad. Sci. U. S. A. *91*, 747–751.

Tajbakhsh, S., Rocancourt, D., Cossu, G., and Buckingham, M. (1997). Redefining the genetic hierarchies controlling skeletal myogenesis: Pax-3 and Myf-5 act upstream of MyoD. Cell *89*, 127–138.

Takiguchi-Hayashi, K., Sato, M., Sugo, N., Ishida, M., Sato, K., Uratani, Y., and Arimatsu, Y. (1998). Latexin expression in smaller diameter primary sensory neurons in the rat. Brain Res. *801*, 9–20.

Tosney, K.W., and Landmesser, L.T. (1985). Development of the major pathways for neurite outgrowth in the chick hindlimb. Dev. Biol. *109*, 193–214.

Treubert-zimmermann, U., Heyers, D., and Redies, C. (2002). Targeting Axons to Specific Fiber Tracts In Vivo by Altering Cadherin Expression. *22*, 7617–7626.

Tripodi, M., Stepien, A.E., and Arber, S. (2011). Motor antagonism exposed by spatial

segregation and timing of neurogenesis. Nature *479*, 61–66.

Tsuchida, T., Ensini, M., Morton, S.B., Baldassare, M., Edlund, T., Jessell, T.M., and Pfaff, S.L. (1994). Topographic organization of embryonic motor neurons defined by expression of LIM homeobox genes. Cell *79*, 957–970.

Usoskin, D., Furlan, A., Islam, S., Abdo, H., Lönnerberg, P., Lou, D., Hjerling-leffler, J., Haeggström, J., Kharchenko, O., Kharchenko, P. V, et al. (2014). Unbiased classification of sensory neuron types by large-scale single-cell RNA sequencing. Nat. Publ. Gr. *18*, 145–153.

Vanderhorst, V.G.J.M., and Holstege, G. (1997). Organization of lumbosacral motoneuronal cell groups innervating hindlimb, pelvic floor, and axial muscles in the cat. J. Comp. Neurol. *382*, 46–76.

Vasyutina, E., and Birchmeier, C. (2006). The development of migrating muscle precursor cells. Anat. Embryol. (Berl). *211*, 37–41.

Vaughn, J.E., and Grieshaber, J.A. (1973). A morphological investigation of an early reflex pathway in developing rat spinal cord. J Comp Neurol *148*, 177–209.

Vogel, A., Rodriguez, C., Warnken, W., Izpisúa Belmonte, J.C., and Izpisua Belmonte, J.C. (1995). Dorsal cell fate specified by chick Lmx1 during vertebrate limb development. Nature *378*, 716–720.

Vogel, a, Rodriguez, C., and Izpisúa-Belmonte, J.C. (1996). Involvement of FGF-8 in initiation, outgrowth and patterning of the vertebrate limb. Development *122*,

1737–1750.

Vrieseling, E., and Arber, S. (2006). Target-Induced Transcriptional Control of Dendritic Patterning and Connectivity in Motor Neurons by the ETS Gene Pea3. Cell *127*, 1439–1452.

Wang, G., and Scott, S. a (2000). The “waiting period” of sensory and motor axons in early chick hindlimb: its role in axon pathfinding and neuronal maturation. J. Neurosci. *20*, 5358–5366.

Wang, L., and Marquardt, T. (2013). What axons tell each other : axon – axon signaling in nerve and circuit assembly §. Curr. Opin. Neurobiol. *23*, 974–982.

Wang, L., Klein, R., Zheng, B., and Marquardt, T. (2011). Anatomical Coupling of Sensory and Motor Nerve Trajectory via Axon Tracking. Neuron *71*, 263–277.

Wang, Z., Li, L.Y., Taylor, M.D., Wright, D.E., and Frank, E. (2007). Prenatal exposure to elevated NT3 disrupts synaptic selectivity in the spinal cord. J. Neurosci. *27*, 3686–3694.

Wang, Z., Li, L., and Frank, E. (2012). The role of muscle spindles in the development of the monosynaptic stretch reflex. 83–90.

Wenner, P., and Frank, E. (1995). Peripheral target specification of synaptic connectivity of muscle spindle sensory neurons with spinal motoneurons. J. Neurosci. *15*, 8191–8198.

White, F. a, Keller-Peck, C.R., Knudson, C.M., Korsmeyer, S.J., and Snider, W.D. (1998). Widespread elimination of naturally occurring neuronal death in Bax-deficient mice. J. Neurosci. *18*, 1428–1439.

Windhorst, U. (2007). Muscle proprioceptive feedback and spinal networks. *73*, 155–202.

Windle, W.F., and Baxter, R.E. (1936). Development of reflex mechanisms in the spinal cord of albina rat embryos. Correlation between structure and function and comparisons with the cat and the chick. J. Comp. Neurol. *63*, 189–209.

Wolpert, L. (1969). Positional information and the spatial pattern of cellular differentiation. J. Theor. Biol. *25*, 1–47.

Woo, S., Lukacs, V., de Nooij, J., Zaytseva, D., Criddle, C., Francisco, A., Jessell, T., Wilkinson, K., and Patapoutian, A. (2015). Piezo2 is the principal mechanotransduction channel for proprioception. Nat Neurosci *73*, 389–400.

Wu, S., Wu, Y., and Capecchi, M.R. (2006). Motoneurons and oligodendrocytes are sequentially generated from neural stem cells but do not appear to share common lineage-restricted progenitors in vivo. Development *133*, 581–590.

Wu, S.X., Koshimizu, Y., Feng, Y.P., Okamoto, K., Fujiyama, F., Hioki, H., Li, Y.Q., Kaneko, T., and Mizuno, N. (2004). Vesicular glutamate transporter immunoreactivity in the central and peripheral endings of muscle-spindle afferents. Brain Res. *1011*, 247–251.

Yakovenko, S., Mushahwar, V., Horst, V.V.A., Holstege, G., Prochazka, A., Mushahwar, V., Vanderhorst, V., Holstege, G., and Prochazka, A. (2002). Spatiotemporal Activation of Lumbosacral Motoneurons in the Locomotor Step Cycle. 1542–1553.

Yashiro, K., Zhao, X., Uehara, M., Yamashita, K., Nishijima, M., Nishino, J., Saijoh, Y., Sakai, Y., and Hamada, H. (2004). Regulation of retinoic acid distribution is required for proximodistal patterning and outgrowth of the developing mouse limb. Dev. Cell *6*, 411–422.

Young, T.R., and Leamey, C.A. (2009). Teneurins: Important regulators of neural circuitry. Int. J. Biochem. Cell Biol. *41*, 990–993.

Zhao, J., Nassar, M.A., Gavazzi, I., and Wood, J.N. (2006). Tamoxifen-Inducible Nav1.8-CreERT2 Recombinase Activity in Nociceptive Neurons of Dorsal Root Ganglia. Genesis *44*, 364–371.